UNIVERSITÉ D'ORLÉANS

ÉCOLE DOCTORALE ENERGIE-MATERIAUX-SCIENCES DE LA TERRE ET DE L'UNIVERS

LABORATOIRE PRISME

THÈSE présentée par :

Padipan TINPRABATH

Soutenue le : **23 avril 2015**

pour obtenir le grade de : **Docteur de l'université d'Orléans**

Discipline : Énergétique

L'Influence des Propriétés Physiques et Chimiques du Biodiesel, Diesel et de leur Mélange sur l'Injection et le Spray

THÈSE dirigée par :

Somchai CHANCHAONA	Maître de conférences, KMUTT University - CERL
Fabrice FOUCHER	Professeur, Université d'Orléans – PRISME

RAPPORTEURS :

Jean-Bernard BLAISOT	Maître de Conférences, Université de Rouen - CORIA
Luis LE MOYNE	Professeur, Université de Bourgogne - ISAT

JURY:

Jean-Bernard BLAISOT	Maître de Conférences, Université de Rouen – CORIA
Somchai CHANCHAONA	Maître de conférences, KMUTT University - CERL
Cyril CRUA	Directeur de recherche, University of Brighton, Président du jury
Fabrice FOUCHER	Professeur, Université d'Orléans - PRISME
Camille HESPEL	Maître de Conférences, Université d'Orléans - PRISME
Luis LE MOYNE	Professeur, Université de Bourgogne - ISAT

Remerciements

Cette thèse a été effectuée dans le cadre d'une collaboration entre l'équipe Energie - Combustion - Moteurs (ECM) du laboratoire PRISME (Université d'Orléans) et de laboratoire CERL, King Mongkul's University of Technology Thonburi (Thaïlande). Mon travail a été soutenu par une bourse de la région et par l'université de Rajamongala (Rajamongala University of Technology Phra Nakhon,Thaïlande).

Dans cet espace dédié, je souhaiterais remercier, malheureusement de manière non-exhaustive, les personnes qui un moment donné ou tout au long de ma thèse m'ont soutenu et qui ont participé à cette aventure qui restera pour moi une expérience inoubliable. Sachez pour les personnes que j'aurais omis de citer et qui le remarqueront, que je les remercie tout autant.

Tout d'abord, je tiens à remercier Cyril Crua, Luis Le Moyne et Jean-Bernard Blaisot de m'avoir fait l'honneur d'accepter de faire parti du jury et de vous êtes déplacés pour assister à ma soutenance. Je les remercie pour l'intérêt qu'ils ont porté à l'égard de cette étude et du temps qu'ils ont consacré à son évaluation. Les rapports avant soutenance et les commentaires durant celle-ci m'ont notamment aidé à appréhender le travail entrepris avec davantage de recul et permis de complémenter / d'améliorer certains aspects des nombreux domaines scientifiques abordés lors de cette thèse. Je vous suis très reconnaissant d'avoir jugé le manuscrit sans traitement de faveur, ce qui lui donne sa juste valeur. Je ne saurais que terminer par vous remercier pour vos compliments.

Je remercie ensuite très chaleureusement ma fantastique (et oui !) équipe encadrante à qui je dois la réussite de cette thèse sous toutes ces formes, aussi bien d'un point de vue scientifique, au plaisir quotidien que j'ai eu à travailler en leur compagnie. Mes remerciements vont donc à Fabrice Foucher qui m'a aidé depuis mon premier jour à Polytech Orléans, pour tous les conseils durant cette thèse, pour m'avoir offert les opportunités d'aller aux conférences à l'étranger. Je remercie également Somchai Chachachaona pour m'avoir aidé à analyser les données et à corriger cette thèse et avoir assisté à ma soutenance. Je tiens à remercier tout particulièrement Camille Hespel pour sa disponibilité, son accompagnement et son implication (comme mon ombre) sur tous les aspects scientifiques de l'atomisation et des sprays ainsi que de m'avoir soutenu dans mes moments de doute (surtout vers la fin ...). Bon nombre des analyses effectuées est le résultat de nos nombreuses discussions (et des gribouillis sur le tableau) qui ont véritablement permis de maintenir une ambiance conviviale et dynamique tout au long de la thèse et en fin pour avoir organisé la soirée inoubliable.

Je remercie Christine Mounaim- Rousselle pour m'avoir offert l'opportunité de faire mes études ici, pour tous les conseils et pour m'avoir de temps en temps invité à la soirée chez elle.

Je souhaiterais ensuite exprimer toute ma reconnaissance pour tous les membres des équipes techniques et administratives du laboratoire Prisme qui ont contribué par leur aide précieuse à ce travail, à savoir : Sylvie Plessard, Bruno Moreau, Yahia Haidous, Benoit Bellicaud et Florian Lespinasse. Je tiens à remercier Julien Lemaire pour m'avoir aidé et préparer les

expériences de la cellule C2, pour m’avoir aidé de résoudre tous les problèmes techniques rencontrés lors des expériences.

Et comment ne pas citer mes cher(e)s ami(e)s, compagnons de tous les jours (mais aussi de soirées et d’autres sorties), docteur ou qui le seront dans un avenir proche, Jérémie, Jianxi, Adrien, Bénedicte, Philippe, Jamil, Arnaud, Amine, Yann-Ael, les deux Pierre, Christophe, Haifa, Shadi, Jean-Baptiste, Sokratis, Charles, Pietro, Ricardo, Medhi, Salim, Antoine, Marco et Ob . Bon courage à tous et surtout ne lâchez rien et profitez-en.

Je finirai par remercier toute ma famille et surtout mes parents pour avoir accepté mes choix. Je vous remercie du fond du cœur pour tout que vous avez fait pour moi et je vous dois tout ce que j’ai pu entreprendre.

Table of contents

List of figures

List of table

Appendix

Nomenclature

Latins Symbols

a	Fuel sound velocity	m/s
A	Projected area of the upstream half of the spray in an image	mm^2
AF	Air - Fuel ratio	-
Ao	Area outlet orifice	mm^2
AR	Area Reduction	-
B	Biodiesel percentage blend	%
Ca	Surface coefficient	-
Cd	Discharge coefficient	-
C_M	Moment coefficient	-
CN	Cetane number	-
Cv	Velocity coefficient	-
D	Nozzle diameter	µm
D_i	Inlet diameter	µm
D_o	Outlet diameter	µm
D_s	Sack chamber diameter of nozzle	µm
K	Cavitatin Number	-
l	Width of the cross section spray	mm
L	Length of the orifice	µm
L/W	Length of the whole / Diameter of the whole	-
M	Momentum flux or spray force	N
$\dot{m}$	Mean mass flow rate	mg/ms
$\dot{m}_e$	Estimated mass flow rate	mg/ms
$\dot{m}_{measured}$	Mean mass flow rate	mg/ms
$\dot{m}_{th}$	Theoretical mass flow rate	mg/ms
$n_{orifice}$	Number of orifices on the nozzle	-
Pb	Back-pressure	MPa
Pi	Injection pressure	MPa

Pv	Saturated vapour pressure	MPa
$p(t)$	Dynamic pressure	MPa
Re	Reynolds number	-
S	Spray tip penetration or penetration length	mm
S_c	Outlet geometric cross-sectional area	mm^2
SG	Specific gravity	-
S_{tube}	Cross-sectional area of the measuring tube	mm^2
V_{th}	Theoretical velocity	m/s
V_{mean}	Mean velocity at the outlet section	m/s
T	Temperature	K
t	Time	µs
t_b, t_r	Break-up time	µs
t_i	Effective injection duration	µs
t_{off}	Time of the injector closed	µs
t_{on}	Time of the injector opening	µs
x_{bio}	Fraction of biodiesel	%
X	Fraction of biodiesel	%

Greeks Symbols

ΔP	Pressure difference ($\Delta P = Pi - Pb$)	MPa
μ	Dynamic viscosity	cP
ν	Kinematic viscosity	mm^2/s
ν_{bio}	Kinematic viscosity of biodiesel	mm^2/s
ν_{mix}	Kinematic viscosity of fuel blend	mm^2/s
ν_T	Kinematic viscosity(variable to temperature)	mm^2/s
ρ	Fuel density	kg/m^3
ρ_a	Air density	kg/m^3
ρ_f	Fuel density	kg/m^3
ρ_T	Fuel density (variable to temperature)	kg/m^3
θ	Angle of spray	°

Abbreviation

DF	Diesel Fuel
HG	Heat of combustion
CN	Cetane Number
FAME	Fatty Acid Methyl Esters
FAAE	Fatty Acid Alkyl Esters
IV	Iodine Value
CI	Cetane Index
CP	Cloud Point
CN	Cavitatin Number
PP	Pour Point
CFPP	Cold Filter Plugging Point
LTFT	Low-Temperature Flow Test
OSI	Oil Stability Index
AOCS	American Oil Chemists' Society
TBHQ	Tres-butylhydroquinone
BHT	Butylated hydroxytoluene
BHA	Hidroxyanisole
PG	Propyl Gallate
APE	Allylic Position Equivalents
BAPE	Bis-Allylic Position Equivalents
MP	Melting Point
BP	Boiling Point
RME	Rapeseed Methyl Ester
EID	Effective Injection Duration
ET	Excitation Time
WD	Winter grade pump-grade diesel
ULSU	Ultra-low sulphur diesel (summer grade)

Introduction: Background and Issues of the study

Current energy reserves are being exhausted, in particular oil which is predicted to be depleted in the next 40 years, making it essential to find alternative fuels. Biodiesel is a very interesting fuel because it is renewable, thus increasing energy security, it is environmentally friendly, and it has a higher cetane number and a lower sulfur and aromatic content than pure Diesel. The main disadvantages of biodiesel are its higher viscosity, lower energy content, higher cloud point and pour point, higher nitrogen oxide (NOx) emissions, lower power and high cost [1]. However, many countries can produce their own biodiesel and blends with diesel fuel of 2–20% [2] and [3]. Governments (e.g. the European Union, the U.S.A.) have stipulated that fuel should be blended with biodiesel [3], although consumers are unconvinced about the use of biodiesel fuel blends in automotive engines because of their concerns about combustion efficiency, pollutant emissions and the impact on engine components. Attention has especially focused on pollutant emissions from biodiesel-fuelled vehicles with the implementation in 2014 of the Euro VI regulations.

The new standards involve problems related to cold-start, namely evaluation of post-treatment strategies and EGR at low temperature. The regulations concerning the quality of cold start at −7 °C will become increasingly stringent [4]. At these temperatures the viscosity is higher. The blending of biodiesel with diesel fuel increases the cloud point, the cold filter plugging point (CFPP), or the pour point, which can clog the fuel lines and filters of the vehicle's fuel system [5]. Whatever the type of fuel, diesel–biodiesel blends under 5% do not impact cold flow properties [6]. That is why it is important to know the behavior of the diesel injector in these conditions for different fuels.

The first important point to consider in the use of biodiesel in vehicle engines is that the combustion efficiency and pollutant emissions depend on the fuel injection process [7, 8]. It is necessary to know the physical properties of injection and flow characteristics inside the injector, the spray tip penetration, spray angle and fuel atomization in order to improve the characteristics of biodiesel, the injector geometry or fuel injection method and thus achieve the highest engine efficiency.

The main objective of this PhD is as follows: characterization of the impact of certain properties of Diesel, Winter diesel, Biodiesel and Biodiesel blend on the phenomena related to the preparation of the mixture for combustion, applied to a diesel engine at room temperature and cold temperatures. The properties that will be focused on are:

- Sound velocity: This is an important thermophysical property of fuel, as it directly characterizes the fuel injection and emissions in diesel engines [9].
- Injection rate: The injection rate is the rate of fuel injection per time. Analysis of the injection rate gives the main characteristics of the injector: discharge coefficient, mean or maximum mass flow rate, opening delay, etc.. The injection rate analysis method used followed Payri et al. [10, 11] and Dernotte et al. [7].

- Discharge coefficient, *Cd*: The discharge coefficient is a property that indicates the efficiency of the injector. The discharge coefficient is a ratio between mass flow rate measurement and theoretical mass flow rate.
- Spray tip penetration: The spray tip penetration or penetration length is the length to which the spray penetrates across the combustion chamber [11]. The speed and extent of spray tip penetration have an important influence on air use and fuel-air mixing rate.
- Spray angle: The spray angle is an important factor in the behavior of spray injection. This angle should be as wide as possible in order to ensure efficient combustion and to limit the impact of the spray on the cylinder or piston walls. A wide spray angle results in a good fuel-air mixing rate and hence a high combustion efficiency as well as a lower spray penetration.

According to the literature, biodiesel fuel produced with vegetable or animal oil can be used with diesel injectors. Most studies focus on biodiesel produced from rapeseed because at the present time this type of fuel is widely used in Europe and Asia. To further our understanding of these mixtures, it is necessary to test a larger range of fuels with a biodiesel fraction of 10 to 50%, and to compare the results with correlations from the literature. During start-up of the engine under cold temperatures, however, no information is available in the literature on the injection rate and spray penetration of Diesel–Biodiesel blends.

The properties investigated in this study are therefore density and kinematic viscosity. Their impact was characterized using various experimental devices. One aspect of this study was the use of simple empirical or theoretical models from the literature and new correlations are proposed to improve their precision but also their range of application.

The present manuscript is divided into four chapters:

1. The first chapter introduces conventional diesel injection and spray, and presents the state of the art of current understanding of the impact of fuel properties on it.

2. The second chapter presents all the experimental methods set up during this study, the associated processing and analysis tools as well as the fuels and their properties.

3. Chapter 3 analyzes the influence of the physical properties of fuel blends at room temperature on the injection rate and spray.

4. In Chapter 4, the influence of fuel blends and negative temperature on injector and spray behavior is investigated.

The final chapter presents the conclusions and future research perspectives.

Introduction: Contexte et enjeux de l'étude **(version français)**

Les réserves énergétiques actuelles s'épuisent, en particulier le pétrole. La chute de production est attendue dans les 40 prochaines années, ce qui rend essentiel de trouver des carburants alternatifs. Le biodiesel est un carburant très intéressant car il est renouvelable, augmentant ainsi la sécurité énergétique, il est ainsi plus respectueux de l'environnement. De plus il a un indice de cétane plus élevé et une faible teneur en souffre et en aromatique que Diesel pur améliorant ainsi quelques performances en terme d'émission dans les moteurs. Les principaux inconvénients de biodiesel sont sa viscosité élevée, sa faible teneur en énergie, son point de trouble et le point d'écoulement plus élevé, des émissions d'oxyde d'azote (NOx) plus importantes, une faible puissance et un coût élevé [1]. Cependant, de nombreux pays peuvent produire leur propre biodiesel et les mélanger avec du carburant diesel de 2 à 20% [2] et [3]. Les gouvernements (par exemple l'Union européenne, les Etats-Unis) ont stipulé que le carburant doit être mélangé avec du biodiesel [3] à hauteur de 8% pour la France et jusqu'à 20% pour certaine flotte aux Etats-Unis. Cette législation sur la composition du carburant n'est très peu connue des consommateurs. Ces deniers restent peu convaincus de l'utilisation de mélanges de carburants de biodiesel dans les moteurs automobiles en raison de leurs préoccupations au sujet de l'efficacité de combustion, les émissions de polluants et de l'impact sur les composants du moteur. Depuis quelques années l'attention s'est surtout focalisée sur les émissions polluantes des véhicules de biodiesel avec la mise en œuvre en 2014 de la réglementation Euro VI.

Les nouvelles normes concernent entre autre les problèmes liés au démarrage à froid, à savoir l'évaluation des stratégies post-traitement et EGR à basse température. Les règlements concernant la qualité de démarrage à froid à -7 ° C deviendront de plus en plus strictes [4]. A ces températures, la viscosité est plus élevée. Le mélange de biodiesel avec du carburant diesel augmente le point de trouble, la température limite de filtration (TLF ; CFPP en anglais), ou le point d'écoulement, ce qui peut conduire à l'obstruction des conduites ou des filtres du véhicule [5]. Quel que soit le type de carburant, les mélanges Diesel-biodiesel de moins de 5% n'ont aucune incidence sur les propriétés de l'écoulement à froid [6]. Pour des taux de mélanges plus élevé il est important de connaître le comportement de l'injecteur pour différentes températures et type de carburant.

Le premier point important à considérer dans l'utilisation du biodiesel dans les moteurs de véhicule est que l'efficacité de la combustion et les émissions polluantes dépendent du processus d'injection de carburant [7, 8]. Il est nécessaire de connaître les propriétés physiques de l'injection et les caractéristiques d'écoulement à l'intérieur de l'injecteur, la longueur de pénétration du carburant, et l'atomisation du jet afin d'améliorer pour les caractéristiques physique des carburant avec du biodiesel, la géométrie de l'injecteur ou la stratégie l'injection de carburant et de réaliser ainsi un rendement moteur plus élevé .

L'objectif principal de cette thèse est le suivant: caractérisation de l'impact de certaines propriétés du Diesel, du Winter diesel, du biodiesel et des mélanges Biodiesel-Diesel ou

Biodiesel-Winter Diesel sur les phénomènes liés à la préparation du mélange pour la combustion, appliqué à un moteur diesel à température ambiante et négatives. Les propriétés sont axées sur :

- la vitesse du son: C'est une propriété thermo physique importante de carburant, car elle influence directement l'injection de carburant et les émissions dans les moteurs diesel [9].
- Le taux d'injection: Le taux d'injection est la vitesse d'injection de carburant en fonction du temps. L'analyse du taux d'injection donne les principales caractéristiques de l'injecteur: coefficient de décharge, débit de masse maximal ou moyen, retard à l'ouverture, etc .. La méthode d'analyse du taux d'injection utilisé suit les publications de Payri et al. [10, 11] et de Dernotte et al. [7].
- Le coefficient de décharge, *Cd*: Le coefficient de décharge est une propriété qui indique l'efficacité de l'injecteur. Le coefficient de décharge est un rapport entre débit massique stationnaire mesuré et débit massique théorique.
- la pénétration liquide su spray : La pénétration ou la longueur de pénétration est la longueur à laquelle le jet pénètre dans la chambre de combustion [11]. La vitesse et l'ampleur du cône d'injection ont une influence importante sur le taux de mélange air-carburant.
- L'angle de spray: L'angle de spray est un facteur important dans le comportement de l'injection. Cet angle doit être aussi large que possible pour assurer une combustion efficace et limiter l'impact du spray sur la paroi du cylindre ou du piston. Un large spray permet un bon taux de mélange air-carburant et donc une grande efficacité de combustion ainsi qu'une pénétration plus faible.

Selon la littérature, le carburant biodiesel produit avec l'huile végétale ou animale peut être utilisé dans des injecteurs diesel sans modification du matériel. La plupart des études se concentrent sur le biodiesel produit à partir de colza, car à l'heure actuelle ce type de carburant est largement utilisé en Europe et en Asie. Pour approfondir notre compréhension de ces mélanges, il est nécessaire de tester un plus grand éventail de carburants biodiesel avec une fraction de 10 à 50%, et de comparer les résultats avec des corrélations de la littérature. Lors du démarrage du moteur, sous des températures froides, aucune information n'est encore disponible dans la littérature sur le taux d'injection, la pénétration liquide des mélanges diesel-biodiesel.

Les propriétés étudiées dans cette étude sont donc la densité et la viscosité cinématique. Leur impact est caractérisé par divers dispositifs expérimentaux. Un aspect de cette étude est l'utilisation de modèles empiriques ou théoriques simples de la littérature et de nouvelles corrélations sont proposées pour améliorer leur précision ainsi que leur champ d'application.

Le présent manuscrit est divisé en quatre chapitres:

1. Le premier chapitre présente l'injection diesel classique et le spray, il résume l'état de l'art sur la compréhension actuelle de l'impact des propriétés du carburant sur l'injection.

2. Le deuxième chapitre présente toutes les méthodes expérimentales mises en place au cours de cette étude, le traitement associé et les outils d'analyse utilisés ainsi qu'une description des propriétés des carburants.

3. Le chapitre 3 analyse l'influence des propriétés physiques des mélanges de carburant à la température ambiante sur le débit d'injection et la répartition du spray liquide.

4. Dans le chapitre 4, l'influence du mélange de carburant et des températures négatives sur le comportement de l'injecteur et du spray sont étudiés.

Le dernier chapitre présente les conclusions et perspectives pour de futures recherches.

CHAPTER 1

Literature Review

The purpose of this chapter is to study the properties of biodiesel, which has a higher cetane number and a lower sulfur and aromatic content than pure diesel. The main disadvantages of biodiesel are its higher viscosity, lower energy content, higher cloud point and pour point, higher nitrogen oxide (NOx) emissions, lower power and high cost. The first important point to consider in the use of biodiesel in engines is the physical properties of injection e.g. flow characteristics inside the injector, spray tip penetration, spray angle and fuel atomization. This chapter reports on: The biodiesel properties

- Biodiesel properties.
- An injection rate analysis from the literature.
- Models of spray tip penetration and spray angle.

Introduction (version français)

Le but de ce chapitre est d'étudier les propriétés du biodiesel. Ce dernier a un indice de cétane plus élevé, une plus faible teneur en soufre et en aromatique que diesel pur. Les principaux inconvénients de biodiesel sont sa viscosité élevée, faible teneur en énergie, point de trouble et le point d'écoulement plus élevé, émission d'oxyde d'azote (NOx) plus importante, faible puissance et le coût élevé. Le premier point important à considérer dans l'utilisation de biodiesel dans les moteurs est la nécessité de connaître les propriétés physiques du carburants, les caractéristiques d'écoulement à l'intérieur de l'injecteur, la longueur de pénétration du carburant, et l'atomisation du jet.

Ce chapitre présente:

- Les propriétés du biodiesel.
- Une analyse du taux d'introduction de la littérature.
- Les modèles de pénétration de l'angle du spray.

1.1 Biodiesel Properties

1.1.1 Introduction

Biodiesel is one of the available Diesel Fuel Fuels (DF) that derived from vegetable oils or animal fats. The trans-esterification of an oil or fat with a monohydric alcohol such as ethanol, methanol yields the corresponding mono-alkyl-esters, which are defined as biodiesel. The highest of introduction increasing use and commercialization of biodiesel in many countries around the world has been accompanied by the development of standards to ensure high product quality and user confidence. Some of the biodiesel standards are ASTM D6751 (ASTM stands for American Society for Testing and Materials) and the European standard EN 14214, which was developed from previously existing standards in individual European countries [13].

The source of production directly affects the properties of the biodiesel, which are influenced by the nature of major as well as minor components arising from production or other sources. Typically, natural components ultimately determine fuel and physical properties. Some of the properties included in standards can be traced to the structure of the fatty esters in the biodiesel. The trans-esterification reaction of an oil or fat leads to a biodiesel fuel with a fatty acid profile corresponding to that of the parent oil or fat. Therefore, biodiesel is largely composed of fatty esters with each ester component contributing to the properties of the fuel [5,13].

The properties of biodiesel that are determined by the structure of its component fatty esters and the nature of its minor components include ignition quality, cold flow, oxidative stability, viscosity, and lubricity. Generally, as it is the least expensive alcohol, methanol is used to produce biodiesel. Biodiesel, in most cases, can be termed the Fatty Acid Methyl Ester (FAME) of a vegetable oil or animal fat. However, both the fatty acid chain and alcohol functionality contribute to the overall properties of a fatty ester. It is necessary to consider the properties imparted by other alcohols yielding Fatty Acid Alkyl Esters (FAAE) which could be used for biodiesel production. Table 1.1 lists the fuel properties of neat fatty acids and esters. The gross heat of combustion (HG) of some fatty compounds [13] is also included in Table 1.1.

Table 1.1: Properties of fatty acids and esters [13]

Trivial(systematic) name; acronym[b]	Melting Point[c] (^oC)	Boiling Point[c,d] (^oC)	Cetane no.	Viscosity[e]	HHV[f] (kcal/mol)
Caprylic (Octanoic);8:0	16.5	239.3			
-Methyl ester		193	33.6 (98.6)[g]	0.99[j]; 1.19[k]	1313
-Ethyl ester	-43.1	208.5		1.37 (25^oC)	1465
Capric (Decanoic); 10:0	31.5	270	47.6 (98.0)[g]		1453.07 (25^oC)
-Methyl ester		224	47.2 (98.1)[k]	1.40[j], 1.72[k]	1625
-Ethyl ester	-20	243-245	51.2 (99.4)[g]	1.99 (25^oC)[j]	1780
Lauric(Dodecanoic); 12:0	44	131[l]			1763.25 (25^oC)
-Methyl ester	5	266	61.4 (99.1)[g]	1.95[j]; 2.43[k]	1940
-Ethyl ester	-1.8	163		2.88[j]	2098
Myristic	58	250.5			2073.91 (25^oC)

(Tetradecanoic): 14:0					
-Methyl ester	18.5	295	66.2(96.5)[g]	2.69[j]	2254
-Ethyl ester	12.3	295	66.9(99.3)[g]		2406
Palmitic (Hexadecanoic); 16:0	63	350			2384.76(25°)
-Methyl ester	30.5	415-418	74.5(93.6)[g];85.9	3.60[j]; 4.38[k]	2550
-Ethyl ester	19.3/24	191	93.1[i]		2717
-Propyl ester	20.4	190	85.0[i]		
-Isopropyl ester	13.4	160	82.6[i]		
-Butyl ester	16.9		91.9[i]		
-2-Butyl			84.8[i]		
-Isobutyl ester	22.5, 28.9	199	83.6[i]		
Stearic (Octadecanoic); 18:0	71	360	61.7[h]		2696.12 (25°)
-Methyl ester	39	442-443	86.9(92.1)[g];101[i]	4.74[j]	2859
-Ethyl ester	31-33.4	199	46.8[h]; 97.7[i]		3012
-Propyl ester			69.9[h]; 90.9[i]		
-Isopropyl ester			96.5[i]		
-Butyl	27.5	343	80.1[h]; 92.5[i]		
-2-Butyl ester			87.5[i]		
-Isobutyl ester			99.3[i]		
Palmitoleic(9(Z)-Hexadecanoic; 16:0					
-Methyl ester			51.0[i]		2521
Oleic(9(Z))-Octadecanoic); 18:1	16	286	46.1[h]		2657.4 (25°)
-Methyl ester	-20	218.5	55[h]; 59.3[i]	3.73[j]; 4.51[k]	2828
-Ethyl ester		216-217	53.9[h]; 67.8[i]	5.50 (25°C)	
-Propyl ester			55.7[h]; 58.8[i]		
-Isopropy ester			86.6[i]		
-Buty ester			59.8[h] ; 61.6[i]		
-2-Butyl ester			71.9[i]		
-Isobutyl ester			59.6[i]		
Linoleic(9Z, 12Z-Octadecadienoic);18:2					
-Methyl ester	-35	215	42.2[h]; 38.2[i]	3.05[j], 3.65[k]	2794
-Ethyl ester		270-275	37.1[h]; 39.6[i]		
-Propyl ester			40.6[h]; 44.0[i]		
-Butyl ester			41.6[h]; 53.5[i]		
Linolenic (9Z,12Z,15Z-Octadecatrienoic); 18:3		-11	230-2[17]	20.4[h]	
-Methyl ester					
-Ethyl ester	-57/-52	109	20.6[g];22.7[i]	2.65[j], 3.14[k]	2750
-Propyl		174	26.7[h]		
-Butyl ester			26.8[h]		
Ricinoleic (12-Hydroxy -9Z-octadecenoic); 18:1, 12-OH	5.5	245			
-Methyl ester		225-227		15.44[k]	
Erucic(13Z-Docosenoic); 22:1	33-34	265			
-Methyl ester		221-222	5.91[j]	3454	
-Ethyl ester		229-230			

[a]Adapted from Ref.[14].

[b]The numbers denote the number of carbons and double bonds. For example, in oleic acid, 18:1 stands for 18 carbons and double bond.

[c]Melting point and boiling point data are from Ref.[15] and [16].
[d]Superscripts denote pressure (mm Hg) at which the boiling point was determined.

[e]Viscosity values determined at 40°C, unless indicated otherwise.
[f]HHV values are from Refs.[17] and [14].
[g]Number in parentheses indicates purity (%) of the material used for CN determination as given in Ref. [18].
[h]Ref. [19].
[i]Ref. [20].
[j]Dynamic viscosity (mPa.s = cP), Ref.[21].
[k]Kinematic viscosity (mm2/s=cSt), Ref.[22].

Table 1.2: Composition of Biodiesels [5]**.**

FAME	S	R	P	SR	RP	SP	SRP	Sf	GP	soy A
C10:0 (caprte)		0.01	0.03		0.02	0.01	0.01			
C12:0 (laurate)		0.04	0.24	0.03	0.20	0.18	0.14	0.02	0.02	
C14:0 (myristate)	0.07	0.07	0.57	0.09	0.54	0.01	0.38	0.07	0.13	
C16:0 (palmitate)	10.76	5.22	42.45	8.90	23.09	25.56	19.07	6.40	10.57	16.18
C16:1(palmitoleate)	0.07	0.20	0.13	0.15	0.17	0.11	0.14	0.09	0.13	
C18:0 (stearate)	3.94	1.62	4.02	2.76	3.02	4.04	3.30	4.22	2.66	3.82
C18:1 (oleate)	22.96	62.11	41.92	52.92	33.13	42.74	23.90	41.05	41.05	28.80
C18:2 (linoleate)	53.53	21.07	9.80	37.51	15.47	31.72	28.08	64.16	36.67	50.46
C18:3 (linolente)	7.02	6.95	0.09	7.02	3.08	3.58	4.68	0.12	7.10	
C20:0 (arachidate)	0.38	0.60	0.36	0.46	0.49	0.39	0.46	0.03	0.44	
C21:1 (eicosenoate)	0.23	1.35	0.15	0.68	0.67	0.20	0.53	0.15	0.67	
C22:0 (behenate)	0.80	0.35	0.09	0.46	0.24	0.32	0.33	0.76	0.45	
C24:0 (lignocerate)		0.22	0.15			0.63				

S and soy A, soybean; R, rapeseed; P, palm; Sf, sunflower; SR, soybean + rapeseed; RP, rapeseed + palm; SP, soybean + palm and SRP, soybean + rapeseed + palm;

1.1.2 Cetane Number

The Cetane Number (CN) is a measure of a fuel's auto ignition characteristics [23]. Generally, biodiesel is composed of many long-chain hydrocarbon groups (with virtually no branching or aromatic structures). It typically has a higher CN than petroleum diesel and increasing the percentage of biodiesel increases the CN of the blend [24]. However, in some cases, increase the percentage effect of reducing the CN of the blend.

Biodiesel produced from feedstock rich in saturated fatty acids (such as tallow and palm) has a higher CN than fuels produced from less saturated feedstock (such as soy and rapeseed). The effect upon CN of branching in the alcohol used to produce the biodiesel is very small, and difficult to discern [25]. The CN of pure FAME molecules increases with chain length but this effect is masked when considering complex mixtures of FAME fuels. On the other hand, the CN of FAME fuels clearly varies with average degree of unsaturation. The literature also reports that an increasing degree of unsaturation leads to a lower CN [26, 27]. Laureate and al. [28] recently proposed a predictive equation for FAME CN that is largely driven by the number of double bonds in the FAME (as well as the FAME's carbon number) [29]. These authors also noted the high correlation between CN and iodine value (IV).

It is noteworthy that no correlation between CN and Cetane Index (CI) is apparent, and that CI has no meaningful correlation with average unsaturation or IV. These observations

suggest that the CI values reported in the literature are not reliable, and highlight the problem that at present, a valid method for computing CI for biodiesel does not exist.

1.1.3 Cold flow properties

Low temperature performance is one of the most important considerations for users of biodiesel. The main problems associated with the use of biodiesel are poor flow properties at low temperature, documented by a relatively high Cloud Point (CP) (CP is the temperature at which crystals first appear) and Pour Point (PP) (PP is the lowest temperature at which the fuel is observed to flow) [5]. The CP, which usually occurs at a higher temperature than the PP, is caused by the temperature at which a fatty material becomes cloudy due to the formation of crystals and solidification of saturates [13]. Solids and crystals rapidly grow and agglomerate, clogging fuel lines and filters and causing major operability problems. When decreasing the temperature, more solids form and the material approaches the PP, the lowest temperature at which the material will still flow. Saturated fatty compounds have significantly higher melting points than unsaturated fatty compounds (Table 1.1) and in a mixture, they crystallize at higher temperatures than the unsaturated compounds. Thus, biodiesel fuels derived from fats or oils with significant amounts of saturated fatty compounds will display higher CP and PP [5].

Moreover, in addition to the CP (ASTM D2500) and PP (ASTM D97) tests, two test methods for the low-temperature flow properties of petrodiesel exist, namely, the Low-Temperature Flow Test (LTFT) (used in North America; e.g., ASTM D4539) and the Cold Filter Plugging Point (CFPP, i.e. the lowest temperature at which a vehicle will operate) (used outside North America; e.g., the European standard EN 116). These methods have also been used to evaluate biodiesel and its blends. Low-temperature filterability tests were stated to be necessary because of correlation with operability tests both of the CP and the PP [13]. However, for fuel formulations containing at least 10 % vol. methyl esters, both LTFT and CFPP are linear functions of the CP [30]. Additional statistical analysis has shown a strong 1:1 correlation between LTFT and CP [31].

Several approaches to the low temperature problems of esters have been investigated, including blending with petrodiesel, winterization, additives, branched-chain esters, and bulky substituents in the chain. The latter approach may be considered a variation of the additive approach, as the corresponding compounds have been investigated in biodiesel at additive levels.

In comparison, the CP of methyl soyate is around 0^{o}C [30, 32]. However, in terms of economics, only isopropyl esters appear attractive as branched-chain esters, even though they are more expensive than methyl esters. Branching in the ester chain does not have any negative effect on the CN of these compounds, as discussed above.

Winterization [33, 34, 35] is based on the lower melting points of unsaturated fatty compounds compared to saturated compounds (Table 1.1). This method removes by filtration the solids formed during the cooling of the vegetable oil esters, leaving a mixture with a higher content of unsaturated fatty esters and thus with lower CP and PP. This procedure can be repeated to further reduce the CPs. Saturated fatty compounds, which have higher CNs (Table 1.1) than unsaturated fatty compounds, are among the major compounds removed by winterization. Thus the CN of biodiesel decreases during winterization. The loss of material is reduced when winterization is carried out in presence of cold flow improvers or solvents such as hexane and isopropanol [35].

1.1.4 Density

Density is defined as mass per unit volume of a fluid. The standard conditions adopted by the petroleum industry are 60^{o}F (15.5^{o}C) and 1 atm [36].

Fuel density is a key property that affects engine performance and pollutant emissions [23]. Because fuel injection pumps metered fuel by volume, not by mass, a greater or lesser mass of fuel is injected depending upon its density. Thus the air-fuel ratio and energy content within the combustion chamber are influenced by fuel density.

Normally, the densities of biodiesel fuels are slightly higher than those of petroleum diesel, and increasing the percentage of biodiesel blends increases the blend's density. As shown in Fig. 1.1, FAME density is strongly affected by the degree of unsaturation, with higher unsaturation leading to increased density [23].

It has been reported in this paper [23] that biodiesel density is also affected by chain length, with higher chain length leading to lower fuel density. However, this does not appear to be the case for the set of 12 biodiesel fuels investigated here, as indicated by the data plotted in Fig. 1.1.

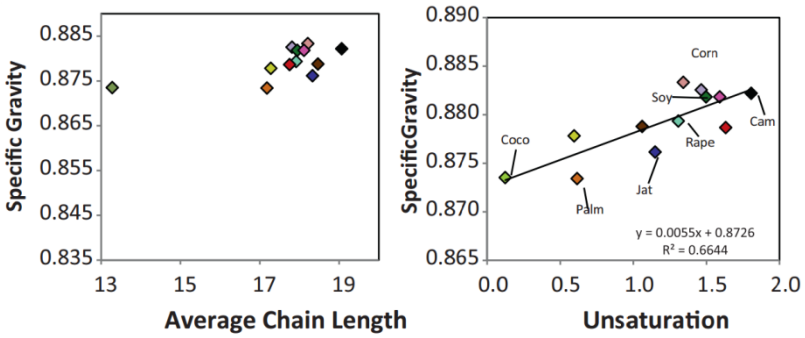

Fig. 1.1 Specific gravity, T= 15.5^{o}C [23]

1.1.5 Viscosity

Viscosity affects the atomization of a fuel upon injection into the combustion chamber and thereby, ultimately the formation of engine deposits [13]. The higher the viscosity, the greater the tendency of the fuel to cause such problems. The viscosity of a transesterified oil, i.e.,

biodiesel, is about one order of magnitude lower than that of the parent oil [5, 13]. High viscosity is the major reason why neat vegetable oils have been largely abandoned as alternative DF. Kinematic viscosity has been included in most biodiesel standards. The difference in viscosity between the parent oil and the alkyl ester derivatives can be used in monitoring biodiesel production [37]. The effect on viscosity of blending biodiesel and petrodiesel has also been investigated [38], and an equation has been derived to calculate the viscosity of such blends.

Kinematic viscosity is defined as the ratio of absolute (dynamic) viscosity μ to absolute density ρ at the same temperature. Values of kinematic viscosity are usually measured and reported at two reference temperatures, 38 ^{o}C (100 ^{o}F) and 99 ^{o}C (210^{o}F) in cSt. However, other reference temperatures of 40^{o}C (104^{o}F), 50^{o}C (122^{o}F) and 60^{o}C (140^{o}F) are also used to report kinematic viscosities of fuel [36].

The prediction of the viscosity of fatty material has received considerable attention in the literature. Viscosity values of biodiesel/mixtures of fatty esters have been predicted from the viscosity of the individual components by a logarithmic equation for dynamic viscosity [39]. Viscosity increases with chain length (number of carbon atoms) and with increasing degree of saturation. This also holds for the alcohol moiety as the viscosity of ethyl ester is slightly higher than that of methyl ester [22]. Factors such as double bond configuration influence viscosity (the cis double bond configuration gives a lower viscosity than the trans configuration), while the double bond position has less effect on viscosity [22]. Thus, a feedstock such as used cooking oil, which is more saturated and contains some amounts of trans fatty acid chains, has a higher viscosity than its parent oil. Branching in the ester moiety, however, has little or no influence on viscosity, again showing that this is a technically promising approach for improving low-temperature properties without significantly affecting other fuel properties. Values for dynamic and kinematic viscosities of neat fatty acid alkyl esters are given in Table 1.1.

1.1.6 Flash point

The flash point [5] is defined as the lowest temperature that at which a fuel gives off sufficient vapors, vapors so that when mixed that air it will ignite momentarily. The flash point for biodiesel is used as the property to limit the level of unreacted alcohol remaining in the finished fuel. The flash point is also of importance in connection with legal requirements and for the safety precautions involved in fuel handling and storage, and is normally specified to in insurance and fire regulations.

The flash point of pure biodiesel is considerably higher than the prescribed limits, but can decrease rapidly with increasing residual alcohol. As these two aspects are strictly correlated, the flash point can be used as an indicator of the presence of methanol in the biodiesel. The flash point is used as a regulation for categorizing the transport and storage of fuels, with different thresholds from region to region, so aligning the standard would possibly require a corresponding alignment of regulations [5].

1.1.7 Oxidative stability

The Oxidative stability[13] of biodiesel has been the subject of considerable research [40, 41]. This issue affects biodiesel primarily during extended storage. The influence of parameters such as the presence of air, heat, traces of metal, antioxidants, and peroxides as well as the nature of the storage container was investigated in the aforementioned studies. Generally, factors such as the presence of air, elevated temperatures, or the presence of metals facilitate oxidation. Studies performed with the automated oil stability index (OSI) method have confirmed that the catalyzing effect of the fatty esters, especially unsaturation as discussed below, was even greater [42]. Numerous other methods, including not only wet-chemical ones such as the acid value and peroxide value, but also pressurized differential scanning calorimetry, magnetic resonance (NMR), and so forth, have been applied in oxidation studies of biodiesel.

Two simple methods for assessing the quality of stored biodiesel are the acid value and viscosity since both increase continuously with increasing fuel degradation, ie., deteriorating fuel quality. The peroxide value is less suitable because it reaches a maximum and then can decrease again due to the formation of secondary oxidation products [43].

A European standard (EN 14112 ; Rancimat method) for oxidative stability has been included in the American and European biodiesel standard (ASTM D6751 and EN 14214). Both biodiesel standards call for determining oxidative stability at 110^{o}C. However, EN 14214 prescribes a minimum induction time of 6 hours by the Rancimat method while ASTM D6751 prescribes 3 hours. The Rancimat method is nearly identical to the OSI method, which is an AOCS (American Oil Chemists' Society) method.

Besides preventing exposure of the fatty material to air, adding antioxidants is a common method to address the issue of oxidative stability. Common antioxidants are synthetic materials such as tres-butylhydroquinone (TBHQ), butylated hydroxytoluene (BHT) butylated hidroxyanisole (BHA), and propyl gallate (PG) as well natural materials such as tocopherols. Antioxidants delay oxidation but do not prevent it, as oxidation will commence once the antioxidants in a material have been consumed.

1.1.8 Iodine value

In European biodiesel standards, the iodine value (IV) [13] is one of the factors for purportedly addressing the issue of oxidative stability and the propensity of the oil or fat to polymerize and form engine deposits. The IV is a measure of the total unsaturation of a fatty material measured in grams of iodine per 100 g of sample when formally adding iodine to the double bonds. An IV of 120 has been specified in EN 14214 and 130 in EN 14213 which would largely exclude vegetable oils such as soybean and sunflower oils as biodiesel feedstock. The IV has not been included in biodiesel standards in the United States and

Australia, and it is limited to 140 in the South Africa standard (which would permit the use of sunflower and soybean oils); the provisional Brazilian standard requires only that it be noted.

The IV of vegetable oil or animal fat is almost identical to that of the corresponding methyl esters. However, the IV of alkyl esters decreases with higher alcohols used in their production since the IV is molecular weight dependent. For example, the IV of methyl, ethyl, propyl, and butyl linoleate is 172.4, 164.5, 157.4, and 150.8, respectively [44].

The use of the IV of a mixture for such purposes does not take into consideration the fact that an infinite number of fatty acid profiles can yield the same IV and that different fatty acid structures can give the same IV, although the propensity for oxidation can differ significantly [44]. Other new structures, termed allylic position equivalent and bis-allylic position equivalent (APE and BAPE), which are based on the number of such positions in a fatty acid chain and are independent of molecular weight, are likely more suitable than the IV [44]. The BAPE index correctly distinguishes mixtures having nearly identical IV by their OSI times. Note that the BAPE index is the decisive index compared to the APE because it relates to the more reactive bis-allylic positions. Engine performance tests with a mixture of vegetable oils of different IVs yielded results that would have justified a low IV [27, 45]. No relationship between the IV and oxidative stability has been observed in another investigation on biodiesel with a wide range of IV [42].

1.1.9 Lubricity

With the advent of low-sulfur petroleum-based DFs, the issue of DF lubricity is becoming increasingly important [13]. Desulfurization of petrodiesel reduces or eliminates the inherent lubricity of this fuel, which is essential for the proper functioning of vital engine components such as fuel pumps and injectors. Several studies [25, 37, 39, 40] on the lubricity of biodiesel or fatty compounds have shown the beneficial effect of these materials on the lubricity of petro biodiesel, particularly low-sulfur petrobiodiesel fuel. Adding biodiesel at a low level (1-2%) restores lubricity to low-sulfur petroleum-derived DFs. However, the lubricity-enhancing effect of biodiesel at low blend levels is mainly caused by minor components of biodiesel such as free fatty acids and monoacylglycerols [28], which have free COOH and OH groups. Other studies [46, 47] also point out the beneficial effect of minor components on biodiesel lubricity, but these studies do not fully agree on which species are responsible [28, 47]. Thus biodiesel is required at 1-2% levels in low-lubricity petrodiesel, in order for the minor components to be effective lubricity enhancers [28]. At higher blend levels, such as 5% the esters are sufficiently effective without the presence of minor components.

While the length of the fatty acid chain does not significantly affect lubricity, unsaturation enhances lubricity slightly; thus an ester such as methyl linolenate improves lubricity more than methyl stearate [24, 28]. In accordance with the above observation on the effect of free OH groups on lubricity, castor oil displays better lubricity than other vegetable oil esters [24, 48, 49]. Ethyl esters have improved lubricity compared to methyl esters [49].

1.2 Injection rate analysis

The main characteristic of an injector is the evolution of the flow in the injector. This depends on cavitation phenomena and the injector discharge coefficient. The analysis of the injection rate therefore makes it possible to determine the sound velocity and the presence of cavitation phenomena, and to calculate the discharge coefficient. The following sections report the main results and methods of analysis of various authors concerning the study and comparison of the injection of different biodiesel fuels.

Desantes et al. [50] conducted an experimental study of biodiesel blends' effects on diesel injection, using a solenoid coil injector. Several experiments were carried out on a commercial diesel fuel with 5.75% of rape methyl ester called B5, another with 30% of the same vegetable oil called B30, and a pure rape methyl ester fuel (called RME). Analyses on the injection rate shape in non-evaporative conditions were performed and studied to compare the effect of these different fuels on the injection process. The results are shown in Fig. 1.2 and 1.3.

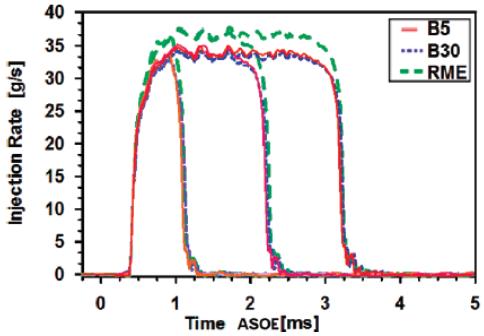

Fig. 1.2 Mass flow rate at 1600 bar (BP = 50 bar, ET = 500, 1000, and 2000 µs) [50].

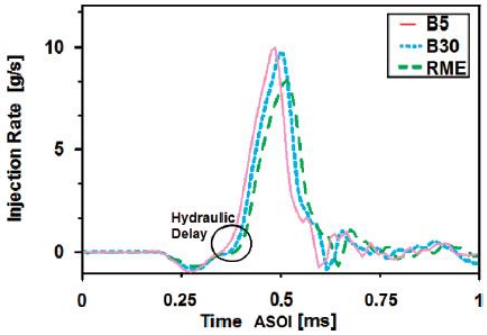

Fig. 1.3 Injection rate at 300 bar, BP = 50 bar [50].

Fig. 1.2 shows that the pure biodiesel fuel (RME) has a higher injection rate than the other two. The difference appears at the top part of the curves, when the needle is fully open. The differences between B5 and B30 are less clear, however, on this graph, as no particular tendency can be observed.

The results shown in Fig. 1.3 clearly show that RME has a slower opening and slower closing than the other fuels. First, at the beginning of the curves, a time difference can be seen; this means that the hydraulic delay is not the same with the three fluids. The difference does not only concern the injector opening delay but also the slope of the injection rate during needle lift. The RME injection rate curve is not as steep as those of B5 and B30, which have highly similar shapes.

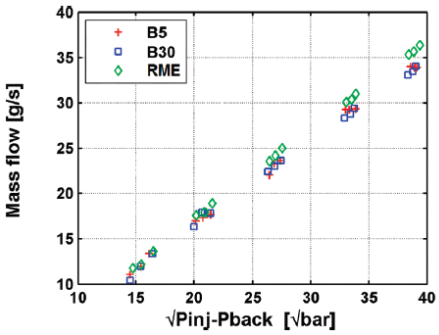

Fig. 1.4 Mass flow rate vs square root of the pressure drop [50].

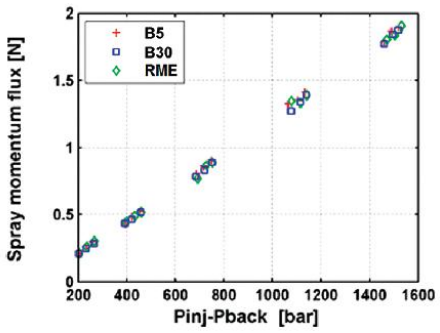

Fig. 1.5 Stabilized spray momentum vs Pressure drop [50].

Fig. 1.4 shows the maximum mass flow rate according to the square root of the pressure difference between injection pressure and back pressure. Experimental results are displayed as five groups of three points. A single group of points represents a characteristic injection pressure and each point in a group corresponds to a different back pressure (20, 50, and 80 bar). These tests were done to determine the stabilized part of the injection; it is a better way to analyze the results in stationary conditions. Only the top part of the longer injection is taken into account to plot these curves. As seen before, the mass flow rate in stabilized conditions is higher with RME; this graph further shows that when the rail pressure increases, the difference also increases.

Fig. 1.5 shows the results of spray momentum for the stationary condition. As for the injection rate, only the stabilized part of the signal was taken into account to plot this graph. There are no significant differences in spray momentum with the fluids tested, even when the injection pressure is changed.

Plamondon et al. [51] developed a simplified dynamic model for a piezoelectric injector using multiple injection strategies with biodiesel/diesel-fuel blends. The injector used in their study was a Bosch CRI 3.3 piezoelectric indirect injector with a micro-sac type nozzle designed to work at pressures up to 2000 bar. The fuels used were pure diesel, biodiesel (colza methyl ester), and a 50% biodiesel blend (B0, B100, and B50, respectively). Injection pressure varied from 700 bar to 1300 bar. The results are shown in Fig. 1.6, 1.7, and 1.8.

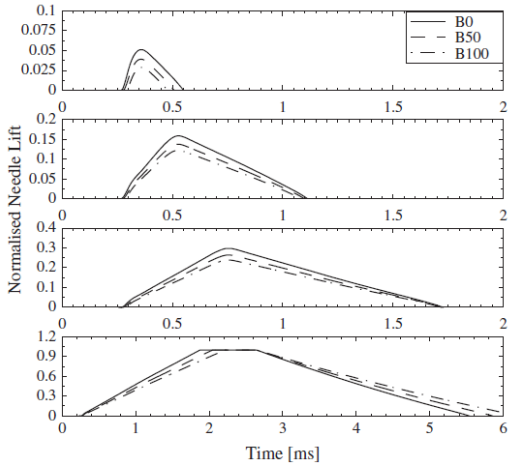

Fig. 1.6 Needle lift for different experimental
Case at *Pi* = 900 bar [51]

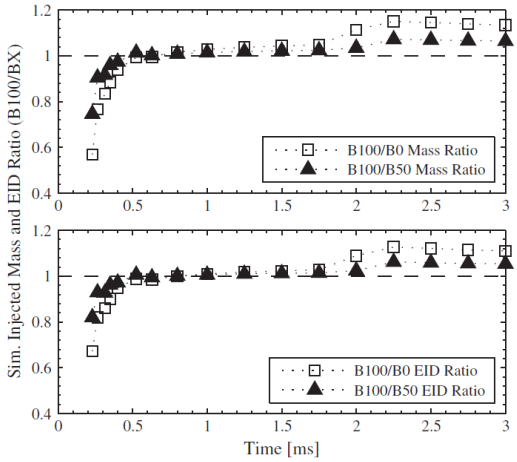

Fig. 1.7 Mass and EID ratio of B100 over B0 and B50 for simulated results at *Pi* = 900 bar [51]

Increased viscosity slowed the needle velocity during the opening and closing displacements. Fig. 1.6 shows the impact of increasing fuel viscosity, with 4 different single injection durations for B0, B50, and B100. First, the injector needle behavior depended on the energizing time and the fuel. For the observed injector configuration, when the injection was very short, the Effective Injection Duration (EID) was shorter for biodiesel and increased with decreasing biodiesel content, thereby decreasing the total mass injected. When the percent of biodiesel in the blend increased or density and viscosity increased, the mass flow rate also tended to increase. When a longer energizing time was used, the overall EID of biodiesel was much closer to that of diesel fuel. Since the opening and closing speeds of diesel are faster than those of biodiesel, the needle reached higher lift but closed slightly later. However, when the needle reached its upper seat, for an excitation time (ET) of around 2 ms the total mass injected for B100 was more than for B50 or B0 (Fig. 1.7).

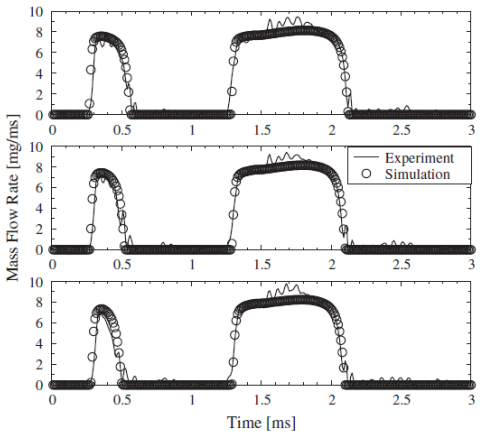

Fig. 1.8 Multiple-injection validation with from top to bottom, B0, B50, and B100 [51].

Fig. 1.8 shows that increasing the biodiesel content shortened the first injection as well as the second, albeit to a lesser extent. The effective durations of the first injection for B0, B50, and

B100 were 0.299 ms, 0.252 ms, and 0.224 ms, respectively, representing a 26% decrease in injection duration, which resulted in a 32.8% reduction in the total injected mass. This effect was less pronounced for a longer injection, as can be seen for the second injection, in which the EID for B0, B50, and B100 were, respectively, 0.842 ms, 0.816 ms, and 0.81 ms for a reduction of less than 4% in injection duration, which represents a 3.3% decrease in the total injected mass.

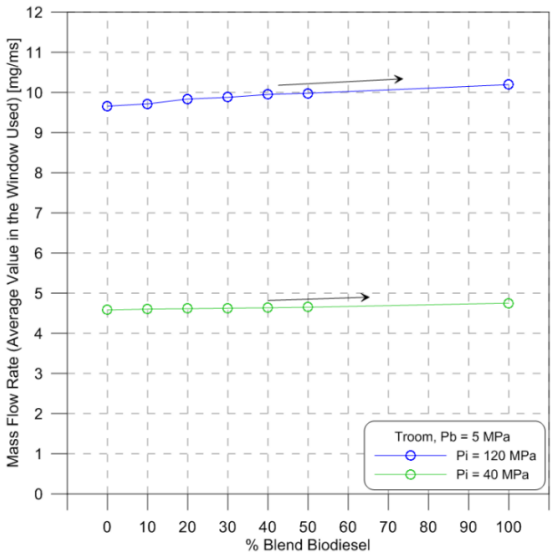

Fig. 1.9 Mean mass flow rate and percentage biodiesel blends-*Pi* = 40, 120 MPa.

Fig. 1.9 shows the mean mass flow rate plotted with the percentage of biodiesel blends. When the biodiesel fraction increases, the mean mass flow rate tends to increase. If diesel fuel is compared with B50 for instance, at *Pi* = 40 MPa the mean mass flow rate increases by 1.46%, and at *Pi* = 120 MPa it increases by 3.32%.

Vergnes et al. [52] studied discharge coefficients for a diesel injector during cold start conditions, by measuring the mass flow rate and discharge coefficient for different injection pressures and ambient cold temperature conditions. Three different fuels were chosen, namely, n-heptane, decane and arctic diesel fuel. The fuel temperatures set up for experiments were 20^{o}C to -20^{o}C. The study focused on spray behavior at the outlet section of the nozzle hole by measuring the mass flow rate and discharge coefficient for different injection pressures at ambient and cold temperature conditions. The fuel properties are shown in Table 1.3 and the results in Fig. 1.10 and 1.11.

Table 1.3: Dynamic viscosity and density of different fuels as a function of ambient temperature.

Physical parameters	**Fuel**	**20^{o}C**	**-5^{o}C**	**-10^{o}C**	**-15^{o}C**	**-20^{o}C**
Viscosity(Pa/s)	n-heptane	0.00050	0.00060	0.00070	0.00094	0.00115
	Decane	0.00098	0.00103	0.00110	0.00160	0.00180
	Arctic diesel	0.00310	0.00590	0.02300	0.12500	0.18000
Density(kg/m^3)	n-heptane	684	708	713	718	723
	Decane	730	749	752	756	760
	Arctic diesel	833	856	859	865	870

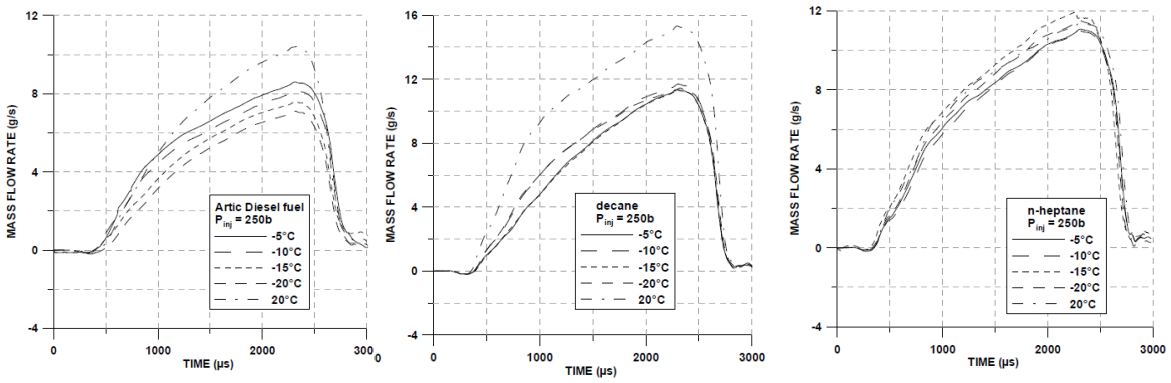

(a) (b) (c)

Fig. 1.10 Evolution of the mass flow rate for the three fuels [52].

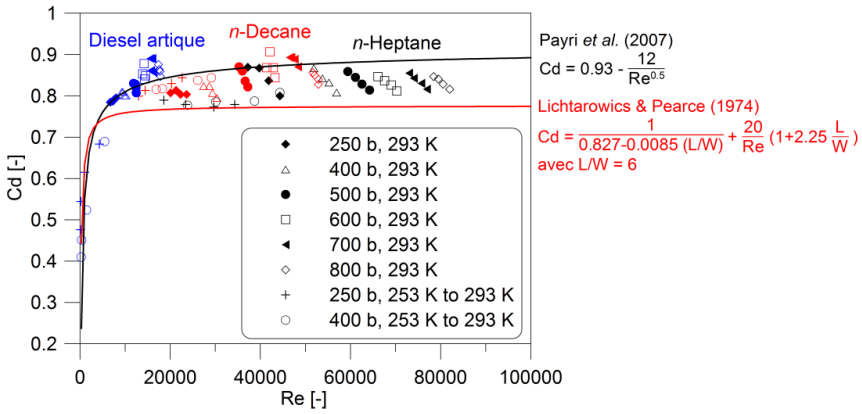

Fig. 1.11 Discharge coefficient versus Reynolds number for all temperature conditions for the three fuels [52].

In Fig. 1.10, it can be observed that no effect of the ambient temperature value is obtained with using n-heptane as fuel. However, for decane and more particularly for arctic fuel it can be seen that the mass flow rate decreases with lower temperature. This is mainly due to the strong increase in the viscosity in comparison to the fuel density change.

For decane and arctic diesel fuel, there is a cavitation phenomenon which can explain the decrease in *Cd* when the Reynolds number increases (Fig. 1.11) The relationship, suggested by Lichtarowicz and Pearce [53], between *Cd*, *Re*, and the geometrical characteristic of the hole, *L/W*, is also indicated on Fig. 1.11. Its expression is:

$$\frac{1}{Cd} = \frac{1}{0.827-0.0085(\frac{L}{W})} + \frac{20}{Re}\left(1 + 2.25\,\frac{L}{W}\right) \qquad (1\text{-}1)$$

for L/W between 2 and 10 and a Reynolds number below 20,000. A relatively good agreement is obtained whatever the injection conditions. According to the following relationship, suggested by Payri et al.[54], also indicated on Fig.11, the best fit curve to their experimental data for decane fuels is found for values of *F*, *G*, and α respectively equal to 0.93, 12 and 0.5.

$$Cd = F - \frac{G}{Re^{\alpha}} \tag{1-2}$$

They concluded that the effect of the temperature on the discharge coefficient values can be neither observed nor quantified. One can note also that the viscosity is only multiplied by 2 when the ambient temperature drops from 20 to -20°C; therefore, few differences are observed in the fuel mass flow rate between normal and cold temperatures, no doubt due to the variations in fuel density. Mass flow rates presented considerable differences between cold and ambient temperatures for the arctic diesel fuel, a few differences for decane, and no difference for n-heptane fuel. The discharge coefficient decreased strongly with an increase in viscosity, inducing a different spray development. Moreover, the needle lift is also affected by the change in viscosity.

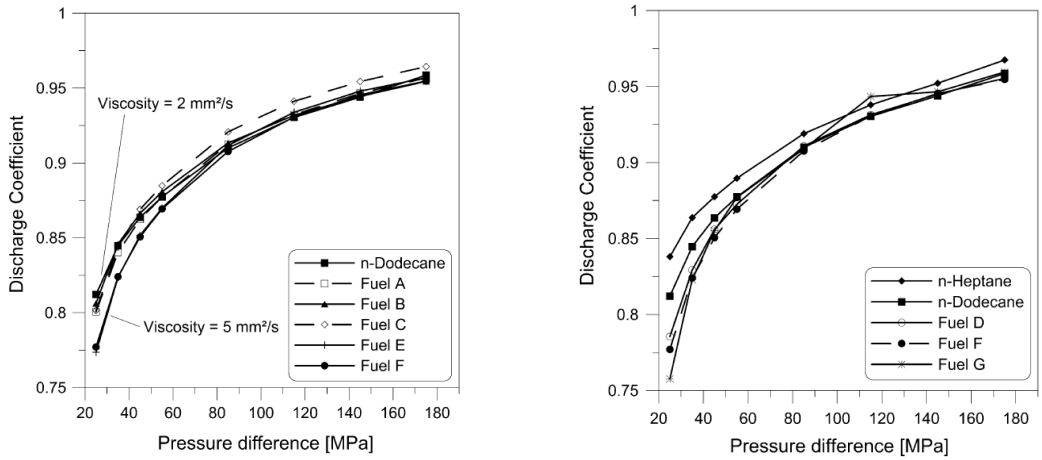

(a) (b)

Fig. 1.12 Impact of fuel viscosity on the discharge coefficient – *Pi* = 30–180 MPa, *Pb* = 5 MPa [55].

Dernotte et al. [55], conducted an experimental investigation into the influence of fuel density and fuel viscosity on the flow characteristics generated by a high pressure diesel injector, equipped with conical orifices. For this purpose, mass flow rate measurements were performed with nine different fuels. Fuel viscosities were varied from 0.6 to 7 mm^2/s and fuel densities from 683 to 876 kg/m^3 at the operating temperature. The results are shown in Fig. 1.12.

Fig. 1.12 (a) indicates that fuels with similar viscosity values fall on the same curve. This means that there is no significant effect of fuel density on the discharge coefficient for the two viscosity levels. Fig. 1.12 (b) shows the effect of fuel viscosity on the discharge coefficient, for n-Heptane, n-Dodecane, and fuels ‘‘D’’, ‘‘F’’ and ‘‘G’’. For these fuels, viscosity varies from 0.6 to 7 mm^2/s. As shown in Fig. 12(b), fuel density does not affect the discharge coefficient; the observed differences were therefore attributed to the influence of viscosity.

Dernotte et al. [55] proposed a new correlation in order to consider the influence of fuel viscosity on the discharge coefficient. This correlation was based on the one defined by Payri et al. [10], which takes into account the orifice geometry. The outlet diameter and the conicity, *AR*, were replaced by their variables. This new correlation is expressed as:

$$Cd = Cd' + K1.v^a.\Delta P^b - \frac{K2.v^c.\Delta P^d}{Re^e} \quad (1\text{-}3)$$

The coefficient values, obtained by minimizing the sum of square errors between the correlation and the experimental data, were: *Cd*' = -5.26, *K*1 = -5.26, *K*2 = -400, *a* = -0.06, *b* = -0.73, *c* = -0.74, *d* = 0.51, *e* = 0.54. The correlation is plotted in Fig. 13 with all the experimental data. In the X-coordinate, the Reynolds number is corrected by multiplying its theoretical value by the discharge coefficient in order to take into account the flow losses on the flow velocity. All the curves represent the function obtained with this new correlation.

$$Re = \frac{D_O.V_{Bernoulli}}{v(1\text{atm})} \quad (1\text{-}4)$$

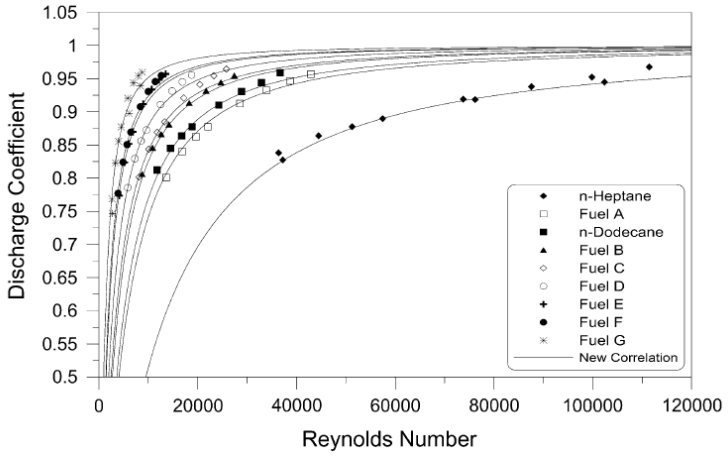

Fig. 1.13 Discharge coefficient versus Reynolds number, *Pi* = 30 to180 MPa, *Pb* = 5 MPa [55].

The study by Dernotte et al. [55] showed that fuel viscosity affects the discharge coefficient for a range of pressure difference between 25 and 55 MPa. For higher pressure differences up to 180 MPa, no significant impact of fuel viscosity was observed. For a given pressure difference from 25 to 55 MPa, when the fuel viscosity is decreased from 7 to 0.6 mm^2/s, the discharge coefficient seems to reach a maximum limit value when the Reynolds number rises to infinity. For higher pressure differences up to 180 MPa, this limit value is constant because fuel viscosity does not impact the discharge coefficient. The fuel density does not have a significant influence on the discharge coefficient. The fact that density variations do not significantly modify the Reynolds number compared to viscosity variations might explain why fuel density does not impact the discharge coefficient. The mass flow rate is proportional to the square root of fuel density. The authors therefore suggested that below 55 MPa, fuel viscosity should be considered. Their new correlation, taking into account the

effect of fuel viscosity and the flow conditions (i.e. the pressure difference and the Reynolds number), was defined for a nozzle operating in turbulent and non-cavitating flow.

In conclusion, Desantes et al. [50] used 3 fuels (B5, B30, RME) to study differences in density and viscosity. Their results showed that the injection rate and mass flow of RME are higher than those of the other two fuels. The injection delay and closing delay of RME are longer than those of the other fuels. In comparison, according to the work of Plamondon et al. [51], the delay in needle lift increases when the percentage of biodiesel increases. This effect on closing delay was observed by Plamondon with a piezoelectric injector only for long ET. Vergnes et al. [52] used 3 fuels (n-heptane, decane and arctic diesel fuel), in cold temperatures. When the temperature decreased, density and viscosity increased. Similarly, the injection rate increased. Their results on the discharge coefficient *Cd* showed that with decane the temperature does not affect the *Cd* but for n-heptane and arctic diesel fuel, the *Cd* strongly decreases when temperature decreases or density and viscosity increase. Dernotte et al. [54] studied 7 fuels with different densities and viscosities. Their results showed that fuel density has no effect on *Cd* but that fuel viscosity affects *Cd* at low injection pressures.

1.3 Spray tip penetration and spray angle

The spray tip penetration or penetration length or spray penetration is the length to which the spray penetrates across the combustion chamber [12]. Spray penetration, *S*, is defined as the distance between the exit hole of the injector and the spray end (see Figure 1.14). The value is dependent on time. Spray penetration has been studied for a long time, one of the earliest studies being that of Miller and Beardsley [56]. Their experiment consisted in injecting a liquid (oil) into a pressurized chamber. The two variables were the injection pressure and the pressure of the ambient gas. It was found that when increasing the injection pressure, the spray penetration increased and, when increasing the pressure of the ambient gas, the spray penetration decreased.

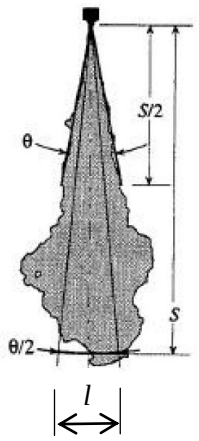

Fig. 1.14 The characteristics of spray studied [57].

The atomization of the liquid (fuel) in the ambient gas (air) at the output of the injector hole generally leads to a conical shape. For reasons of simplicity, they defined the angle of spray,

θ, as the angle of the cone (see Fig. 1.14). The spray angle depends on the density ratio, $\frac{\rho_f}{\rho_a}$. Liquid has more trouble penetrating a gas having a high density. This is due to aerodynamic forces which greatly slow down the droplets at the injector outlet. The problem is that they are driven by the continuous flow of liquid out of the nozzle, which tends to push the droplets already present to the sides and thus to increase the angle of the cone.

In order to better understand the spray penetration of diesel, biodiesel and biodiesel blends, it is necessary to first review the various spray penetration models reported in the literature. We will point out the parameters taken into account to model the spray length (density, viscosity, etc.).

1.3.1 Model of Naber & Siebers

Naber & Siebers [57] developed a penetration correlation involving two steps: (1) derivation of a relationship for the spray tip velocity, and (2) integration of the velocity relationship to obtain a correlation for tip penetration time versus penetration distance. Fig. 1.15 shows a schematic of the conceptual spray model used in the analysis to develop the spray tip velocity relationship. The "model" spray is defined as one with a uniform velocity profile at any x-location that has the same mass and momentum fluxes as the equivalent “real” spray at the same x-location. As illustrated in Fig. 1.15, the model plots a perfect cone in which the fuel mixture is assumed to be homogeneous. It should be recalled that the spray pattern includes the following assumptions:

- A uniform velocity profile.
- A constant injection velocity with an instantaneous start.
- No velocity slip between the fuel and the entrained air.
- Quasi-steady flow with a uniform growth rate.

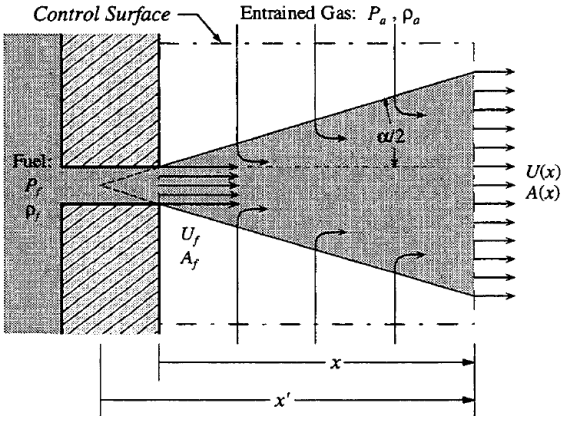

Fig. 1.15 Schematic description of the model jet Naber & Siebers [57].

This model is described by the set of equations Eq. 1-5 to Eq. 1-9, where *S* is the penetration length of the spray, $\tilde{S}$ and $\tilde{t}$ respectively are dimensionless penetration and dimensionless time with. Note that in our case, the effective diameter of output used is the geometric diameter. This model was then improved by Musculus & Kattke [58] to highlight the waves

of air entrained in diesel jets. However, these improvements result in greater complexity which is not necessary to understand the results of the present study.

$$S = \tilde{S}.x^{+} \tag{1-5}$$

$$\tilde{S} = \left[\left(\frac{1}{\tilde{t}}\right)^{n} + \left(\frac{1}{\tilde{t}^{0.5}}\right)^{n}\right]^{\frac{-1}{n}} = \frac{\tilde{t}}{\left(1+\tilde{t}^{n/2}\right)^{1/n}} \quad (n = 2.2) \tag{1-6}$$

$$\tilde{t} = \frac{t}{t^{+}} \tag{1-7}$$

Where $x^{+}$and t^{+} are respectively the length scales and the time scales. They are defined in the following:

$$x^{+} = \frac{D_o.\left(\frac{\rho_f}{\rho_a}\right)^{0.5}}{a.tan\left(\frac{\theta}{2}\right)} \tag{1-8}$$

$$t^{+} = \frac{D_o.\left(\frac{\rho_f}{\rho_a}\right)^{0.5}}{a.tan\left(\frac{\theta}{2}\right).V_{ef}} \tag{1-9}$$

These can be compared to Eq. (1-6), applied to an ideal spray (cone-like shape), which is used in order to explain the observed trends. This model has already proven its ability to take into account the effect of the operating conditions (P_i, ρ_a, T_a) and the nozzle parameters (D_o, L/D) if the implemented quasi-steady spray spreading angle θ is correct and the constant a is adjusted. Its response for different fuels is validated in the study by Dernotte et al [8].

$$S = C_v\sqrt{\frac{2\Delta P}{\rho_f}}.\frac{1}{\left[1+\left(\left(\frac{a.C_v}{C_a.D_o}\right)\left(\frac{\tan\left(\frac{\theta}{2}\right)\sqrt{2\Delta P.\rho_a}}{\rho_f}\right)t\right)^{1.1}\right]^{1/2.2}}.t \tag{1-10}$$

And the spray angle;

$$tan\left(\frac{\theta}{2}\right) = 0.40\left(\frac{\rho_a}{\rho_f}\right)^{0.19} \tag{1-11}$$

Siebers [59] proposed a spray angle estimated by taking into account the density variations. It depends only on the ratio of the liquid and gas densities as well as a constant:

$$tan\theta = 0.260.\left[\left(\frac{\rho_a}{\rho_f}\right)^{0.19} - 0.0043\left(\frac{\rho_f}{\rho_a}\right)^{0.5}\right] \tag{1-12}$$

1.3.2 Model of Hiroyasu & Arai

Hiroyasu and Arai [60] proposed equations (1-13) and (1-14), which are derived from results in their previous investigations published in (Hiroyasu et al. [61]). They are based on Levich's jet disintegration theory [62].

$$0 < t < t_b; \quad S = 0.39\left(\frac{2\Delta P}{\rho_f}\right)^{0.5}.t \tag{1-13}$$

$$t > t_b; \quad S = 2.95\left(\frac{\Delta P}{\rho_a}\right)^{0.25}.(D.t)^{0.5} \tag{1-14}$$

And the spray angle:

$$\theta = 83.5\left(\frac{L}{D}\right)^{-0.22}.\left(\frac{D}{D_s}\right).\left(\frac{\rho_a}{\rho_f}\right)^{0.26} \tag{1-15}$$

The spray penetration follows two different developments in the break-up time, t_b. The first proportional change takes place at time t and the second at the square root. The passage from one to the other is called the break-up time, t_b.

1.3.3 Models of Desantes et al. and Payri et al.

The models developed by Desantes et al. [63] and Payri et al.[64] to characterize spray penetration are similar to that proposed by Naber and Siebers [57], but with slight modifications. These two models distinguish between two regions of different behavior: initial to transient time (t_r), the first characterized by a linear penetration behavior with time $S \propto t$, while the second is a region of fully developed spray where the penetration behaves proportional to the square root of time $S \propto \sqrt{t}$:

-If $0 < t < t_r$; $$S(t) = C_v.\sqrt{\frac{2\Delta P}{\rho_f}}.t \tag{1-16}$$

-If $t \geq t_r$; $$S(t) = 1.26.M^{\frac{1}{4}}.\rho_a^{-1/4}.t^{1/2}.(\tan\frac{\theta}{2})^{1/2} \tag{1-17}$$

When $$M = C_a.C_v^2.2.A_o.\Delta P \tag{1-18}$$

The results correlate the spray angle with the parameters identified as influential:

- Gas density, represented by the ratio of densities between the gas and fuel ρ_a/ρ_f.
- Turbulence intensity. The parameter that best characterizes the turbulence intensity is the area contraction coefficient C_a, which has values close to unity for fully developed turbulence, and decreases as turbulence decreases.
- Nozzle geometry. In this case the only difference between nozzles is the nozzle diameter or its dimensionless equivalent parameter, the length to diameter relation *L/D*.

Thus, the spray angle expressed in terms of the tangent of the half angle is:

$$tan\left(\frac{\theta}{2}\right) = 0.8113.\left(\frac{\rho_a}{\rho_f}\right)^{0.3316}.C_a^{7.319}.\left(\frac{L}{D}\right)^{-0.1872} \tag{1-19}$$

1.3.4 Model of Sazhin et al.

Sazhin et al. [65] analyzed the influence of an air jet on spray dynamics in the area beyond the vicinity of the nozzle. The dynamics of both droplets and entrained air can be described in terms of a two-phase flow with a zero relative velocity between air and droplets. The basic properties of this flow can be derived from the conservation of mass and momentum. Spray penetration is calculated as follows:

$$S = \frac{\sqrt{v_{in}.D_o.t}}{(1-\propto_d)^{1/4}.\rho_a{}^{1/4}.\sqrt{tan\frac{\theta}{2}}} \quad (1\text{-}20)$$

Where $v_{in} = Cd.\sqrt{2\Delta P/\rho_f}$, θ is the spray angle and $\propto_d$ is the volume fraction of droplets in the spray.

1.3.5 Conclusion of the models of spray penetration and spray angle

The conclusions of this review of models of spray penetration and spray angle are summarized in Table 1.4.

Table 1.4: Spray penetration and spray angle models.

Model	Spray penetration	Spray angle
Naber & Siebers [57]	$S = C_v\sqrt{\frac{2\Delta P}{\rho_f}}.\frac{1}{\left[1+\left(\left(\frac{a.C_v}{C_a.D_o}\right)\left(\frac{\tan\left(\frac{\theta}{2}\right)\sqrt{2\Delta P.\rho_a}}{\rho_f}\right)t\right)^{1.1}\right]^{1/2.2}}.t$	$tan\left(\frac{\theta}{2}\right) = 0.40\left(\frac{\rho_a}{\rho_f}\right)^{0.19}$ $tan\theta = 0.260.\left[\left(\frac{\rho_a}{\rho_f}\right)^{0.19} - 0.0043\left(\frac{\rho_f}{\rho_a}\right)^{0.5}\right]$ Siebers [59]
Hiroyasu and Arai [60]	$0 < t < t_b;\quad S(t) = 0.39\left(\frac{2\Delta P}{\rho_f}\right)^{0.5}.t$ $t \geq t_b;\quad S = 2.95.\left(\frac{\Delta P}{\rho_g}\right)^{0.25}.(D.t)^{0.5}$	$\theta = 83.5\left(\frac{L}{D}\right)^{-0.22}.\left(\frac{D}{D_s}\right).\left(\frac{\rho_a}{\rho_f}\right)^{0.26}$
Desantes et al. and Payri et al. [63, 64]	$0 < t < t_r;\quad S(t) = C_v.\sqrt{\frac{2\Delta P}{\rho_f}}.t$ $t \geq t_r;\quad S(t) = 1.26.M^{\frac{1}{4}}.\rho_a^{-1/4}.t^{1/2}.(\tan\frac{\theta}{2})^{1/2}$ When; $M = C_a.C_v^2.2.A_o.\Delta P$	$tan\left(\frac{\theta}{2}\right) = 0.8113.\left(\frac{\rho_a}{\rho_f}\right)^{0.3316}.C_a^{7.319}.\left(\frac{L}{D}\right)^{-0.1872}$
Sazhin et al. [65]	$S = \frac{\sqrt{v_{in}.D_o.t}}{(1-\propto_d)^{1/4}.\rho_a{}^{1/4}.\sqrt{\tan\left(\frac{\theta}{2}\right)}}$ When; $v_{in} = C_d.\sqrt{2\Delta P/\rho_f}$	
Arregle et al. [66]	$S = D^{0.307}.P_{inj}^{0.262}.\rho_a{}^{-0.406}.t^{0.508}$	$tan\left(\frac{\theta}{2}\right) = D^{0.508}.P_{inj}^{0.00943}.\rho_a^{0.335}$

The Naber & Siebers model of spray penetration and spray angle will be used in the analysis and compared with experimental results on the room temperature and cold temperatures in the following chapter.

1.4 Conclusions

Before using biodiesel, we need to understand biodiesel fuel properties at room temperature and cold temperature. At cold temperatures, no information is available in the literature. The present chapter has examined:

- Biodiesel properties
- Injection rate analysis
- Spray tip penetration and spray angle models

Chapter 2 will report the experimental setup and processing used to analyze fuel properties in the present study. Physical properties at room temperature are reported in chapter 3 and at cold temperature in chapter 4. The physical properties of fuel and injector involve the measurement of:

- Density
- Viscosity
- Sound velocity
- Injection rate
- Discharge coefficient
- Spray tip penetration
- Spray angle

❖ Conclusions (version français)

Avant d'utiliser différents carburants et entre autre le biodiesel, nous devons connaître leurs propriétés physique pour différentes températures. A basse température (inférieur à 0°C), aucune information n'est disponible dans la littérature concernant le biodiesel. Le présent chapitre a examiné:

- les propriétés du biodiesel
- l' analyse des taux d'injection
- les modèles d'angle et de pénétration du spray

CHAPTER 2

Experimental setup, processing and fuel properties

The fuel injection rate was analyzed according to the Bosch method with an IAV$^{@}$ Injection Rate system. Visualization of the spray was based on Dernotte et al. using a high speed camera. The fuel density and viscosity were analyzed by an Anton Paar$^{@}$ Stabinger Viscosimeter. This chapter reports on:

- The measurement of the injection rate
- The characterization of macroscopic growth of the spray
- The method of measurement under cold conditions
- The correlation of density and viscosity
- The sound velocity of fuels

Introduction (version français)

Le taux d'introduction du carburant a été analysé selon le procédé Bosch avec un système d'injection IAV$^{@}$ de la société AVL. Le montage de visualisation du spray avec une caméra rapide et le traitement d'image associé est basé sur le travail de Dernotte et al. La densité et la viscosité du combustible ont été analysés par un viscosimètre Anton Paar$^{@}$. Ce chapitre présente:

- La mesure du débit d'injection
- La caractérisation macroscopique du développement du spray
- La méthode de mesure dans des conditions froides
- La corrélation entre la température et la densité ou la viscosité
- La vitesse du son de carburants

2.1 Operating principle of piezoelectric injector technology

Two piezo-electric injectors Bosch® type CRI 3.1 which can withstand injection pressures up to 2000 bar were used in the experiments. The first nozzle with three holes was used to study the injection rate and characterize the spray at room temperature and in cold conditions. The second nozzle has seven holes for the injection rate at room temperature.

The injectors used are of the indirect piezoelectric type. Fig. 2.1 is a sectional view of such an injector. The needle is not controlled directly by the piezoelectric elements. These elements control the opening of a valve at the entry to a control chamber full of fuel. The pressure level in this chamber controls the needle.

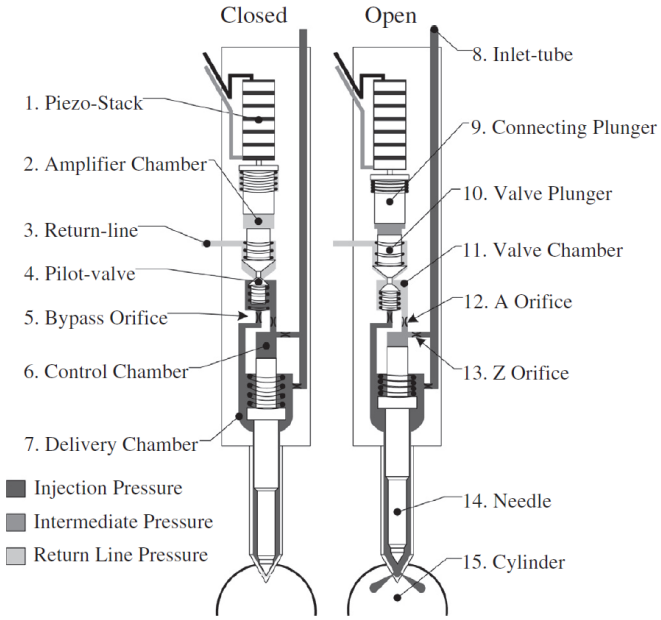

Fig. 2.1 Sectional view of a Bosch injector CRI 3.1[51].

The injector is qualified as indirect since the valve is not directly actuated by the piezostack (1) itself but by means of a hydraulic amplifier (2), as shown in Fig. 2.1. When the injector is closed, the pressure in the hydraulic amplifier chamber on the valve downstream side valve (4) and in the return-line (3) are the same, while the pressure everywhere else is equal to the injection pressure. In this condition, the valve assembly consisting of the valve itself and the valve plunger (10) is forced upward against the valve seat, thereby sealing the exit port. The needle-valve (14) is pushed against the needle seat by the pressure in the control chamber (6) and the pre-load spring, preventing any fuel leak through the nozzle holes [51].

To lift the injector needle, the piezo-stack is charged, expands, and pushes the connecting plunger (9) downward in the amplifier chamber, increasing the fuel pressure. Valve opening (4) is then possible through the hydraulic amplification caused by the surface ratio between the connecting plunger (9), the valve plunger (10), and the valve itself (4). When the pressure in the amplifier chamber (2) is sufficient to overcome the force exerted on the valve side, the valve assembly moves downward, opening the exit port and exposing the valve chamber (11) to the return-line (3) pressure. As the valve (4) reaches its maximum stroke, it closes the

bypass orifice (5), preventing fuel flow from the delivery chamber (7) into the valve chamber. Once the exit port starts opening, flow is established in the A (12) and Z orifices (13), decreasing the pressure in the control chamber (6) and allowing the needle-valve to open when the pressure forces acting on the bottom side of the needle overcome that on the top and the needle spring force. As soon as the needle starts moving upward, the micro-sac starts filling and the injection process begins. The closing process begins as soon as the piezo-stack is discharged. The connecting plunger (9) moves up, decreasing the pressure in the amplifier chamber (2) and allowing the valve assembly to return to its initial position. The bypass orifice (5) is now open and allows flow from the delivery chamber (7) through the valve chamber (11), inversing the flow in the A orifice (12) and contributing to filling the control chamber (6) with the Z orifice (13). The pressure in the control chamber starts increasing until it is sufficient to close the needle-valve, which ends the injection event [51].

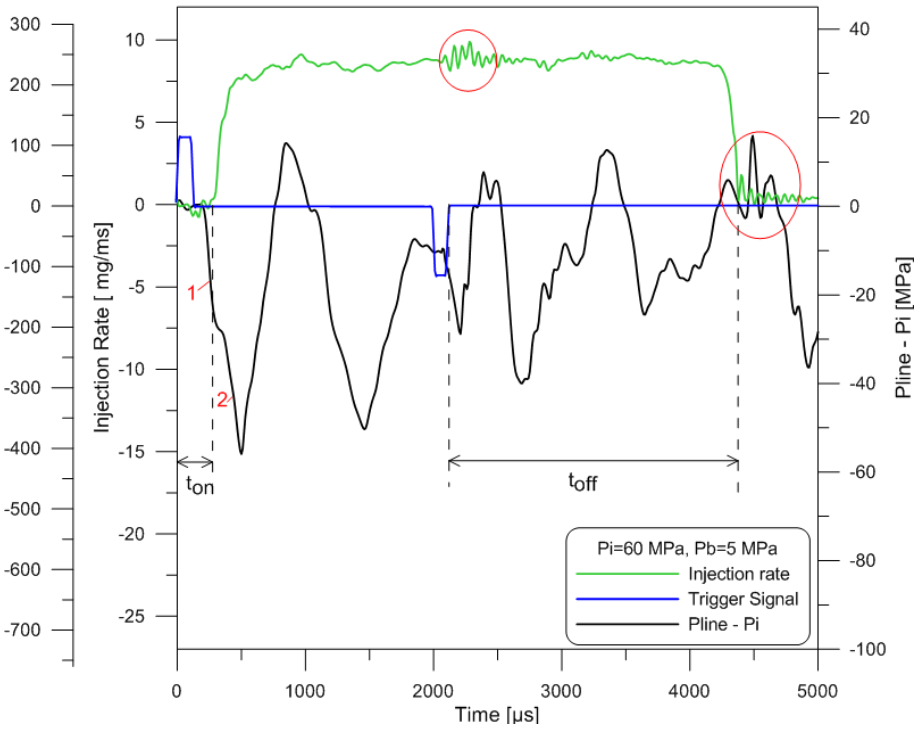

Fig. 2.2 Mean mass flow rate, Trigger signal and *Pline*, *Pi* = 60 MPa, *Pb* = 5 MPa.

This type of injector has a typical pressure evolution signature just upstream of the injector (cf. Fig 2.2). *Pi* is the initial injection pressure, *Pline* is the pressure upstream of the injection and *Pb* is the pressure in the cylinder. It is characterized by activation of the injector with a pressure drop due to the opening of the valve after x microseconds (see Fig.2.2 graph *Pline-Pi*, period 1). This opening of the valve results in a pressure imbalance which allows the needle to lift. This needle movement generates a second pressure drop (see Fig.2.2 graph *Pline-Pi*, period 2). Then the pressure wave propagates in the body of the injector. The amplitude depends on the damping and thus the viscosity of the fluid. At the close command, the valve closes and the needle goes down. The effective closure of the injector generates a hammer.

Both nozzles are of the micro-sac type with converging conical holes with rounded hydro-eroded entries (Fig. 2.3). Conical holes and hydro-eroded entries were chosen because of their ability to moderate the cavitation phenomenon, a parameter that could mask the effects of fuel properties by reducing the fluid /wall interactions (Soteriou et al. [67], Giannadakis et al. [68]). This type of injector is currenly used in diesel engines because of its lower deviation over time (longer service life, better hydraulic performance) due to less erosion of the injection holes.

The nozzle characteristics are summarized in Table 2.1. The values of the geometric holes in this table are those used for data processing, particularly for calculating the discharge coefficient. The discharge coefficient values given in the Results section are for information only because we did not have access to the exact value of the output diameter. However, the values obtained are of the same order of magnitude as the values provided by Payri et al. [10, 69] with a similar hole geometry. The injector drive by Ipod EFS® case (model 8370), and the adjustment of parameters is taken from Dernotte et al. [70].

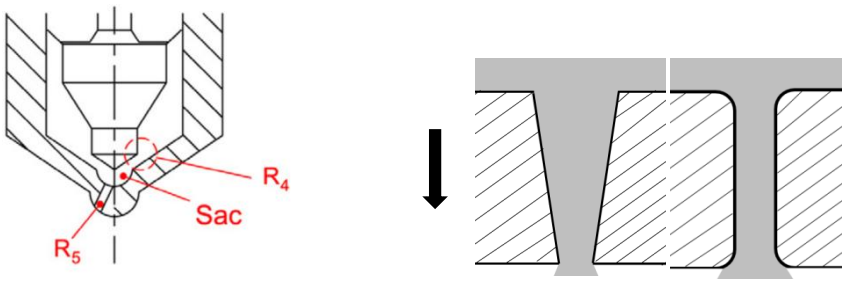

(a) (b)

Fig. 2.3 Representation of an injector sac (a) and diagram of the geometry of the converging conical holes with hydro-eroded entries (b) [70].

Table 2.1: Geometric characteristics of the nozzle three-hole and seven-hole nozzles [70].

	Nozzle 3 holes	**Nozzle 7 holes**
Diameter input	120.4 µm	157 µm
Diameter output	value used : 100 µm	143 µm
The length of the orifice, *L*	680 µm	933.3 µm
L/D	6.80	6.53
Degree of conicity (area reduction) $AR = \frac{D_i^2 - D_o^2}{D_i^2} \times 100$	outlet diameter used : 17%	17%
$k - factor = 100 \times \frac{D_i - D_o}{L}$	Given by Bosch : 3	1.5
Angle axis orifices / axis injector	78^o	78^o
Angle entrance axis orifices	120^o (3 orifices)	51.43^o (7 orifices)

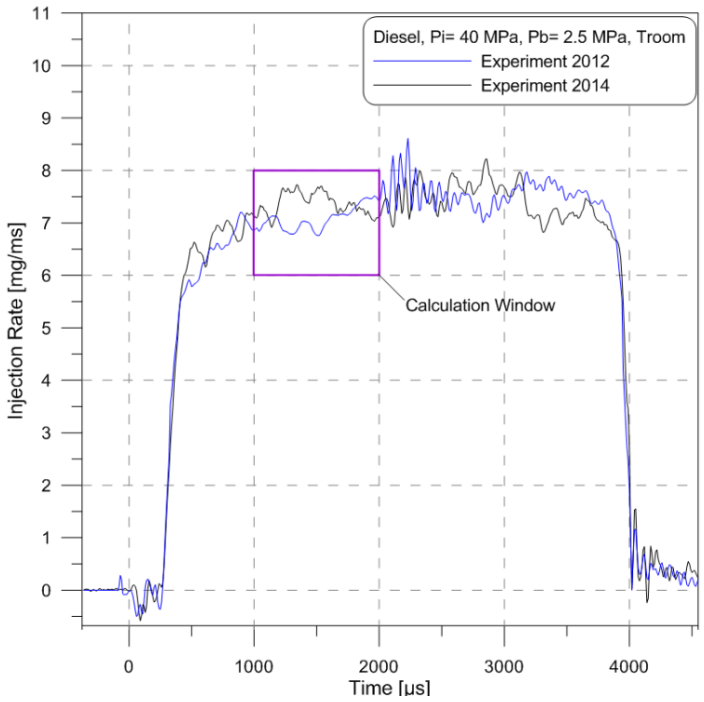

Fig. 2.4 Injection rate, comparison experiment in 2012 and 2014, Diesel, Troom, *Pi*= 40 MPa, *Pb*= 2.5 MPa.

Fig.2.4 compares the injection rate of experiment in 2012 and 2014 for Diesel for piezoelectric injector with the 3 holes nozzle. It can be observed that, the start and stop of injection are the same but the behaviors on injection period are different. The injection rates are different by 5% for calculation window and this may be caused by wearing out of the injector.

2.2 Introduction to measurement of the injection rate

The injection rate measures the fuel flow across the injector with high temporal resolution. It allows the determination of the instantaneous flow, total mass of fuel injected per shot after integration of the time signal, the opening and closing delays, and calculation of the discharge coefficient; it also provides information on cavitation. Depending on the technique, it is possible to obtain the kinetic moment of the spray and so decouple the discharge coefficient Cd, the surface coefficient Ca, and the velocity coefficient Cv: $Cd = Ca.Cv$ [10, 11, 59].

2.2.1 Dynamic pressure measurement method

Fig. 2.5 presents the block diagram of the system used to measure the injection rate by means of the "Injection Analyzer" (Version K-025-50, IAV GmbH®) [71]. The flow is measured with a temporal resolution of 10 µs, with a measurement accuracy of +/- 0.2 mg / stroke, approximately +/- 1% (if 20 mg / stroke). To adjust the counter-pressure (the pressure of the fuel injector output) from 0.5 to 18 MPa, a nitrogen cylinder is connected to compress the fuel in the unit via a piston. The generating pressure (that is to say, the injection pressure) is

created with the aid of a Maximator® pressure amplifier (model M 189 D) to achieve injection pressures up to 200 MPa. The sensor connected in the tube above the injector is a Kistler® piezoelectric pressure sensor (type 4067A3000A0) to measure the pressure fluctuations close to the entrance of the injector.

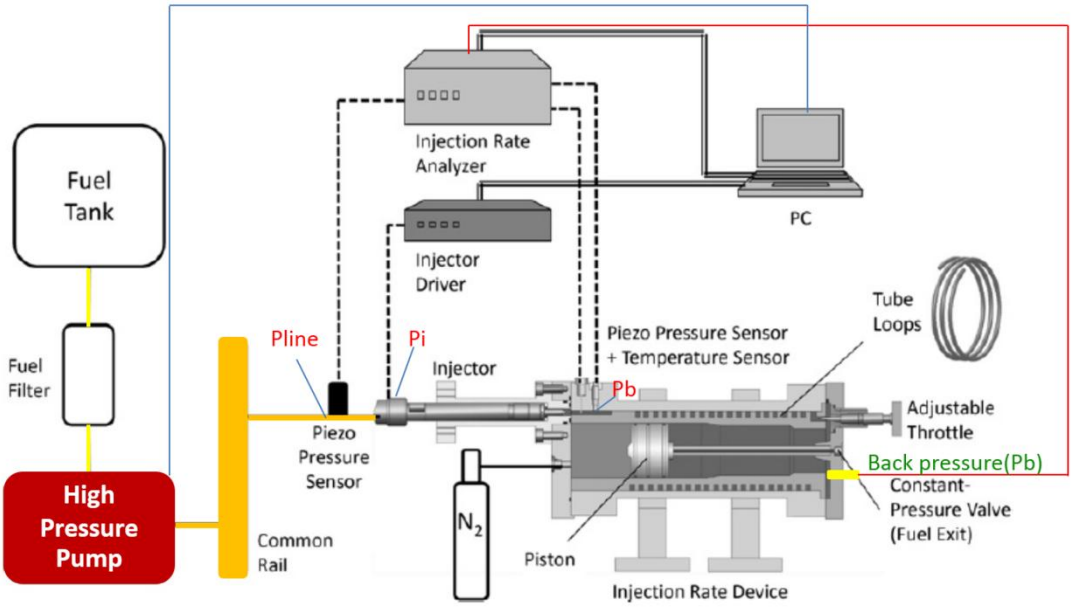

Fig. 2.5 Injection rate experimental setup (from IAV GmbH® technical specification) [71].

-*Principle of the measurement of the injection rate*

In the measurement of the injection rate based on the Bosch method [72], the principle of operation is as follows: an injector debiting in a pipe filled with fuel creates an acoustic wave that propagates in the tube (Fig. 2.6). The dynamic pressure measured with a piezoelectric pressure sensor is directly proportional to the fuel flow as shown in Eq. 2-1 (the equation is derived in Appendix I.), where ρ_f is the fuel mass flow, S_{tube} is the internal geometric section of the tube, a is the sound velocity in the fluid and $p(t)$ the dynamic pressure. The role of the serpentine tube is to lengthen the pressure wave travel time and avoid a disturbing reflection measurement. A thermocouple measures the average temperature of the fuel near the nozzle of the injector. At the end of the tube, an adjustable screw adjusts the amplitude of the reflection waves.

$$\dot{m} = \frac{S_{tube}}{a}.p(t) \qquad (2\text{-}1)$$

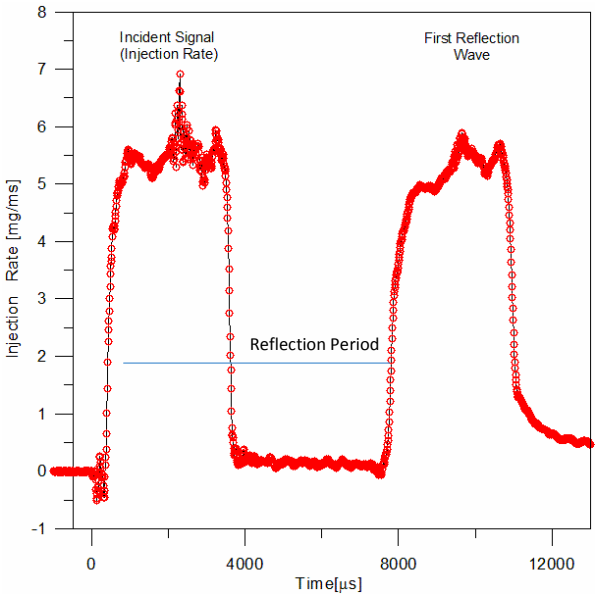

Fig. 2.6 Sound velocity measurement principle - Incident signal and first reflection.

2.2.2 Injection rate analysis

From the injection rate measurements, it is possible to obtain information on:

- the injector opening and closing times to calculate the opening and closing delays;
- the flow rate during the stabilization phase and thus the discharge coefficient;
- the flow velocity and the initial time of the spray in the orifice outlet section (with the assumption that the effective area is equal to the geometric surface area);
- the flow regime (Reynolds number);
- the impact of cavitation on the discharge coefficient.

- Detecting the instant of injector opening and closing

Detection of the instants of injector opening and closing was performed from the determination of the slopes at these two transitions (Fig. 2.7).

The abscissa at the origin corresponds to the times of opening and closing of the injector, which are not absolute values due to identifiable disturbances in Fig. 2.7. However, the gap between time and effective detection does not exceed 50 µs and represents a small proportion of the mass of fuel injected. The repeatability of the opening and of the closure is respectively +/- 10 µs and +/- 25 µs.

The opening or closing delays are the difference between the beginning or the end of the injector command and the injection rate data.

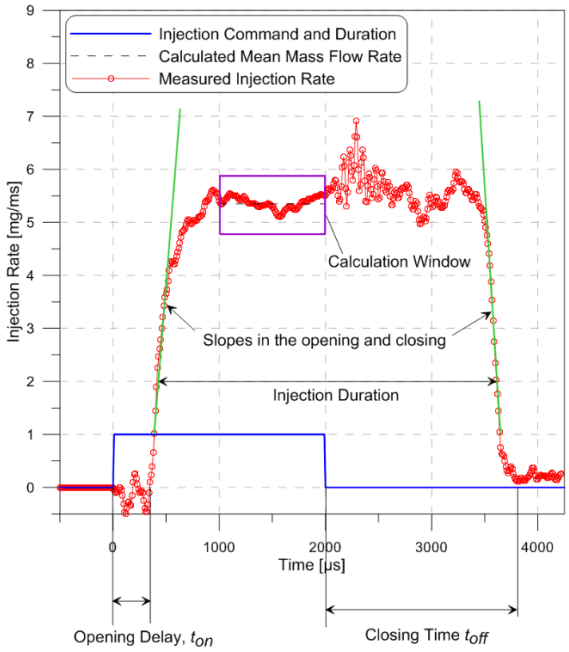

Fig. 2.7 Principle of detecting the instant of mean mass flow rate calculation window during the quasi steady state period-case of diesel fuel, *Pi* = 30 MPa, *Pb* = 5 MPa.

-Average flow during the stabilization phase and discharge coefficient

The injection rate analysis method used followed Payri et al. [10, 11] and Dernotte et al. [7]. Eq. 2-2 was used to calculate the discharge coefficient Cd by mean mass flow rate, $\dot{m}_{measured}$ from the quasi-steady state period 1000 - 2000 µs after the start of activation (SOA)(Fig. 2.7).

This period avoids the transient phenomena related to the opening and closing phases of the injector [7]. The theoretical mass flow rate (Eq.2-3) is derived from a combination of the continuity equation (Eq.2-4) and Bernoulli's equation (Eq.2-5), assuming that the inlet velocity was negligible:

$$Cd = \frac{\dot{m}_{measured}}{\dot{m}_{th}} \tag{2-2}$$

$$\dot{m}_{th} = n_{orifice} \,.\, S_c \sqrt{2\Delta P . \rho_f} \tag{2-3}$$

$$\dot{m}_{th} = n_{orifice} \,.\, \rho_f . S_c . V_{th} \tag{2-4}$$

$$V_{th} = \sqrt{\frac{2.\Delta P}{\rho_f}} \tag{2-5}$$

where $n_{orifice}$ is the number of orifices on the outlet geometric cross-sectional area of the orifice, ΔP the pressure differential (ΔP = injection pressure, *Pi* – back pressure, *Pb*), ρ_f the fuel density at the experimental temperature, and V_{th} the theoretical velocity at the fuel outlet section.

The maximum relative error on the discharge coefficient is estimated at +/- 1.5%, imputed as:

• the error in the measurement of sound velocity of +/- 0.2% (section 2)

• the error in the estimate of the density at the operating temperature of +/- > 0.8%

• an error of +/- 0.5% related to the position and size of the window used to calculate the discharge coefficient (Fig. 2.3). This was determined by changing the position and size of the calculation window by +/- 200 µs.

-Reynolds number and fuel mean velocity

The Reynolds number, *Re*, defines the fluid flow regime. It can be either laminar (*Re* < 2000), transitional (2000 < *Re* < 3000) or turbulent (*Re* > 3000) (Lefebvre [73]). The Reynolds number *Re*, is calculated by Eq. 2-6,

$$Re = \frac{V_{mean} \cdot D_O}{\nu} \tag{2-6}$$

where V_{mean} is the fuel mean velocity at the orifice exit, D_o is the geometric outlet diameter and ν is the kinematic viscosity of the fuel at the experimental temperature. V_{mean}, the fuel exit mean velocity (Eq. 2-7) can be determined by measuring the mass flow rate and using the continuity equation under the assumption that there is no cavitation. Flow losses are attributed to losses of flow velocity.

$$V_{mean} = \frac{\dot{m}_{measured}}{n_{orifice} \cdot S_c \cdot \rho_f} \tag{2-7}$$

This method of calculation of the flow velocity by considering the geometric section S_c output port requires making a hypothesis on the surface coefficient Ca (ratio of actual surface to the geometric area) since it was not was measured. However, according Payri et al. [11], there is no flow contraction caused by a possible cavitation, smaller than the outlet section (Ca = 1) for a conical orifice. We can also assume that Cd evolves in the same way whatever the fuel properties. As a result, the pressure losses will be allocated to speed losses ($Cd = Cv$).

-Calculating the initial moment of spray

The time of the spray in the output section can be written as the product of mass flow measurement by the flow velocity in the outlet section:

$$M = \dot{m}_{measured} . V_{mean} \tag{2-8}$$

Replacing $\dot{m}_{measured}$ and V_{mean} by their respective expression:

$$M = Cd^2 . n_{orifice} . S_c . 2\Delta P \tag{2-9}$$

This is the function of Cd^2, which is also called the moment coefficient C_M. In the expression above, we see that the initial moment does not depend on the density of the fuel.

- *The cavitation number*

Two definitions of the cavitation number can be encountered: one commonly called Cavitation Number, *CN* (Soteriou et al. [74], Chaves et al. [75]), whose value increases when the system approaches cavitation, the second being the reverse (Payri et al. [10], Vergnes et al. [52]). The second definition was chosen for the present study (Eq. 2-10).

$$K = \frac{P_i - P_v}{P_i - P_b} \tag{2-10}$$

It represents the ratio of pressure variables involved in the cavitation phenomenon. P_v is the saturated vapor pressure of the fuel that is neglected due to its very low value (close to zero). A variation of this term has also been proposed by other authors (Suh et al. [76]).

2.3 Macroscopic characterization of the spray in non-vaporization conditions

Characterization of the macroscopic development (far field) of the spray was accomplished by rapid shadowgraph visualization. This simple technique provides information on the temporal evolution of the overall morphology of the spray (angle and length). It is also possible to extract information on the air-fuel ratio. Conducting these experiments under non-vaporizing conditions eliminates volatility in fuel properties.

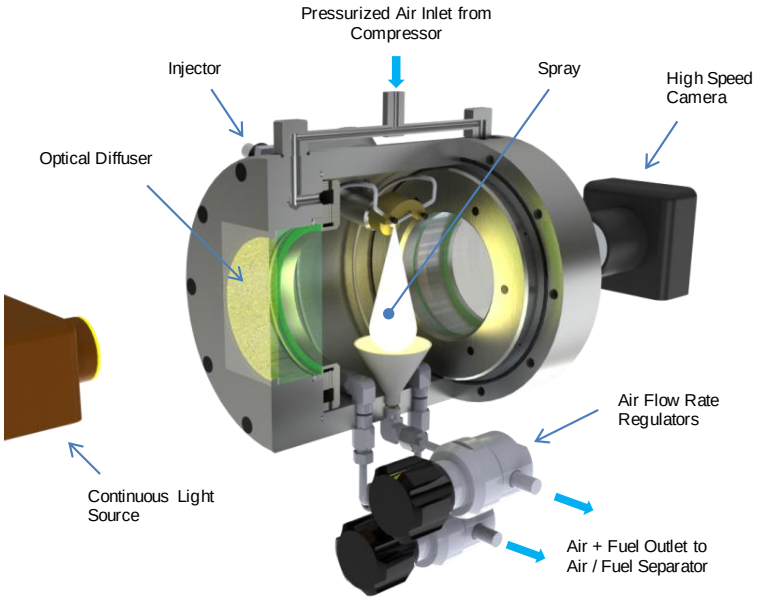

Fig. 2.8 Diagram (partial sectional view) of the experimental setup for the sprays visualization [70].

2.3.1 Method used: shadowgraph visualization

Visualization of the sprays was performed according to a shadowgraph method as shown by Fig. 2.9 based on Dernotte et al. [8]. The vessel has an internal volume of 2.5 dm^3. Optical access is provided by two 100 mm diameter windows located on either side of the vessel. The fuel injector is located on the top side of the vessel with one spray out of three, the one under

study, oriented to the bottom of the vessel on its vertical axis. The vessel is pressurized with air at room temperature coming from a 0 – 2.5 MPa air tank pressurized by an air compressor. Therefore, it is possible to reproduce engine gas density at the injection phasing (respectively from 11.8 to 29.4 kg/m^3).

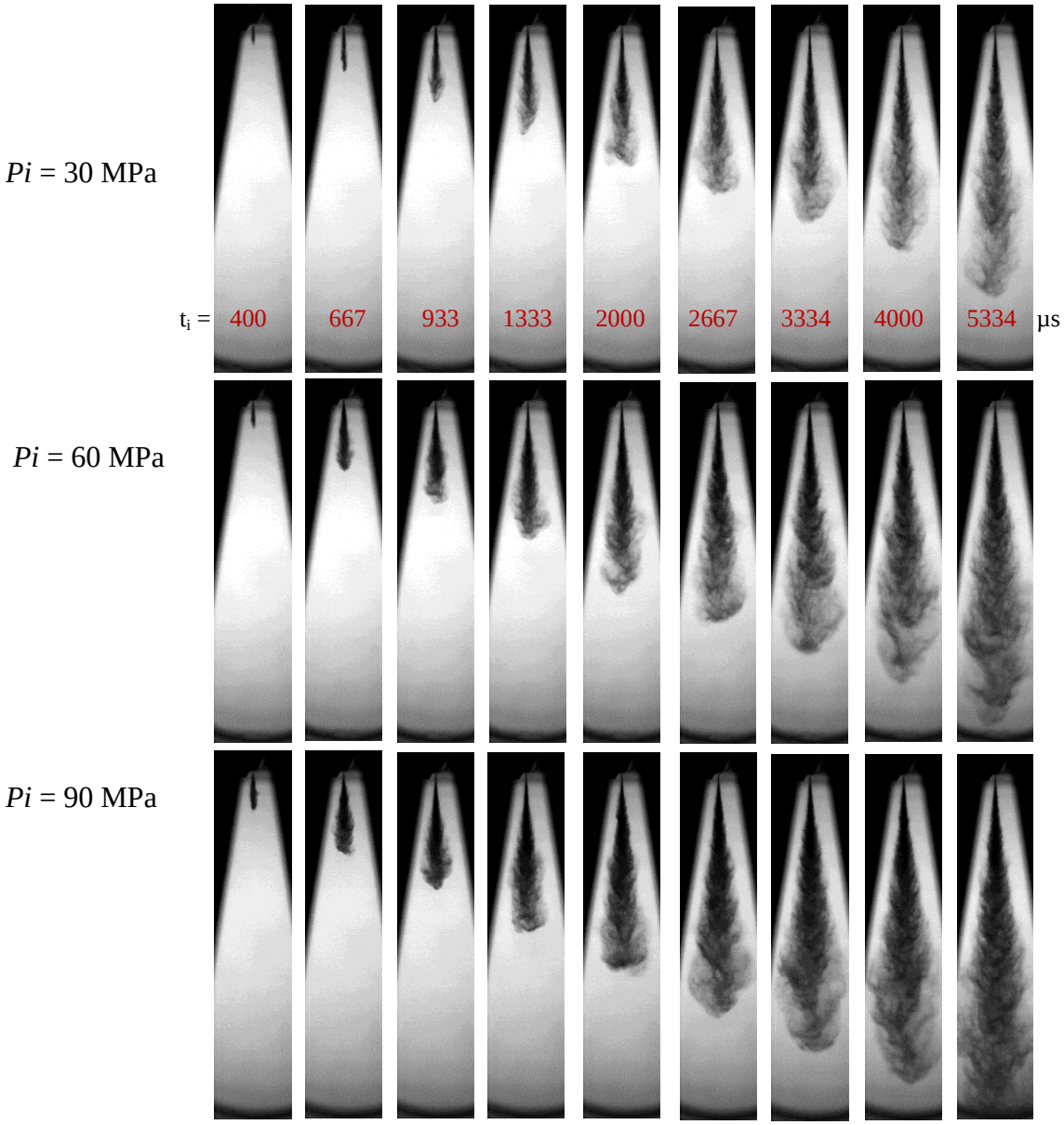

Fig. 2.9 Example of spray development – diesel fuel- *Pi*=30, 60, 90 MPa, *Pb* = 2.5 MPa.

To reduce window fouling, a continuous low air flow rate was created through the vessel without affecting the spray development process. Pressure and temperature sensors are also mounted on the vessel. To monitor the spray development, high-speed imaging diagnostics were used, with a continuous 150 W halogen lamp and an 8 bit (256 grey levels) high speed camera (Photron® PowerView™ HS-2000) triggered with the injector command. An optical diffuser is placed between the light source and the spray vessel in order to obtain a relatively homogeneous background. The camera is equipped with a 50 mm, f/1.4 lens and is set at 15000 frames per second ($\Delta t \approx 66.7$ µs) with an exposure time of ~ 8.3 µs and a resolution of 128x512 pixels.

For every operating condition, 50 injection sequences were recorded. Raw images (Fig. 2.9) were analyzed by using a digital image processing program to determine the spray tip penetration *S* and the spray angle.

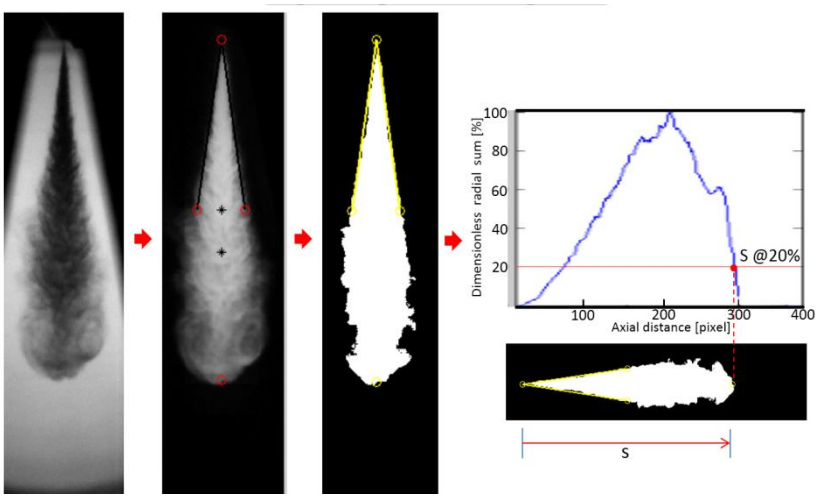

(a) (b) (c) (d)

Fig. 2.10 Processing steps for sprays images: (a) Raw image; (b) Noise removed and reversed image; (c) binarized image (d) Radial rescaled sum of pixels as a in function of axial distance for the determination of penetration length.

2.3.2 Processing of spray images

This section describes the image processing method used to obtain the geometric quantities of spray (penetration length and angle).

-Methodology

Analysis of the raw images to determine the penetration length of spray or spray tip penetration *S* and spray angle comprises four steps:

1. Subtraction of the background noise and inversion of the image (negative) (Fig. 2.10 (a) and (b)). The average image of the background noise is obtained by averaging the first five images acquired in the beginning of each sequence before the appearance of the spray (the delay in the opening).

2. The binarization of the images from a threshold of intensity, by the method of Otsu [77] to "separate" the spray, the background of the image (Fig. 2.10 (c)).

3. Determination of the penetration length *S* from the longitudinal profile of binary images (Fig. 2.10(d)). The penetration length or spray width is defined as corresponding to 20% of the maximum as shown in Fig. 2.10(d). The determined

length is very insensitive to this threshold value due to the large cumulated intensity gradient in the end spray: for a variation of the threshold from 10 to 30%, the change in the penetration length is less than 1% for the case presented below. A threshold of 20% for any transfer was used to exclude "packages" standing out from the end of the spray and to overcome its non-symmetrical shape. For the width the sensitivity of the threshold is more important.

4. Finally, from binarized (digitized images), the spray angle is determined at axial distances from the tip and at *S*/2. We measured at:

$$tan\left(\frac{\theta}{2}\right) = \frac{l/2}{S/2} \quad (2\text{-}11)$$

2.4 Method of measurement under cold conditions

During start-up of the engine under cold temperatures, conditions can be different when biodiesel is used due to the low fuel injection pressure and the high cloud point and high pour point. It is consequently of interest to understand the behavior of the injector under cold conditions when operating with biodiesel.

Two experimental test rigs were used: an injection test rig (Fig.2. 11) and a visualization test rig (Fig.2.12). For the two experiments, a prototype Bosch CRI 3.1 piezoelectric injector with a pump and a pressure fuel tank were used (see section 2.2.2). All the injection and visualization equipment was installed in the climatic chamber to control the temperature in the experiment to within +/-1^{o}C. Injection pressures were set at 30-60 MPa to be close to start-up conditions. The fuel injection rate was analyzed with an IAV$^{@}$ Injection Rate system (model K-025-50). The experimental setup and injection rate analysis are the same as in section 2.2.2.

Macroscopic visualization was accomplished using a constant-volume vessel with optical access and a constant circulation of air near the window as shown in Fig. 2.12. To obtain the desired density conditions inside the vessel, the pressure was adjusted; the system is designed for a maximum pressure of 3 MPa. The fuel injector is located at the top of the vessel. An 8-bit (256 gray levels) high speed camera (Photron$^{@}$PowerViewTMHS-2000) recording at 15,000 frames per second was used to capture the three sprays by Mie scattering. Illumination was provided by a continuous 150 W halogen lamp. The camera and lamp are outside the climatic chamber, only a fiber light is inside. For each operating condition, 50 injections at a frequency of 1 Hz were recorded to ensure convergence of the results.

The temperature in the climatic chamber can be adjusted from Troom to -25 ^{o}C and controlled to within +/-1^{o}C. An accumulator tank was also installed for high-pressure fuel to control the temperature before injections to +/-1^{o}C. For visualization, we installed dry air in the chamber injection and a mirror (see Fig.2.12) for cleaning and removal of water vapor.

To study injection, five fuels were tested: diesel fuel, winter diesel fuel, two diesel–biodiesel blends (B20, B50) and pure biodiesel (B100), and to study the spray behavior Winter diesel fuel and B100 were used. Injection pressures were set at 30-60 MPa. The experimental temperatures studied were room temperature, -5°C and -8°C. -8°C is the lowest temperature, or cold filter plugging point (CFPP), at which a vehicle will operate with biodiesel fuel. Particular attention was paid to the control of initial and boundary conditions for all measurements. The test rig consists of a climatic chamber supplied with dry air and temperature controlled (Troom to -25°C). Temperature sensors (type K thermocouple) are positioned in areas considered important to the control of the boundary conditions (see Fig.2.11 and 12):

- In the cell (T_clim)
- In the fuel inside the high-pressure rail (T_rail)
- In the HP tube to the skin of the injector inlet (2.0 cm nut) (T_line)
- In the output of the fuel return line (2cm from the injector) (T_fuel)
- In the Injection Analyzer (T_rate)
- In dry air enclosure visualization (T_cell)

The measurements were acquired and experiments started when all sensors reach the set temperature to +/-1°C.

Within this chamber is arranged a pressurized rail of a large volume of 300 cm^3. The pressure control is carried out outside the chamber via a hydraulic pressure multiplier. The injection pressure reaches the set pressure +/-10 bar. For each injection, temperature and injection pressure are recorded. Moreover a fast acquisition card 500 kHz saves the current and voltage of the signal sent to the injector driver IPOD and also the evolution of pressure (*Pline*) at the HP pipe.

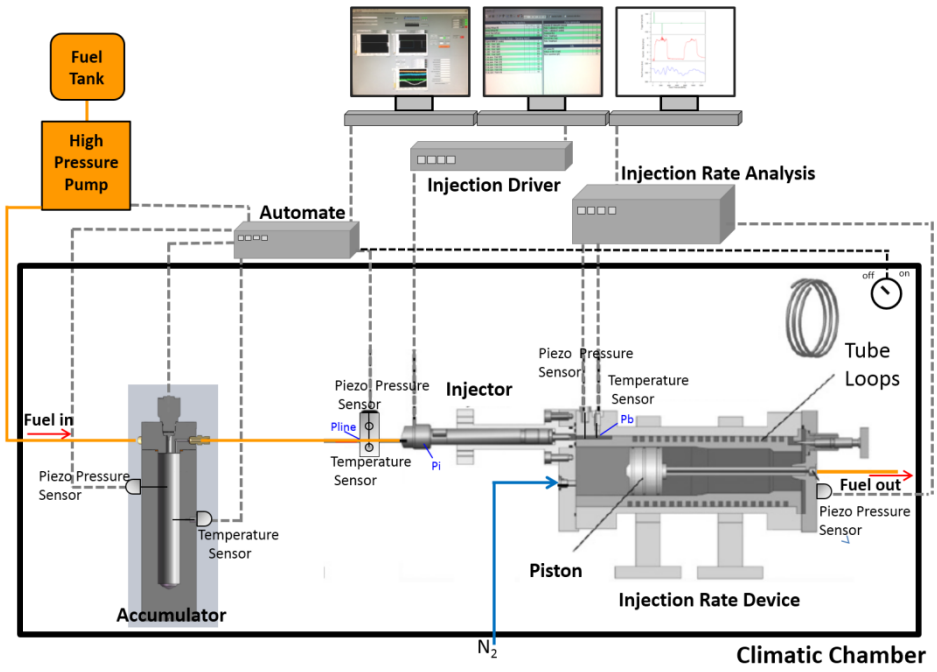

Fig. 2.11 Injection rate experimental setup under cold conditions.

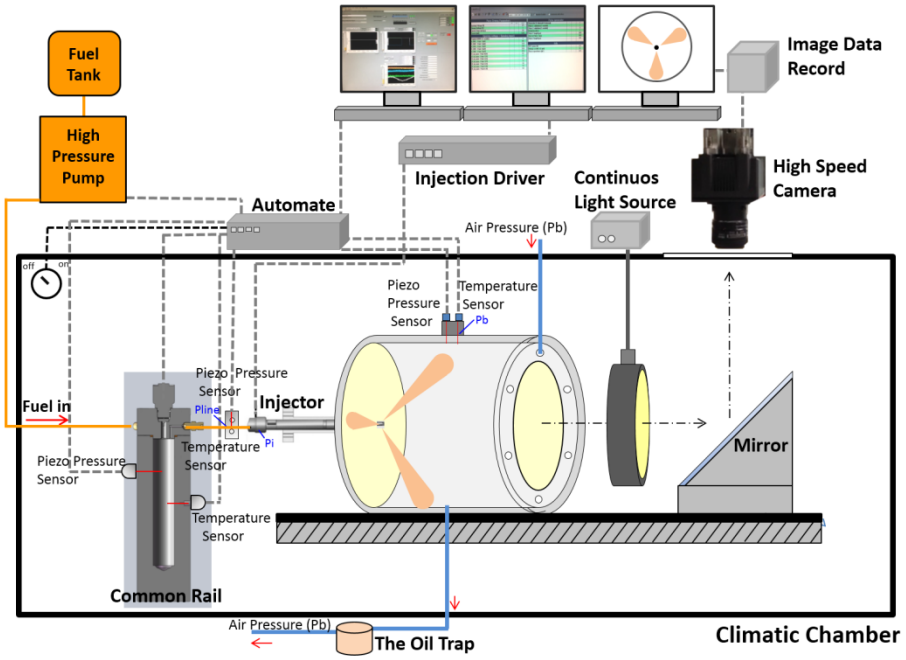

Fig. 2.12 Experimental setup for spray injection under cold conditions.

2.4.1 Spray image analysis

A film of the macroscopic development of the spray is shown in Fig. 2.13. For spray image analysis, raw images were analyzed using a digital image processing program to determine the spray tip penetration S and spray angle θ at $S/2$.

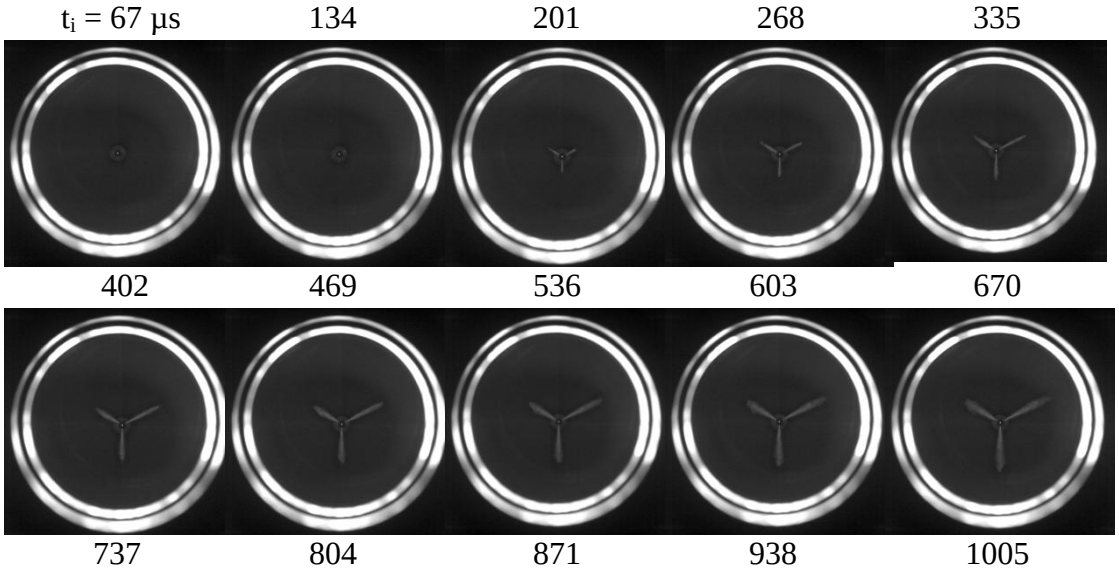

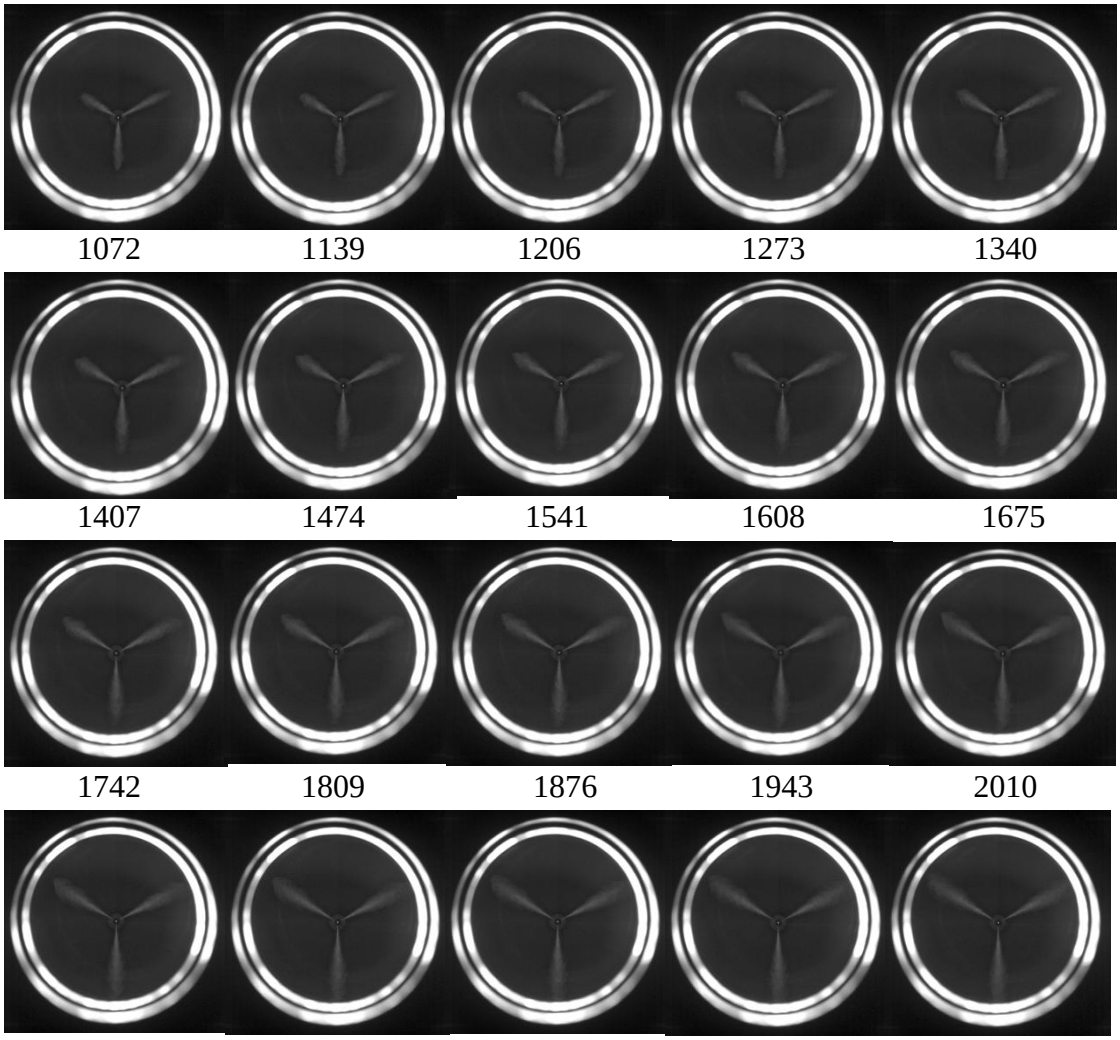

Fig. 2.13 Example of development of a spray – diesel fuel- *Pi*=60 MPa, *Pb*= 1.7 MPa,Troom.

In summary, the image processing comprises three main steps (Fig 2.14):

-First, the background is subtracted from the spray region and only a spray is selected

-Second, the image is binarized by applying an intensity threshold level according to the Otsu method.

-Third, from the digitized images, the spray tip penetration *S* is measured with the position of the last pixel and the area of spray is calculated.

-The angle is calculated with this expression:

$$tan\left(\frac{\theta}{2}\right) = \frac{A}{(S/2)^2} \quad (2\text{-}12)$$

A is projected area of the upstream half of the spray in an image.

- After rotating the image by 120°, the second spray can be analyzed.

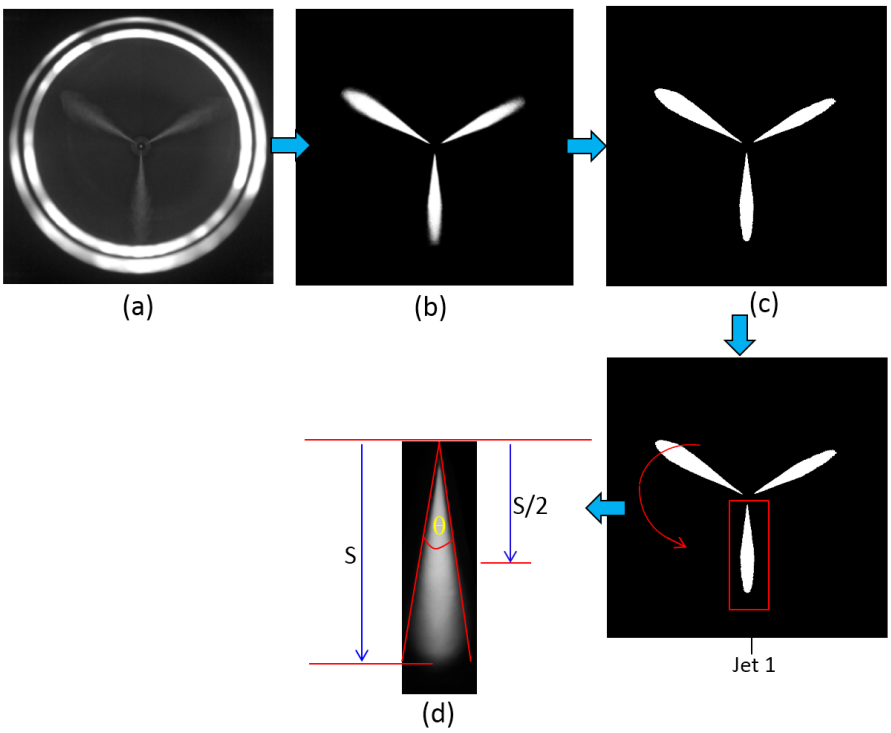

Fig. 2.14 Processing steps of spray images: (a) Raw image; (b) Noise removed and reversed image; (c) image binarized with the Otsu method (d) Radial rescaled sum of pixels as a function of axial distance for determination of the spray penetration *S* and the spray angle at *S/2*.

2.5 Fuel properties

We selected the following fuels for testing: Diesel, Winter diesel, Biodiesel (B100) (produced from rapeseed), and 6 Biodiesel blends between Diesel and B100, namely: B10, B20, B30, B40, B50 and B50(W) (Biodiesel 50% blend with Winter diesel 50%). For the study at room temperature 7 fuels were used: Diesel, B10, B20, B30, B40, B50 and B100, fuel B30, B40 and B50 expand percentage biodiesel blend more than literature. For the study in cold condition 5 fuels were used: Diesel, Winter diesel, B20, B50 and B100, all fuel no information is available in the literature.

2.5.1 Viscometer

The fuel density and viscosity were analyzed with an Anton Paar® Stabinger Viscometer (model SVM 3000/G2) [78]. The SVM 3000 Stabinger Viscometer measures the dynamic viscosity and density according to ASTM D7042. A tube (outer rotor) (Fig. 2.15, 2.16) filled with sample liquid rotates at a constant speed. A hollow measuring rotor (Titanium rotor) floats freely in the tube. Due to its low density, the measuring rotor is centered in the heavier liquid by buoyancy forces. The measuring gap is formed between the tube and the rotor. The

rotor is guided axially by a built-in permanent magnet. The rotating magnetic field delivers the speed signal and induces eddy currents in the surrounding copper casing. Two different torques influence the rotor speed:

- The driving force is caused by the shear stress of the rotating sample and is therefore proportional to the difference in speed between the outer and inner cylinder.

- The above-mentioned eddy currents are responsible for the retarding force.

The viscosity measurement for Newtonian fluid can therefore be reduced to a single speed measurement. Due to the completely frictionless floating rotor bearing, the linearity of the eddy current brake and the high-resolution digital speed measurement, a single measuring cell geometry is sufficient for the entire measuring range.

The conversion of the measuring value from dynamic to kinematic viscosity requires knowing the density. Determination of the sample density was undertaken by the integrated density measuring cell which uses the proven principle of the oscillating U-tube (also used in the DMA series of density meters). The integrated thermostat with cascaded Peltier elements and Platinum thermometer as well as the low thermal mass of the measuring cell enable rapid changes and exact adjustments to the measuring temperature. The measurement of viscosity over temperature curves can therefore be performed very quickly. The measuring temperatures were -56 to 105^{o}C, the accuracy for viscosity: +/-0.35%, density: 0.0005 g/cm^{3}. The fuel properties are listed in Appendix I and in Fig. 2.17.

Fig. 2.15 Anton Paar® Stabinger Viscometer [78].

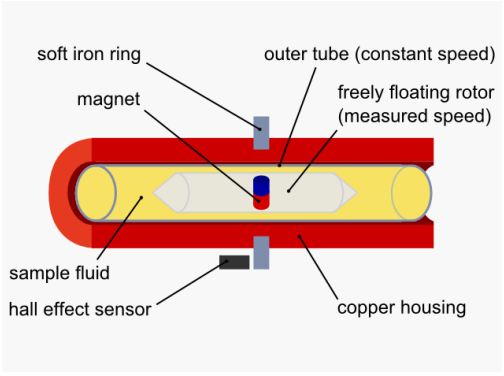

Fig. 2.16 Viscometer principle [78].

2.5.2 Density of fuel

In order to cover operation in cold conditions, we compare our measurement to the correlation from Riazi [79], Eq. 2-13.

$$\rho_T = 0.99.SG - (2.34 - 1.898SG).(T - 288.7) \quad (2\text{-}13)$$

where SG is Specific Gravity, and T = Temperature (K). The result comparing correlation and experimental data is shown in Fig. 2.18. The maximum percentage difference between

correlation and experimental data was 0.5 %, showing that Riazi's correlation is suitable for all temperatures.

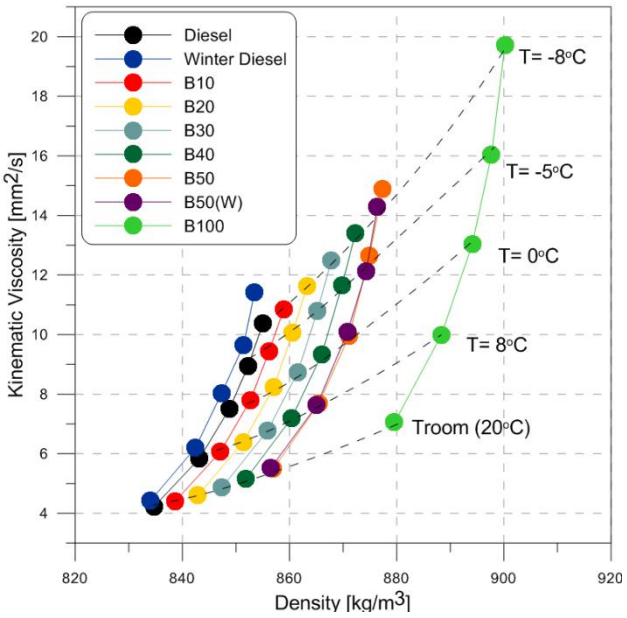

Fig. 2.17 Fuel matrix-predicted viscosity versus density, experimental data.

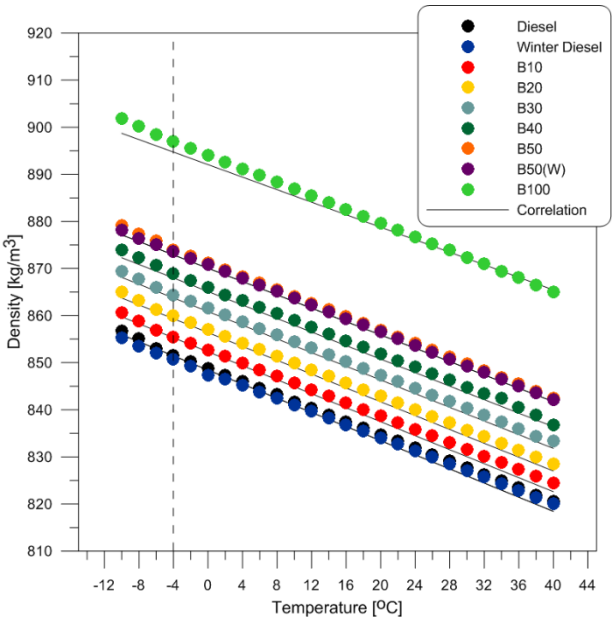

Fig. 2.18 Density experimental data and correlation.

2.5.3 Fuel viscosity

Little information is available on the viscosity of Diesel and Biodiesel blends in cold conditions. For the present study, it was necessary to determine viscosity at room temperature

and at cold temperatures. To predict viscosity, we tested viscosity correlations from Riazi [79] Eq. 2-14, Yilmaz [80] Eq. 2-17, Wang et al. [81] Eq. 2-18, Tesfa et al. [82] Eq. 2-19 and Verduzco et al. [83] Eq. 2-20.

Riazi's correlation:

$$Log(v_T) = A.\left(\frac{311}{T}\right)^B.T - a \quad (2\text{-}14)$$

$$A = Log\left(v_{311(100)}\right) + a \quad (2\text{-}15)$$

$$B = b.Log\left(v_{311(100)}\right) + c \quad (2\text{-}16)$$

where T is the temperature (K), $v_{311(100)}$ is the Kinematic viscosity at 311 K or 38°C, and a = 0.8696, b = 0.2801 and c = 1.8616. To fit the experimental results as closely as possible, the coefficients were recalculated by the least squares method, taking into account all the results of all the fuels: a = -0.0593, b = -5.6832 and c = 8.3112, R^2 = 0.9780.

Yilmaz's correlation:

$$\mu = exp\left(a + \frac{b}{T} + \frac{c}{T^2}\right) \quad (2\text{-}17)$$

Where ; μ is the Dynamic viscosity (cP), T is the temperature (°C), coefficient for type of fuel;

Fuel	*a*	*b*	*c*	R^2
Diesel	-2.6	338.129	232417	-
B20	3.6	-3417.5	816809	-
B100	11	-9115.8	1927596	-
New coefficient				
Diesel	5.9081	-4905	1037500	0.9990
B20	12.426	-8640	1579400	0.9977
B50	29.025	-18171	2960960	0.9892
B100	22504	-14300	2411200	0.9926

Wang et al.'s correlation:

$$v = A.exp(B + C.T) + D \quad (2\text{-}18)$$

where T is the temperature (K). The coefficients A, B, C and D are defined in the following table for each of the fuels.

Fuel	*A*	*B*	*C*	*D*	R^2
WD*	1.0277	1.14	-0.0310	1.043	0.992
ULSD*	1.2622	1.33	-0.0304	1.205	0.998
New coefficient					
Diesel	0.1646	3.6513	-0.0404	1.3519	0.9959
Winter Diesel	0.5992	2.4693	-0.0422	1.2857	0.9878

B50	0.5378	2.864	-0.0421	1.3729	0.9892
B100	0.6584	2.9520	-0.0421	1.3801	0.9884

*WD = Winter grade pump-grade diesel, ULSD = Ultra-low sulfur diesel (summer grade)

Tesfa's correlation (fuel blends only):

$$\ln(v) = (a.T + b).X - c.T + d \tag{2-19}$$

where T is the temperature (K), X is the volume fraction of biodiesel ($0 < X < 100$), and a = -0.0012, b = 0.8456, c = -0.0234 and d = 8.64. The new coefficients recalculated by the least squares method, taking into account all the results of all the fuels, where: a = -0.01275, b = 4.23, c = -0.0292 and d = 10, R^2 = 0.9679.

Verduzco's correlation (fuel blends only):

$$v = exp\left(a + bX + \frac{c}{T} + \frac{dX}{T^2}\right) \tag{2-20}$$

where T is the temperature (K), X is the volume fraction of biodiesel ($0< X<100$), and a = -4.47, b = 1.8168, c = 1735 and d = 397.5. The new coefficients recalculated by the least squares method, taking into account all the results of all the fuels, where: a = -6.36, b = -1.41, c = 2282 and d = 160480, R^2 = 0.9804.

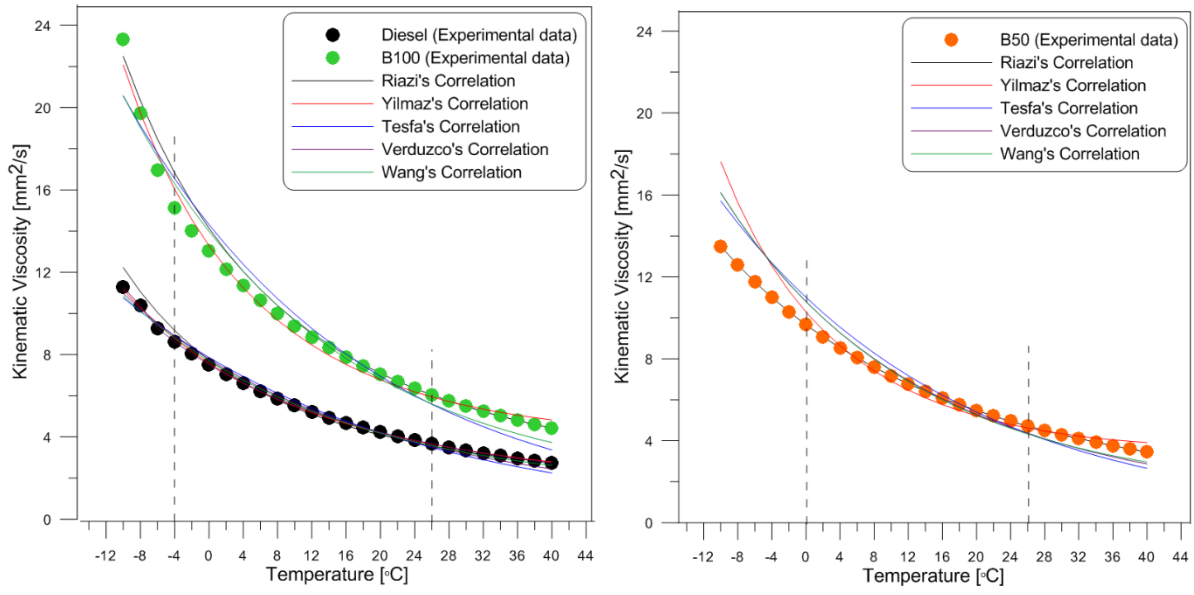

Fig. 2.19 Viscosity: experimental data and correlation.

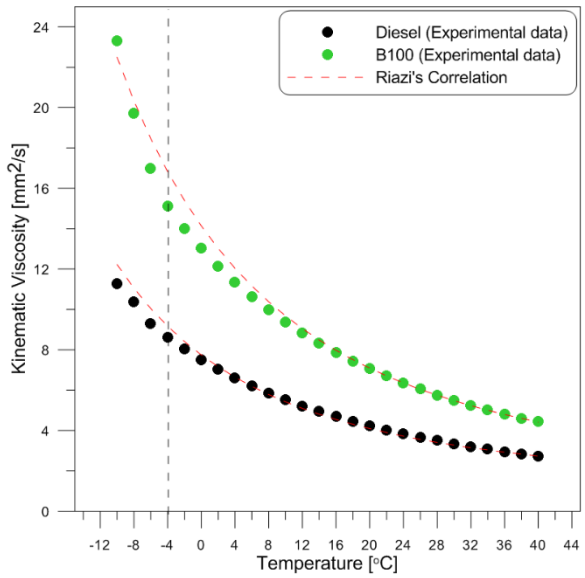

Fig. 2.20 Riazi's correlation.

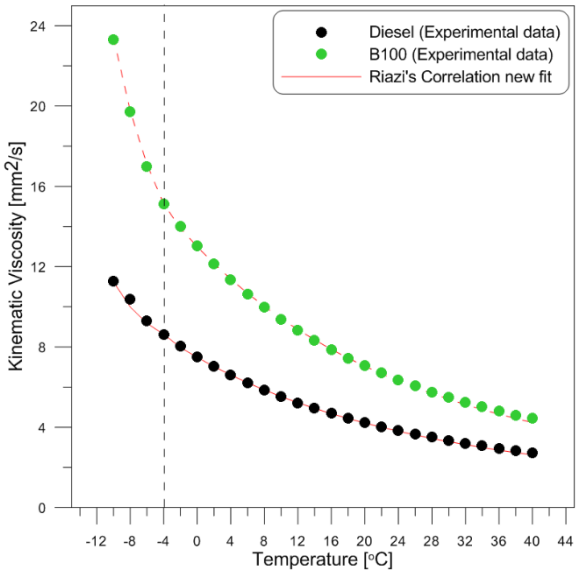

Fig. 2.21 Riazi's correlation new fit.

Fig. 2.19 shows the Kinematic viscosity correlation for Diesel fuel, Biodiesel and B50. The result shows that Riazi's correlation and Yilmaz's correlation are good predictors and that in the case of B50, Riazi's correlation is the best. The Tesfa and Verduzco correlations are good predictors only for biodiesel blends from T = 0 to 26°C (Fig.2.19) because the correlations do not cover cold conditions. Wang's correlation is based on cold conditions but the coefficients only fit for WD and ULSU fuels, and the results reported in [81] did not include viscosity results in cold conditions (-4°C to -10°C). In the present work, Riazi's correlation was therefore selected as it uses only 1 set of coefficients to predict the viscosity of all fuels.

Fig. 2.20 shows the experimental data and the correlation from Riazi. It can be observed for diesel fuel from T = 20°C to 40°C that Riazi's correlation accurately describes the experimental data, but at cold temperatures the values differ from experimental data. For B100 the results are the same. The choice of a single set of coefficients is not valid for the whole temperature range to describe the evolution of viscosity. We therefore separated the curve into two parts.

For temperatures from -4°C to 40°C, Eq. 2-14 were used. The coefficient values *a*, *b*, *c* were obtained by minimizing the sum of square errors between correlation and experiment: *a* =1.1865, *b* = -0.4144, *c* = 2.0082 and R^2 = 0.9897.

For temperature from -4°C to -10°C; $$log(v_T) = A.\left(\frac{269}{T}\right)^B - a \quad (2\text{-}20)$$

$$A = Log_{10}\left(v_{269(100)}\right) + a \quad (2\text{-}21)$$

$$B = b.Log_{10}\left(v_{269(100)}\right) + c \quad (2\text{-}2)$$

where $v_{269(100)}$ is the Kinematic viscosity at 269 K or -4°C. The coefficient values *a*, *b*, *c* were obtained by minimizing the sum of square errors between correlation and experiment: *a* = -0.8639, *b* = -87.6560, *c* = 124.30 and R^2 = 0.9939.

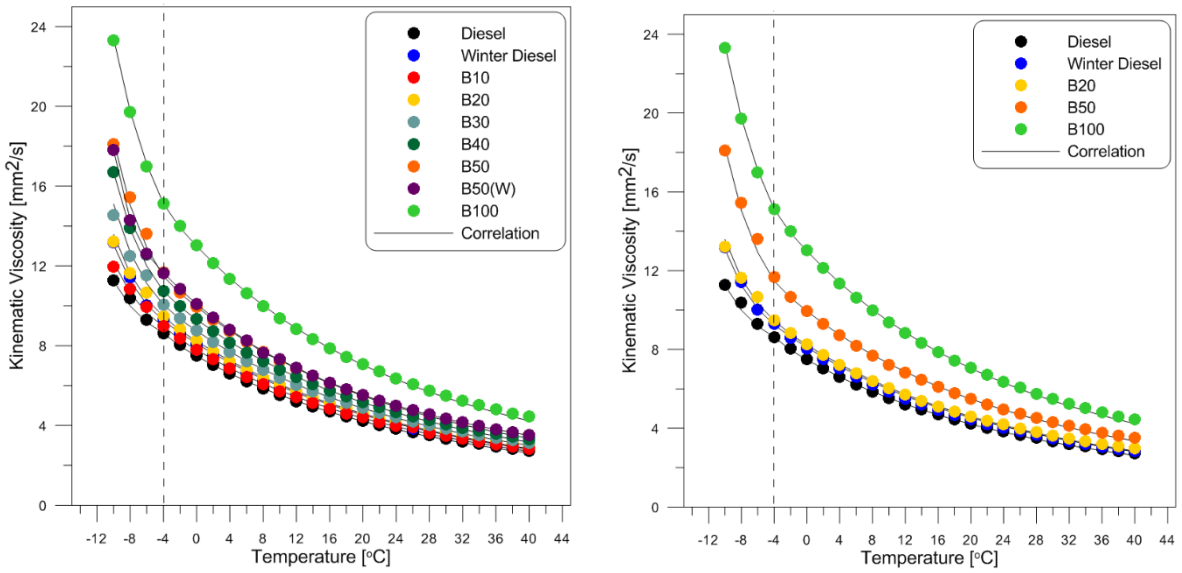

Fig. 2.22 Kinematic viscosity experimental data and correlation.

The results from experimental data and correlation are shown in Fig. 2.21 and Fig. 2.22. The results for the new fit are very good for Riazi's correlation. The maximum percentage difference between correlation and experimental data is 4.6 %. It can be observed that Riazi's correlation used viscosity for calculation, unlike the other correlations. However, it is necessary to know the fuel viscosity for 2 temperatures (-4°C and 38°C) in order to use Riazi's correlation.

When the viscosity of Diesel or Winter diesel and B100 is known from experiment, we can use a mixed correlation [49] to predict the viscosity of the fuel blend:

$$\ln v_{mix} = x_{bio} ln(v_{bio}) + (1 - x_{bio}) \ln(v_{diesel}) \qquad (2\text{-}23)$$

The result of the predicted viscosity of biodiesel blends is shown in Fig. 2.23. The correlation is a good predictor for biodiesel blends with both Diesel and Winter diesel.

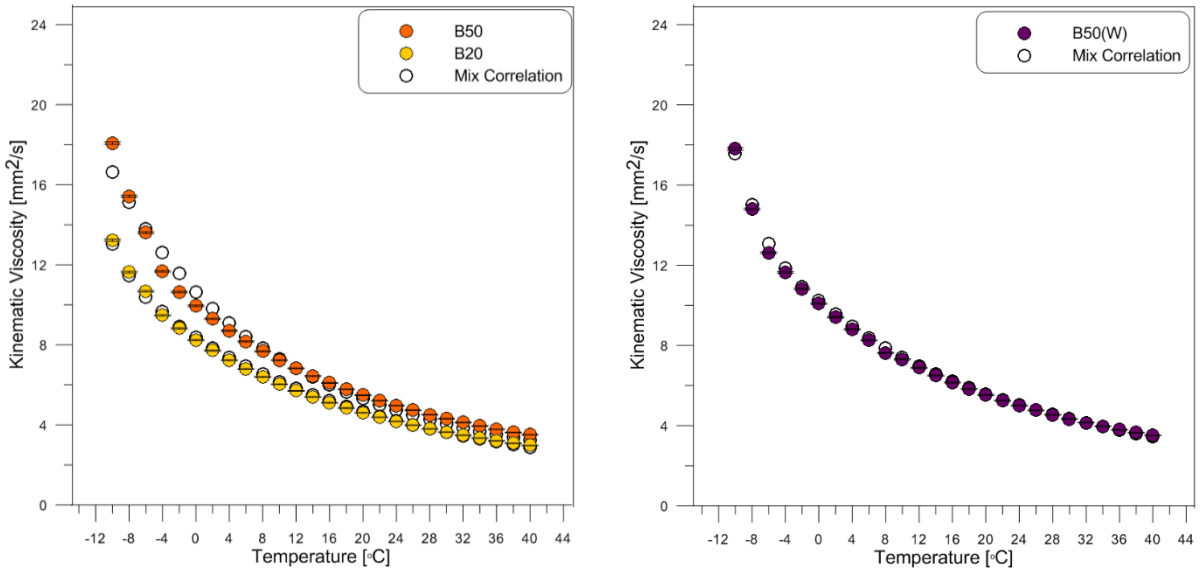

(a) B20 and B50 (b) B50(W)

Fig. 2.23 Kinematic viscosity: experimental data and mixed correlation.

2.6 Sound velocity measurement

Sound velocity is an important thermophysical property of fuel, as it directly characterizes the fuel injection and emissions in diesel engines [9]. Sound velocity is necessary to determine the mass flow rate (see Eq. (2-1)). The injection rate device can be used to estimate sound velocity [7, 84]. The method is based on determination of the time delay between the incident signal induced by the injection event and the first reflection wave (Fig. 2.5). We used the same experiment test bench as Dernotte et al. [7]. They measured the length of the tube loops using two liquids whose sound velocity is known. The two liquids selected were n-Heptane and n-Dodecane and their sound velocity values were taken from the NIST Chemistry WebBook. The distance travelled by the pressure wave is 10.2 m with a maximum error of 0.3%.

2.6.1 Sound velocity correlation

The acoustic wave is generated by an injection at 30 MPa in the injection rate system under a back-pressure from 1 to 5 MPa at room temperature. Tat et al. [85] proposed a three-variable polynomial to fit the sound velocity (Eq. 2.24). The variables are the temperature, T (K), the pressure, P (MPa) and the Biodiesel percentage (B). The coefficients C depend on the Diesel and Biodiesel characteristics.

$$a = C_1.T + C_2.P + C_3.B + C_4.T.P + C_5.P.B + C_6.P^2 + C_7.B^2 + C_8 \quad (2\text{-}24)$$

In our case (Fig. 2.24 and 2.25), we chose a linear fit to show that the sound velocity increases approximately linearly with back-pressure. These experimental values are close to the measurements made by Dernotte et al. [7] and differ by +/-2.1% from the results of Freitas et al. [9] and the experimental values at cold temperatures are close to the

measurements made by Kegl et al. [86]. From the correlation of Tat et al. (Eq. 2-24) based on temperatures from 20°C to 40°C, we fitted Eq. 2-24 for biodiesel blends, and temperature variable from -8°C to 20°C, The coefficients C_1 to C_8 are obtained by minimizing the sum of square errors between the correlation and experiment. The values obtained are: C_1 = -3.3498, C_2 = -325.04, C_3 = 2679.70, C_4 = -0.0026, C_5 = 0.0028, C_6 = 5.0130, C_7 = -3780.40, C_8 = 7137.70, R^2 = 0.9966. The comparison between correlation and experimental data in Fig.2.26 shows that the maximum error is 0.5 %. Eq.2-24 and the new coefficient are good predictors of sound velocity in cold conditions.

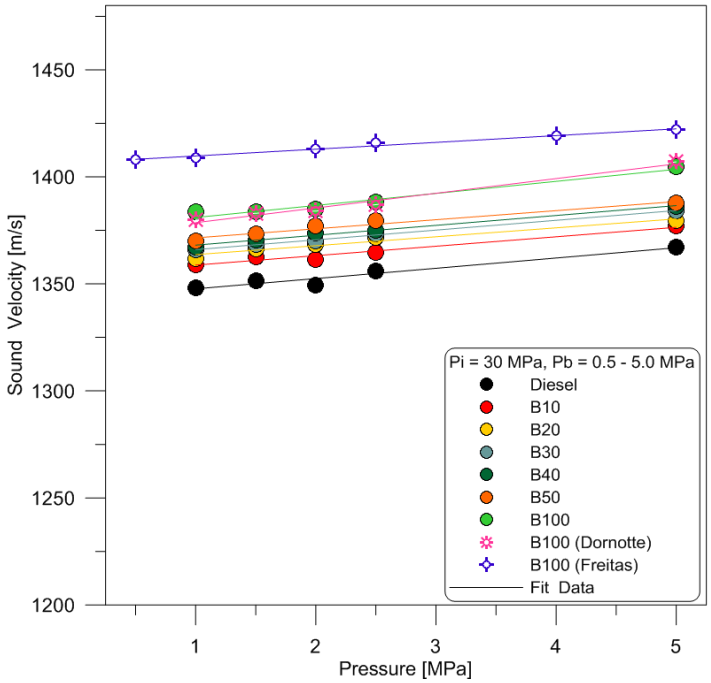

Fig. 2.24 Sound velocity as a function of the different fuels at room temperature.

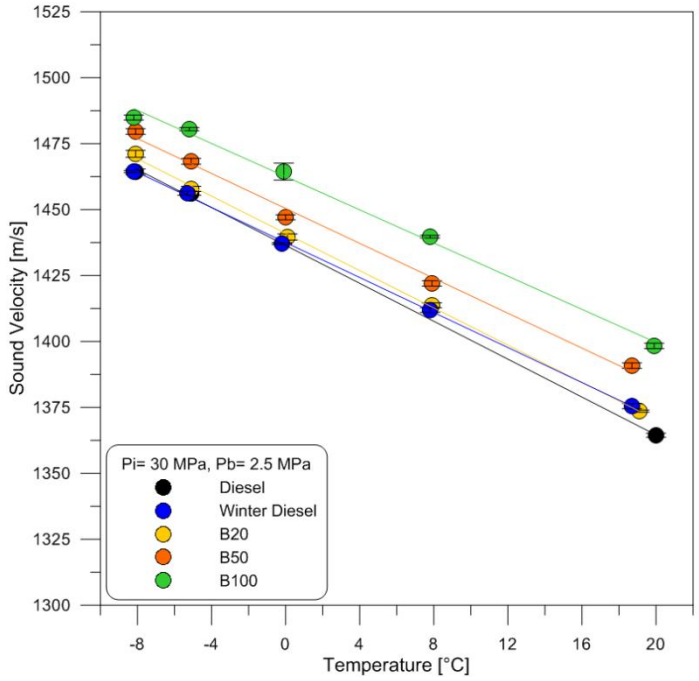

Fig. 2.25 Sound velocity as a function of the different fuels-*Pi* = 30 MPa, *Pb* = 2.5 MPa.

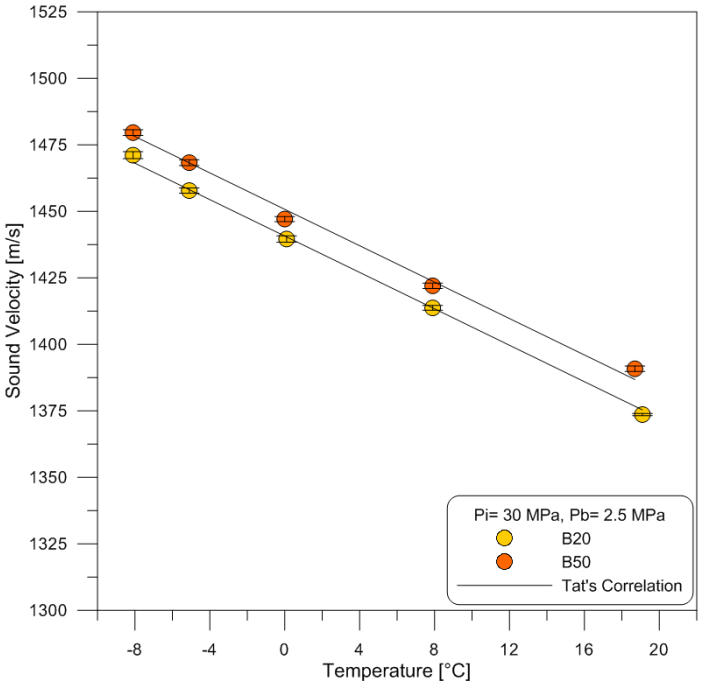

Fig. 2.26 Sound velocity experimental data and Tat's correlation -*Pi* = 30 MPa.

2.7 Conclusions

This chapter has presented the experimental means used, their operating principle and the associated processing methods. Fig. 2.27 summarizes the results, indicating the quantities that have been characterized and the properties of the fuels that have been studied.

1. Hydraulic injector

-Injection rate measurement from dynamic pressure (Bosch method) 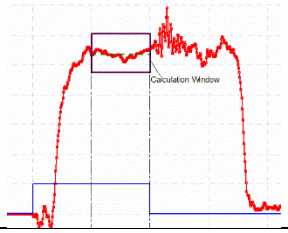	**Quantities characterized** Mass flow / Discharge coefficient Reynolds Number / Cavitation/ Opening time and initial closing / Sound velocity	**Fuels and properties considered** -Diesel, B10, B20, B30, B40, B50 and B100 -Density, Kinematic viscosity

2. Development of macroscopic spray (non-vaporizing conditions)

-Visualization by absorption with a fast camera in a pressurized chamber. 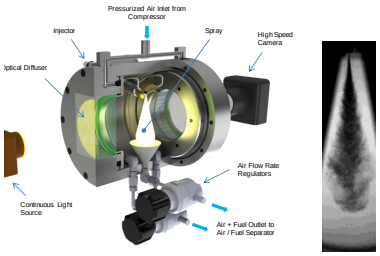	**Quantities characterized** Angle *S*/2 / penetration length	**Fuels and properties considered** -Diesel, B10, B20, B30, B40, B50 and B100 -Density, Kinematic viscosity

3. Hydraulic injector under cold conditions

-Injection rate measurement from dynamic pressure (Bosch method) 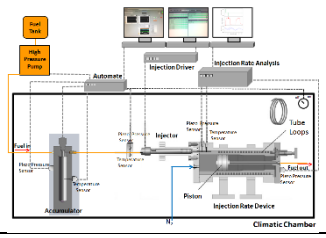	**Quantities characterized** Mass flow / Discharge coefficient Reynolds Number / Cavitation/ Opening time and initial closing / Sound velocity	**Fuels and properties considered** -Diesel, B20, B50, B50(W), B100 and Winter diesel -Density, Kinematic viscosity

4. Development of macroscopic spray under cold conditions

-Visualization by Mie scattering with a fast camera 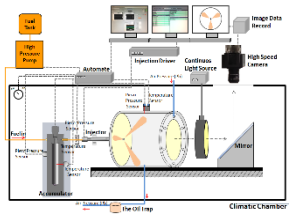	**Quantities characterized** Angle *S*/2 / penetration length	**Fuels and properties considered** -Diesel, B20, B50, B50(W), B100 and Winter diesel -Density, Kinematic viscosity

Fig. 2.27 Summary of experiments, quantities and properties of fuels studied.

❖ Conclusions (version français)

Ce chapitre a présenté les moyens expérimentaux utilisés, leur principe de fonctionnement et les méthodes de traitement associés. Les points suivant résument les moyens, les quantités et les carburants étudiés. De plus des corrélations étendus aux températures négatives ont été établis afin de prédire l'évolution de la densité ou de la viscosité cinématique sur une plus large gamme de température.

1. Le taux d'introduction à température ambiante et basse température

Mesure du taux d'introduction par analyse d'une onde acoustique (la méthode du tube Bosch) 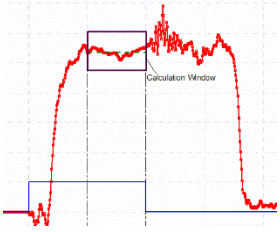	**Quantités caractérisées** Débit, coefficient de décharge, délai d'ouverture et de fermeture, phénomène de cavitation, vitesse du son	**Carburants et propriéts considérées** -Diesel, B10, B20, B30, B40, B50 and B100 (temperature ambiante) -Diesel, B20, B50, B50(W), B100 and Winter diesel (temperature negative) -Densité, viscosité cinématique

2. Développement macroscopique du spray (condition non évaporante)

A température ambiante Visualisation par absorption avec une camera rapide dans une chambre pressurisée rapide 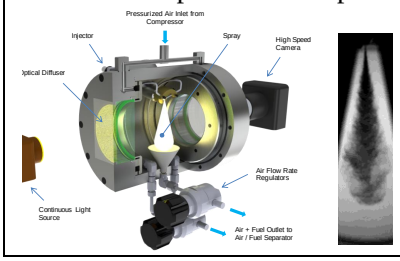	**Quantités caractérisées** Angle *S*/2, longueur de pénétration	**Carburants et propriéts considérées** -Diesel, B10, B20, B30, B40, B50 and B100 (temperature ambiante) -Diesel, B20, B50, B50(W), B100 and Winter diesel (temperature negative) -Densité, viscosité cinématique

A température négative Visualisation par diffusion de Mie 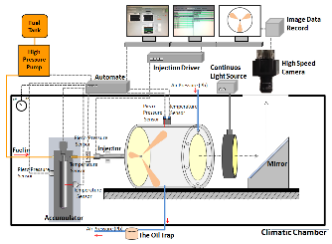 		

Fig. 2.28 Résumé des experiences.

CHAPTER 3

Influence of physical properties of fuel blends at room temperature on the injection rate and the spray

In this chapter the results obtained at room temperature are reported. After an introduction on fuel properties and experimental conditions, the results are presented in for parts:

- The effect of fuel blend properties on injection rate.
- The effect of fuel blend properties on discharge coefficient and discharge coefficient correlation.
- The effect of fuel blend on pressure evolutions.
- The effect of fuel blend on spray injection behavior: spray tip penetration, spray angle.

Introduction (version français)

Dans ce chapitre les résultats obtenus à température ambiantes sont reportés. Après une introduction sur la description des carburants utilisés et des conditions expérimentales, les résultats sont présentés en quatre parties.

- L'effet des propriétés des différents carburants sur le taux d'introduction.
- L'effet des propriétés des carburant sur le coefficient de décharge et détermination des nouveaux coefficients corrélant le coefficient de décharge aux propriétés des carburants (viscosité et densité) pondérés par les conditions d’injection.
- L'effet des mélanges de carburant sur les fluctuations de pression en amont de l’injecteur
- L'effet des mélanges de carburant sur le comportement du spray: longueur et angle de spray

3.1 Fuels used and experimental conditions

The seven fuels chosen in this study are Diesel and a mass mixes between Diesel and rapeseed Biodiesel. They are referenced in this study as follows: Diesel, B100 (biodiesel 100 % produced from rapeseed), B10 (diesel 90%, biodiesel 10 %), B20 (diesel 80%, biodiesel 20 %), B30 (diesel 70%, biodiesel 30 %), B40 (diesel 60%, biodiesel 40 %), and B50 (diesel 50%, biodiesel 50 %). The percentage is a mass fraction. The fuel properties are listed in Table 3.1.

Table 3.1: Fuel matrix in standard conditions.

Abbreviation	Fuel	Density @ 15°C (kg/m^3)	Kinematic viscosity @ 40°C (mm^2/s)	Injector CRI 3.1 3 holes	Injector CRI 3.1 7 holes
Diesel	Diesel	837	3.66	✓	✓
B10	10% biodiesel	841	3.89	✓	
B20	20% biodiesel	845	4.09	✓	
B30	30% biodiesel	850	4.22	✓	
B40	40% biodiesel	854	4.41	✓	
B50	50% biodiesel	859	4.57	✓	✓
B100	100% biodiesel	881	5.49	✓	✓

The injection rate experiment was carried out at room temperature (24°C +/-3°C). The injection pressure, *Pi*, varied from 30 – 180 MPa and the back-pressure, *Pb*, from 1 – 5 MPa. The duration of electrical activation of the injector was set at 2000 µs for an effective injection duration of about 4000 µs. Each injection event was reproduced 50 times. The injection frequency was set at 1 Hz to allow the pressure waves in the injection device and in the duct upstream of the injector to be completely dampened [7]. The discharge coefficient (*Cd*) calculated for each condition corresponding to the mass flow rate was averaged between 1000 and 2000 µs after the start of activation (SOA) during the quasi-steady state period.

The spray injection experiment was also conducted at room temperature (24°C +/-3°C). The injection pressure, *Pi* varied from 30 - 150 MPa and the back-pressure, *Pb*, from 1 - 2.5 MPa for a variation in density from 11.8 - 29.4 kg/m^3 representing the gas density at the Top Dead Centre (TDC) of conventional diesel engines. The injection duration was set at 4000 µs and the injection frequency at 1 Hz.

The same injector Bosch CRI 3.1 body was used with 2 nozzles for study injection rate behavior. The first nozzle has 3 holes and the second seven holes. We use only the nozzle with 3 holes for study spray behavior.

3.2 Effect of fuel blend properties on injection rate

3.2.1 Effects on mean behavior and pressure evolution

Mean mass flow rates at different injection pressure are shown in Fig. 3.1 (a) and (b). The starts of injection are nearly the same for all fuels however a greater dispersion for the

closing delay is observed. Increasing of biodiesel blends or viscosity affect significantly less the opening behavior of this type of injector then the closing behavior, as discussed later. On the quasi-steady state period (Fig 3.1(a)), it can be observed that when biodiesel content increases injection rate tends to increase. On the end of injection, the closing delay of fuel injection increases with the biodiesel content, with the B100 fuel showing the most delayed closing (Fig. 3.2 and 3.4). The needle displacement due to the pressure drop inside the injector depends on frictional forces and thus on the fuel viscosity. This behavior is typical for this injector technology. With piezo activation, the movements of the needle on the opening and the closing of injector are more difficult with a higher viscous fluid [87]. The fuel viscosity increases with an increase of biodiesel blend. So the closing delay increases and leads to an increase in injection duration. These results are similar to those reported by Kegl [84].

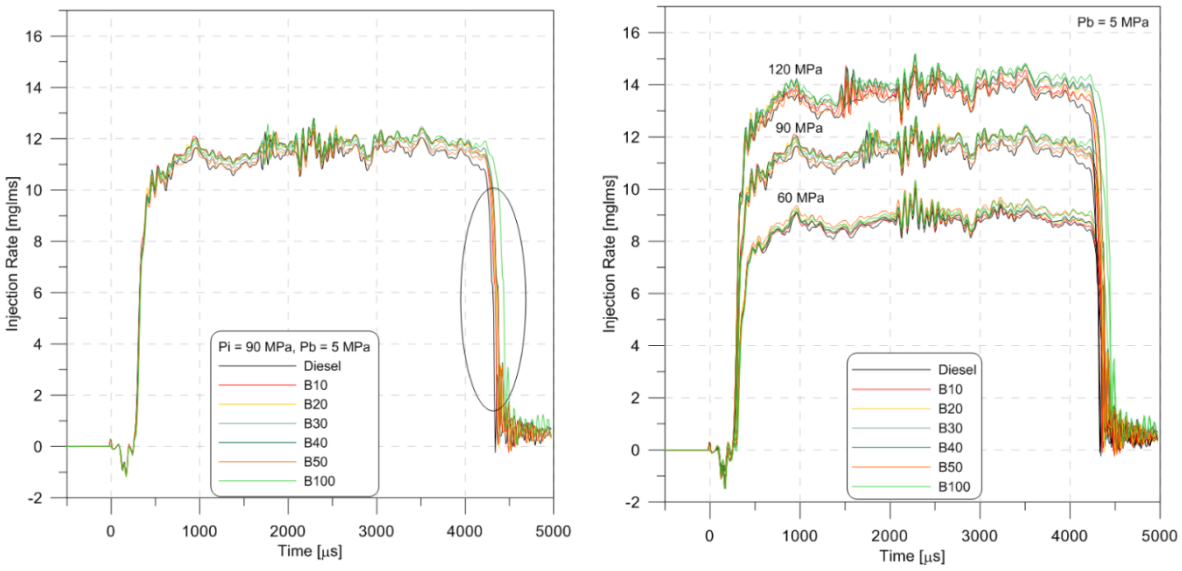

(a) *Pi* = 30 MPa (b) *Pi* = 60, 90 and 120 MPa

Fig. 3.1 Mean mass flow rate at injection pressure, *Pb* = 5 MPa, 3 holes injector.

The delay depends on valve and needle displacement. Fig. 3.3 shows the mean mass flow rate and variation of pressure upstream of injector for all fuels at *Pi* = 30, 60, 90 MPa. The pressure drop is caused by the opening of the valve. The decrease of the pressure in the control chamber drives the start of the needle movement by pressure disequilibrium. With the B100, the pressure decreasing is slower (Fig. 3.3 (a) in a circle), the start of needle lift is slightly delayed, thus explaining the increase of hydraulic delay of 30µs on *Pi* = 30 MPa (Fig. 3.3 (a) and (b)). This shift is much more important at closing like observed in this work and by Plamandon [51]. Once the needle reaches its seat the increased viscosity with increased biofuel content in Diesel slows down the needle velocity during its closing displacement. When the injection pressure increases, the behavior of the pressure evolutions is the same for all fuels (Fig. 3.3 (c) and (e)).

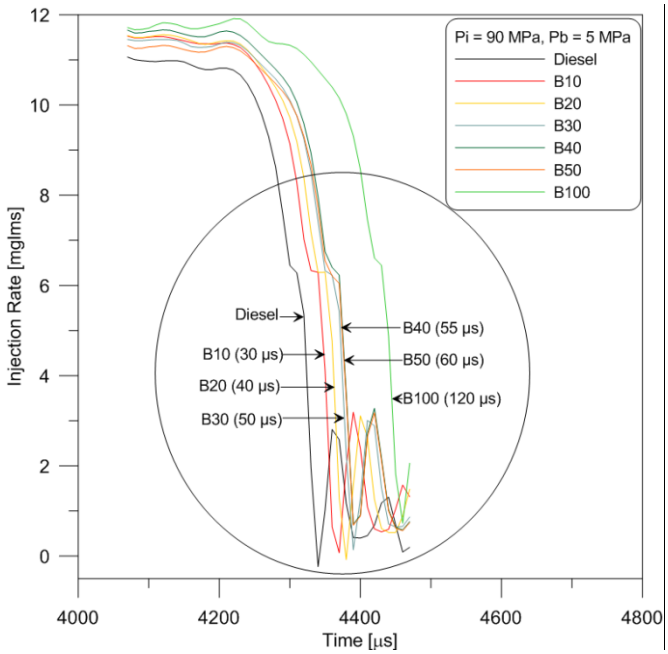

Fig. 3.2 Mean mass flow rate at injection pressure, *Pb* = 5 MPa, 3 holes injector.

3.3 Effect of fuel blend properties on discharge coefficient

3.3.1 In case used injector CRI 3.1 (3 holes)

The discharge coefficient (Cd) is calculated by Eq. 2-2. Fig. 3.5 (a) and (b) show the discharge coefficient versus the pressure difference for different fuels. Cd increases when the pressure difference increases. No significant difference of the discharge coefficient with Diesel or biodiesel blends was observed in the range of injection pressures used here. However a slight decrease is observed with B100 for injection pressures up to 120 MPa. Beyond this pressure cavitation phenomena can occur with low back-pressure.

The discharge coefficient does not change significantly when the fraction of biodiesel in the diesel fuel increases. The density changes from 837-859 kg/m^3 (an increase of 0.5 – 2.6 %), and viscosity varies from 3.66 – 4.57 mm^2/s (an increase of 6.2 – 24.8%). This means that there is only small influence of fuel density and viscosity on the discharge [7]. However in the case of B100 (which at 881 kg/m^3 is denser than Diesel and 50% more viscous than Diesel) the discharge coefficient is smaller than that of the other fuels. The results are similar to those reported by Park et al. [88], Seykens et al. [89] and Desantes et al. [50].

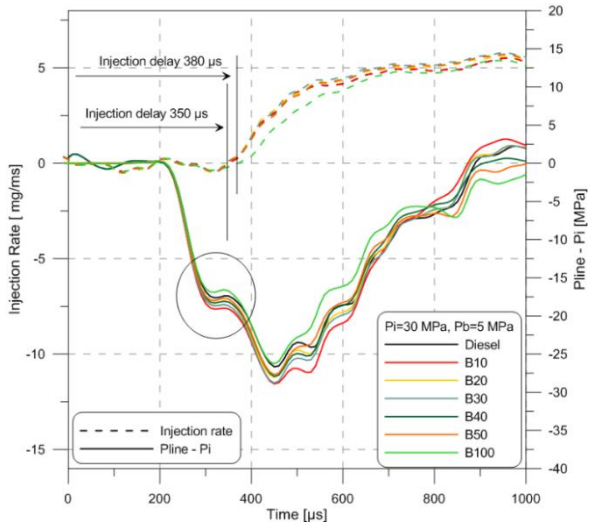

(a) All fuel- *Pi*= 30 MPa

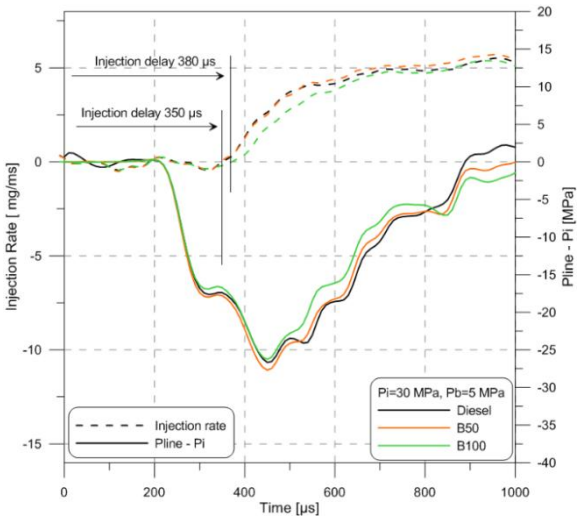

(b) Diesel, B50, B100- *Pi*= 30 MPa

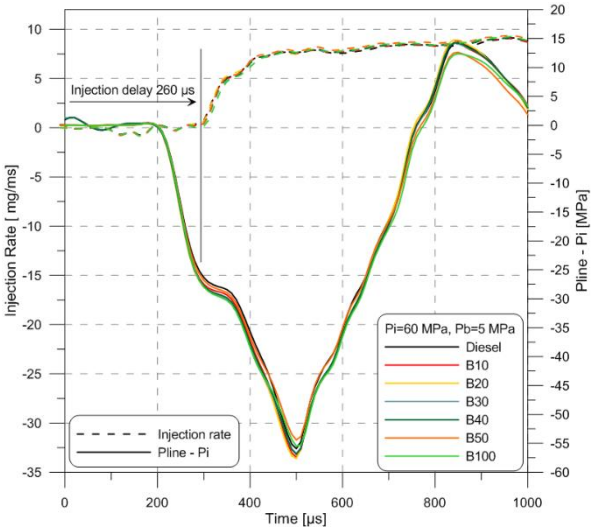

(c) All fuel- *Pi*= 60 MPa

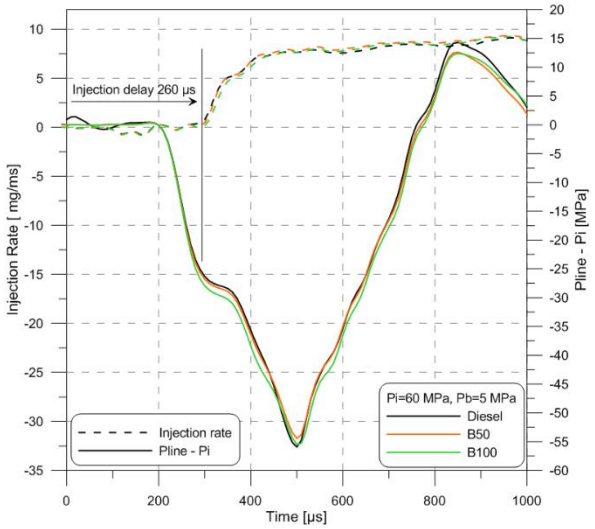

(d) Diesel, B50, B100- *Pi*= 60 MPa

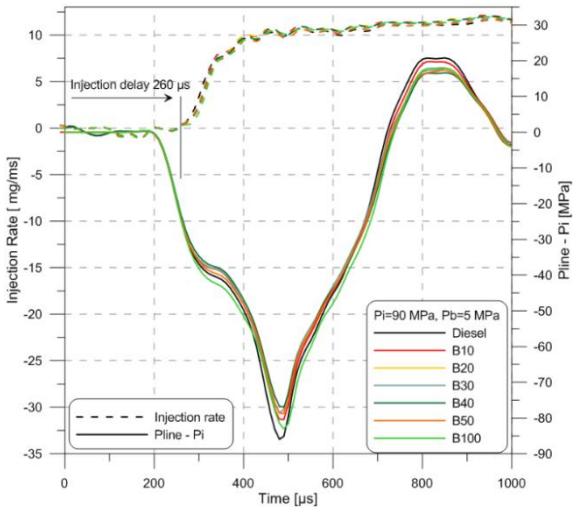

(e) All fuel- *Pi*= 90 MPa

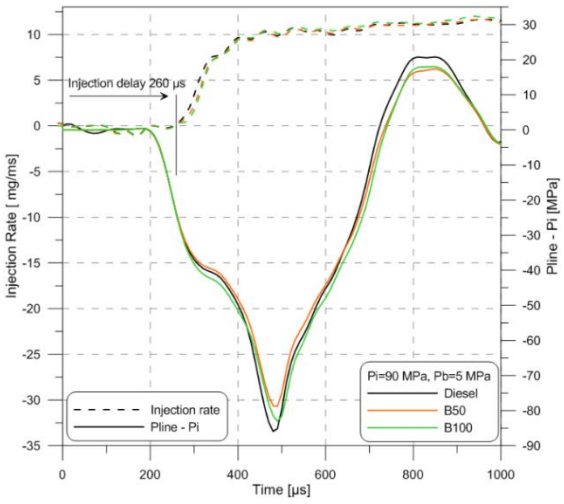

(f) Diesel, B50, B100- *Pi*= 90 MPa

Fig. 3.3 Mean mass flow rate and *Pline, Pi, Pb*=5 MPa, 3 holes injector.

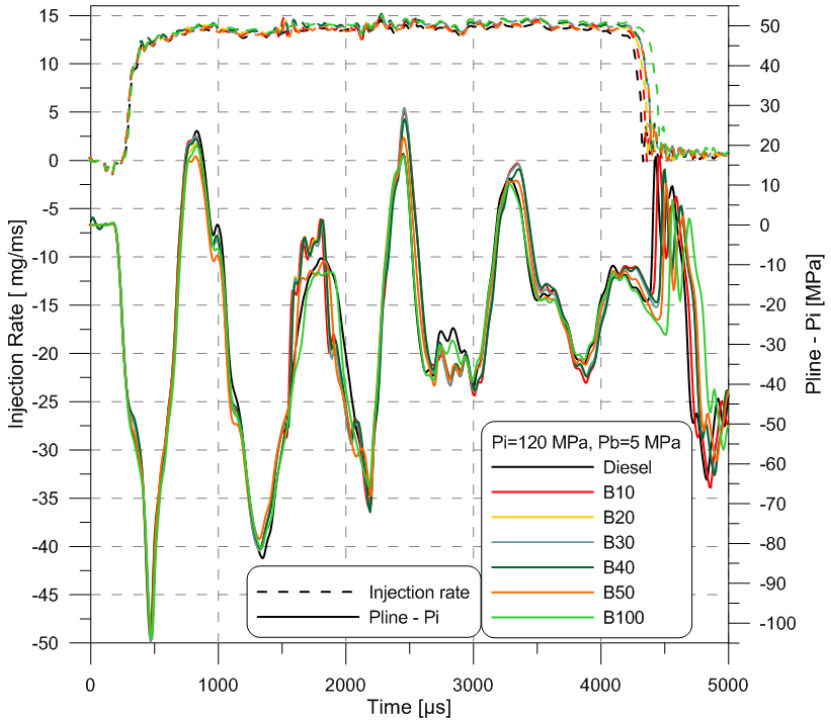

Fig. 3.4 Mean mass flow rate and *Pline*, *Pi* = 120 MPa, *Pb* = 5 MPa, 3 holes injector.

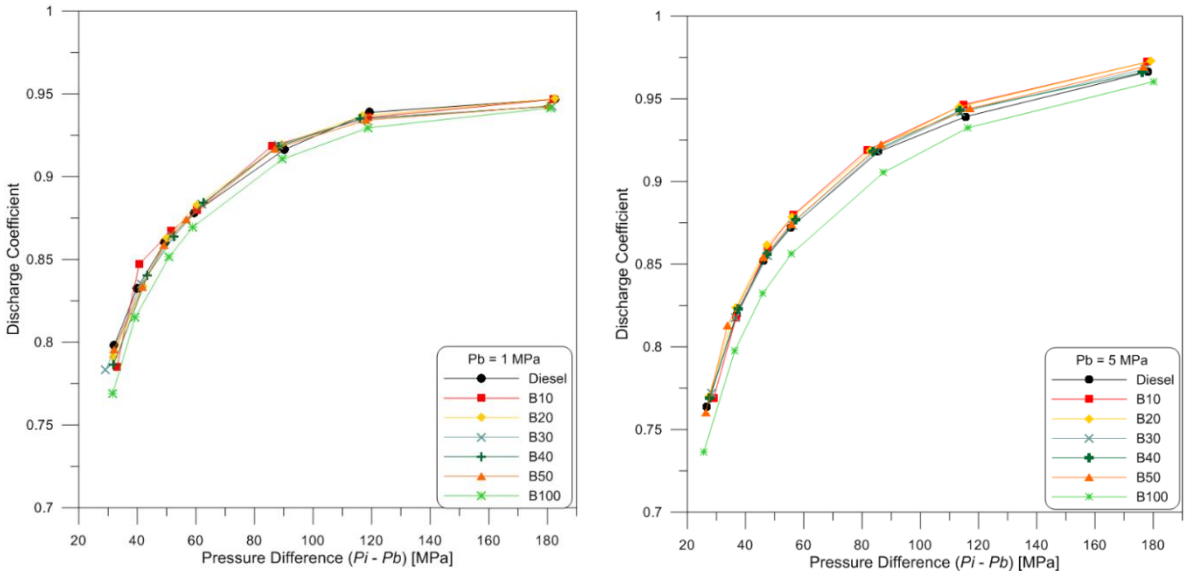

(a) *Pb* = 1 MPa (b) *Pb* = 5 MPa

Fig. 3.5 Impact of fuel blend on discharge coefficient, *Pi* =30 to 180 MPa, 3 holes injector.

3.3.2 In case used injector CRI 3.1 (7 holes)

We verify these first conclusions by using another nozzle with the same injector body. Only the needle, the number and the shape of hole change. Fig. 3.6 (a and b) shows the discharge coefficient versus the pressure difference for different fuels at *Pb* = 1, 5 MPa. It increases when the pressure difference increases. At injection pressure (30-120 MPa), the discharge coefficient of Diesel is highest for all fuels and the discharge coefficient of B100 is lowest for all fuels. After injection pressure more than 120 MPa, no significant differences of the discharge coefficient of all fuels.

With the 3 holes-nozzle no significant differences are observed on discharge coefficient for different blends between 0-30-40% of biodiesel and Cd decreases a little between 40-50 and 100% of biodiesel. With the 7 holes-nozzle, the discharge coefficient slight decreases with percentage blend, especially at low injection pressure. For B100, the discharge coefficient is lowest all fuels with both injectors. These observations are visible on Fig. 3.7 (a) and (b). It is noted when used more than 50% biodiesel blends at low injection pressure the discharge coefficient strongly decreases, but at high injection pressure, no significant differences of the discharge coefficient are found.

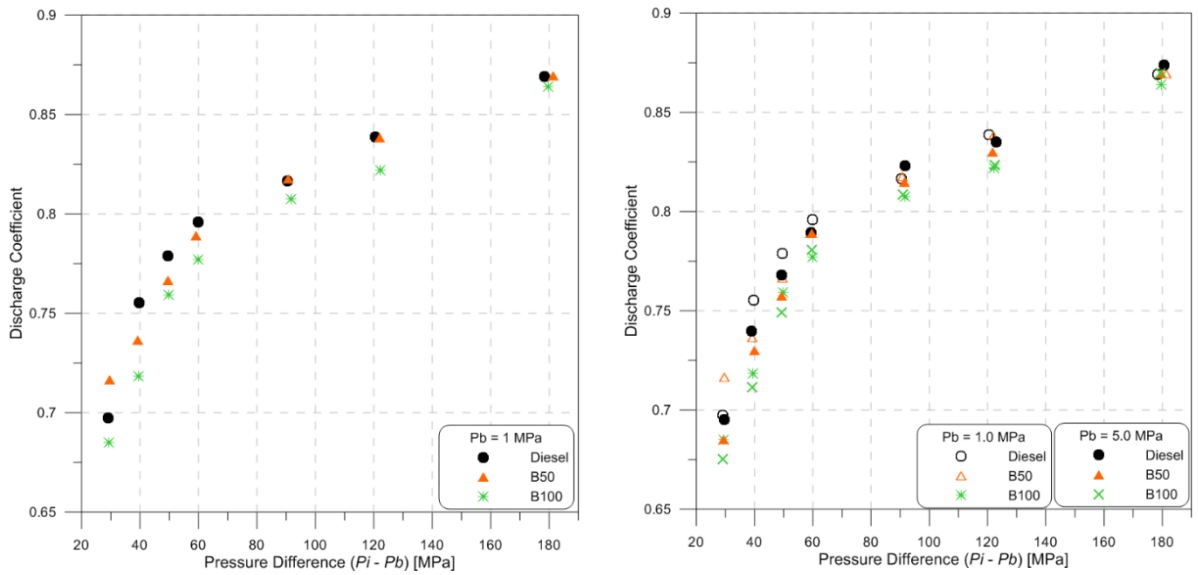

(a) *Pb* = 1 MPa (b) *Pb* = 5 MPa

Fig. 3.6 Impact of fuel blend on discharge coefficient, *Pi* = 30 to 180 MPa, 7 holes injector.

3.3.3 Discharge coefficient correlation

We tested two correlations. The first is an empirical correlation adapted from Payri et al. [10] by Dernotte [7]. Considering Eq. 3-1, the parameter *Cd*', *K1* and *K2* now depend on the nozzle geometry. This parameter changes with a type of nozzle. The superscripts *a*, *b*, *c*, *d* and *e* are obtained by minimizing the sum of square errors between the correlation and experiment (Table 3.2) and *Re* from Eq. 2-6.

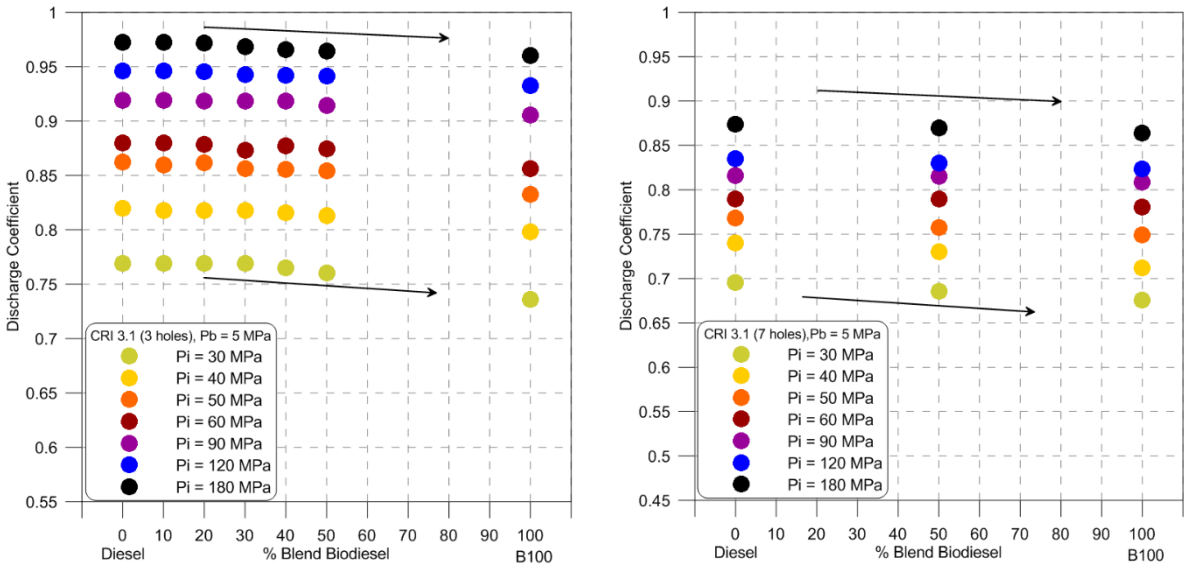

(a) 3 holes injector (b) 7 holes injector

Fig. 3.7 Discharge coefficient versus percentage of biodiesel blend, *Pi*=30–180 MPa.

$$Cd = Cd' + K1.v^a.\Delta P^b - \frac{K2.v^c.\Delta P^d}{Re^e} \quad (3\text{-}1)$$

Table 3.2: Payri et al. and Dernotte et al. correlation for estimating the discharge coefficient – values of the coefficients

Nozzle	*Cd'*	*K1*	*K2*	*a*	*b*	*c*	*d*	*e*	R^2
3 holes	1	-3.37	2.67E+5	-0.02	-0.73	-1.89	0.04	1.58	0.9794
7 holes	1	-1.03	2.67E+5	-0.02	-0.73	-1.89	0.04	1.58	0.9780

The second correlation is based on the work by Soteriou et al. [68] and Dernotte et al. [7] and applies the generalized Bernoulli principle:

$$\frac{1}{2}\rho_f.V_i^2 = P_i - P_{back} - \Delta P_c = \Delta P - \Delta P_c \quad (3\text{-}2)$$

Rearranging Eq. 2-2, Eq. 2-5 and Eq. 3-2, the expression of the discharge coefficient becomes:

$$Cd = \sqrt{\frac{\Delta P - \Delta P_c}{\Delta P}} \quad (3\text{-}3)$$

The Cd drop is assimilated as a pressure loss. If *Cd* =1, it means that there is no pressure loss (ΔP_c = 0). The pressure loss is determined by the following empirical correlation, where *A* and *B* are parameters for orifice type loss and *C* and *D* for viscous type loss:

$$\Delta P_c = A.v^D.\dot{m}_{th}^{(C.v+B)} \quad (3\text{-}4)$$

The coefficient values *A,B,C,D* are obtained by minimizing the sum of square errors between the correlation and experiment in Table 3.3.

Table 3.3: New correlation for estimating the discharge coefficient – values of the coefficients

Nozzle	*A*	*B*	*C*	*D*	R^2
3 holes	95.32	0.33	-0.02	-0.49	0.9864
7 holes	2496	1.24	-0.02	-0.49	0.9762

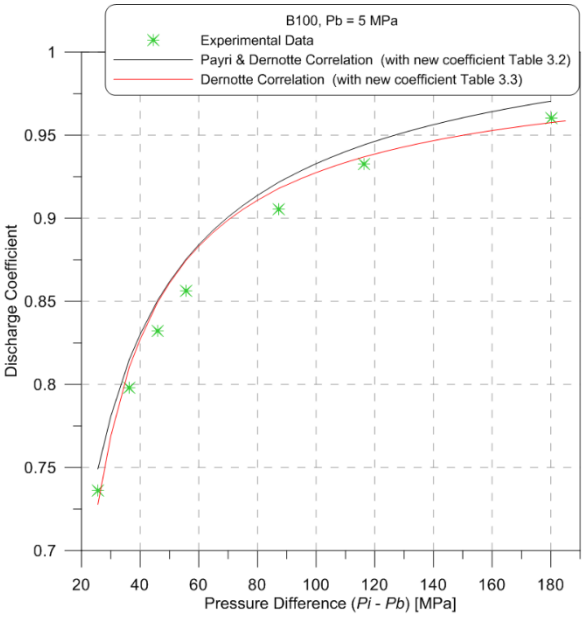

Fig. 3.8 Discharge coefficient: experimental results for B100 and correlation, B100, *Pi* = 30 to180 MPa, *Pb* = 5 MPa.

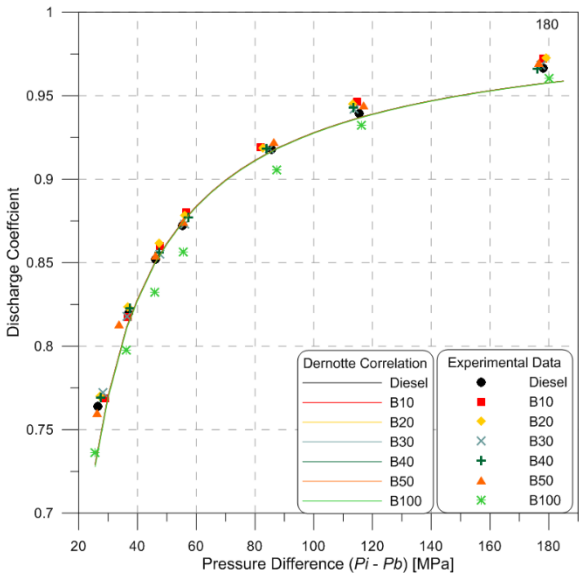

Fig. 3.9 Discharge coefficient: experimental results compared with Dernotte correlation, *Pi* = 30 to180 MPa, *Pb* = 5 MPa.

Fig. 3.8 compares the discharge coefficient correlation from Eq. 3-1 and Eq. 3-3 with experimental data for pure biodiesel, at pressure differences from 30 to 180 MPa. The average error is +/-2%. The result is better (+/-0.5%) for the second correlation on high pressure difference. The performance of this new correlation is similar (+/-2.0%) for all fuels (cf. Fig. 3.9).

Fig. 3.10 shows that cavitation starts to affect the discharge coefficient at 90 MPa for a *Pb* around 2.5 MPa. At 120 MPa, from 1 to 2.5 MPa of *Pb*, the discharge coefficient is definitely affected by cavitation. In fact for a same Reynolds number the Cd decreases when the back pressure decreases. At 5 MPa, the curves seem to follow the same trend. So the injector seems to be not affected by cavitations. So for the next experimentations we analyze only the

results under high back-pressure or for low injection pressure to avoid the cavitations phenomena.

The Dernotte correlation is plotted in Fig. 3.11 with all the experimental data. The x-coordinate is the Reynolds number and the y-coordinate is the discharge coefficient.

Considering these correlations obtained in non-cavitation conditions for each fuel, it can be stated that the discharge coefficient depends not only on the Reynolds number but also on the geometry and the fuel. Unlike Payri et al. [90], for a medium Reynolds number we observe a distinct curve for each fuel (Fig. 3.11). The new correlation with only four parameters gives a good estimation of the discharge coefficient for all fuels and for all experimental conditions without cavitation.

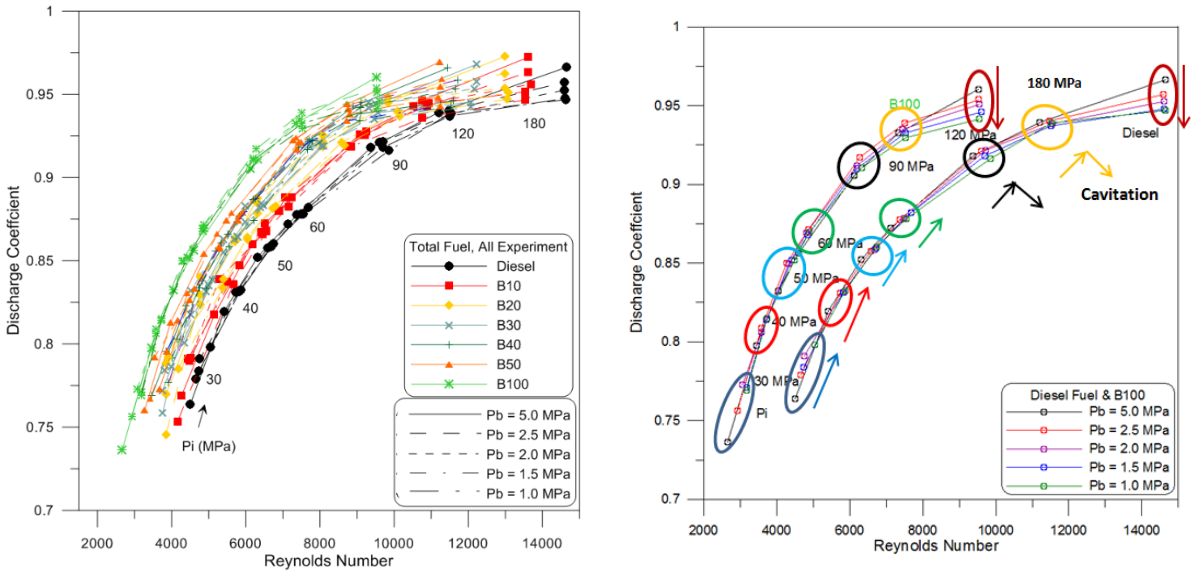

(a) Total data (b) B100 and Diesel

Fig. 3.10 Discharge coefficient versus Reynolds number for all the fuels, *Pi*=30 to 180 MPa, *Pb*= 1 to 5 MPa.

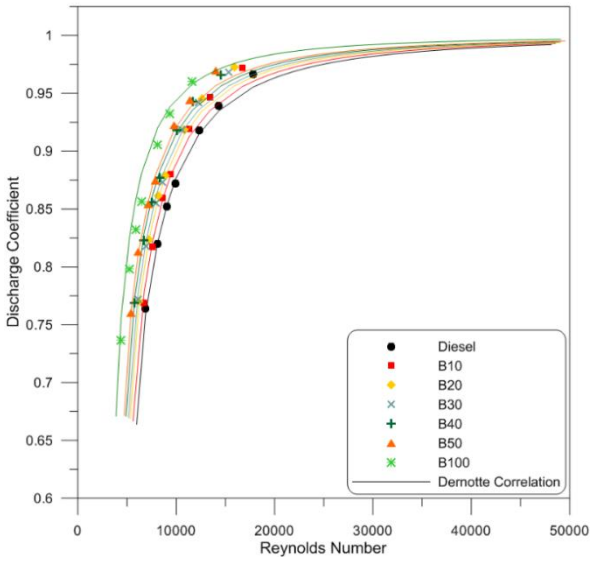

Fig. 3.11 Discharge coefficient versus Reynolds number for all the fuels, *Pi* = 30 to 180 MPa, *Pb* = 5 MPa.

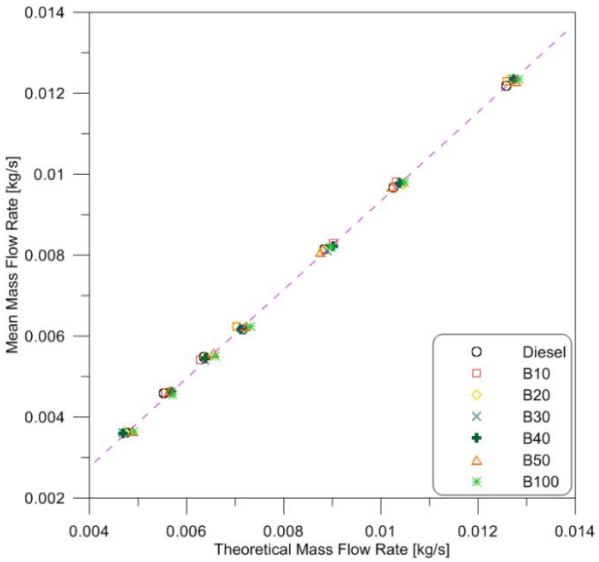

Fig. 3.12 Mean mass flow rate (experimental data) versus theoretical mass flow rate, *Pb* = 5 MPa.

The mass flow rate is exclusively a function of $\sqrt{2\rho\Delta P}$ or square root density [7, 10]. The decrease of 3.6% in the discharge coefficient with B100 is not visible on Fig. 3.12.

Fig. 3.13 compares the discharge coefficient correlation from Eq. 3-1 and Eq. 3-3 with experimental data for pure biodiesel with 7 holes nozzles, at pressure differences from 30 to 180 MPa. The average error is +/-2.1% for first correlation and +/-1.7% for the second correlation. The performance of this Dernotte correlation (shows in Fig.3.14) is good for prediction the discharge coefficient for injector CRI 3.1 (7 holes).

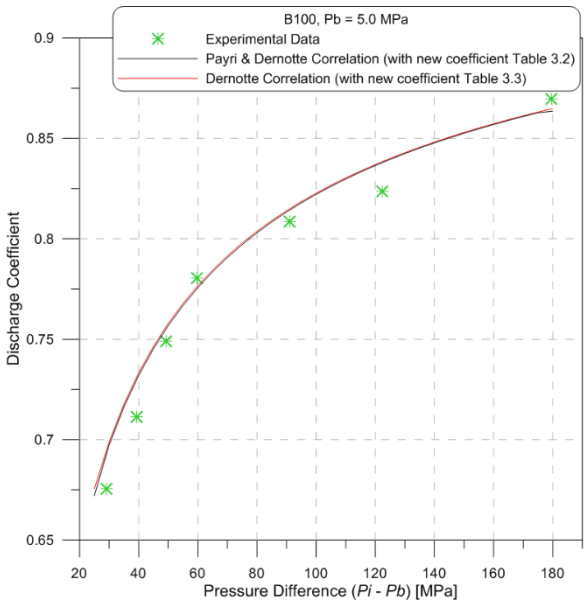

Fig. 3.13 Discharge coefficient: experimental results for B100 and correlation, B100, *Pi* = 30 to 180 MPa, *Pb* = 5 MPa.

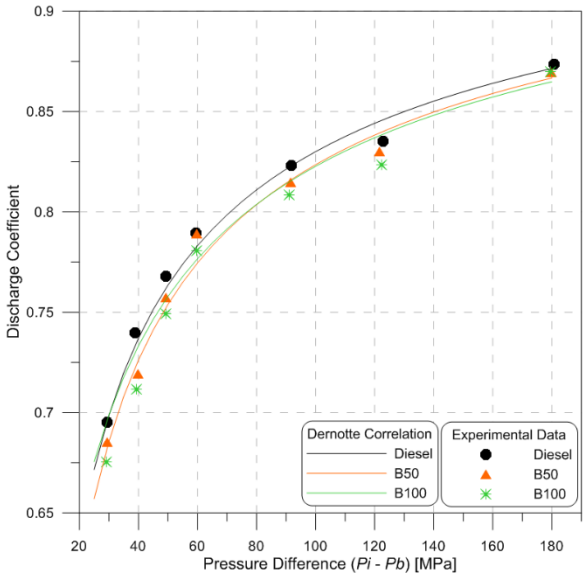

Fig. 3.14 Discharge coefficient: experimental results compared with Dernotte correlation, *Pi* = 30 to 180 MPa, *Pb* = 5 MPa.

3.4 Effect of fuel blend on spray injection behavior

3.4.1 Spray tip penetration analysis 84

The raw images were analyzed with a digital image processing program to determine the spray tip penetration *S* and spray angle θ. Fig. 3.15 shows the average image (average from 50 image) at t_i = 400, 993 and 2000 µs after injection when *Pi* = 90 MPa, *Pb* = 1 MPa. It can be noted that diesel fuel and biodiesel-blended fuel have a similar spray penetration but the penetration length with B100 is longer than the other fuels at the start of injection. These results are similar to those of Chen et al. [91].

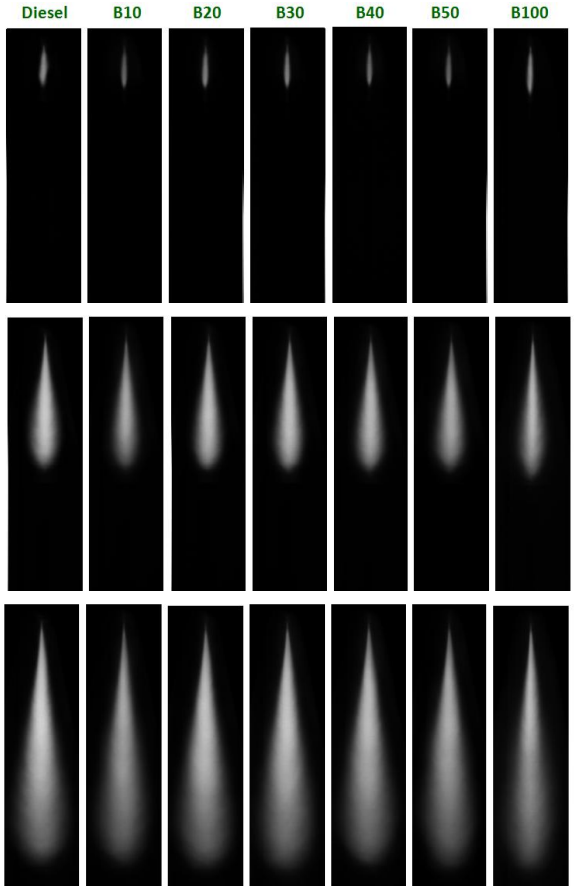

Fig. 3.15 Comparison of spray development : average image 400 µs, 993 µs, 2000 µs after injection, *Pi* = 90 MPa, *Pb* = 1 MPa.

In this work, the spray tip penetration can be calculated from analysis raw image using Matlab program. We use the Naber & Siebers correlation [57], Eq.1-9 (see chapter 1 section 1.4.1). The correlation is based on the mass and momentum conservation equations, applied to an ideal spray (where $\Delta P, \rho_a, \rho_f$ and *t* are data from operating conditions, *Do* data from the nozzle, angle θ from average θ in quasi-steady). The coefficient *a* from Naber & Siebers using 0.66 and Dernotte et al. [8] using 0.9, Dernotte et al. found the maximum error of +/- 5 %. For this work following Dernotte et al. we used *a* = 0.9 because we used similar

piezoelectric injector (Bosch CRI 3.1). For discharge of velocity, *Cv* is need to use Naber & Siebers correlation, this work assumes *Cv* = *Cd*, the area coefficient *Ca* = 1 for a conical orifice under "non-cavitating condition" as shown by Payri et al. [8]. So it's necessary to know the discharge coefficient. We test two definitions. The first is "*Cd* average". It is calculated by mean mass flow rate from the quasi-steady state period in 1000 to 2000 µs (*Cd* experiment of topic 3.3). The second is call "*Cd* variable" is calculated by instantaneous mass flow rate from start of actual injection period to actual end of injection to follow the transient phase.

$$1.Cd \text{ average (quasi-steady state)} = \frac{\dot{m}_{quasi-steady\ state}}{\dot{m}_{th}} \tag{3-5}$$

$$2.Cd \text{ variable} = \frac{\dot{m}_{measured}(t)}{\dot{m}_{th}} \tag{3-6}$$

The results shown in Fig. 3.16 are penetration length calculated with these two definitions of *Cd*. Using a variable Cd does not improve the model even during the transients phases. So for the remainder of the study we will use a constant Cd ("*Cd* average"). Fig. 3.17 shows the penetration length of diesel fuel, B50 and B100 from *Cd* average (quasi-steady state) and they are compared with the experimental data with the variables *Pi* from 30 to 150 MPa and Pback (*Pb*) 2.5 MPa. The differences can be explained by the modification of spray angle during the injection.

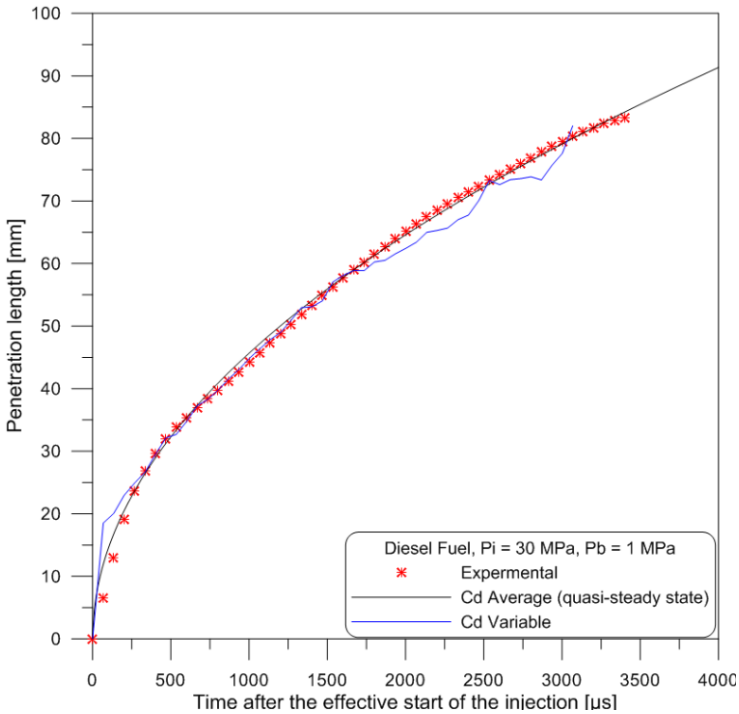

Fig. 3.16 The penetration length from experiment data and estimated values by change *Cd*.

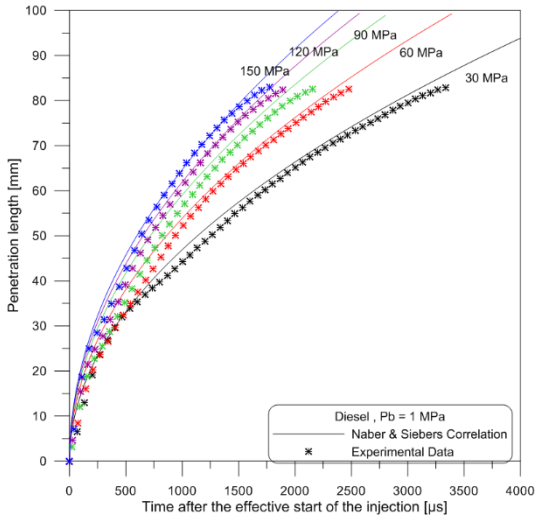

(a) Diesel, *Pb* = 1 MPa

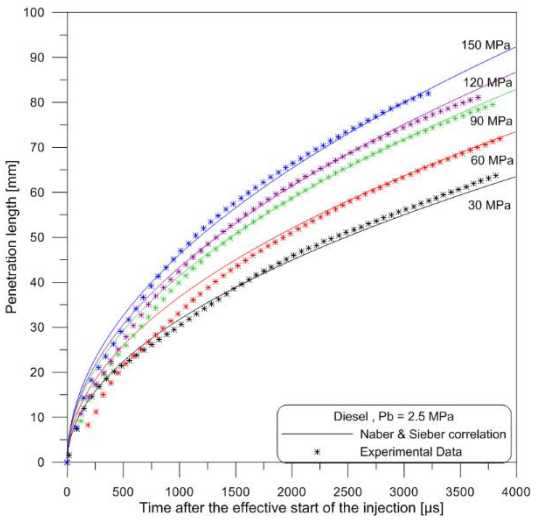

(b) Diesel, *Pb* = 2.5 MPa

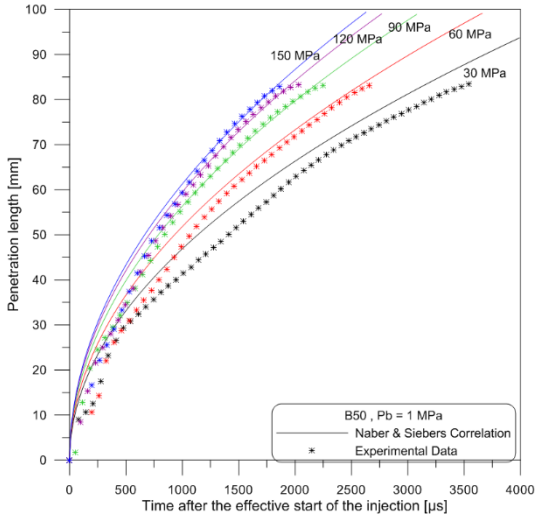

(c) B50, *Pb* = 1 MPa

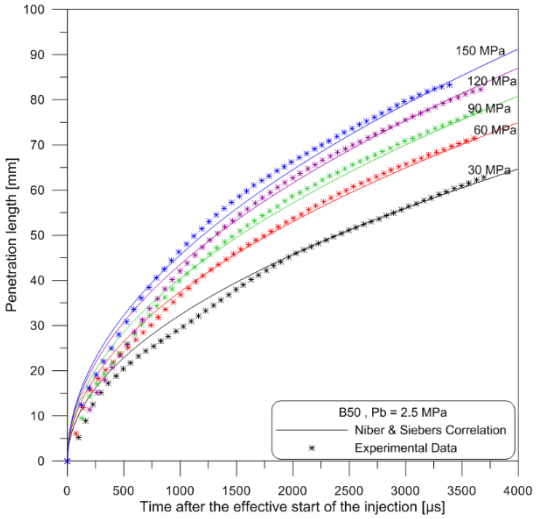

(d) B50, *Pb* = 2.5 MPa

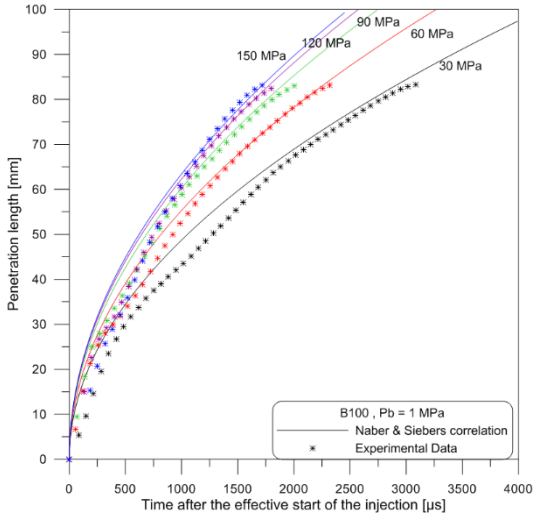

(e) B100, *Pb* = 1 MPa

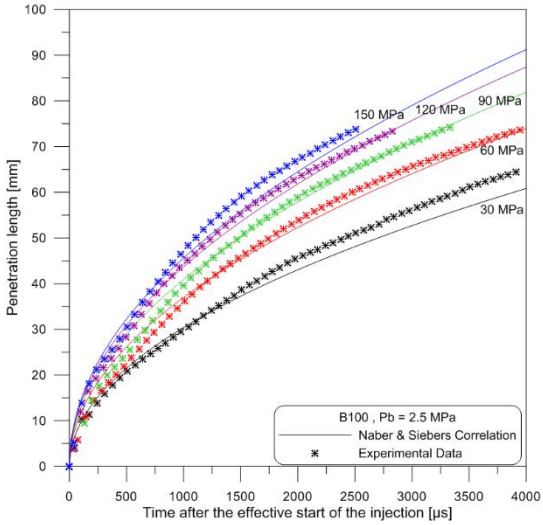

(f) B100, *Pb* = 2.5 MPa

Fig. 3.17 The penetration length from experiment data and estimated values, *Pi* = 30 to 150 MPa, *Pb* = 2.5 MPa.

3.4.2 Results of Spray tip penetration

The effect of blended fuels on the spray behavior is shown in Fig. 3.18 (a, c). This figure shows the time evolution of penetration length at *Pi* = 30, 120 MPa and *Pb* = 1 or 2.5 MPa for all fuels. For the blended fuel and Diesel the penetration lengths are similar. In line with Fig. 3.18 only B100 has a slightly different behavior (Fig. 3.18 (b, d)), with a higher penetration length. These results are the same as those of Desantes et al. [50], Chen et al. [91], Bang et al. [92] and Gao et al. [93].

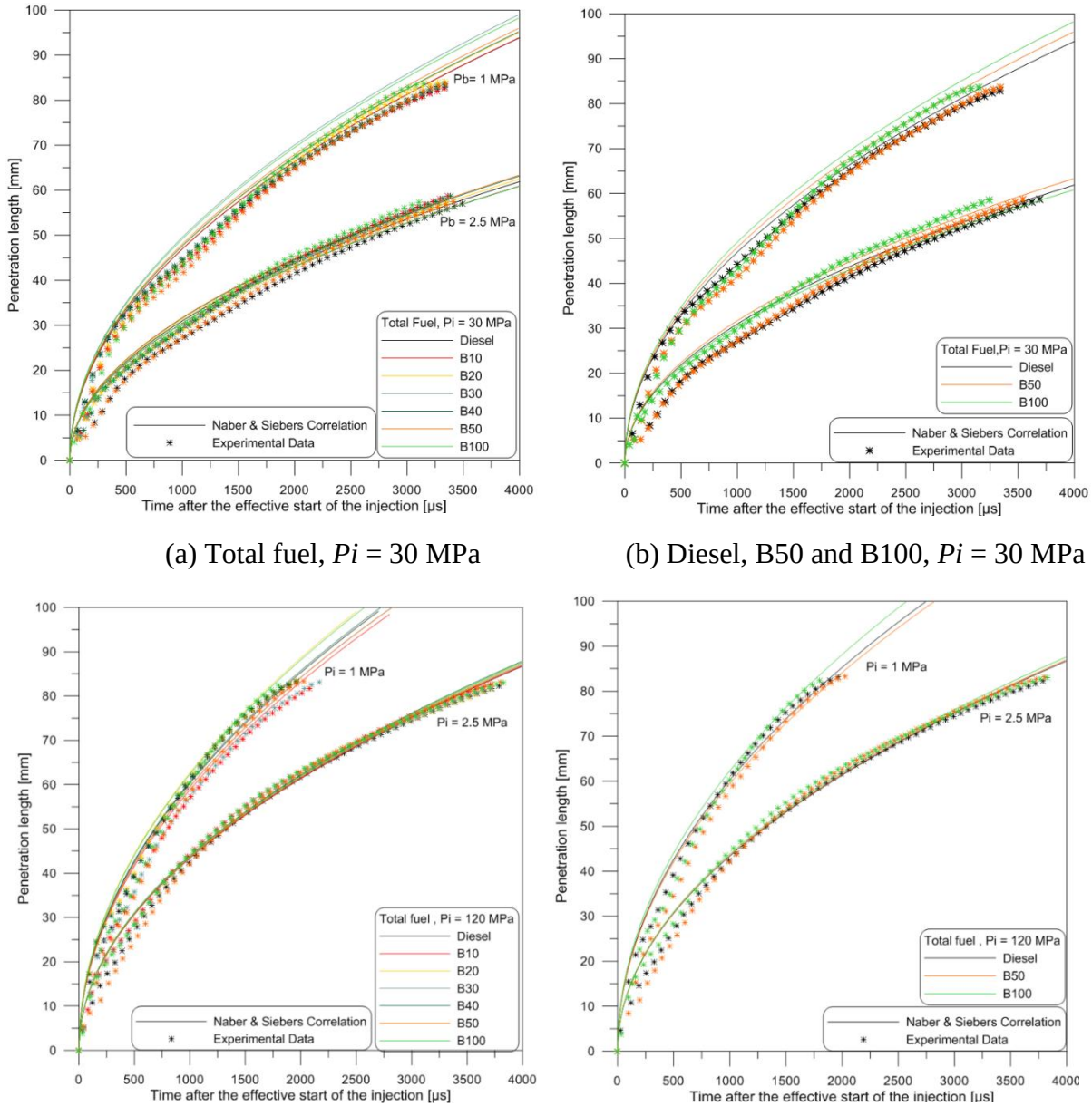

(a) Total fuel, *Pi* = 30 MPa (b) Diesel, B50 and B100, *Pi* = 30 MPa

(c) Total fuel, *Pi* = 120 MPa (d) Diesel, B50 and B100, *Pi* = 120 MPa

Fig. 3.18 The penetration length from experiment data and estimated values of total fuel.

3.4.3 Spray angle analysis

The differences observed between the correlation and the actual measurement of the penetration lengths are due that the assumption of a constant spray angle over time which is not experimentally observed. Here we invert the same correlation to determine the time evolution of the spray angle as a function of the penetration depth.

The expression becomes:

$$tan\frac{\theta(t)}{2} = \frac{D_0}{a.Cd}.\frac{\rho_f}{\sqrt{2\Delta P.\rho_a}}.\frac{1}{t}.\left[\left(\frac{Cd.\sqrt{2\Delta P}}{S(t).\sqrt{\rho_f}}.t\right)^{2.2} - 1\right]^{\frac{1}{1.1}} \quad (3\text{-}7)$$

In this case the model is extended to conditions where the angle and flow rate are not constant. However the spray is considered as a succession of stationary states.

Two definitions of *Cd* were again tested ("C*d* average" and "C*d* variable") and the experimental spray angle was measured using an image processing program (chapter 2 section 2.3.2)

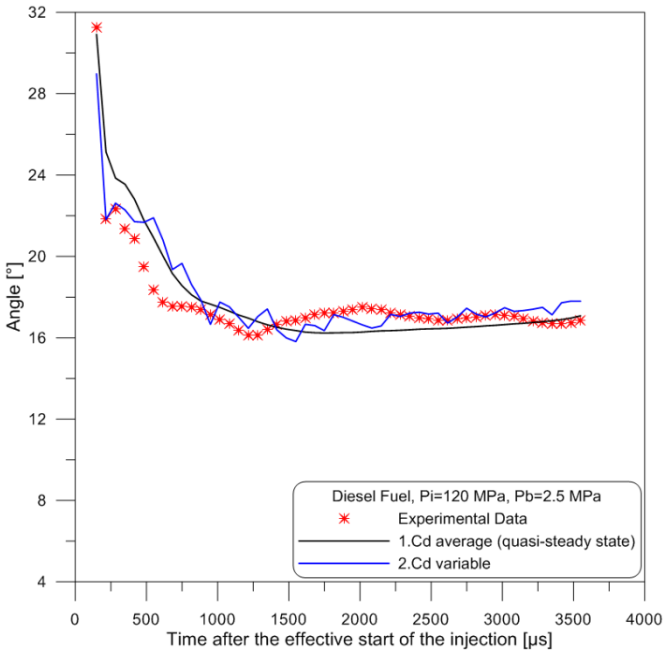

Fig. 3.19 The spray angle from experimental data and estimated values by changing *Cd.*

Fig. 3.19 shows the impact of choice *Cd* on the spray angle. "Cd variable" gives better result. But the gain is not enough important and the curve shows more fluctuations. The choice of *Cd* modifies the average angle by +/-7.3%. So it is possible to obtain a good estimation of spray angle with Naber & Siebers correlation with a constant *Cd*.

Fig. 3.20 shows that the correlation of Naber & Siebers [57] with a constant *Cd* and a=0.9 gives a good estimation of average angle for the steady phase and maximum angle for

transient phase with an accuracy of 12.3%. The only measurement of penetration length is sufficient to estimate the spray angle. This estimation is less sensitive to image processing error because the determination of the spray tip penetration is less sensitive to threshold than θ.

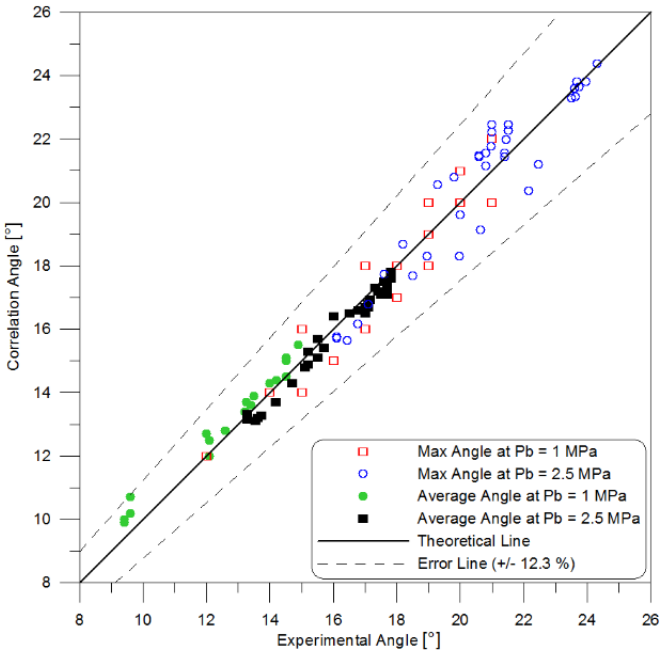

Fig. 3.20 Experimental angle versus correlation angle, *Pb* = 1 and 2.5 MPa.

Fig. 3.21 shows the experimental and estimated time evolution of the spray angle. There are two distinct phases: the transient phase and the constant phase over 1800 µs. During the transient phase, the spray angles are different for each fuel. For the constant phase the spray angles are similar for blended fuel and Diesel at all back-pressures and pressure differences. These results are the same as literature values (Desantes et al. [50], Chen et al. [91]) and Gao et al. [93]So the viscosity has a bigger impact during the transient phase.

These last point is visible on the next figures :

- Fig. 3.22 shows the maximum spray angle during the transient phase versus the injection pressure. The angle increases when the injection pressure increases. Fig. 3.23 shows that the angle tends to decrease when the fraction of biodiesel increases. This trend is stronger for low back-pressure and low injection pressure.
- Fig. 3.24 shows the average spray angle during the steady phase versus the percentage of Biodiesel in Diesel. During this phase, the average angles are very similar. Only the spray angle with B100 is smaller.

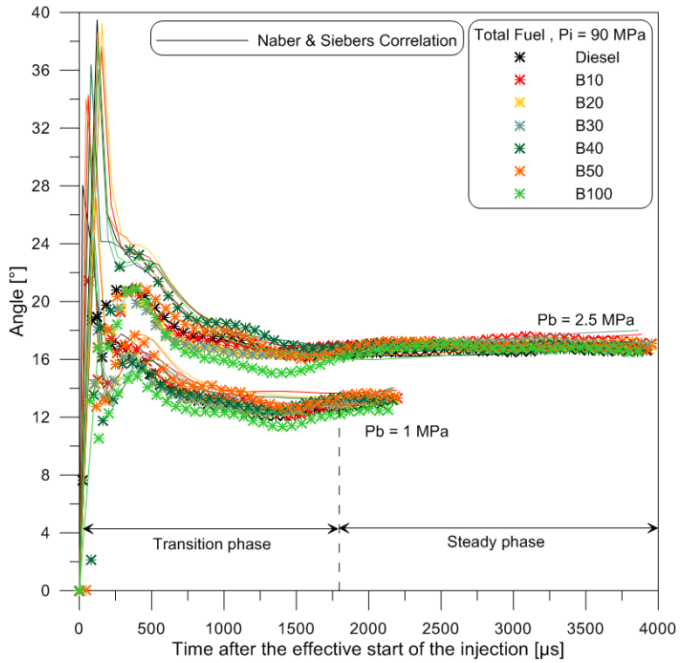

Fig. 3.21 The spray angle from experimental and estimated fuel values, *Pi* = 90 MPa, *Pb* = 1 and 2.5 MPa.

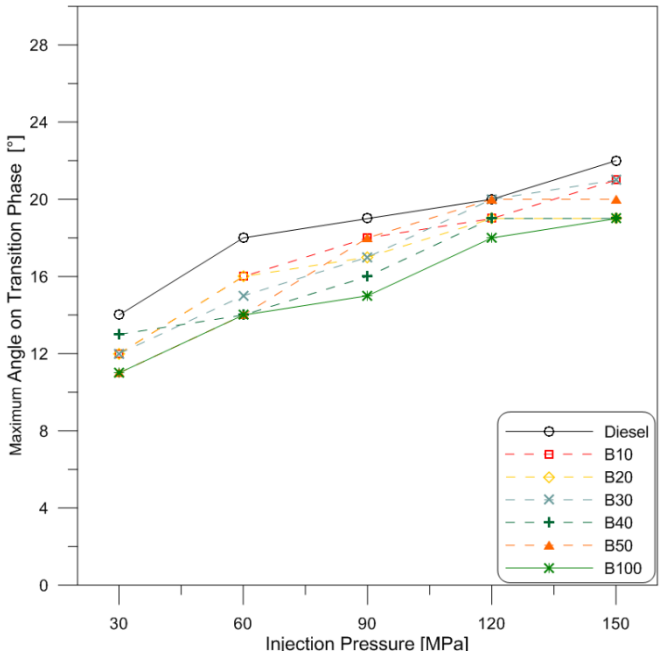

Fig. 3.22 Maximum angle in transition phase (t_i < 1800 µs), *Pb* = 1 MPa.

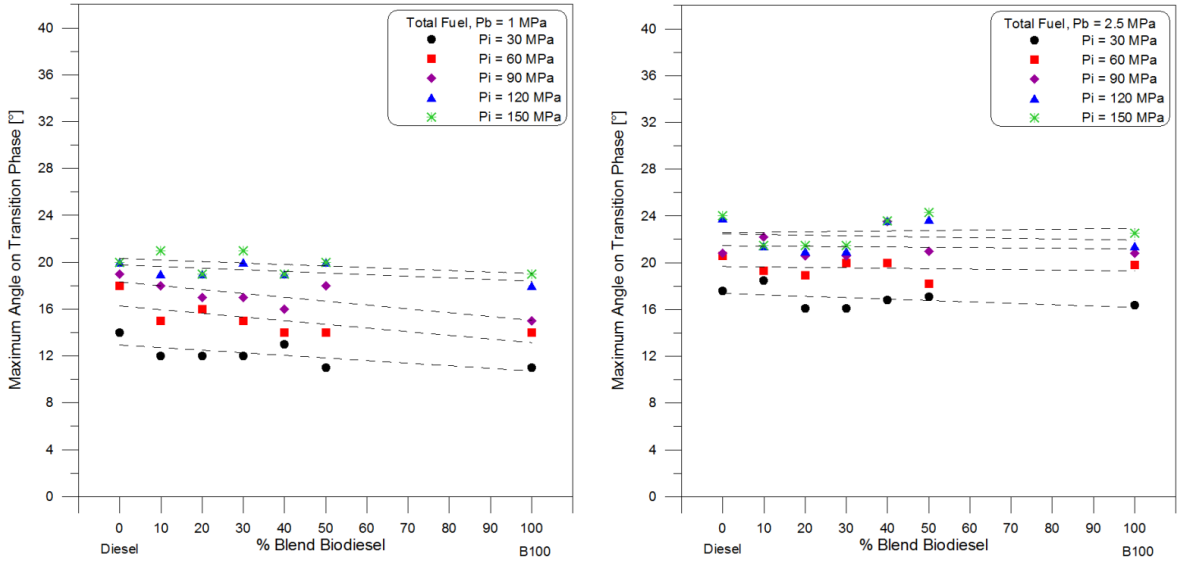

(a) *Pb* = 1 MPa (b) *Pb* = 2.5 MPa

Fig. 3.23 Maximum angle in transition phase versus percentage of biodiesel blend.

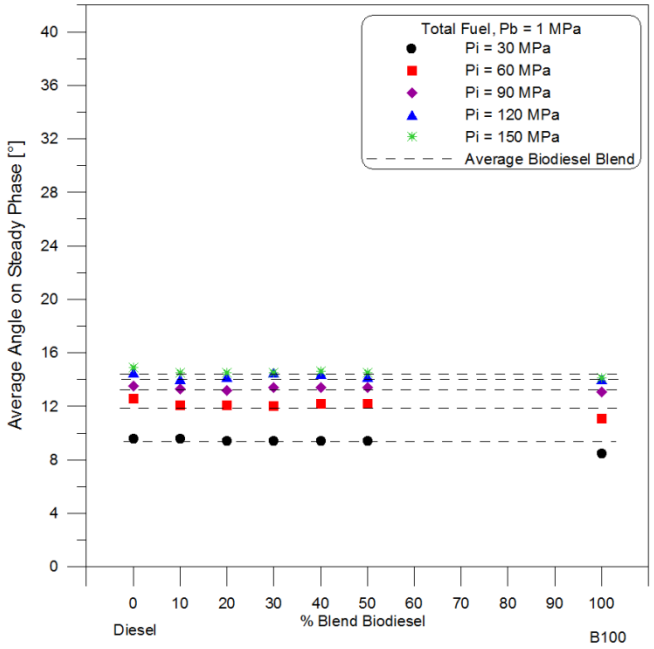

Fig. 3.24 Average angle in steady phase versus percentage biodiesel blend, *Pb* = 1 MPa.

3.5 Conclusions

The study of the influence of biodiesel and diesel blends on the injection rate and spray injection behavior in non-vaporizing conditions was conducted using an injector with three or seven conical convergent orifices. Measurements of the mass flow rate and visualization of the spray with diesel fuel, biodiesel blends and Biodiesel (B100) were made. The conclusions of this study are summarized as follows:

By increasing the fraction of biodiesel the closing delay increases (20-70 µs for biodiesel blends and 70-170 µs for B100).

By increasing the fraction of biodiesel in the blend the discharge coefficient does not change significantly when used injector CRI 3.1 (3 holes) and when used injector CRI 3.1 (7 holes) the discharge coefficient tends to slightly decrease especially at low injection pressure. However, with B100 the discharge coefficient tends to be lower than that of diesel and biodiesel blended fuels.

The spray penetration of diesel fuel and biodiesel blended fuels is similar while with B100, the spray penetration is higher than with diesel and biodiesel blended fuels. This difference is the result of a smaller spray angle with B100. The fraction of Biodiesel seems to have a slight influence during the transient phase. For low back and injection pressures the maximum spray angle decreases with the percentage of Biodiesel in the fuel.

In this work the fraction of biodiesel in the fuel did not exceed 50% which is in line with the use of biodiesel in many countries (where a biodiesel fraction of 2-20% is mandatory). The results show that increasing the fraction of biodiesel in the blend does not have a significant influence on the discharge coefficient or on macroscopic the spray behavior.

❖ Conclusions (version français)

L’'influence de la quantité de biodiesel dans les mélanges de carburant (diesel-biodiesel) sur le débit injecté et le comportement du spray a été réalisée dans des conditions de non-évaporation en utilisant un injecteur à trois ou sept orifices coniques convergents. Différentes mesures du débit massique et l’analyses des images du spray obtenues avec différents carburants (diesel, mélanges, pur biodiesel (B100))ont été effectués. Les conclusions de cette étude sont résumées comme suit:

En augmentant la fraction de biodiesel le retard de fermeture de l’injecteur augmente de 20 à 70 ms pour les mélanges de biodiesel et de 70 à 170 ms pour B100.

En augmentant la fraction de biodiesel dans le mélange le coefficient de décharge pour l’injecteur CRI 3.1 (3 trous) reste relativement constant mais ce dernier tend à diminuer légèrement en particulier sur la pression d'injection faible pour l’injecteur 7 trous. Cependant, avec le B100 le coefficient de décharge est toujours inférieur aux autres carburants

La pénétration du spray pour le Diesel ou les mélanges est similaire tandis qu'avec B100 la pénétration est supérieure. Cette différence est le résultat d'un angle de pulvérisation plus petite avec le B100. La fraction de biodiesel semble avoir une légère influence pendant la phase transitoire. Pour des faibles contre-pressions ou de faibles pressions d'injection l'angle de spray maximal diminue avec le pourcentage de biodiesel dans le carburant.

Dans ce travail, la fraction de biodiesel dans le carburant ne dépasse pas 50%, ce qui est en lien avec l'utilisation du biodiesel dans de nombreux pays (où une fraction de biodiesel de 2-20% est obligatoire). Les résultats montrent que l'augmentation de la fraction de biodiesel dans le mélange n'a pas une grande influence sur le coefficient de décharge ou sur le comportement macroscopique du spray pour des températures ambiantes supérieures à 15°C.

CHAPTER 4

Influence of fuel blends and negative temperature on behavior of injector and spray

The new standards involve problems related to cold-start, namely evaluation of post-treatment strategies and EGR at low temperature. The regulations concerning the quality of cold start at −7°C will become increasingly stringent [4]. During start-up of the engine under cold temperatures, conditions can be different when Biodiesel is used due to the low fuel injection pressure and the high cloud point and high pour point. It is consequently of interest to understand the behavior of the injector under cold conditions when operating with Biodiesel and the impact on the combustion process. The results are presented in five parts:

- The fuel used and experimental conditions.
- The effect of fuel blend properties on injection rate.
- The effect of fuel blend on pressure evolutions for different temperatures.
- The effect of fuel blend properties on discharge coefficient and discharge coefficient correlation for cold conditions.
- The effect of fuel blend properties on spray injection behavior: spray tip penetration, spray angle.

Introduction (version français)

Les nouvelles normes concernant les problèmes liés à démarrage à froid, à savoir l'évaluation des stratégies post-traitement et l'EGR à basse température apparaissent. Les règlements concernant la qualité de démarrage à froid à -7 °C deviendront de plus en plus strictes [4]. Lors du démarrage du moteur, les températures froides et les faibles pressions d'injection peuvent être problématiques lorsque le biodiesel est utilisé en raison d'un point trouble et point d'écoulement et de sa viscosité plus élevés. Il est donc intéressant de comprendre le comportement de l'injecteur à froid avec du biodiesel. Les résultats sont présentés en cinq parties:

- Le carburant utilisé et les conditions expérimentales.
- L'effet des propriétés du carburant (mélange ou pas) sur le taux d'introduction.
- L'effet de la fraction de biodiesel dans le carburant sur les évolutions de pression tube pour différentes températures.
- L'effet des propriétés du carburant sur le coefficient de décharge et détermination d'une corrélation entre coefficient de décharge et viscosité cinématique pour les conditions froides.
- L'effet des propriétés du carburant sur le comportement du spray: longueur et angle de spray.

4.1 Fuels used and experimental cold conditions

The five fuels chosen in this study were Diesel, Winter diesel and mixtures with rapeseed Biodiesel. They are referred to in this study as follows: Diesel, Winter diesel, B100 (100% biodiesel produced from rapeseed), B20 (diesel 80%, biodiesel 20%), B50 (diesel 50%, biodiesel 50%) and B50(W) (winter diesel 50%, biodiesel 50%). We tested this fuel which is doubly interesting because of its viscosity identical with that of B20 and of its density identical with that of diesel whatever the temperature (Fig. 2.21). The fuel properties were measured at the operating temperature and at ambient temperature 8°C, 0°C, −5°C, and −8°C (very close to the Cold Filter Plugging Point (CFPP) of Biofuel). The fuel properties are listed in Table 4.1. The various settings and measurement protocols follow those already exposed in Chapter 3. To compare each condition, a measurement protocol is followed to be sure that during the 50 strokes, all the parameters (temperature, pressure) are constant. The Fig. 4.1 shows that the stroke by stroke variations of injection pressure, injected mass or fuel temperature are very low.

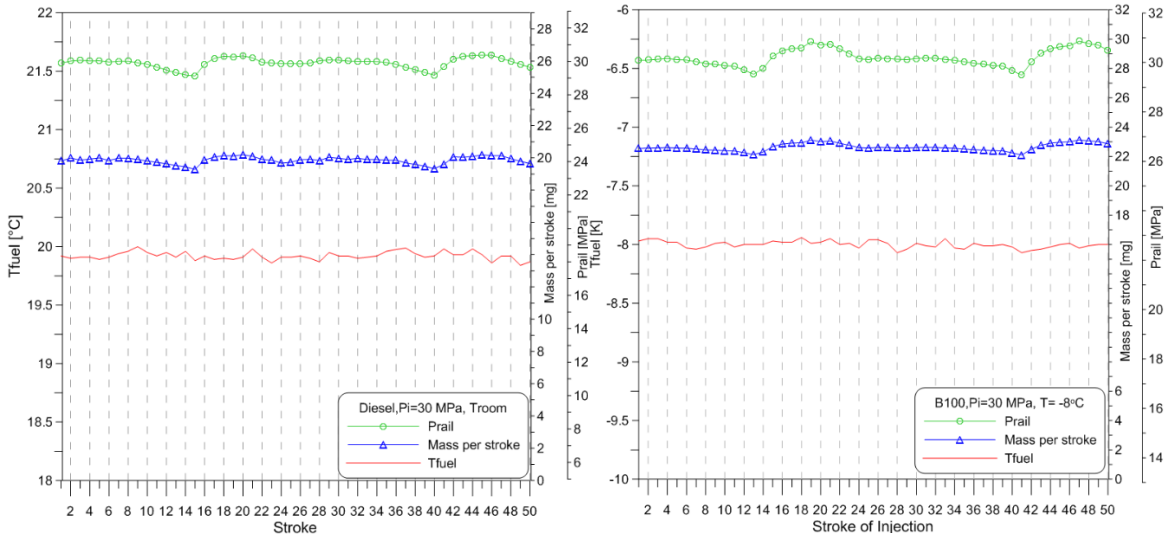

(a) Diesel fuel, Troom. b) B100, T = −8 °C.

Fig. 4.1 Tfuel, mass and Prail per stroke.

The injection pressure, *Pi*, varied from 30 to 60 MPa (typical of start-up of the engine). The back-pressure, *Pb* varied from 1 – 2.5 MPa for studying injection rate behavior and for the visualizations *Pb* varied from 1.2 – 1.7 MPa for a variation in density from 14.3 – 20.13 kg/m^3 The effect of cavitation is here avoided by use conical nozzle injector and low injection pressures.

Table 4.1: Fuel matrix in standard conditions.

T(°C)	Density, ρ, (kg/m^3)						Kinematic viscosity, v (mm^2/s)					
	Diesel	Winter diesel	B20	B50	B50(W)	B100	Diesel	Winter diesel	B20	B50	B50(W)	B100
-8	855.1	853.5	863.3	877.4	876.4	900.2	10.38	11.43	11.63	15.42	14.36	19.72
-5	852.3	851.4	860.6	874.9	874.3	897.7	8.95	9.65	10.07	12.64	12.11	16.04
0	848.8	847.4	857.1	871.1	870.8	894.1	7.51	8.04	8.24	9.95	10.09	13.03
8	843.2	842.4	851.4	865.5	865.1	888.3	5.85	6.19	6.40	7.68	7.63	9.97
20	834.7	834.1	842.9	856.9	856.5	879.6	4.23	4.43	4.61	5.49	5.53	7.05

4.2 Effect of cold temperature and blended fuel properties on injection rate

4.2.1 Mass and pressure evolution

In chapter 3 we showed that the increase in viscosity had an impact on the closing delay. This aspect is confirmed by results at low ambient temperature (Fig 4.2). The opening delay remains constant around the 260 µs – 350 µs while closing delay increases linearly as a function of viscosity (Fig 4.3). The closing delay increases with the biodiesel content, with the B100 fuel showing the biggest delay.

The fuel viscosity increases with a decrease in temperature. So the closing delay increases and leads to an increase in injection duration like reported by Kegl [94].

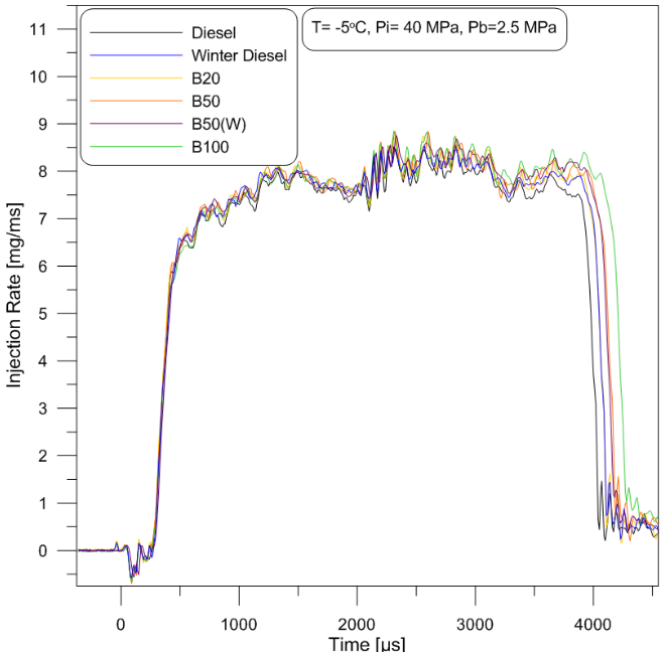

Fig. 4.2 Injection rate, T = -5°C.

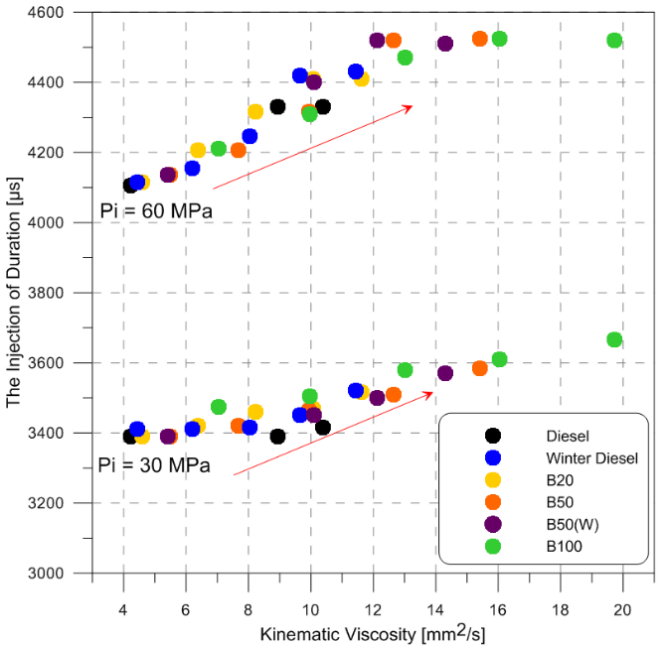

Fig. 4.3 The duration of injection

Two points can explain the increase in injected mass. First point, in cold conditions the fuel density increases, and so an increase in the mass flow is expected [93]. Second point in cold conditions the fuel viscosity increases and causes the increases of the duration of injection and hence the quantity of injected fuel. This result is illustrated in Fig. 4.4 where it is shown that the total fuel mass injected increases when the fuel temperature decreases. The second point is main explication, for the same viscosity (in the present case, 10 mm^2/s), a change in the density does not lead to an increase in the total mass of fuel injected.

The temperature variation or the percentage of biodiesel has no impact on the displacement of the valve of the control chamber. It always goes down at the same time explaining that hydraulic delay remains relatively constant. Decreasing the temperature still affects the amplitude of the pressure fluctuations. Lower temperatures over these fluctuations are damped (see Fig. 4.5). The fluctuation amplitude also depends on the type of fuel. Injections with Winter diesel generate pressure fluctuations with larger amplitudes. For the next analysis of pressure data (*Pline-Pi*), we used *Pline-Pi* averaged from 50 injections.

Fig. 4.6 shows mean mass flow rate and *Pline-Pi* of Winter diesel data from injection rate and visualization experiment at injection pressure 30 MPa temperature -8^oC. It can be observed that the amplitudes are not the same. There are risks that the mass flow rates different between these two measurements and the *Cd* determined on the first experimentation (injection rate) is probably not valid for the visualization.

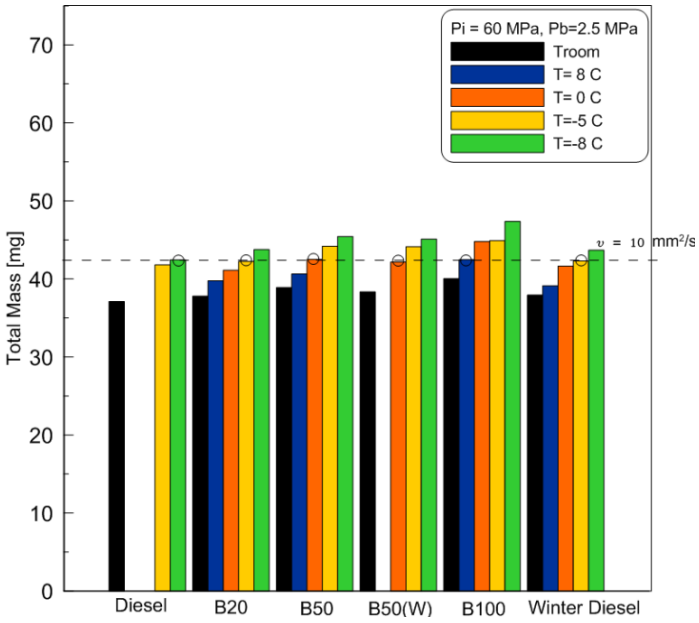

Fig. 4.4 Total mass injected at *Pi* = 60 MPa.

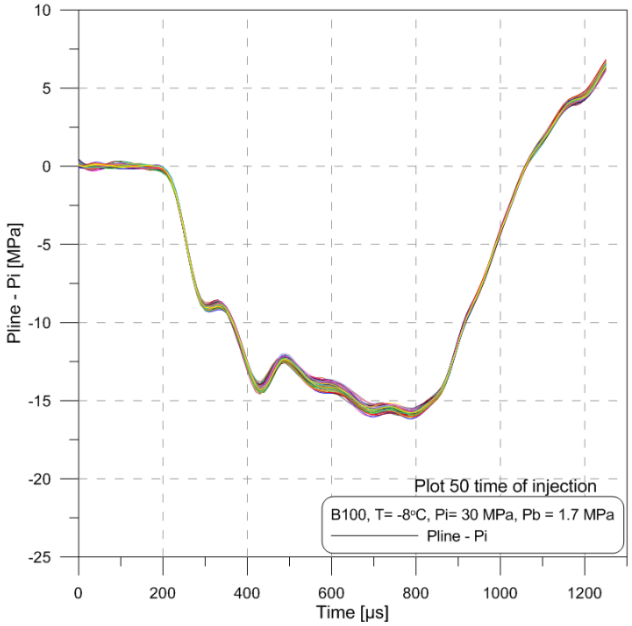

Fig. 4.5 *Pline – Pi*, plot 50 time of injection, T= -8°C, *Pi*= 30 MPa, *Pb*= 1.7 MPa.

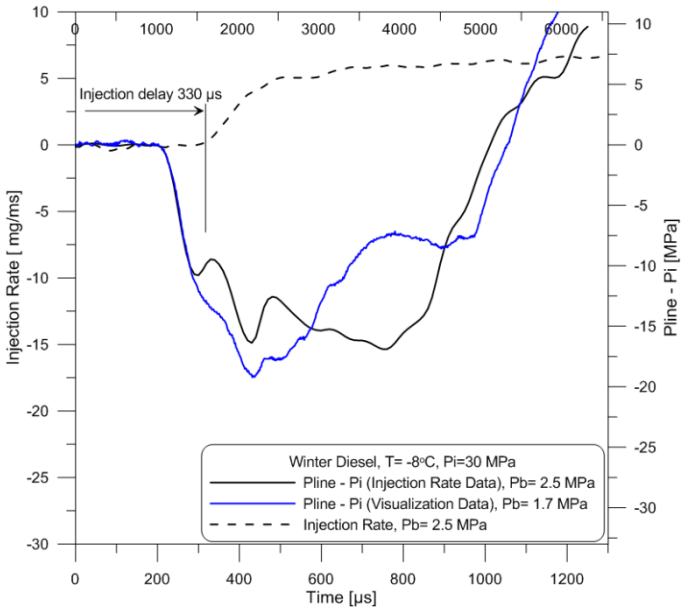

Fig. 4.6 Mean mass flow rate and *Pline - Pi* (average) data from injection rate and visualization experiment ,*Pi*= 30 MPa.

Fig. 4.7 shows the mean mass flow rate and variation of pressure upstream of the injector for winter diesel and B100 at *Pi* =30 MPa. The pressure drop is caused by the opening of the valve. The acoustic pressure waves are perturbed again (local maximum pressure around 300 µs) by now the lifting of the needle. With B100 at low temperature, the pressure decrease is slower and the lifting of the needle is slightly delayed which explains the 10 µs (Fig. 4.7(e)) increase in hydraulic delay. This shift is greater on closing than on opening, as shown on Fig.4.8(c) (injection rate).

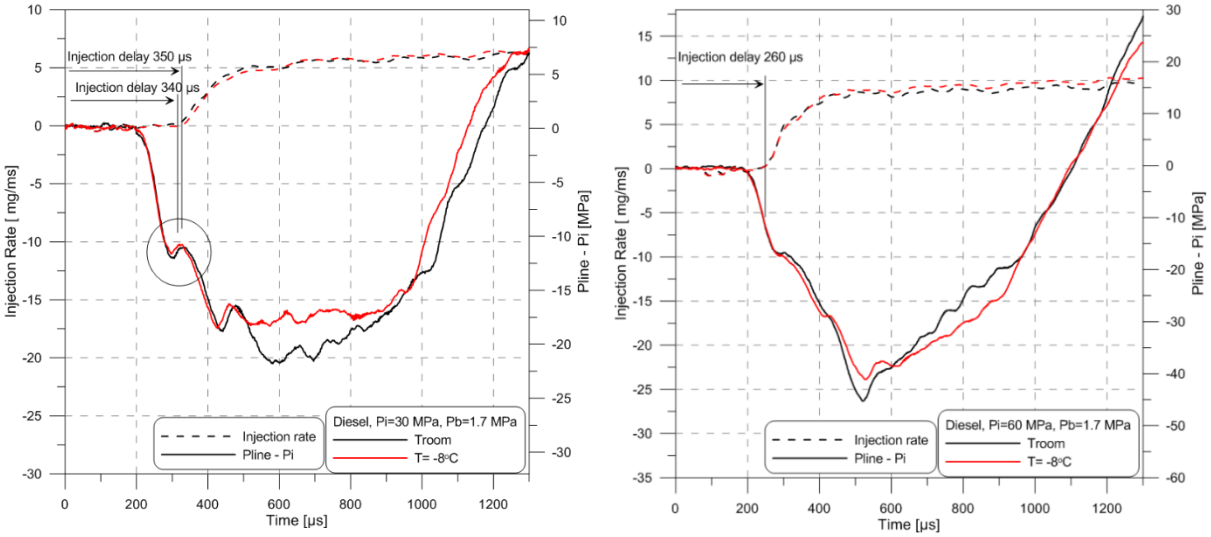

(a) Diesel, *Pi* = 30 MPa

(b) Diesel, *Pi* = 60 MPa

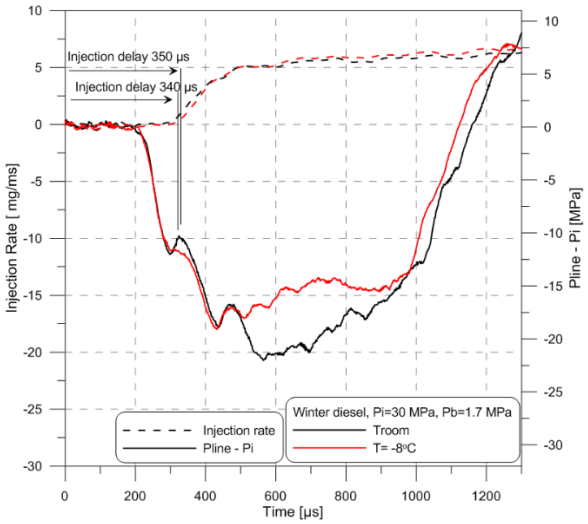

(c) Winter diesel, *Pi* = 30 MPa

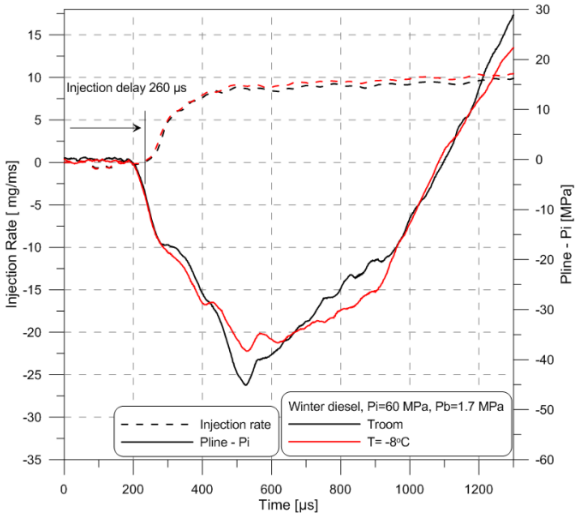

(d) Winter diesel, *Pi* = 60 MPa

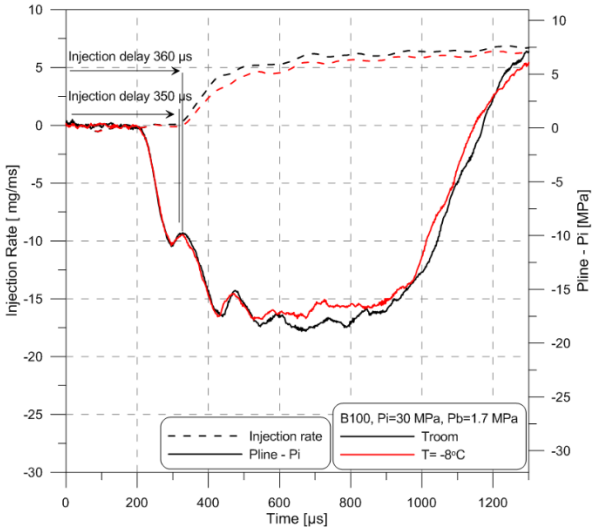

(e) B100, *Pi* = 30 MPa

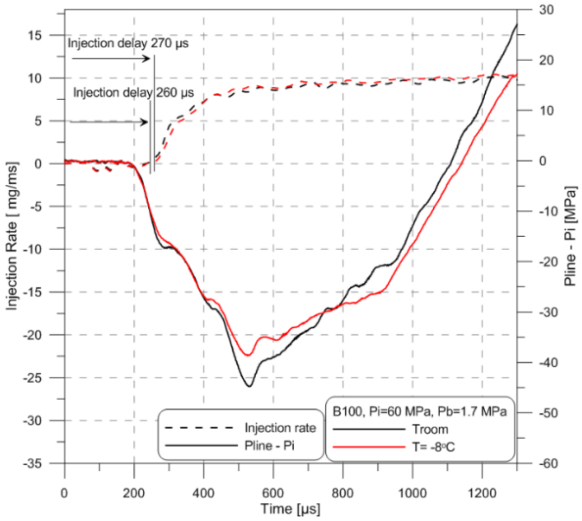

(f) B100, *Pi* = 60 MPa

Fig. 4.7 Mean mass flow rate and *Pline – Pi*, *Pb* = 1.7 MPa.

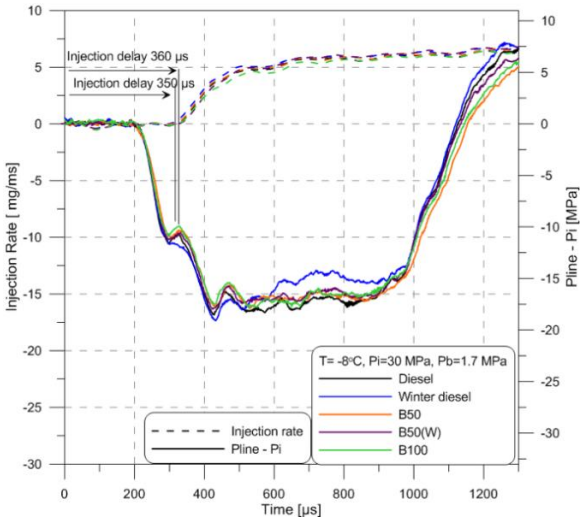

(a) All fuel

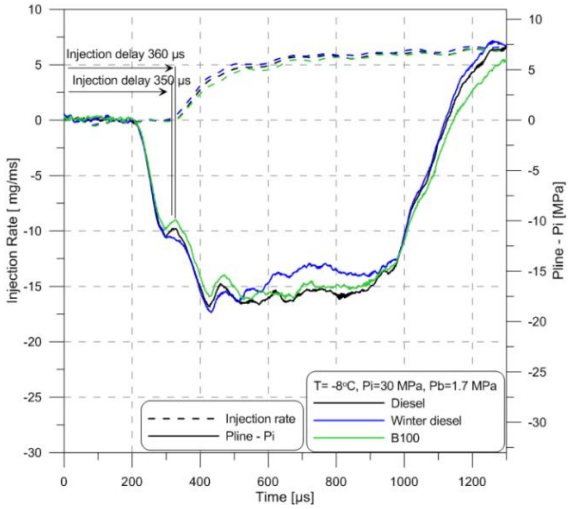

(b) Diesel, Winter diesel, B100

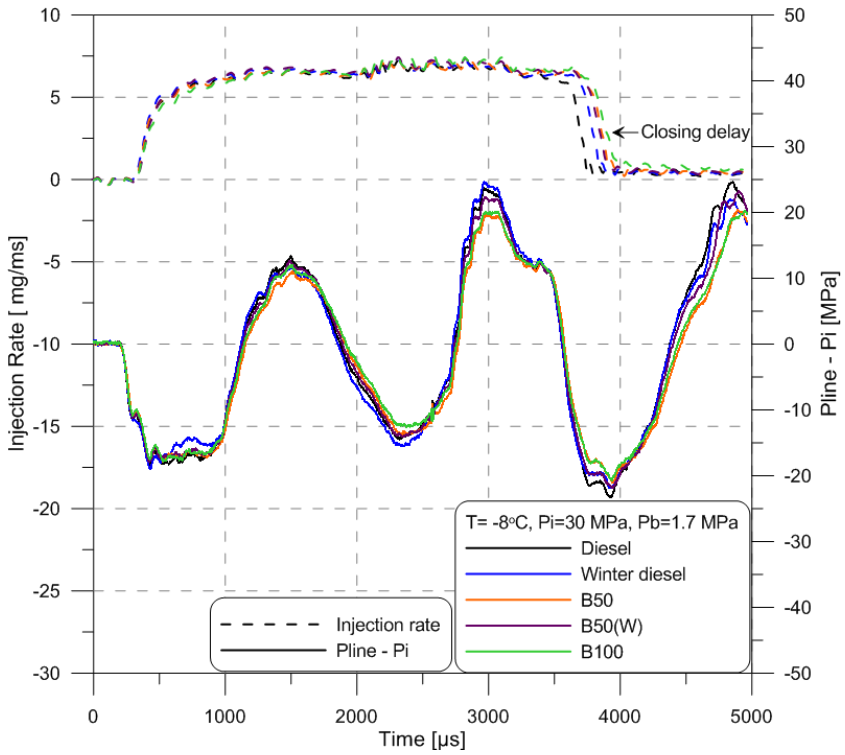

(c)

Fig. 4.8 Mean mass flow rate and *Pline – Pi*, T = -8°C, *Pi*=30 MPa, *Pb*= 1.7 MPa.

When comparing the injection pressures 30 and 60MPa for B100 (Fig. 4.7 (d) & (f)), the hydraulic delays are the same. For Diesel (Fig. 4.7 (a) & (b)) and Winter diesel (Fig. 4.7 (c) & (d)) they do not have the increase of hydraulic delay for 60MPa. As shown on Fig. 4.9, when the injection pressure is increased to 60 MPa, the peak pressure of B100 in the

maximum period is slightly lower than that of the other fuels. The difference on closing delays does not depend on the injection pressure.

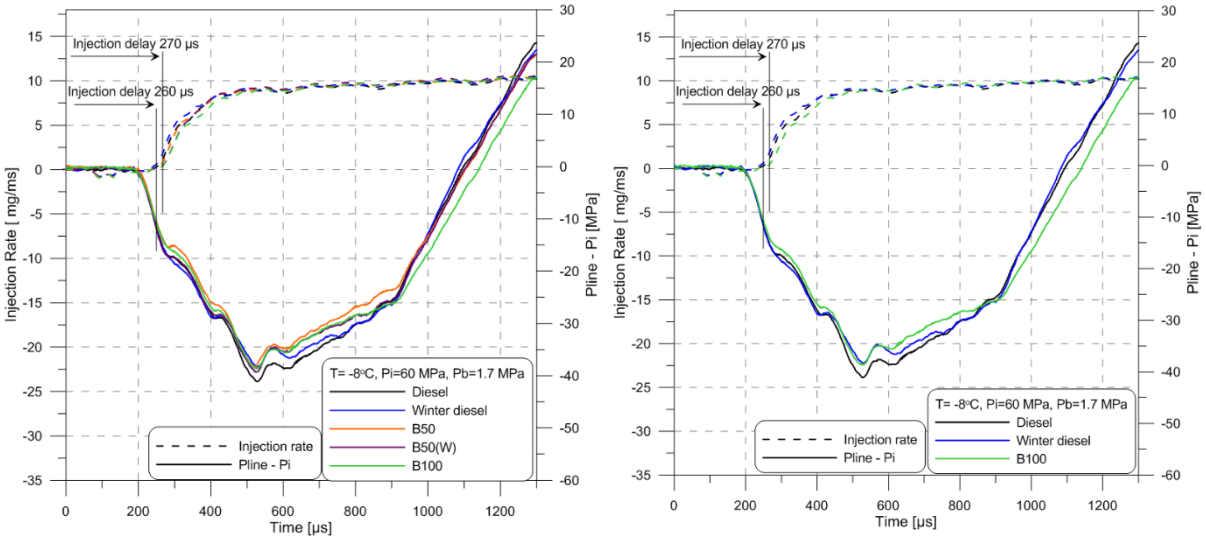

(a) all fuel (b) Diesel, Winter diesel, B100

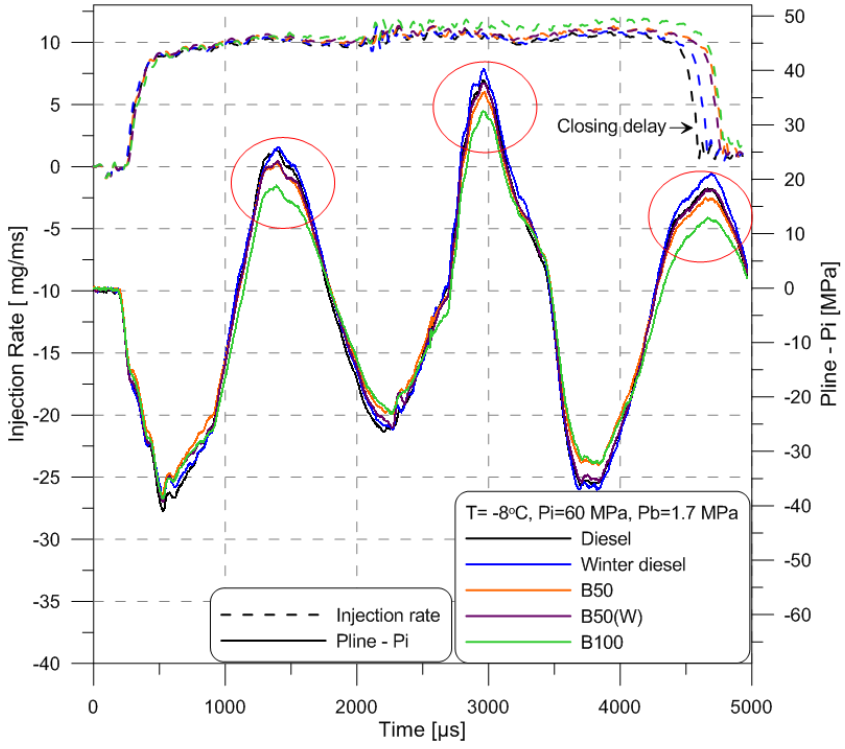

(c)

Fig. 4.9 Mean mass flow rate and *Pline – Pi*, T = -8°C, *Pi*=60 MPa, *Pb*= 1.7 MPa.

4.3 Effect of blended fuels and cold conditions on discharge coefficient in quasi steady state period

The injection rate was analyzed following the method of Payri et al. [11] and [69], Dernotte et al. [68] and Tinprabath et al. [95] as explained in chapter 2 section 2.2. The period between 1000-2000 µs after the start of activation (SOA) is selected as the quasi-steady state period, since this corresponds to the steady state period for injection rate (cf. Figs. 2.7 and 4.10). The injection rate values for all fuels are very close (Fig. 4.10). The average flow rate of B100 is slightly higher than that of Diesel. In this case, the difference in density between Diesel and B100 is about 5% and the viscosity of B100 is 2 times higher than that of diesel.

Fig. 4.11 shows that when the temperature is reduced from Troom to -8^{o}C, the average mass flow rate for *Pi*= 60MPa is the same for all fuel. Substantial changes in viscosity or density do not alter the average mass flow rate during the quasi-steady period. These values are the result of trade-off between density and viscosity. In cold conditions and/or with Biodiesel, the fuel density increases and so an increase in the mass flow rate can be expected. However, in cold conditions or with biodiesel, the fuel viscosity also increases. This leads to higher frictional forces and contrary to the influence of density, a decrease in the injection rate can be expected. The changes in viscosity compensate almost completely for the changes in density. From the analysis it can be concluded that only a change in viscosity or in density can impact on the fuel flow rate.

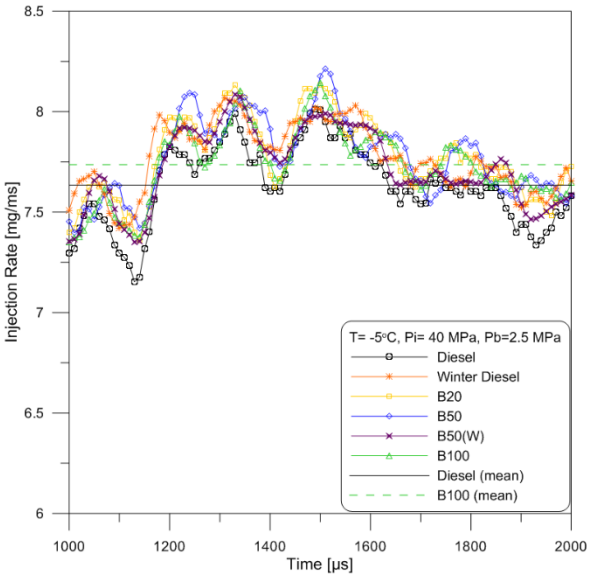

Fig. 4.10 Injection rate at the interval of 1000 to 2000 µs.

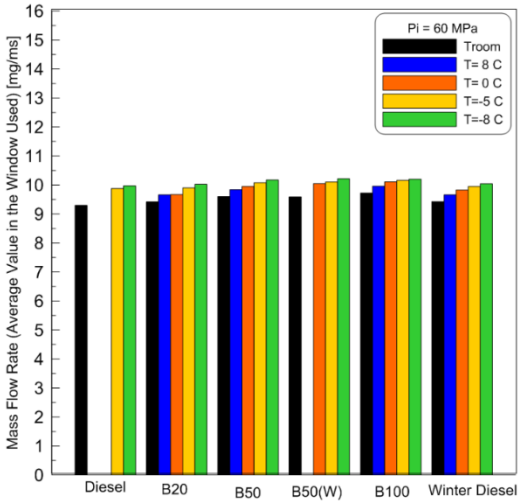

Fig. 4.11 Mass flow rate (average value in the window used), *Pi*= 60 MPa.

The data were analyzed according to Eq. 2-2 to extract discharge coefficients. Unlike the *Cd* rate is sensitive to the type of fuel. Here the density effect is corrected by the theoretical mass flow. The results are given in Fig. 4.12(a) which shows the discharge coefficient versus the

pressure difference for different fuels at room temperature. The discharge coefficient is affected by the Biodiesel blend or increase in viscosity at room temperature. These decreases are greater for small injection pressures: 2.6% for *Pi* = 30 MPa and 0.6% for *Pi* = 60 MPa. The results are similar to the findings of Desantes et al. [50], Park et al. [88], Seykens et al. [89], and Tinprabath et al. [95]. This behavior is confirmed down to 0°C. In Fig. 4.12(b) the *Cd* decreases linearly with viscosity at an injection pressure of 30 MPa.

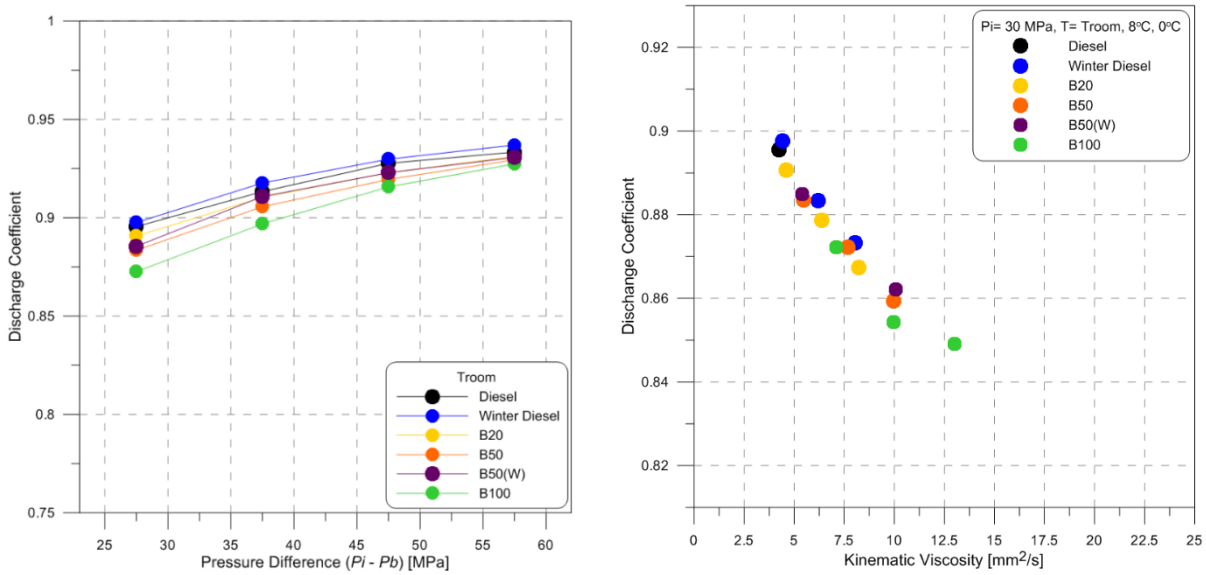

(a) *Cd* as function of pressure difference, Troom (b) *Cd* as function of *v*, Troom, 8°C, 0°C

Fig. 4.12 Impact of fuel blends and temperature on the discharge coefficient – *Pi* = 30 to 60 MPa.

For the same density (Fig. 4.13) the curve arrangement depends on the fuel viscosity except for winter diesel. The discharge coefficient of diesel fuel tends to be the lowest of all fuels and the maximum difference is 2.6%.

Likewise, Fig. 4.14(a) shows the discharge coefficient versus the pressure difference for different fuels at a temperature of -8°C, which is close to the CFPP of Biodiesel fuel. The results show that the discharge coefficient of Winter diesel fuel is the highest, even if it has the same kinematic viscosity as B20. No significant differences of the discharge coefficients for Diesel or Biodiesel blends are observed in the range of test injection pressures. However, the discharge coefficient of B100 fuel decreases strongly. At -5°C and -8°C the *Cd* values for fuel blends are not determined only by viscosity. In Fig. 4.14(b), the points are more dispersed; this dispersion can be explained by the fact that fuel additives for Winter diesel and diesel improve the discharge coefficient. Moreover the temperature is very low (-8°C), close to the CFPP of B100 and it is possible that Biodiesel begins to crystallize.

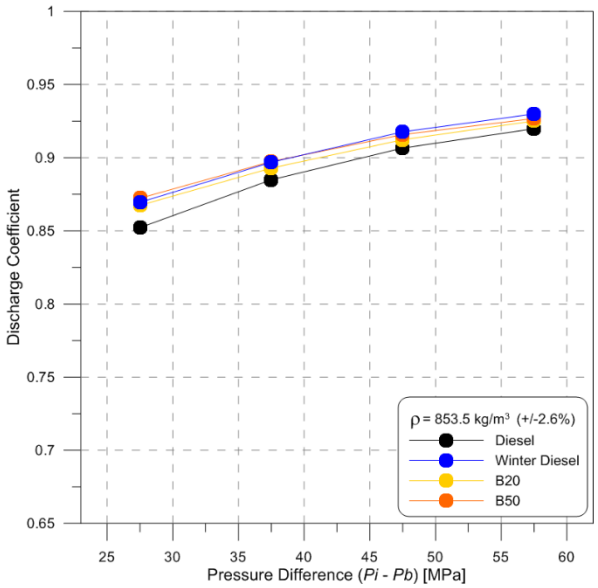

Fig. 4.13 Impact of the same fuel density on the discharge coefficient at the same density, *Pi* = 30 to 60 MPa.

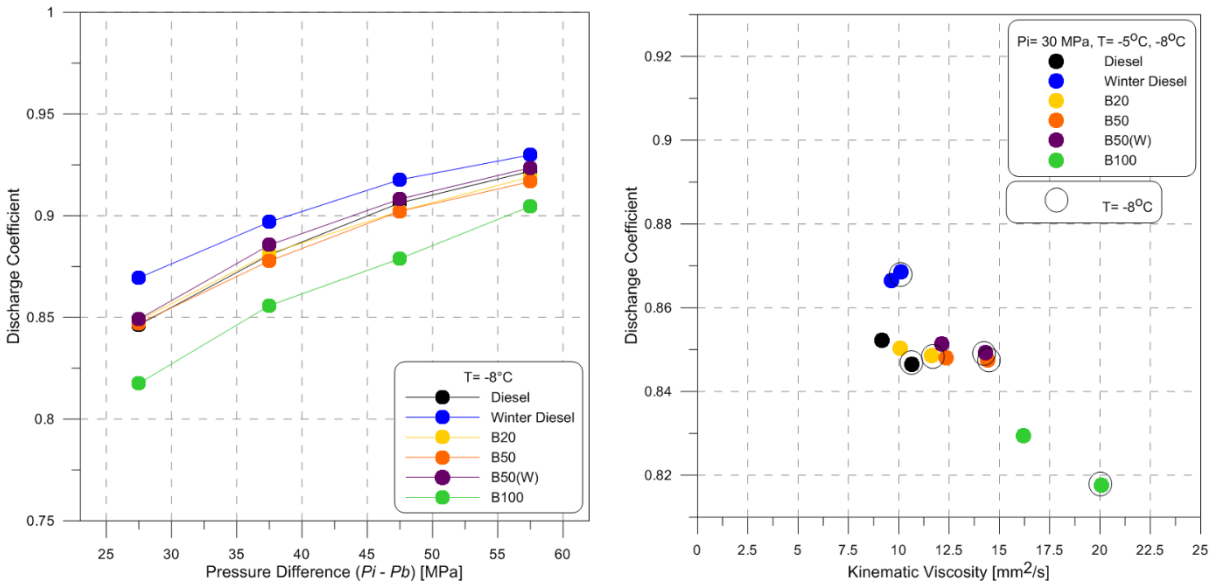

(a) *Cd* as function of pressure difference, T= -8°C (b) *Cd* as function of *v*, T= -5°C, -8°C.

Fig. 4.14 Impact of fuel blends and temperature on the discharge coefficient, *Pi* = 30–60 MPa.

Fig. 4.15 shows discharge coefficient versus kinetic viscosity. It is observed when increasing pressure, the discharge coefficient of all fuels increases. When kinematic viscosity increasing, the discharge coefficient of all fuels decreases. But on low injection pressure *Pi* = 30 MPa (Fig. 4.14(b)), the discharge coefficient of Biodiesel blends does not vary with the kinetic viscosity.

Moreover, Fig. 4.15 for *Pi* = 50 MPa and *Pi* = 60 MPa, the discharge coefficients are close and vary to the kinetic viscosity or temperature.

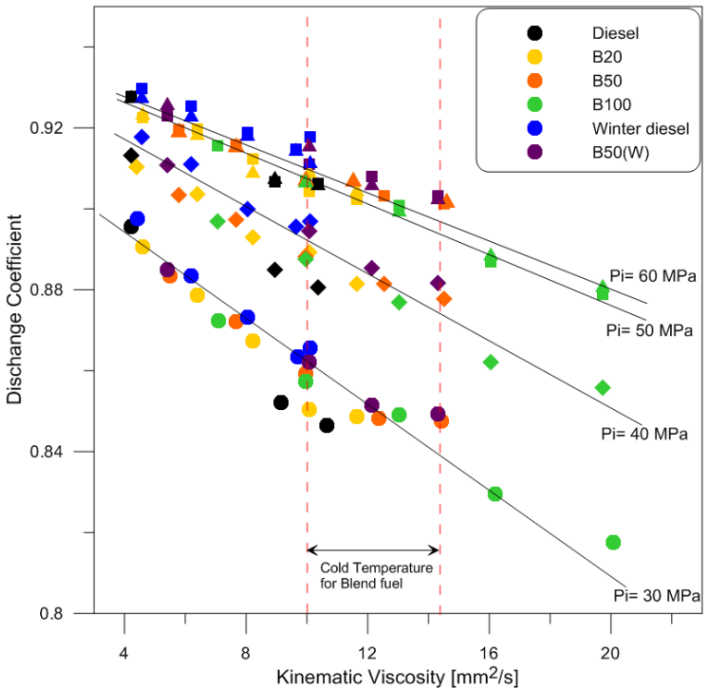

Fig. 4.15 Kinematic viscosity and discharge coefficient, *Pi* = 30 to 60 MPa.

So using correlations taking into account that only the viscosity and density, estimates the coefficient of discharge obtained will be less accurate at low temperature because the dispersion of the experimental points (Cd as a function of viscosity) is larger at these negative temperatures.

4.3.1 Discharge coefficient correlation for cold cold conditions

Two correlations Payri et al. [10] & Dernotte et al. [7] and Dernotte [70] were used again. The first is an empirical correlation adapted as shown in Eq. 3-1, the parameters *Cd*', *K1* and *K2* depend on the nozzle geometry fixed in chapter 3. The superscripts *a*, *b*, *c*, *d* and *e* are obtained by minimizing the sum of square errors between the correlation and experiment and *Re* from Eq. 2-6 shows in Table 4.2. (data fit 1). From data fit 1 it is shown that R^2 is 0.8122 and the maximum percentage difference from experimental data is 2.73%. For the B100 and temperature of -8°C the maximum percentage difference from experimental data is 5.26%.

The second correlation (Eq-3-3) is developed by Dernotte et al. [7], the parameters *C* and *E* depend on the nozzle geometry fixed in chapter 3. The superscripts *A* and *B* are obtained by minimizing the sum of square errors between the correlation and experiment as shown in Table 4.3. (data fit 1). From data fit 1 it is shown that R^2 is 0.7687 and the maximum percentage difference from experimental data is 5.26%. For the B100 and temperature of -8°C the maximum percentage difference from experimental data is 14.73%.

In chapter 3, two correlations are good for prediction discharge coefficient and the maximum percentage difference from experimental data is 2%. It is noticed from Fig. 2.4 that the behavior on injection period on calculation window is not the same caused by wearing out of the injector. The "geometric" parameters cannot be fixed as chapter 3 section 3.3. We fit Eq. 3-1 and Eq. 3-2 again by minimizing the sum of square errors between the correlation and experiment for all superscripts. The results for Eq. 3-1 show in Table 4.2. (data fit 2). From data fit 2 it is shown that R^2 is 0.9525 and the maximum percentage difference from experimental data is 3.08%. The results for Eq. 3-3 show in Table 4.3. (data fit 2). From data fit 2 it is shown that R^2 is 0.9577 and the maximum percentage difference from experimental data is 1.67%. As expected the correlation ratio (R^2) for these measurements is lower than that obtained at room temperature only (R^2=0.97 seen chapter 3). These two correlations are compared with experimental data for Diesel and pure Biodiesel on Fig 4.16

Table 4.2: Payri et al. correlation for estimating the discharge coefficient - values of the coefficients

	Cd'	*K1*	*K2*	*a*	*b*	*c*	*d*	*e*	R^2
Fit 1	1	-2.67	-1.8464E+6	-0.02	-0.73	-1.89	-0.04	1.58	0.8122
Fit 2	1	-1.67	-5.7385E+6	-0.18	-0.80	-1.94	-0.36	1.43	0.9525

Table 4.3: Dernotte correlation for estimating the discharge coefficient-values of the coefficients

	A	*B*	*C*	*D*	R^2
Fit 1	310.19	-0.49	-0.02	0.70	0.7687
Fit 2	40.70	0.22	-0.002	0.43	0.9577

The performance of this Dernotte correlation is good for prediction the discharge coefficient for injector CRI 3.1 and it is confirmed for other fuel in Fig 4.17 (*Cd* versus pressure difference) and Fig 4.18 (*Cd* versus Reynolds number)

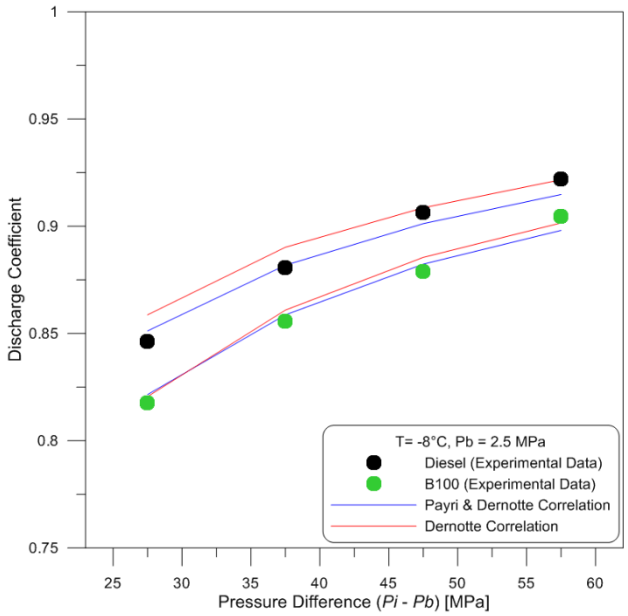

Fig. 4.16 Discharge coefficient: experimental results and correlation for Diesel, B100, *Pi* = 30 to 60 MPa, *Pb* = 2.5 MPa.

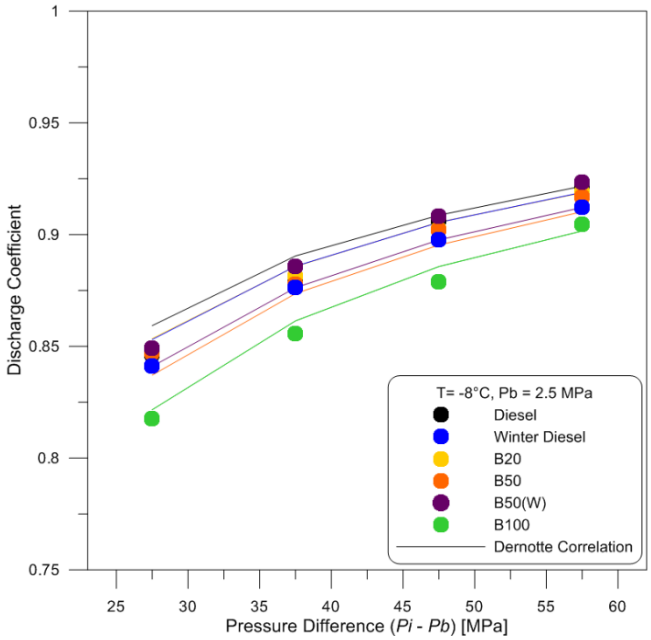

Fig. 4.17 Discharge coefficient: experimental results compared with the Dernotte correlation, *Pi* = 30 to 60 MPa, *Pb* = 2.5 MPa.

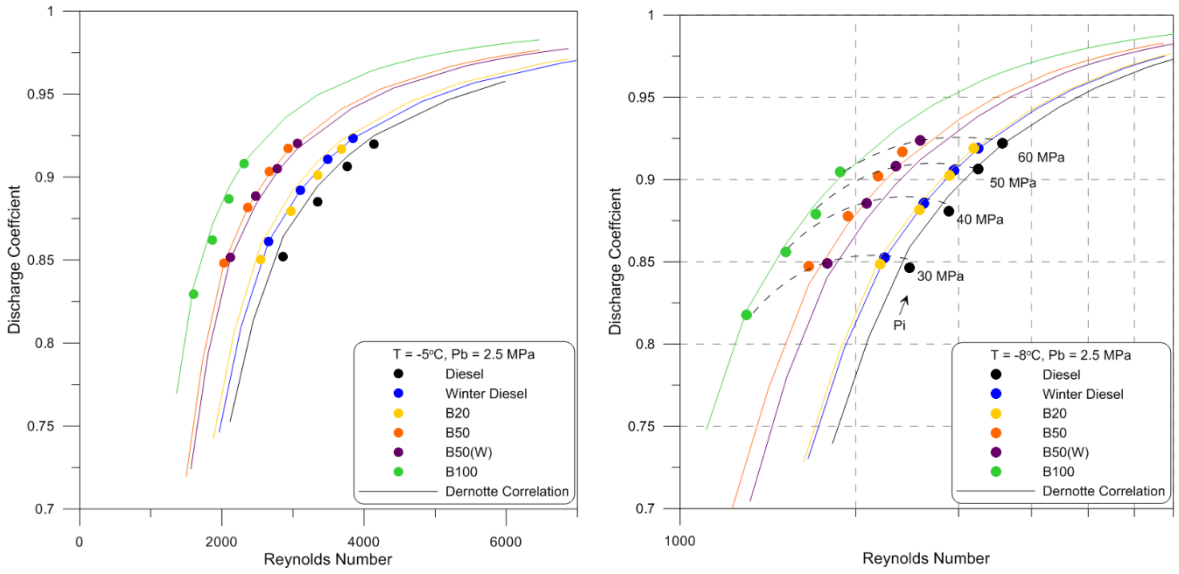

(a) T = -5°C (b) T = -8°C

Fig. 4.18 Impact of fuel blends and temperature on the discharge coefficient, *Pi* = 30 to 60 MPa.

Considering these correlations obtained in cold conditions for each fuel, it can be stated that the discharge coefficient depends not only on the Reynolds number but also on the geometry and fuels. Unlike Payri et al. [90], for a medium Reynolds number we observe a distinct curve for each fuel (Fig. 4.18). The Dernotte correlation with only four parameters gives a good estimation of the discharge coefficient for all the fuels and for all experimental conditions without cavitation.

Moreover, we test another correlation from Payri et al. [87] for prediction the discharge coefficient for all the fuel and temperature cover Troom and cold temperature. The global behavior shows that the discharge coefficient, *Cd* can be written by this type of equation (Eq. 4-1) [87]:

$$Cd = A - \frac{B}{Re} \tag{4-1}$$

Cases *A* and *B* depend on the injection pressure because at high injection pressure the effect of viscosity is reduced. The coefficient values *A* and *B* are obtained by minimizing the sum of square errors between the correlation and experiment as shown in Table 4.4 and Fig. 4.19.

Table 4.4: Values of the coefficients for discharge coefficient correlation

Pi (MPa)	*A*	*B*	R^2
30	0.9071	128.4	0.8905
60	0.9371	109.3	0.9086

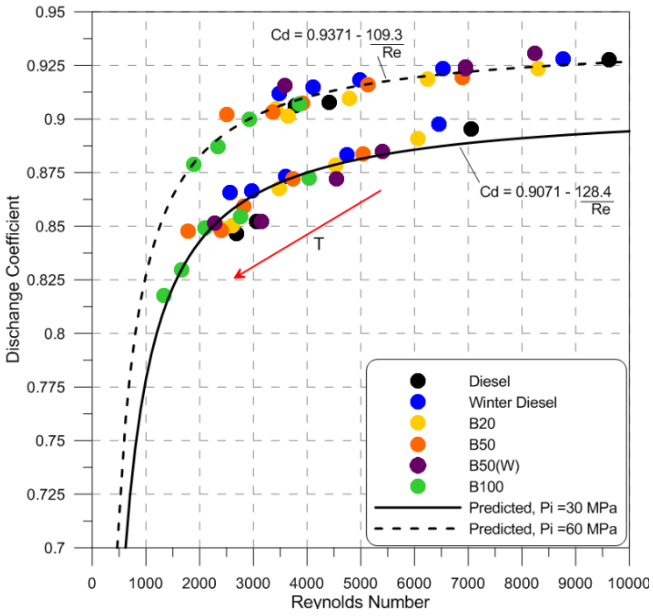

Fig. 4.19 Discharge coefficient versus Reynolds number for all fuels, *Pi* = 30, 60 MPa.

With study of evolution of *A* and *B* in function of injection pressure we can show that:

$$Cd = \underbrace{Cd' + K1.P_i}_{A} - \frac{\overbrace{K2 + K_3.P_i}^{B}}{Re} \qquad (4\text{-}2)$$

Where; $P_i \leq 50$ MPa: $A = \begin{cases} Cd' = 0.8623 \\ K_1 = 0.0015\text{x}10^{-6}\ [\text{Pa}^{-1}] \end{cases}$

$B = \begin{cases} K_2 = 156.43 \\ K_3 = -0.925\text{x}10^{-6}\ [\text{Pa}^{-1}] \end{cases}$

$P_i > 50$ MPa: $A = 0.9377$

$B = 109.9$

With this type of correlation we observe a distinct curve for each injection pressure.

In case of using B50(W); which is produced from Biodiesel 50 % and Winter diesel 50 %, the fuel property of B50(W) (density and viscosity (Fig.2.19, 2.22)) are the same as B50 (produced from Biodiesel 50% and Diesel 50%). The behavior of injection rate on Troom and cold temperature are the same as B50 (Fig. 4.2 - 4.4). However, the discharge coefficient for the two fuels is slightly different. This difference remains constant during the decrease in temperature while the Winter diesel offers performance on *Cd* much greater than diesel. Adding in the winter diesel biodiesel not significantly improves the discharge coefficient (Fig 4.20). Fig. 4.20(a)-(d) summarizes the impact of the percentage of Biodiesel on the discharge coefficient at room temperature, 0, -5 and -8^{o}C, respectively.

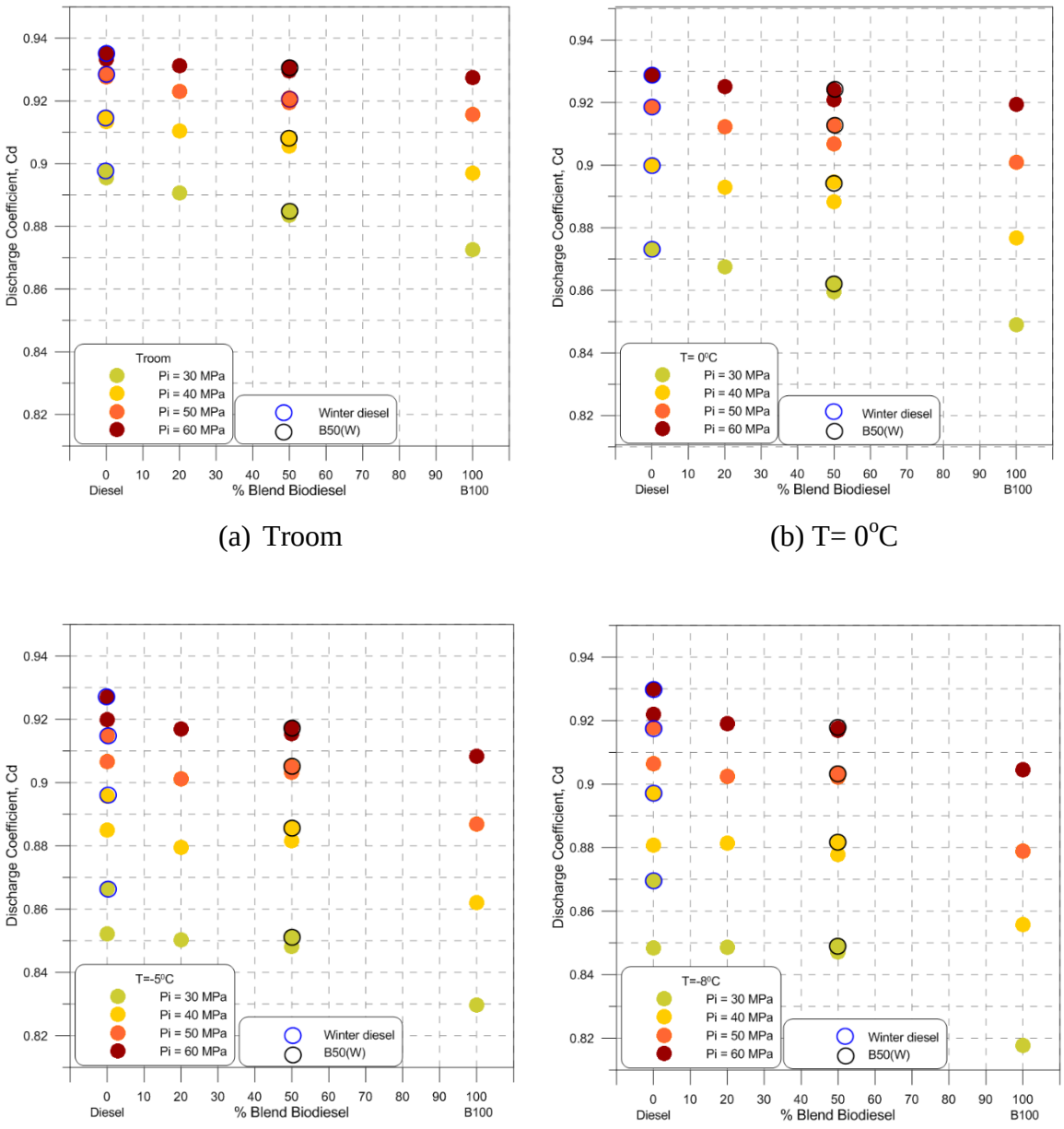

(a) Troom (b) T= 0°C

(c) T= -5°C. (d) T= -8°C

Fig. 4.20 Discharge coefficient versus percentage of biodiesel blend for all fuels, *Pi*=30–60 MPa.

At positive temperatures (Fig. 4.12), when the amount of Biofuel increases, the discharge coefficients decrease. The results are similar to those reported in the literatures [50, 86, 87, 95]. At subzero temperatures (Fig. 4.14), the mixtures and Diesel reach the same discharge coefficient. Only the discharge coefficient of B100 is smaller. At these negative temperatures, the additives in diesel cancel out the influence of viscosity on the discharge coefficient.

4.4 Effect of blended fuels and cold conditions on spray injection behavior

4.4.1 Spray tip penetration analysis

The raw images were analyzed with a digital image processing program to determine the spray tip penetration *S* and spray angle θ. Fig. 4.21 shows the average image 52, 160, 346 and 748 µs after injection when *Pi* = 30 MPa, and *Pb* = 1.2 MPa. It can be noted that diesel fuel and biodiesel-blended fuel have a similar spray penetration but that the penetration length with B100 is longer than that of other fuels at the start of injection. These results are similar to those of Chen et al. [13].

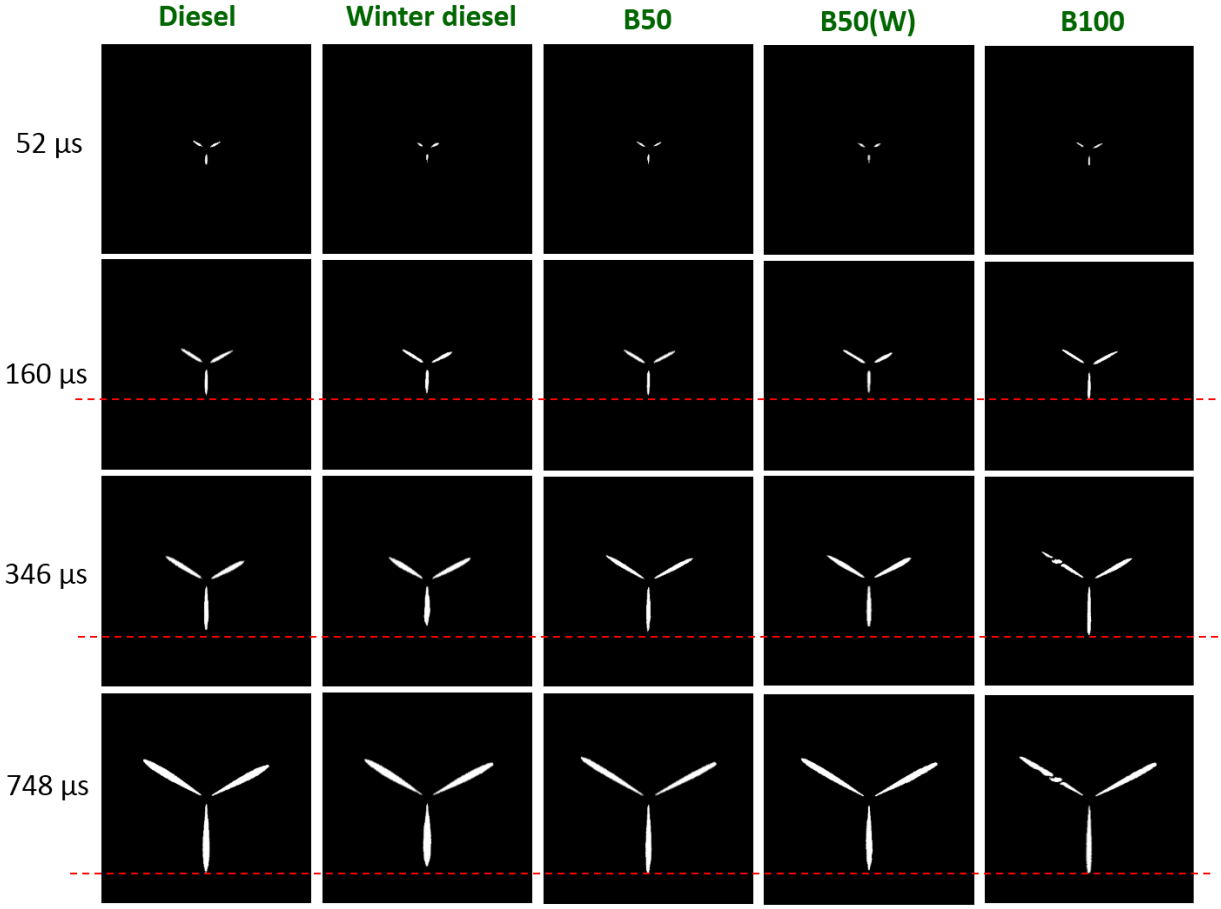

Fig. 4.21 Comparison of spray development : average image 52 µs, 160 µs, 346 µs and 748 µs after injection, T= -8^{o}C, *Pi* = 30 MPa, *Pb* = 1.2 MPa.

4.4.2 Results of Spray tip penetration

The type of fuel and temperature affects to penetration length shows in Fig. 4.22 (a, b). The spray penetration of Diesel slightly different between two temperatures but it can be seen that the spray penetration of B100 on cold temperature is the higher than on room temperature.

Fig.4.23 (a, c, e) shows that the penetration lengths of all fuels at room temperature are very similar. Fig. 4.23(b, d, f) shows that at -8 ^{o}C, the spray penetration of B100 is stronger higher than of the other fuels, the spray penetration of Winter diesel is the lowest, and the spray penetrations of Diesel, B50 and B50(W) are a median behavior between Winter diesel and Biodiesel. In the case of B50(W), the spray penetration behavior is similar to that of Diesel. So in cold conditions, the spray penetration behavior depends on viscosity: when the viscosity increases strongly due to the cold temperature, the spray penetration also increases strongly. The experimental results show that when Winter diesel is used the spray penetration is lower than that of the other fuels although the viscosity [8, 95].

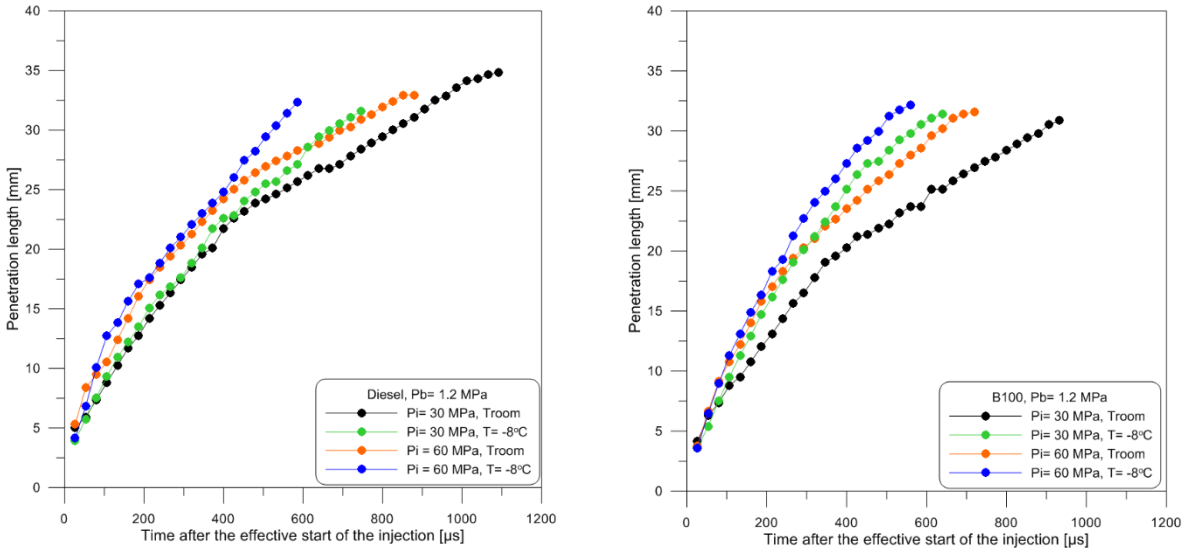

(a) Diesel (b) B100

Fig. 4.22 Penetration length –*Pi*= 30, 60 MPa, *Pb*= 1.2 MPa.

4.4.3 Spray tip penetration correlation

The image field only allows to study the first injection millisecond, so only when the opening phase of nozzle. In addition it was noted that the evolution of the pressure when visualizations or flow rate measurements is different (Fig 4.7). The actual flow rate during the spray visualization is not known. By default we will keep discharge coefficients determined on the stationary phase during flow rate measurements. To that Naber and Siebers correlations [57] (same as topic 3.3) correspond better to the experiences, the coefficient “a” is adjusted again. The increase in the latter from 0.9 to 1.7 can compensate for a decrease in the *Cd* when condition of visualizations.

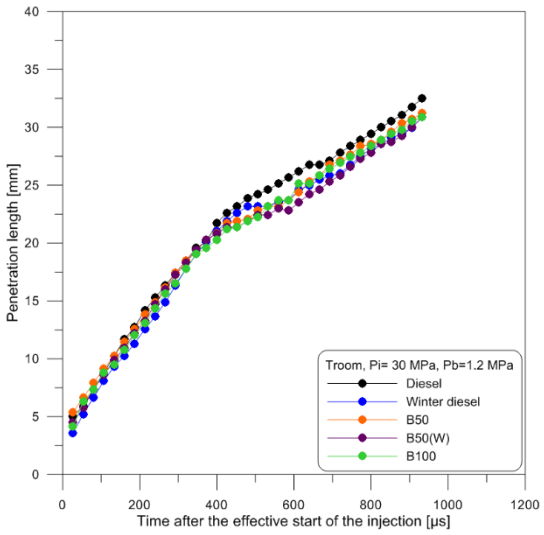

(a) Troom, *Pi*=30 MPa, *Pb*= 1.2 MPa.

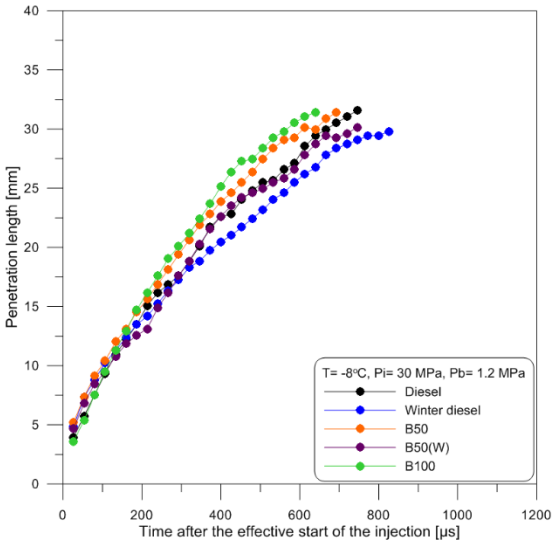

(b) T= -8°C, *Pi*=30 MPa, *Pb*= 1.2 MPa.

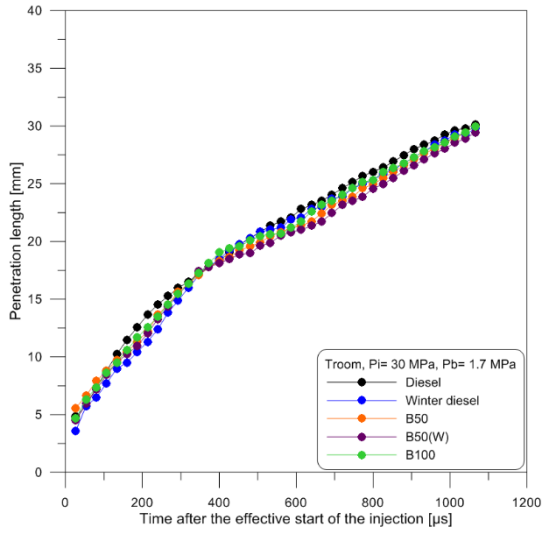

(c) Troom, *Pi*=30 MPa, *Pb*= 1.7 MPa.

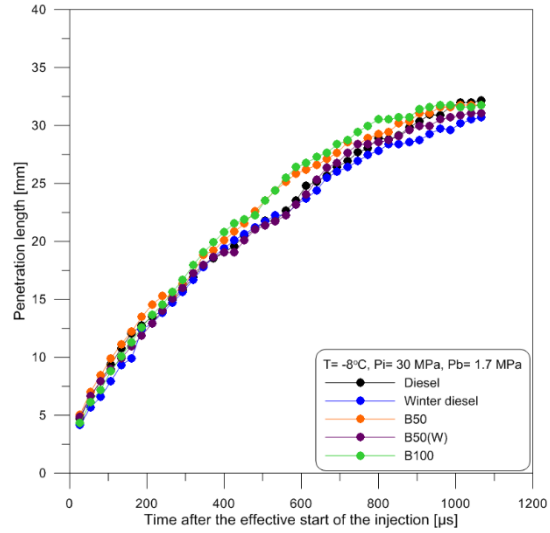

(d) T= -8°C, *Pi*=30 MPa, *Pb*= 1.7 MPa.

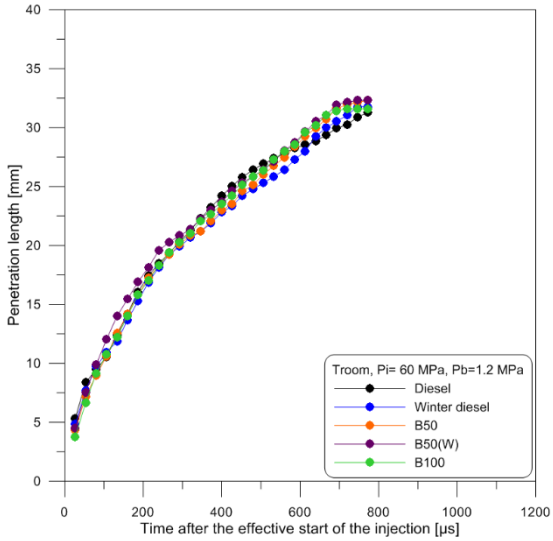

(e) Troom, *Pi*=60 MPa, *Pb*= 1.2 MPa.

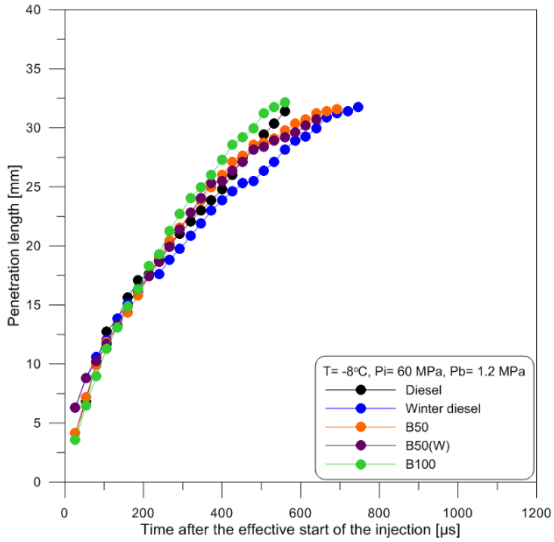

(f) T= -8°C, *Pi*=60 MPa, *Pb*= 1.2 MPa.

Fig. 4.23 Penetration length all fuel–*Pi*= 30, 60 MPa.

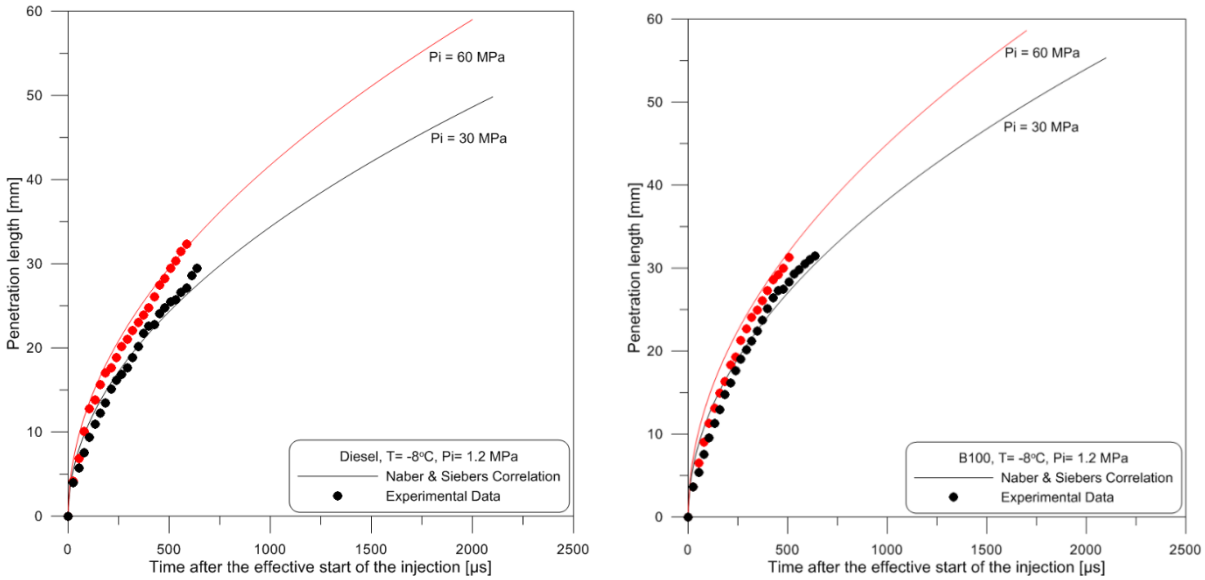

(a) Diesel, T= -8°C (b) B100, T= -8°C

Fig. 4.24 Penetration length from experiment data and estimated values.

The results are shown in Fig. 4.24, the maximum error with these new adjustment is +/- 5 %. With this new value of "a" coefficient, The Naber & Siebers correlation give a good estimate of spray penetration length on the cold condition.

4.4.4 Results of spray angle

The experimental data of spray angle were compared using the Naber & Siebers correlation (3.7)[54]. The experimental spray angle was measured using an image processing program. It follows Eq.2-11 where *A* is the projected area of the upstream half of the spray in an image. *S* is the penetration length.

The spray angle results are shown in Fig. 4.25-4.27. At room temperature (Fig.4.25) the spray angles are almost the same for all fuels and same result as in topic 3.4 (Fig. 3.20). At cold temperature (-8 °C), the spray angles differ (Fig. 4.26(a)), with B100 having the lowest spray angle and Winter diesel the highest, while the spray angle for Diesel fuel (Fig.4.26(b)) is between B100 and Winter diesel.

As the injection pressure increases, it can be noted in Fig.4.27 that the spray angles of Diesel, B50 and B50(W) are similar and slightly higher than at *Pi* = 30 MPa but that the spray angle of B100 remains the lowest.

The fact that spray angle behaviors differ under cold conditions for different duel is significant, because the spray angle directly affects the air-fuel ratio [5]. B50(W), which is produced from the same additive as Winter diesel, cannot produce a large spray angle.

During engine start-up in cold conditions, the only fuel that has a larger spray angle behavior is Winter diesel.

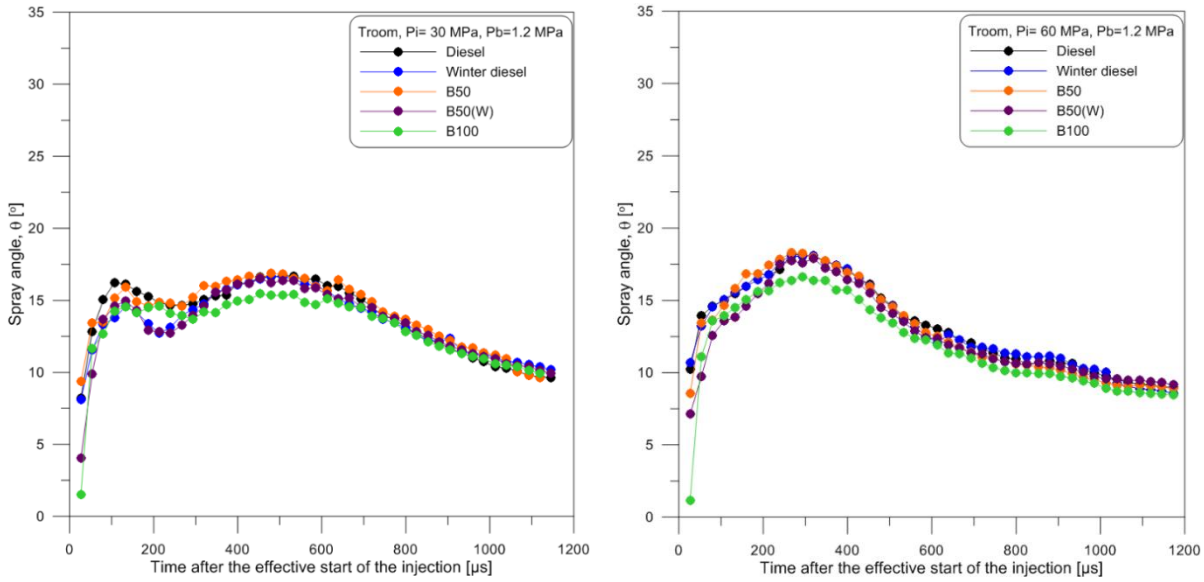

(a) *Pi* = 30 MPa (b) *Pi* = 60 MPa

Fig. 4.25 The spray angle, Troom.

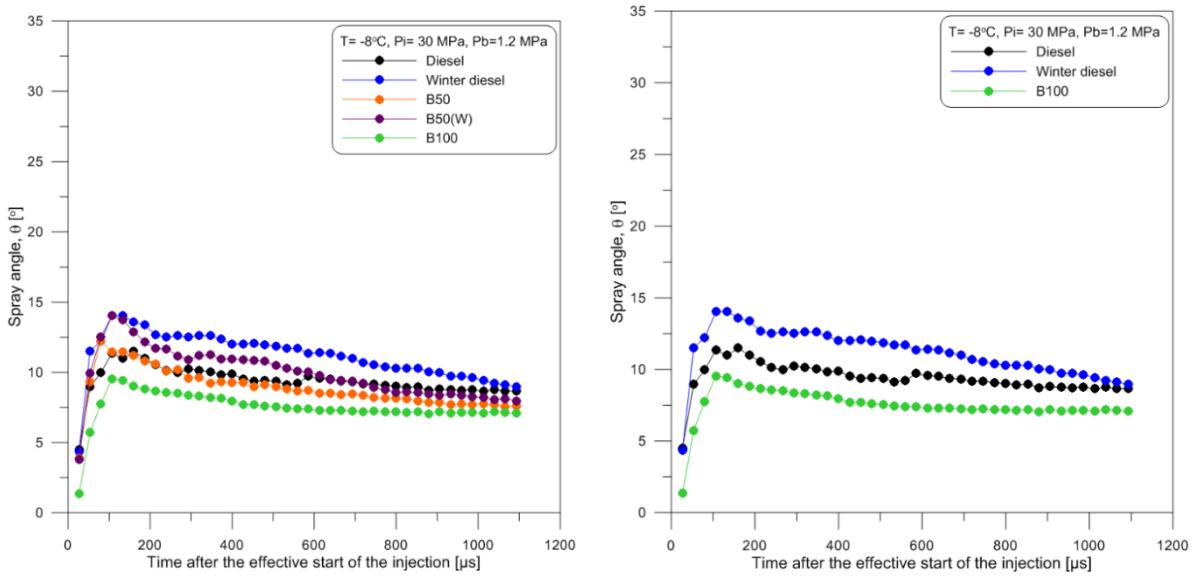

(a) All fuel (b) Diesel, Winter diesel and B100

Fig. 4.26 The spray angle, *Pi* = 30 MPa, T= -8^{o}C.

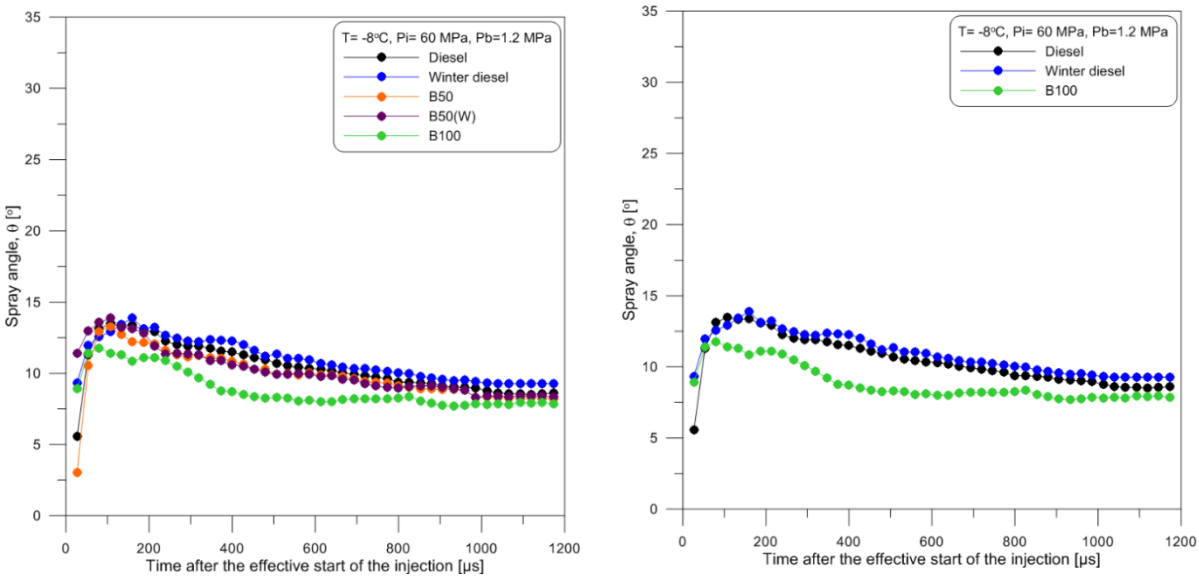

(a) All fuel (b) Diesel, Winter diesel and B100

Fig. 4.27 The spray angle, *Pi* = 60 MPa, T= -8°C.

4.4.5 Spray angle correlation

Fig. 4.28(a) shows the average spray angle. The cold temperature reduces radial expansion of the spray. The spray angle does not depend only on density; it is in fact more sensitive to variations in viscosity (Fig. 4.28(b)). We compared the experimental data with a correlation from Dernotte et al. [8] using Eq. 4-2. The spray angle versus viscosity is shown in Fig. 4.28(b), with the coefficient values *A*, *B*, *C*, *D* and *E*. They were obtained by minimizing the sum of square errors between the correlation and experiment as listed in Table 4.5. While several authors (Siebers [59], Hiroyasu [60], Payri et al. [64], Reitz & Bracco [36]) have proposed correlations to estimate the spray angle based on the injector geometry or injection conditions, only the correlation proposed by Dernotte et al. is in agreement with our results, with a maximum error of +/-13.2%.

Table 4.5: values of the coefficients for discharge coefficient

A	*B*	*C*	*D*	*E*	R^2
0.3	0.11	-0.13	-0.15	-0.46	0.9219

$$tan\left(\frac{\theta}{2}\right) = A.\left(\frac{\rho_a}{\rho_f}\right).\Delta P^C.f(v) \qquad (4\text{-}2)$$

When; $f(v) = \exp\left(D.\Delta P^E.v\right)$ and v is in mm^2/s, ΔP in MPa.

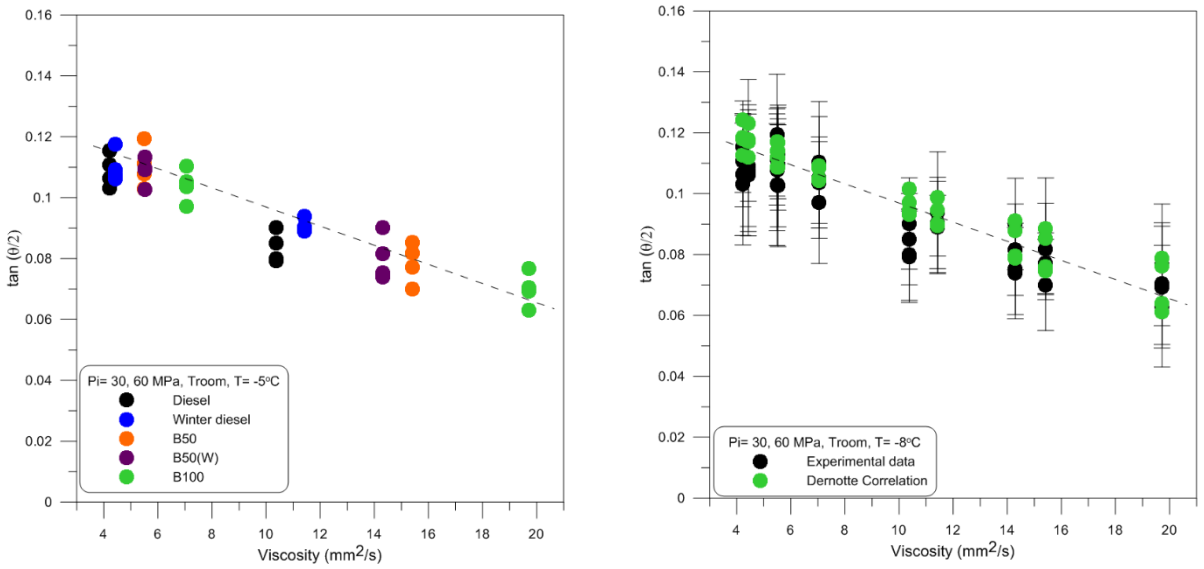

(a) Experimental data (b) Dernotte correlation

Fig. 4.29 The average spray angle versus viscosity, *Pi* = 30, 60 MPa.

4.5 Conclusions

The study of the influence of biodiesel and diesel blends on the injection rate in cold conditions was conducted using a Bosch CRI 3.1 piezoelectric injector. Measurements of the mass flow rate and visualization of spray with diesel fuel, Winter diesel fuel, Biodiesel blends and Biodiesel (B100) were made.

The study was carried out to discover a new understanding of the injection rate behaviors such as fuel viscosity and density under cold conditions and to focus on low injection pressures, the relationship between the discharge coefficient and the percentage of Biodiesel in the blends, and the relationship between the discharge coefficient and the decrease in temperature. New coefficient values for a kinematic viscosity correlation adapted for cold conditions were determined. Spray behaviors were studied, such as: comparison of spray development, spray penetration, spray penetration correlation on cold temperature, spray angle, average spray angle correlation and effect of fuel blend on pressure evolutions. New coefficient values for an average spray angle correlation adapted for cold conditions were determined.

The results are compared with data available in the literature. The conclusions of this study are summarized as follows:

- For this type of injector, the fuel viscosity changes the injection duration and hence for the same duration of pulse, it also changes the total mass injected.
- Concerning the performance of the injector shown by the value of the discharge coefficient, two behaviors were observed:

  - at positive temperatures or for fuels without additives (B100), the discharge coefficient decreases linearly with increasing viscosity;
  - at negative temperatures for fuels with additives (Winter Diesel, Diesel or blends), the viscosity measured at atmospheric pressure is not the only property which modifies the discharge coefficient. The effect of additives cancels out the impact of viscosity and the Diesel and fuel blends then it gives the same discharge coefficient value. For winter diesel with other additives the discharge coefficients are better.
- The spray angle is smaller when the temperature decreases or when the viscosity increases. The cold temperature seems to reduce the spray atomization.
- The spray penetration is longer when the temperature decreases or when the viscosity increases.
- The pressure evolution behaviors are the same for all fuel types, but the injection delay of B100 increases slightly compared with the other fuels.
- The spray performance (*Cd*, length and angle) is better with Winter diesel.
- When using B50(W) which is produced from Biodiesel 50% and Winter diesel 50%, the injection rate and spray behaviors are similar to those of Diesel and Biodiesel blends.

❖ Conclusions (version français)

L'étude de l'influence du taux de biodiesel dans les mélanges de carburant (diesel-biodiesel ou Winter Diesel-Biodiesel) sur le débit injecté et sur le comportement macroscopique du spray dans des conditions froides a été effectuée à l'aide d'un injecteur piézoélectrique Bosch CRI 3.1. Les mesures du débit massique et la visualisation du spray ont été faites avec du carburant Diesel, Winter Diesel, le biodiesel (B100) et quelques mélanges

L'étude a été effectuée pour mieux comprendre le comportement de l'injecteur et du spray sous des conditions de froid à des pressions d'injection faible. Ce comportement ce traduit par la description d'une nouvelle la relation entre le coefficient de décharge et le pourcentage de biodiesel dans les mélanges, et la relation entre le coefficient de décharge et la diminution de la température. Le comportement du spray a été étudié : extension du modèle de pénétration liquide aux températures négatives, déterminations de nouveau coefficients adaptée aux faibles températures pour la fonction de corrélation entre l'angle moyen du spray, la viscosité du carburants, le rapport de densité et la différence de pression entre la pression d'injection et la contre-pression. Les résultats sont comparés avec les données disponibles dans la littérature. Les conclusions de cette étude sont résumés comme suit:

- Pour ce type d'injecteur, la viscosité du combustible change la durée d'injection et,ainsi, pour la même durée d'impulsion, la masse totale injectée augmente.
- En ce qui concerne la performance de l'injecteur représenté par la valeur du coefficient de décharge, deux comportements ont été observés:

  - aux températures positives ou sans additifs pour carburants (B100), le coefficient de décharge diminue linéairement avec l'augmentation de viscosité;
  - aux températures négatives pour les carburants avec additifs (Winter Diesel, Diesel ou les mélanges), la viscosité mesurée à pression atmosphérique n'est pas la seule propriété qui modifie le coefficient de décharge. L'effet des additifs annule l'effet de la viscosité. En effet les mélanges biodiesel-Diesel ou 100% Diesel ont le même coefficient de décharges. Avec le Winter Diesel et des mélanges avec ce carburant cet effet n'est pas observé. La présence d'autres additifs améliore le coefficient de décharge.
- L'angle de spray est plus petit lorsque la température diminue, ou lorsque la viscosité augmente. La température froide semble réduire l'expansion du spray.
- La longueur de pénétration est plus longue lorsque la température diminue ou quand la viscosité augmente.
- Les fluctuations de pression en amont de l'injecteur de la pression sont les même pour tous les types de carburant. Cependant le délai hydraulique du B100 est plus grand par rapport aux autres combustibles.
- La performance de l'injecteur (coefficient de décharge, longueur et angle du spray) est meilleur avec Winter Diesel.
- Lorsque vous utilisez B50 (W) qui est produit à partir de biodiesel 50% et 50% du Winter Diesel, le débit et le comportement du spray sont similaires à ceux obtenus avec du diesel ou des mélanges Diesel-Biodiesel.

Conclusions and future research perspectives

The Influence of Physical Properties of Biodiesel, Diesel and Blended Fuels on Injection and Spray

Synthesis

The aim of this thesis was to further our understanding of the effects of the physical and chemical properties of Diesel, Biodiesel and blended fuels on injection and spray.

First, a literature review was carried out in order to determine the most relevant physical and chemical parameters to be investigated and the expected potential effects on combustion and injection. This synthesis helped to build a matrix comprising: Diesel, Winter diesel, Biodiesel and Biodiesel blends (6 fuels) and variations of the following properties: density, and kinematic viscosity.

In a second step, several studies related to injection were conducted. The characterization of the flow in the injector nozzle was determined from injection rate measurements.

The development of macroscopic spray under non-vaporization conditions was viewed in a pressure vessel.

Finally, the injection rate measurements and the development of macroscopic spray were studied under cold conditions.

To analyze the results, simple models based on physical and empirical correlations were used and improved.

The effects of fuel properties on injection and spray can be summarized in the following way:

- ***Influence of the biodiesel blends***

When the fraction of biodiesel in a blend increases, the density and viscosity of the fuel also increase. This leads to an increase in the mass flow which is proportional to the square root of the density as stipulated by the theory of Bernoulli. It is observed that the closing delay of the injector when the biodiesel fraction increases.

In the quasi-steady state, increasing the fraction of Biodiesel in the blend does not change the discharge coefficient significantly for high injection pressures. However, with B100 the discharge coefficient tends to be slightly lower than that of Diesel and Biodiesel blended fuels and at low injection pressure the discharge coefficient tends to decrease.

The spray penetrations of Diesel fuel and Biodiesel blended fuels are similar while with B100, the spray penetration is higher than that of Diesel and Biodiesel blended fuels. This difference is the result of a smaller spray angle with B100. The biodiesel fraction seems to have a slight influence during the transient phase. For low back and injection pressures the maximum spray angle decreases with the percentage of Biodiesel in the fuel.

In conclusion, in this work the fraction of Biodiesel in the fuel did not exceed 50% ain order to do not have a significant influence on the discharge coefficient or on the spray behavior.

- ***Influence of the biodiesel blends under cold conditions***

When the fuel temperature decreases, the closing delay, injection duration and total mass increase because viscosity increases.

At negative temperatures for fuels with additives (Winter diesel, Diesel or blends), the viscosity measured at atmospheric pressure is not the only property that modifies the discharge coefficient. The effect of additives cancels out the impact of viscosity and the Diesel and fuel blends, thereby giving the same discharge coefficient value. For Winter diesel with other additives the discharge coefficients are better. However, for B50(W) which is produced from Biodiesel 50% and Winter diesel 50%, the injection rate and spray behaviors are the same as those of Diesel and Biodiesel blends. The spray penetration is longer and the spray angle is smaller when the temperature decreases or when the viscosity increases. The pressure evolution behaviors are the same for all fuels, but the injection delay of B100 slightly increases compared with the other fuels.

In conclusion, the cold temperature reduces the radial expansion of spray and air entrainment.

Conclusion

This study has shown that in the "normal" operating conditions of a diesel engine, that is to say a thermally stabilized engine, the physical properties of fuels (density, viscosity) do not affect the injection step and the spray structure (injection rates, spray penetration, angle, strongly enough to impact the development of diesel combustion.

Under cold conditions and engine start-up (low injection pressure), Winter diesel gives a good injection behavior (injection rate, spray penetration, angle). For Diesel and Biodiesel blends, the behaviors are poorer and Biodiesel produces a negative spray behavior. Biodiesel blended with Winter diesel does not help improve spray efficiency.

Prospect

For fuel to be viable, it must present good operating characteristics under cold conditions. This phase of diesel engine operation is becoming increasingly problematic, due firstly to its inclusion in the cycles of normalized emission of pollutants (EURO 6). Secondly, as the engines of tomorrow increasingly use hybrid systems (electric motors, alternator starters), the phases of cold boost will become more frequent. Under these conditions, we have shown that the physical properties of fuels, including viscosity, may significantly influence the Diesel spray (flow angle, grain size). However, the link with the combustion process is still poorly understood. The impact of the quality of the spray on combustion and particularly the

interaction between the liquid phase and the diffusion flame and premixed flame require further fundamental studies to better control the combustion.

The main contribution of this study is to have provided information on the impact of the physical properties of fuels complemented by considering the impact of the chemical properties of alternative fuels (concentration of oxygen, esters, etc.).

For lack of time, we have not been able carry out tests with a motor to measure the emission of pollutants (NOx, particulates, HC, CO) and consumption, while varying the diluent concentration (EGR). The objective would be to work on a NO_X / particles tradeoff with properties such as fuel variables to assess their impact.

Conclusions et perspectives (version français)

L'Influence des Propriétés Physiques et Chimiques du Biodiesel, Diesel et de leur Mélange sur l'Injection et le Spray

Synthèse

Le but de ce travail de thèse est d'apporter des éléments de compréhension sur les effets de propriétés physiques des carburants tel le Diesel, le biodiesel et les mélanges Diesel-Biodiesel sur le comportement de l'injecteur et la morphologie macroscopique du spray.

Un premier travail de synthèse de la littérature a été réalisé afin de déterminer les paramètres physiques et chimiques les plus pertinents à étudier afin de mesurer leur effet potentiel sur la combustion et l'injection. Ce travail de synthèse a permis de cerner notre étude sur l'impact de la densité et la viscosité sur le comportement de l'injecteur et du spray généré. Une matrice de carburant a été construite. Les carburants étudiés sont du Diesel, Winter diesel, Biodiesel issu de l'estérification d'huile de colza et différents mélanges de ces-dits carburants. Six types de combustibles ont donc été investigués à différentes températures permettant un balayage large de la densité et de la viscosité.

La deuxième étape concerne l'impact du carburant sur le comportement de l'injecteur à température ambiante. La caractérisation de l'écoulement en sortie de la buse de l'injecteur a été réalisée à partir de la mesure du débit d'injection.

Le développement macroscopique du spray dans des conditions non-vaporisation a été réalisé dans une enceinte sous-pression

Ces mêmes mesures ont été ensuite réalisés sous différentes températures afin d'étudier l'impact des conditions froides sur les performances de l'injecteur.

Dans le cadre de l'analyse des résultats, des modèles simples basés sur des corrélations physiques et empiriques ont été utilisées et améliorées afin de mieux rendre compte de l'impact de la viscosité à faible pression d'injection sur le comportement de l'injecteur et du spray.

Les effets des propriétés des carburants sur l'injection et le spray peuvent être résumés de la façon suivante:

- ***Influence du pourcentage de biodiesel dans les mélanges***

En augmentant la quantité de biodiesel dans les mélanges la densité et la viscosité du carburant augmentent. L'augmentation de la densité comme stipulé par la théorie de Bernoulli conduit à une augmentation du débit massique proportionnellement à la racine carrée de la densité. L'augmentation de la viscosité génère un délai de fermeture plus important. Cette augmentation de la fraction de biodiesel dans le mélange ne change pas de

façon significative le coefficient de décharge pour des pressions d'injection élevées. Cependant, avec B100 le coefficient de débit tend à être légèrement inférieur à celui des autres carburants. Pour des pressions d'injection à faible (< 600 bars) le coefficient de décharge tend à diminuer avec l'augmentation de biodiesel

La longueur de pénétration du spray est similaire pour tous les carburants comportant une fraction de Diesel. Avec 100% de Biodiesel (B100), la pénétration du spray est plus longue. Cette différence est le résultat d'un angle de spray moins large avec le B100. Tout fois la réponse de l'angle durant la phase d'ouverture varie avec la fraction de biodiesel. Pour des faibles pressions d'injection, l'angle maximal observé diminue avec le pourcentage de biodiesel dans le carburant.

En conclusion, la fraction de biodiesel dans le carburant ne doit pas excéder 50% pour ne pas subir une influence significative sur le coefficient de décharge ou sur le comportement du spray.

- ***Influence de la mélanges de biodiesel dans des conditions froides***

En diminuant la température du carburant on augmente de façon exponentielle la viscosité. Celle dernière agit comme un frein au mouvement et à la dynamique de l'aiguille ainsi le délai de fermeture, la durée d'injection augmentent ainsi que et la masse totale.

Aux températures négatives, la viscosité mesurée à la pression atmosphérique pour les carburants avec additifs (Winter diesel, diesel ou mélanges) n'est pas la seule propriété qui peut expliquer l'évolution du coefficient de décharge. L'effet des additifs pourrait annuler l'effet de la viscosité. En effet un même coefficient de décharge est mesuré pour des valeurs de viscosité des carburants testés différents. Le Winter diesel avec des additifs permettant une meilleure tenue au froid du carburant améliore la valeur du coefficient de décharge. Cependant, pour B50 (W) qui est produit à partir de biodiesel 50% et 50% de Winter diesel, le comportement du débit d'injection du spray sont équivalents au comportement observé avec diesel ou au mélange biodiesel/Diesel

La pénétration du spray est plus longue et l'angle du spray est donc plus petite lorsque la température diminue ou lorsque la viscosité augmente. Plus la température baisse plus le délai d'apparition du spray augmente. Ce retard est d'autant plus important pour le B100. L'impact de la pression d'injection est le même quel que soit le carburant.

En conclusion, la température froide réduit l'expansion radiale du spray et l'entrainement d'air.

Conclusion

Cette étude montre que dans des conditions de fonctionnement "normal" ou moteur diesel est stabilisé thermiquement, les propriétés physiques des carburants (densité, viscosité) n'affectent pas significativement l'injection et la structure du spray (débits d'injection, la

pénétration, l'angle) et donc de devraient pas directement le développement de la combustion du diesel.

Dans des conditions froides (températures négatives) et de démarrage du moteur (faible pression d'injection), les performances de l'injecteur sont détériorées en utilisant du Diesel ou des mélanges Biodiesel/Diesel. De plus à ces températures l'ajout biodiesel réduit l'entrainement d'air. Par contre ces effets négatifs sont très limités avec l'utilisation de 100% de Winter Diesel. Mais l'ajout de Winter diesel dans un mélange 50% Biodiesel 50% Winter diesel n'améliore pas le comportement de l'injecteur et l'efficacité du spray.

Perspective

Un bon choix de combustible doit être présenté de bonnes caractéristiques que ce soit à chaud ou à froid. La phase de fonctionnement à froid du moteur diesel est de plus en plus problématique, en raison d'une part de son inclusion dans les cycles d'émission normalisée de polluants (EURO 6). Deuxièmement, comme les moteurs de demain utilisent plus de systèmes d'hybridation (moteurs électriques, démarreurs alternateur), les phases de démarrage à froid seront plus fréquentes. Dans ces conditions, nous avons montré que les propriétés physiques des carburants, notamment la viscosité, peuvent influencer de manière significative la pulvérisation du carburant. Cependant, le lien avec le processus de combustion est encore mal compris. L'impact de la qualité de la pulvérisation lors de la combustion et notamment de l'interaction entre la phase liquide et la flamme de diffusion ou/et pré mélange nécessite de nouvelles études fondamentales

Notre étude donne essentiellement des informations sur l'impact des propriétés physiques des carburants qui seraient nécessaires d' approfondir en tenant compte de l'impact des propriétés chimiques tels que par exemple la concentration d'oxygène, le nombre de double liaison, la taille des molécules… des différents biocarburants

Par manque de temps, nous n'avons pas été en mesure de réaliser des essais moteur afin de mesurer les émissions de polluants (NOx, particules, HC, CO) et d'estimer la consommation, et d'étudier l'impact de la concentration de diluant (EGR) sur les ces résultats. L'objectif serait de travailler sur le compromis NOx / particules avec des propriétés telles que les variables taux de biodiesel ou température afin d'évaluer son impact.

Appendix

Appendix I

Fuel properties

Fuel properties from experiment and correlation follow topic 2.5, Fig 2.17 and 2.18. The fuel density and viscosity were analysed with an Anton Paar® Stabinger Viscometer (model SVM 3000/G2) [78]. The SVM 3000 Stabinger Viscometer measures the dynamic viscosity and density according to ASTM D7042.

Table: I.I Density (kg/m^3)

	Diesel		Winter Diesel		B10		B20		B30	
T(^{o}C)	Corre.	Exp.	Corre.	Exp.	Corre.	Exp.	Corre.	Exp.	Corre.	Exp.
-10	855.95	856.80	855.95	855.30	859,75	860,70	863,74	865,00	868,11	869,45
-8	854.45	855.05	854.45	853.50	858,26	858,90	862,27	863,30	866,66	867,80
-6	852.95	853.00	852.95	852.10	856,78	856,90	860,80	861,30	865,21	865,95
-4	851.45	851.60	851.45	850.75	855,29	855,50	859,33	859,90	863,75	864,40
-2	849.95	850.20	849.95	849.35	853,81	854,10	857,86	858,45	862,30	863,00
0	848.44	848.80	848.44	847.35	852,32	852,70	856,39	857,05	860,85	861,55
2	846.94	847.40	846.94	846.55	850,84	851,30	854,92	855,60	859,40	860,10
4	845.44	845.95	845.44	845.15	849,35	849,90	853,45	854,20	857,95	858,75
6	843.94	844.50	843.94	843.75	847,86	848,50	851,98	852,80	856,49	857,30
8	842.44	843.20	842.44	842.40	846,38	847,10	850,51	851,40	855,04	855,90
10	840.94	841.70	840.94	841.00	844,89	845,70	849,04	849,90	853,59	854,50
12	839.44	840.30	839.44	839.65	843,41	844,30	847,57	848,50	852,14	853,10
14	837.94	838.90	837.94	838.25	841,92	842,90	846,10	847,10	850,68	851,70
16	836.44	837.50	836.44	836.85	840,44	841,50	844,63	845,70	849,23	850,25
18	834.94	836.10	834.94	835.45	838,95	840,10	843,16	844,30	847,78	848,80
20	833.44	834.70	833.44	834.05	837,46	838,65	841,69	842,90	846,33	847,40
22	831.93	833.30	831.93	832.70	835,98	837,25	840,22	841,50	844,88	846,00
24	830.43	831.90	830.43	831.25	834,49	835,85	838,75	840,00	843,42	844,55
26	828.93	830.45	828.93	829.90	833,01	834,45	837,29	838,60	841,97	843,15
28	827.43	829.10	827.43	828.50	831,52	833,05	835,82	837,20	840,52	841,75
30	825.93	827.65	825.93	827.10	830,04	831,65	834,35	835,70	839,07	840,30
32	824.43	826.30	824.43	825.70	828,55	830,15	832,88	834,30	837,61	838,85
34	822.93	824.90	822.93	824.30	827,06	828,75	831,41	832,90	836,16	837,40
36	821.43	823.50	821.43	822.90	825,58	827,35	829,94	831,50	834,71	836,00
38	819.93	821.85	819.93	821.35	824,09	825,85	828,47	829,90	833,26	834,40
40	818.43	820.50	818.43	820.00	822,61	824,40	827,00	828,55	831,80	833,30

Table: I.I Density (kg/m^3)

	B40		B50		B50(W)		B100	
T(^{o}C)	Corre.	Exp.	Corre.	Exp.	Corre.	Exp.	Corre.	Exp.
-10	872,29	874,00	877,14	879,10	877,14	878,20	898.71	901.90
-8	870,86	872,30	875,72	877,35	875,72	876,40	897.38	900.15
-6	869,42	870,70	874,31	875,85	874,31	875,00	896.05	898.40
-4	867,99	868,90	872,89	874,00	872,89	873,60	894.72	897.00
-2	866,55	867,50	871,47	872,60	871,47	872,20	893.39	895.50
0	865,11	866,00	870,06	871,10	870,06	870,80	892.06	894.10
2	863,68	864,30	868,64	869,70	868,64	869,35	890.73	892.60
4	862,24	863,20	867,22	868,30	867,22	867,90	889.40	891.20
6	860,81	861,80	865,81	866,90	865,81	866,50	888.07	889.75
8	859,37	860,40	864,39	865,45	864,39	865,10	886.74	888.30
10	857,94	858,95	862,98	864,00	862,98	863,70	885.41	886.85
12	856,50	857,50	861,56	862,60	861,56	862,25	884.08	885.40
14	855,07	856,10	860,14	861,20	860,14	860,80	882.75	883.95
16	853,63	854,70	858,73	859,80	858,73	859,40	881.42	882.50
18	852,19	853,30	857,31	858,35	857,31	857,95	880.09	881.05
20	850,76	851,90	855,90	856,90	855,90	856,50	878.76	879.60
22	849,32	850,45	854,48	855,50	854,48	855,10	877.43	878.15
24	847,89	849,05	853,06	854,10	853,06	853,65	876.10	876.75
26	846,45	847,60	851,65	852,70	851,65	852,25	874.77	875.30
28	845,02	846,40	850,23	851,20	850,23	850,80	873.44	873.85
30	843,58	844,80	848,81	849,75	848,81	849,35	872.11	872.35
32	842,15	843,35	847,40	848,30	847,40	847,95	870.78	870.95
34	840,71	842,45	845,98	846,90	845,98	846,45	869.45	869.45
36	839,27	840,45	844,57	845,50	844,57	845,05	868.12	868.05
38	837,84	838,90	843,15	843,95	843,15	843,60	866.79	866.50
40	836,40	836,75	841,73	842,45	841,73	842,10	865.46	865.00

Table: I.II Kinematic Viscosity (m^2/s)

	Diesel		Winter Diesel		B10		B20		B30	
T(^oC)	Corre.	Exp.	Corre.	Exp.	Corre.	Exp.	Corre.	Exp.	Corre.	Exp.
-10	11.24	11.27	13.07	13.16	12,19	11,96	13,59	13,23	15,11	14,53
-8	9.99	10.38	11.25	11.43	10,64	10,85	11,60	11,63	12,68	12,48
-6	9.18	9.28	10.07	10.02	9,64	9,93	10,33	10,68	11,11	11,52
-4	8.63	8.63	9.24	9.28	8,96	8,96	9,47	9,47	10,06	10,06
-2	7.97	8.04	8.65	8.59	8,31	8,35	8,77	8,82	9,32	9,37
0	7.48	7.51	8.10	8.04	7,79	7,80	8,22	8,24	8,73	8,74
2	7.02	7.04	7.60	7.51	7,31	7,30	7,72	7,71	8,19	8,18
4	6.60	6.60	7.15	7.02	6,87	6,85	7,25	7,23	7,69	7,66
6	6.22	6.21	6.72	6.59	6,47	6,44	6,82	6,79	7,24	7,20
8	5.86	5.85	6.33	6.19	6,10	6,06	6,42	6,40	6,81	6,77
10	5.53	5.52	5.97	5.83	5,75	5,72	6,06	6,03	6,42	6,39
12	5.23	5.22	5.64	5.50	5,43	5,41	5,72	5,70	6,06	6,03
14	4.94	4.94	5.33	5.20	5,14	5,12	5,41	5,39	5,73	5,70
16	4.68	4.68	5.05	4.92	4,86	4,85	5,12	5,11	5,42	5,40
18	4.44	4.44	4.78	4.66	4,61	4,60	4,85	4,85	5,13	5,13
20	4.21	4.23	4.53	4.43	4,37	4,41	4,60	4,61	4,86	4,87
22	4.00	4.02	4.30	4.21	4,15	4,17	4,36	4,38	4,61	4,63
24	3.80	3.84	4.09	4.00	3,94	3,97	4,14	4,18	4,38	4,41
26	3.62	3.66	3.89	3.82	3,75	3,89	3,94	3,99	4,16	4,21
28	3.45	3.50	3.70	3.64	3,57	3,62	3,75	3,80	3,96	4,02
30	3.28	3.35	3.53	3.48	3,41	3,47	3,57	3,64	3,77	3,84
32	3.13	3.21	3.36	3.33	3,25	3,32	3,41	3,48	3,60	3,68
34	2.99	3.07	3.21	3.19	3,10	3,18	3,25	3,34	3,43	3,52
36	2.86	2.95	3.07	3.06	2,96	3,05	3,11	3,20	3,28	3,38
38	2.74	2.83	2.93	2.93	2,84	2,93	2,97	3,08	3,13	3,25
40	2.62	2.74	2.81	2.83	2,71	2,84	2,84	2,97	3,00	3,13

Table: I.II Kinematic Viscosity (m^2/s)

	B40		B50		B50(W)		B100	
T(^oC)	Corre.	Exp.	Corre.	Exp.	Corre.	Exp.	Corre.	Exp.
-10	16,70	16,70	18.3	18.1	18,60	17,80	23.42	23.31
-8	13,85	13,90	15.0	15.4	15,31	14,30	19.75	19.72
-6	11,99	12,57	12.9	13.6	13,14	12,61	17.09	16.97
-4	10,73	10,73	11.5	11.7	11,65	11,65	15.12	15.12
-2	9,94	9,99	10.6	10.6	10,63	10,83	13.91	14.00
0	9,31	9,33	9.9	9.9	9,95	10,09	12.99	13.03
2	8,73	8,71	9.3	9.3	9,32	9,41	12.15	12.15
4	8,19	8,16	8.7	8.7	8,74	8,81	11.38	11.35
6	7,70	7,66	8.2	8.2	8,22	8,26	10.67	10.63
8	7,25	7,20	7.7	7.7	7,73	7,63	10.02	9.97
10	6,83	6,79	7.3	7.2	7,28	7,30	9.42	9.38
12	6,44	6,41	6.9	6.8	6,86	6,89	8.87	8.83
14	6,08	6,06	6.5	6.4	6,48	6,50	8.35	8.33
16	5,75	5,73	6.1	6.1	6,12	6,15	7.88	7.87
18	5,44	5,44	5.8	5.8	5,79	5,83	7.44	7.44
20	5,16	5,16	5.5	5.5	5,48	5,53	7.04	7.05
22	4,89	4,91	5.2	5.2	5,20	5,25	6.66	6.69
24	4,64	4,68	4.9	5.0	4,93	5,00	6.31	6.36
26	4,41	4,46	4.7	4.7	4,68	4,76	5.98	6.05
28	4,20	4,26	4.5	4.5	4,45	4,54	5.68	5.74
30	3,99	4,07	4.2	4.3	4,24	4,32	5.40	5.50
32	3,81	3,89	4.0	4.1	4,04	4,15	5.13	5.23
34	3,63	3,73	3.8	3.9	3,85	3,97	4.88	5.02
36	3,46	3,57	3.7	3.8	3,67	3,80	4.65	4.80
38	3,31	3,43	3.5	3.6	3,51	3,65	4.44	4.60
40	3,16	3,31	3.4	3.5	3,35	3,51	4.23	4.44

Appendix II

SAE Technical paper: 2013-24-0032

ICE 2013, 11th International Conference on Engine & Vehicle, Naples, Italy

SAE INTERNATIONAL

Influence of Biodiesel and Diesel Fuel Blends on the Injection Rate and Spray Injection in Non-Vaporizing Conditions

2013-24-0032
Published
09/08/2013

Padipan Tinprabath and Camille Hespel
Universite d'Orléans

Somchai Chanchaona
King Mongkut's University Thonburi

Fabrice Foucher
Universite d'Orléans

doi:10.4271/2013-24-0032

ABSTRACT

Fossil fuel reserves are being depleted due to increasing energy requirements. One of the solutions is to partly replace fossil fuel by renewable biodiesel fuel. However, the physical properties of biodiesel fuels need to be thoroughly investigated before applying biodiesel or diesel-biodiesel blends in diesel engines, in order to improve the combustion efficiency.

This paper presents the experimental study of diesel fuel and biodiesel blends on injection flow characteristics and fuel spray behavior. Seven fuels were tested: diesel fuel, five diesel-biodiesel blends: 10%(B10), 20%(B20), 30%(B30), 40%(B40), 50%(B50), and pure biodiesel(B100) in a diesel engine equipped with a piezo injector. Injection pressures were set at 30-180 MPa for the study of the injection flow characteristics and at 30-150 MPa for the study of spray behavior in non-vaporizing conditions. The experimental results show that the injection flow characteristics and fuel spray behavior are the same with biodiesel blends as with diesel fuel. With pure biodiesel (B100), which has a density that is 5.2% higher and a viscosity 50% higher than diesel fuel, the discharge coefficient decreases by 3.63% but at injection pressure values of over 55 MPa, the effect on the discharge coefficient is insignificant. At the beginning of the injection period (up to 2000μs), the spray penetration and spray angle of B100 are different but after 2000 μs the spray behavior is similar to that of the other fuels. Correlations based on the work of Payri et al., Soteriou et al. and Naber & Siebers were used for comparison with the experimental data.

INTRODUCTION

Current energy reserves are being exhausted, in particular oil which is predicted to be depleted in the next 40 years, making it essential to find alternative fuels. Biodiesel is a very interesting fuel because it is renewable, thus increasing energy security, environmentally friendly, and has a higher cetane number and a lower sulfur and aromatic content. The main disadvantages of biodiesel are its higher viscosity, lower energy content, higher cloud point and pour point, higher nitrogen oxide (NOx) emissions, lower power and high price [1]. However, many countries can produce their own biodiesel and blends with diesel fuel of 2-20% [2,3]. Governments (e.g. the European Union, the U.S.A.) have stipulated that fuel should be blended with biodiesel [3], although consumers are unconvinced about the use of biodiesel fuel blends in automotive engines because of concerns about combustion efficiency, pollutant emissions and the effects on engine components.

The first important point to consider in the use of biodiesel in vehicle engines is that the combustion efficiency and pollutant emissions depend on the fuel injection process [4,5].

It is necessary to know the physical properties of injection and flow characteristics inside the injector, the spray tip penetration, spray angle and fuel atomization in order to improve the characteristics of biodiesel, the injector geometry or fuel injection method and thus achieve the highest engine efficiency.

Studies show that the side mass flow rate in the nozzle decreases slightly due to the increase in viscosity [6,7] and that biodiesel blended fuels have a Sauter Mean Diameter (SMD) greater than diesel fuel due to an increase in the flow friction loss [8,9]. The fraction of biodiesel in the blended fuel increases the density and viscosity of the fuel. This modification does not affect the discharge coefficient [4,5,10] but when pure biodiesel is used, the discharge coefficient decreases slightly [11]. Several studies show that when the percentage of biodiesel is increased, spray tip penetration also increases and the spray angle decreases [5,6,9,12,13]. This is because the increase in viscosity increases the spray SMD and reduces the atomization capacity [11]. According to the literature, biodiesel fuel produced with vegetable or animal oil can be used with diesel injectors. In this paper, we focus on biodiesel produced from rapeseed because at the present time this type of fuel is widely used in Europe and Asia. The only published study on biodiesel produced from rapeseed is the research by Desantes et al. [9], in which two biodiesel blends (5% and 30%) and pure biodiesel were studied. The results showed that only pure biodiesel has an effect on the spray behavior. To further our understanding of these mixtures, it is necessary to test a larger range of fuels with a biodiesel fraction of 10 to 50%, and to compare the results with correlations from the literature.

In the present study, the fuels chosen were diesel fuel, biodiesel (rapeseed biodiesel), and diesel fuel blended with 10%, 20%, 30%, 40% and 50% rapeseed biodiesel. The fuel properties were measured at the operating temperature. We investigated the effect of biodiesel and diesel fuel blends on the injection rate and spray behavior in non-vaporizing conditions e.g. discharge coefficient, fuel mass flow rate, spray tip penetration and spray angle, using the diesel injector over the operating conditions encountered in current engine strategies. In this study the correlations based on work by Payri et al. [10], Soteriou et al. [14] and Naber & Siebers [15] were used for comparison with the experimental data.

SETUP AND METHOD

Experimental Setup for Injection Rate

The fuel injection rate was analyzed according to the Bosch method [16] with an IAV@ Injection Rate system (model K-025-50), based on Dernotte et al. [4]. A high pressure pump develops the injection pressure in a conventional common rail. A Bosch CRI 3.1 piezoelectric injector was used for injection into tube loops filled with fuel (Fig.1). This duct is pressurized by an adjusted nitrogen supply. A piezoelectric sensor and temperature sensor are installed downstream of the injector nozzle and detect the dynamic pressure. The injection rate is computed by Eq.1, where $\dot{m}$ is the mass flow rate, S_{tube} the cross sectional area of the tube, a the fuel sound velocity and $p(t)$ the dynamic pressure. The injector is a micro-sac type with three nozzles with conical-shaped orifices. The outlet diameter (D_o) of the orifice is 100 µm, and the degree of conicity AR is 38% [17], where $AR = 100 \times (D_i^2 - D_o^2)/D_i^2$.

$$\dot{m} = \frac{S_{tube}}{a_s} p(t) \qquad (1)$$

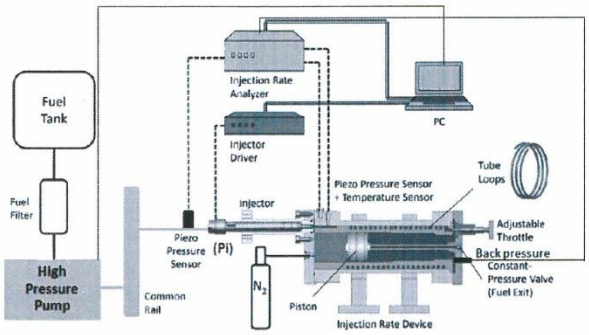

Figure 1. Injection rate experimental setup (from IAV@ technical specification) [4].

Experimental Setup for Spray Injection

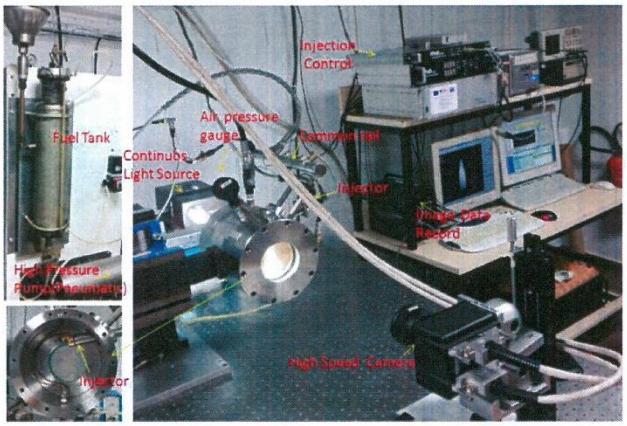

Figure 2. Experimental setup for spray injection.

Visualization of the spray (Fig. 2) is based on Dernotte et al. [5]. The injector and high pressure pump are the same as for the injection rate setup. The fuel injector is located at the top of the vessel with one spray out of three, the one under study, oriented toward the bottom of the vessel on its vertical axis. The 8-bit (256 gray levels) high speed camera (Photron@PowerView™HS-2000) equipped with a 50 mm, f/1.4 Nikon lens and a continuous 150 W halogen lamp records 15,000 frames per second with a resolution of 128 × 512 pixels^2. The vessel is pressurized with air at room temperature from 0 - 2.5 MPa, to reproduce the engine gas density in the injection phase (from 11.8- 29.4 kg/m^3). For

each operating condition, 50 injection sequences were recorded to ensure convergence of the results.

Experimental Test Fuel

The seven fuels chosen in this study are Diesel and a mixes between Diesel and rapeseed Biodiesel. They are referenced in this study as follows: Diesel, B100 (biodiesel 100 % produced from rapeseed), B10 (diesel 90%, biodiesel 10 %), B20 (diesel 80%, biodiesel 20 %), B30 (diesel 70%, biodiesel 30 %), B40 (diesel 60%, biodiesel 40 %), and B50 (diesel 50%, biodiesel 50 %). The fuel properties are listed in Table 1.

Table 1. Fuel matrix in standard conditions.

Abbreviation	Fuel	Density @ 288 K (kg/m^3)	Kinematic viscosity @ 313 K (mm^2/s)
Diesel	Diesel	837	3.66
B10	10% biodiesel	841	3.89
B20	20% biodiesel	845	4.09
B30	30% biodiesel	850	4.22
B40	40% biodiesel	854	4.41
B50	50% biodiesel	859	4.57
B100	100% biodiesel	881	5.49

Operating Conditions

The injection rate experiment was carried out at room temperature (297 K +/−3 K). The injection pressure, *Pi*, varied from 30 - 180 MPa and the back-pressure, *Pb*, from 1 - 5 MPa. The duration of electrical activation of the injector was set at 2000 µs for an effective injection duration of about 4000 µs. Each injection event was reproduced 50 times. The injection frequency was set at 1 Hz to allow the pressure waves in the injection device and in the duct upstream of the injector to be completely dampened [4]. The discharge coefficient (*Cd*) calculated for each condition corresponding to the mass flow rate was averaged between 1000 and 2000 µs after the start of activation (SOA) during the quasi-steady state period (Fig. 3).

The spray injection experiment was also conducted at room temperature (294 K +/− 3 K). The injection pressure, *Pi* varied from 30 - 150 MPa and the back-pressure, *Pb*, from 1 - 2.5 MPa for a variation in density from 11.8 - 29.4 kg/m^3 representing the gas density at the Top Dead Centre (TDC) of conventional diesel engines. The injection duration was set at 4000 µs and the injection frequency at 1 Hz. Additional information about cavitation for these conditions can be found in Dernotte et al. [5]. These injector and operating conditions were chosen so as to avoid or to limit cavitation phenomena [4,5,14]

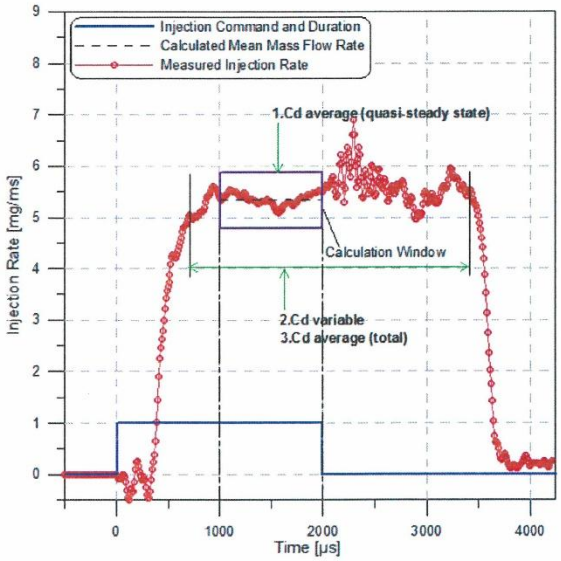

Figure 3. Mean mass flow rate calculation window during the quasi steady state period-case of diesel fuel - Pi= 30 MPa, Pb= 5 MPa.

Injection Rate Analysis

The injection rate analysis method used followed Payri et al. [10,17] and Dernotte et al. [4]. Eq. 2 was used to calculate the discharge coefficient *Cd*, by mean mass flow rate, $\dot{m}_{measured}$ from the quasi-steady state period 1000 - 2000 µs after the start of activation (SOA)(Fig. 3).

This period avoids the transient phenomena related to the opening and closing phases of the injector [4]. The theoretical mass flow rate (Eq.3) is derived from a combination of the continuity equation (Eq.4) and Bernoulli's equation (Eq.5), assuming that the inlet velocity was negligible:

$$Cd = \frac{\dot{m}_{measured}}{\dot{m}_{th}} \quad (2)$$

$$\dot{m}_{th} = n_{orifice} \cdot S_c \sqrt{2\Delta P \cdot \rho_f} \quad (3)$$

$$\dot{m}_{th} = n_{orifice} \cdot \rho_f \cdot S_c \cdot V_{th} \quad (4)$$

$$V_{th} = \sqrt{\frac{2.\Delta P}{\rho_f}} \quad (5)$$

where $n_{orifice}$ is the number of orifices on the outlet geometric cross-sectional area of the orifice, ΔP the pressure differential (ΔP = injection pressure, *Pi* - back pressure, *Pb*), ρ_f the fuel density at the experimental temperature, and V_{th} the theoretical velocity at the fuel outlet section. *Re* the Reynolds

number is calculated by Eq. 6, where V_{mean} is the fuel mean velocity at the orifice exit, D_o is the geometric outlet diameter and ν is the kinematic viscosity of the fuel at the experimental temperature. V_{mean}, the fuel exit mean velocity (Eq. 7) can be determined by measuring the mass flow rate and using the continuity equation under the assumption that there is no cavitation. Flow losses are attributed to losses of flow velocity.

$$Re = \frac{V_{mean} \cdot D_O}{\nu} \quad (6)$$

$$V_{mean} = \frac{\dot{m}_{measured}}{n_{orifice} \cdot S_c \cdot \rho_f} \quad (7)$$

Spray Images Analysis

Raw images were analyzed using a digital image processing program to determine the spray tip penetration S and spray angle Θ at $S/2$ using the same methodology as Dernotte et al. [5]. Figure 4 shows the image processing steps from raw spray images. In summary there are three main steps. First, the background is subtracted from the spray region and then it is converted to a negative image. Second, the image is binarized by applying an intensity threshold level according to the Otsu method [18], to "separate" the spray from the background. Third, from the digitized images, the spray tip penetration S is measured (here defined as the value corresponding to 20% of the maximum value based on the axial profile), as well as the spray angle at $S/2$.

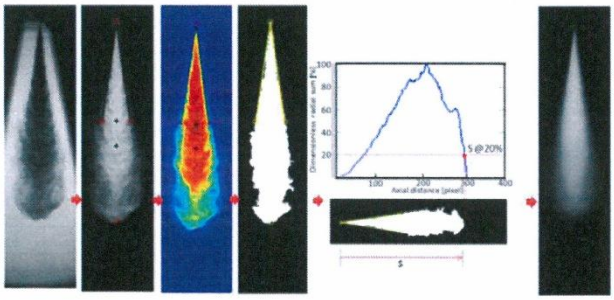

Figure 4. Image analysis process from raw spray image: a) From raw image change to 2 colors; b) Change from two colors to number of pixels and calculate spray penetration; c) Find average spray image.

Sound Velocity Measurement

Sound velocity is an important thermophysical propertie of fuel, as it directly characterizes the fuel injection and NOx emissions in diesel engines [19]. It is necessary in order to determine the mass flow rate (see Eq. 1). The injection rate device can be used to estimate sound velocity [4,20]. The method is based on determination of the time delay between the incident signal induced by the injection event and the first reflection wave [4]. The distance travelled by the pressure wave is 10.2 m with a maximum error of 0.3%. The acoustic wave is generated by an injection at 30 MPa in the injection rate system under a back-pressure from 1 to 5 MPa at room temperature. Tat et al. [21] proposed a three-variable polynomial to fit the sound velocity (Eq. 8). The variables are the temperature (T), the pressure (P) and the Biodiesel percentage (B). The coefficients C depend on the Diesel and Biodiesel characteristics.

$$a_s = C_1.T + C_2.P + C_3.B + C_4.T.P + C_5.P.B + C_6.P^2 + C_7.B^2 + C_8 \quad (8)$$

In our case (Fig.5), we chose a linear fit to show that the sound velocity increases approximately linearly with back-pressure. These experimental values are close to the measurements made by Dernotte et al. [4] and differ by +/ −2.1% from the results of Freitas et al. [19].

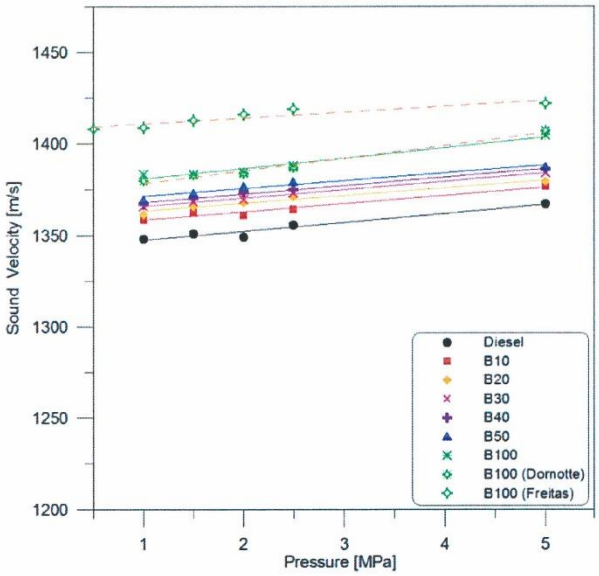

Figure 5. Sound velocity as a function of the different fuels at room temperature.

RESULTS AND DISCUSSION

Effect of Blended Fuel Properties on Discharge Coefficient

Figures 6 and 7 shows the discharge coefficient versus the pressure difference for different fuels. The discharge coefficient is calculated by Eq. 2. It increases when the pressure difference increases. No significant difference between the discharge coefficient with Diesel or biodiesel blends was observed in the range of injection pressures used here. However a slight decrease is observed with B100 for injection pressures up to 120 MPa. Beyond this pressure cavitation phenomena can occur with low back-pressure.

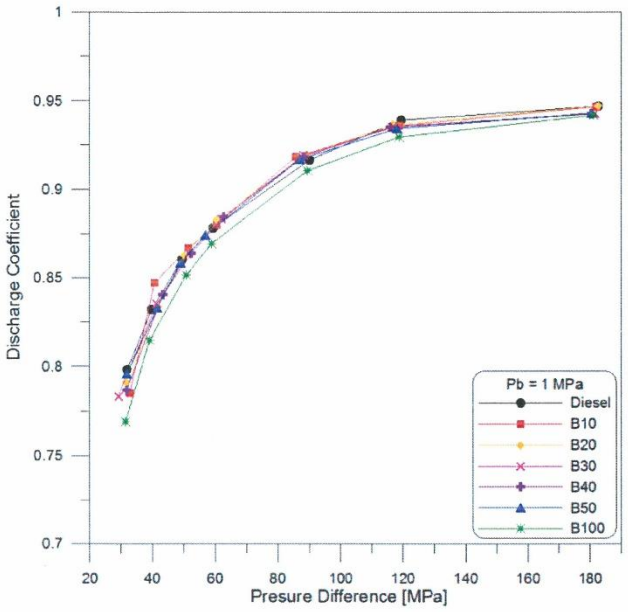

Figure 6. Impact of fuel blend on discharge coefficient - Pi= 30 - 180 MPa, Pb= 1 MPa.

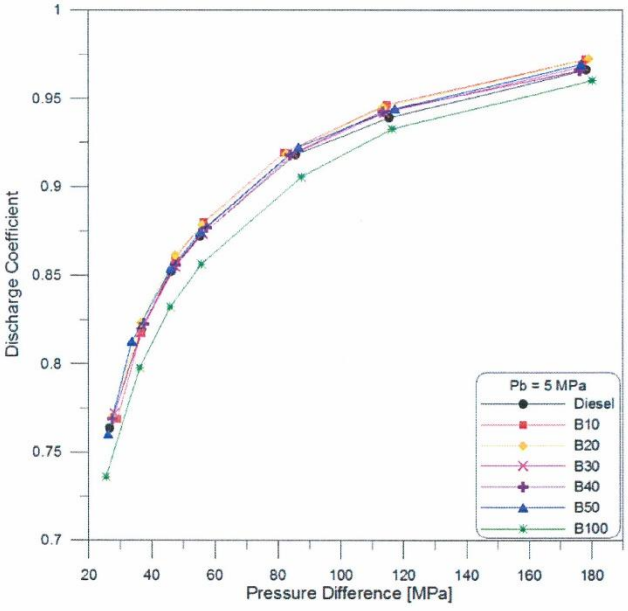

Figure 7. Impact of fuel blend on discharge coefficient - Pi =30 - 180 MPa, Pb = 5 MPa.

The discharge coefficient does not change when the fraction of biodiesel in the diesel fuel increases. The density changes from 837-859 kg/m^3 (an increase of 0.5 - 2.6 %), and viscosity varies from 3.66 - 4.57 mm^2/s (an increase of 6.2 - 24.8%). This means that there is no significant influence of fuel density and viscosity on the discharge [4]. However in the case of B100 (which at 881 kg/m^3 is denser than Diesel and 50% more viscous than Diesel) the discharge coefficient is poorer than that of the other fuels. The results are similar to the findings of Park et al. [11], Seykens et al. [7] and Desantes et al. [9].

We tested two correlations. The first is an empirical correlation adapted from Payri et al. [10] by Dernotte [4]. Dernotte et al. kept the shape of the equation and replaced the outlet diameter and the conicity by our variables: viscosity and pressure difference.

Considering Eq. 9, the parameter Cd', $K1$ and $K2$ now depend on the nozzle geometry. The superscripts a, b, c, d and e are obtained by minimizing the sum of square errors between the correlation and experiment: Cd'=1, $K1$=−3.37, $K2$=−2.67E+5, a=−0.02, b=−0.73, c=−1.89, d=0.04, e=1.58 and Re from Eq. 6.

$$Cd = Cd' + K1.v^a.\Delta P^b - \frac{K2.v^c.\Delta P^d}{Re^e} \quad (9)$$

The second correlation is based on the work by Soteriou et al. [14] and applies the generalized Bernoulli principle: the flow rate $\dot{m}_e$ is estimated by taking the friction loss into account.

$$\frac{1}{2}\rho_f \dot{m}_e{}^2 = P_i - P_{back} - \Delta P_c = \Delta P - \Delta P_c \quad (10)$$

Rearranging Eq. 2, Eq. 3 and Eq. 10, the expression of the discharge coefficient becomes:

$$Cd = \sqrt{\frac{\Delta P - \Delta P_c}{\Delta P}} \quad (11)$$

The Cd drop is assimilated as a pressure loss. If Cd=1, it means that there is no pressure loss (ΔP_c = 0). The pressure loss is determined by the following empirical correlation, where A and B are parameters for orifice type loss and C and D for viscous type loss:

$$\Delta P_c = A.v^D.\dot{m}_{th}^{(C.v+B)} \quad (12)$$

The coefficient values A,B,C,D are obtained by minimizing the sum of square errors between the correlation and experiment: A=95.32, B =0.33, C=−0.02, D=−0.49 for Eq. 12.

Figure 8 compares the discharge coefficient correlation from Eq. 9 and Eq. 11, at pressure differences of 30 - 180 MPa, with experimental data for pure biodiesel. The average error is +/−2%. The result is better (+/−0.5%) for the second correlation on high pressure difference. The performance of this new correlation is similar (+/−2.0%) for all fuels (cf. Fig. 9).

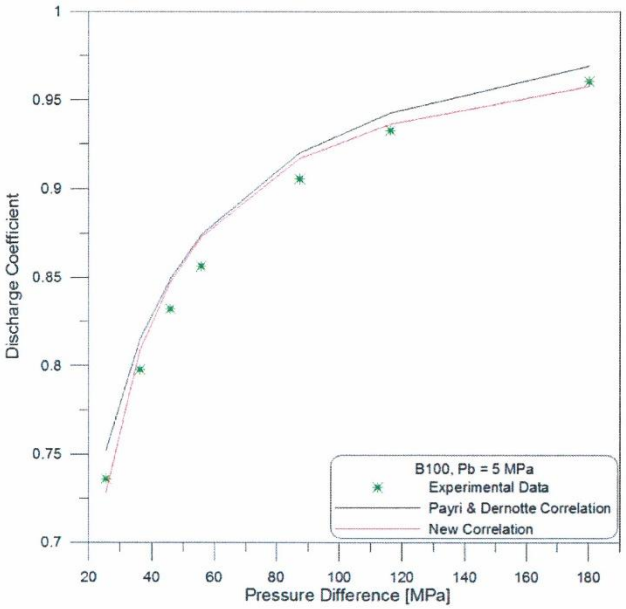

Figure 8. Discharge coefficient: experimental results for B100 and correlation, B100 - Pi = 30-180 MPa, Pb = 5 MPa.

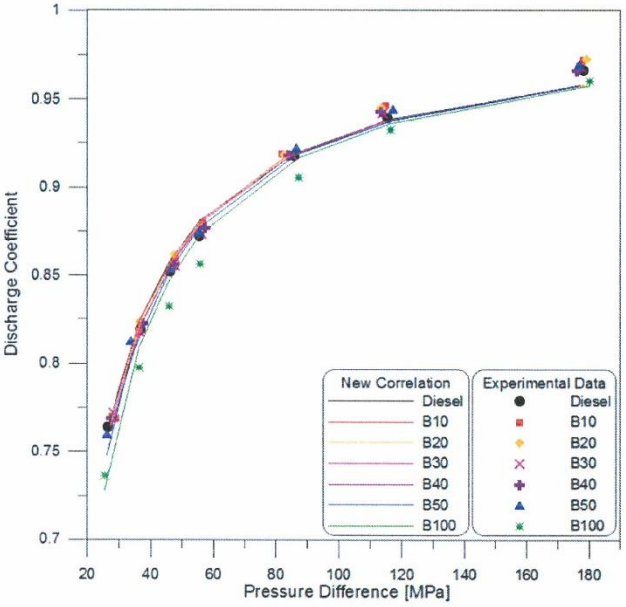

Figure 9. Discharge coefficient: experimental results compared with the new correlation - Pi = 30-180 MPa, Pb = 5 MPa.

Figure 10 shows that cavitation starts to affect the discharge coefficient at 90 MPa for a *Pb* around 2.5 MPa. At 120 MPa, from 1 to 2.5 MPa of *Pb*, the discharge coefficient is definitely affected by cavitation. At 5.0 MPa, a sudden drop is observed in the discharge coefficient as the Reynolds number increases, so there is no effect of cavitation for this back-pressure.

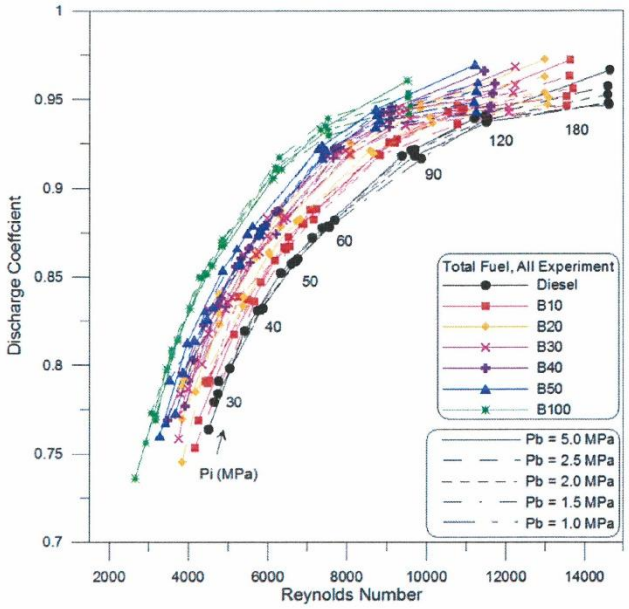

Figure 10. Discharge coefficient versus Reynolds number for all the fuels - Pi=30-180 MPa, Pb= 1-5 MPa.

The new correlation is plotted in Fig.11 with all the experimental data. The x-coordinate is the Reynolds number and the y-coordinate is the discharge coefficient.

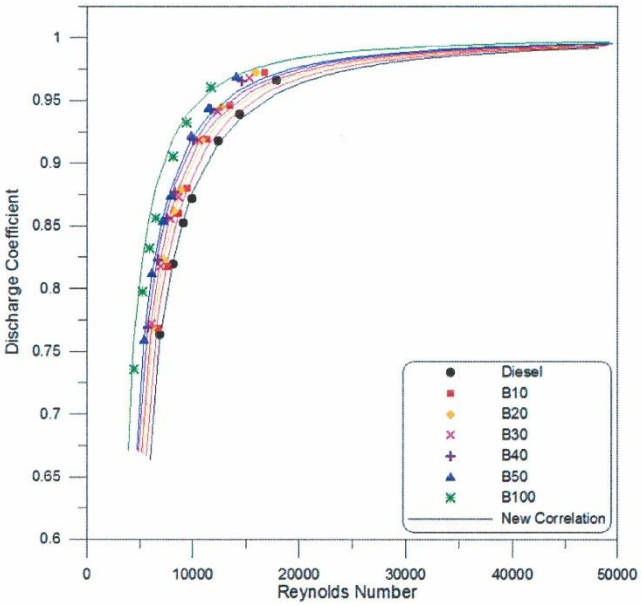

Figure 11. Discharge coefficient versus Reynolds number for all the fu els - Pi = 30-180 MPa, Pb = 5 MPa.

Considering these correlations obtained in non-cavitation conditions for each fuel, it can be stated that the discharge coefficient depends not only on the Reynolds number but also on the geometry and the fuel. Unlike Payri et al. [22], for a medium Reynolds number we observe a distinct curve for each fuel (Fig. 11). The new correlation with only four parameters gives a good estimation of the discharge

coefficient for all the fuels and for all experimental conditions without cavitation.

The mass flow rate is exclusively a function of $\sqrt{2\rho\Delta P}$ or square root density [4,10]. The decrease of 3.6% in the discharge coefficient with B100 is not visible on Fig.12.

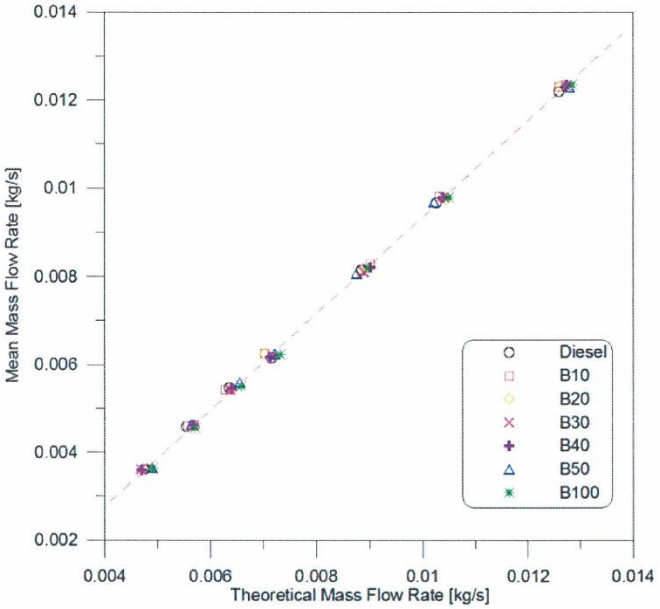

Figure 12. Mean mass flow rate (experimental data) versus theoretical mass flow rate - Pb = 5 MPa.

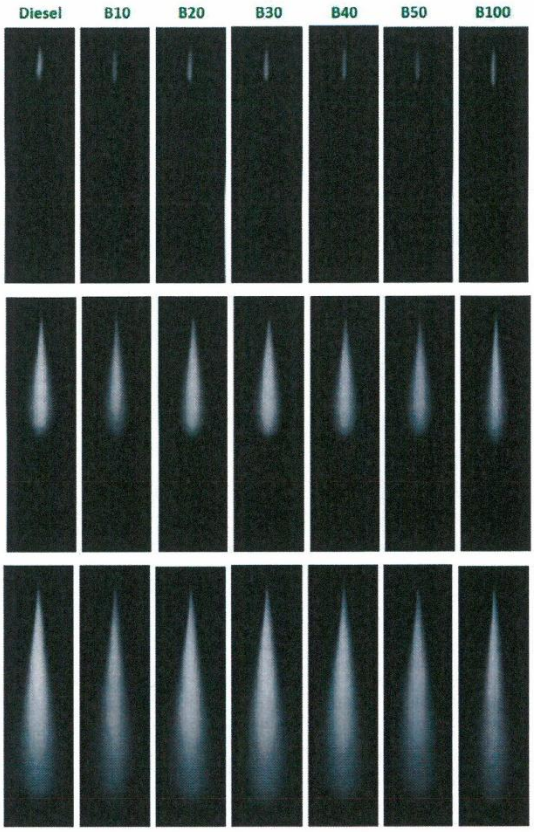

Figure 13. Comparison of spray development : average image 400 µs, 993 µs, 2000 µs after injection - Pi = 90 MPa, Pb = 1 MPa.

Effect of Fuel Blend on Spray Injection Behavior

Spray Tip Penetration Analysis

The raw images were analyzed with a digital image processing program to determine the spray tip penetration S and spray angle θ. Figure 13 shows the average image 400, 993 and 2000 µs after injection when Pi = 90 MPa, Pb = 1 MPa. It can be noted that diesel fuel and biodiesel-blended fuel have a similar spray penetration but that the penetration length with B100 is longer than with the other fuels at the start of injection. These results are similar to those of Chen et al. [13].

The effect of blended fuels on the spray behavior is shown in Fig.14. This figure shows the time evolution of penetration length at Pi = 30 MPa and Pb = 1 or 2.5 MPa for all fuels. For the blended fuel and Diesel the penetration lengths are very similar. In line with Fig. 13 only B100 has a slightly different behavior (Fig.15), with a higher penetration length. These results are the same as those of Bang et al. [6], Desantes et al. [9], Gao et al. [12] and Chen et al. [13].

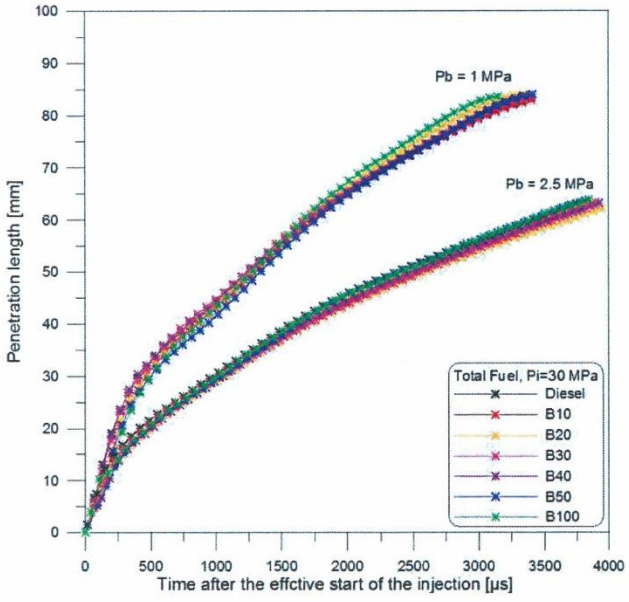

Figure 14. The penetration length from experimental data of total fuel - Pi = 30 MPa, Pb = 1 and 2.5 MPa.

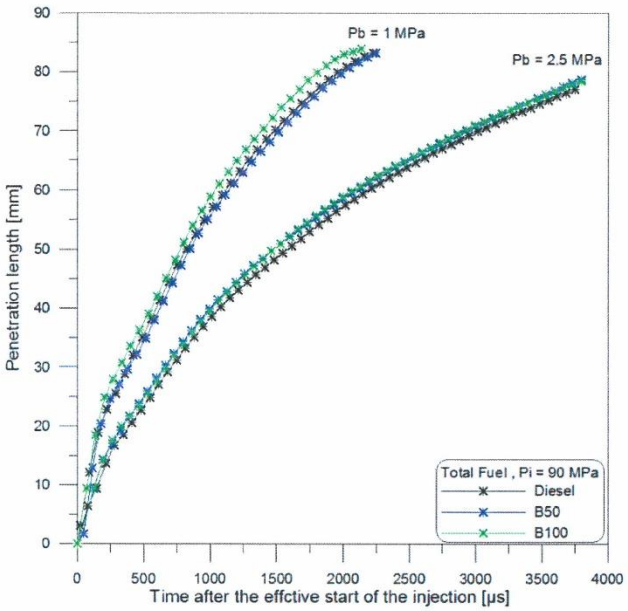

Figure 15. The penetration length from experimental data of total fuel - Pi = 90 MPa, Pb = 1 and 2.5 MPa.

Spray Angle Analysis

The experimental data of spray angle were compared using the Naber & Siebers correlation [15]. The experimental spray angle was measured using an image processing program. It follows Eq.13 where $A_{p,s/2}$ is the projected area of the upstream half of the spray in an image. S is the penetration length.

$$\theta = tan^{-1}\left(\frac{Ap,s/2}{(S/2)^2}\right) \qquad (13)$$

The correlation is based on the mass and momentum conservation equations, applied to an ideal spray. The major assumptions for spray analysis are: (a) uniform velocity profile, (b) instantaneous injection start, (c) no velocity slip between the fuel and entrained air, and (d) constant flow and spray angle. In [14], ΔP, ρ_a, ρ_f are data from the operating conditions, D_o data from the nozzle, and angle Θ from the average Θ in the quasi-steady state. Under non-cavitating conditions, Cv can be assumed equal to Cd [23]. With the same injector, Dernotte et al. [5] showed that the correlation is efficient when coefficient a is 0.9 and that it achieves a maximum error of +/−5%.

$$S(t) = C_v.\frac{\sqrt{2\Delta P}}{\sqrt{\rho_f}}.\frac{1}{\left[1+\left(\frac{a.C_v}{D_o}.\frac{\tan\left(\frac{\theta}{2}\right)\sqrt{2\Delta P.\rho_a}}{\rho_f}.t\right)^{1.1}\right]^{\frac{1}{2.2}}}.t \qquad (14)$$

We tested the performance of this correlation to estimate the time evolution of the spray angle. The expression becomes:

$$tan\frac{\theta(t)}{2} = \frac{D_0}{a.Cd}.\frac{\rho_f}{\sqrt{2\Delta P.\rho_a}}.\frac{1}{t}.\left[\left(\frac{C_d.\sqrt{2\Delta P}}{S(t).\sqrt{\rho_f}}.t\right)^{2.2} - 1\right]^{\frac{1}{1.1}} \qquad (15)$$

In this case the model is extended to conditions where the angle and flow rate are not constant. However the spray is considered as a succession of stationary states.

Three definitions of Cd were tested (Fig. 3):

1. Cd average (quasi-steady state) $= \frac{\dot{m}_{quasi-steady\ state}}{\dot{m}_{th}}$
2. Cd variable $= \frac{\dot{m}_{measured}(t)}{\dot{m}_{th}}$
3. Cd average (total) $= \frac{m_{total}}{\dot{m}_{th}.t_{inj}}$ with t_{inj} the effective injection duration

Figure 16 shows the impact of Cd on the spray angle. The three definitions of Cd give similar results. The choice of Cd modifies the average angle by +/−7.3%. So it is possible to obtain a good estimation of spray angle with Naber & Siebers' correlation with a constant Cd.

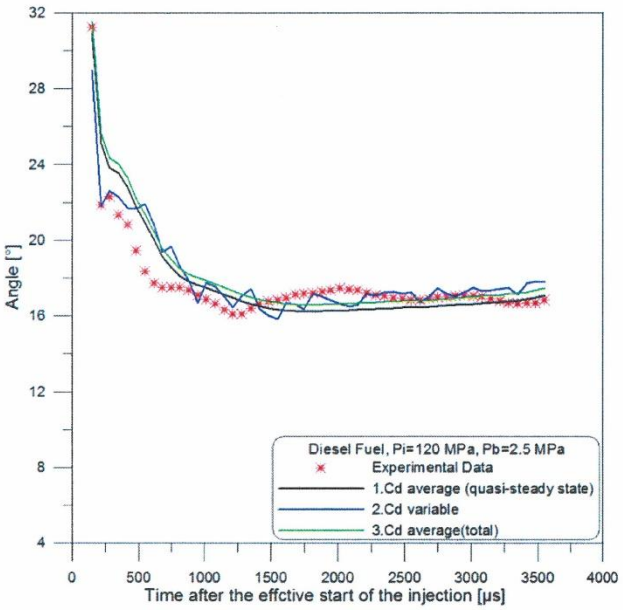

Figure 16. The spray angle from experimental data and estimated values by changing Cd.

Figure 17 shows the experimental and estimated time evolution of the spray angle. There are two distinct phases: the transient phase and the constant phase over 2000 µs. During the transient phase, the spray angles are different for each fuel. For the constant phase the spray angles are similar for blended fuel and Diesel at all back-pressures and pressure differences. These results are the same as literature values (Desantes et al. [9], Gao et al. [12] and Chen et al. [13]).

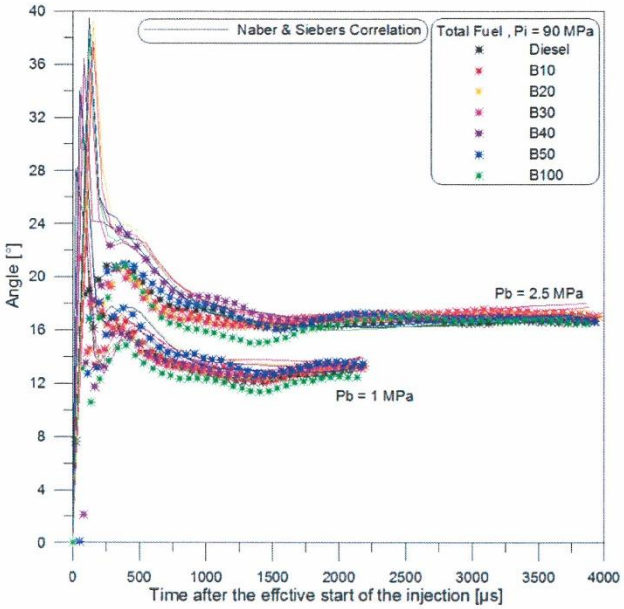

Figure 17. The spray angle from experimental and estimated fuel values - Pi=90 MPa, Pb= 1 and 2.5 MPa.

Figure 18 shows the maximum spray angle during the transition phase versus the injection pressure. The angle increases when the injection pressure increases. Figures 19 and 20 show that the angle tends to decrease when the fraction of biodiesel increases. This trend is stronger for low back-pressure and low injection pressure.

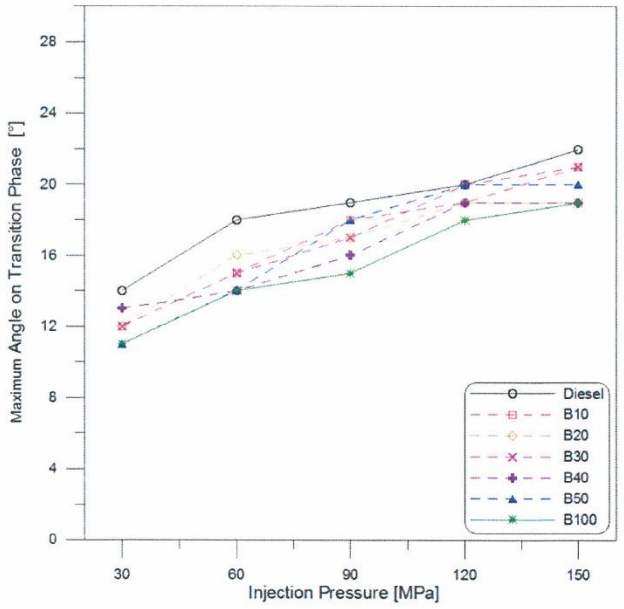

Figure 18. Maximum angle in transition phase - Pb = 1 MPa.

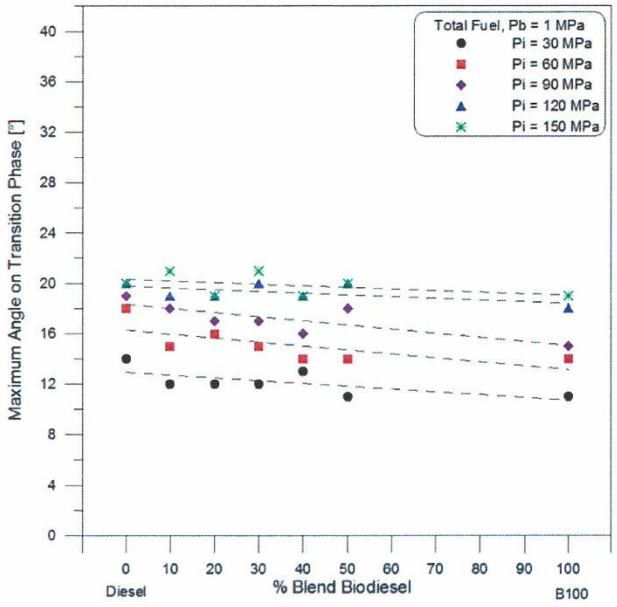

Figure 19. Maximum angle in transition phase versus percentage of biodiesel blend - Pb = 1 MPa.

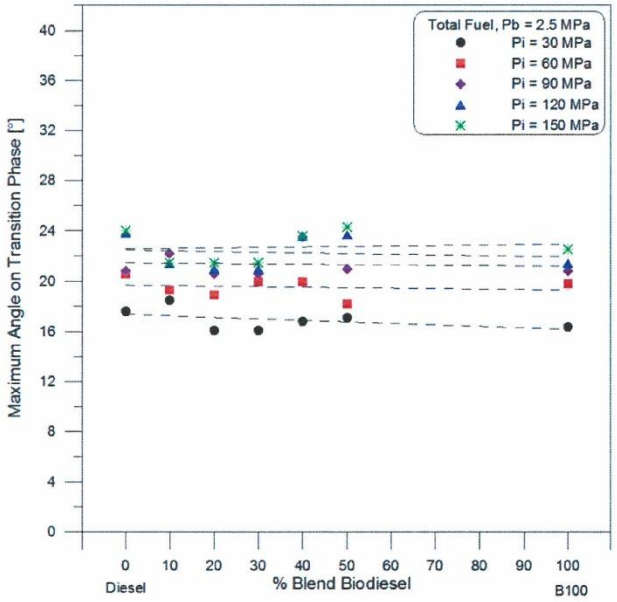

Figure 20. Maximum angle in transition phase versus percentage of biodiesel blend - Pb = 2.5 MPa.

Figure 21 shows the average spray angle during the steady phase versus the percentage of Biodiesel in Diesel. During this phase, the average angles are very similar. Only the spray angle with B100 is smaller.

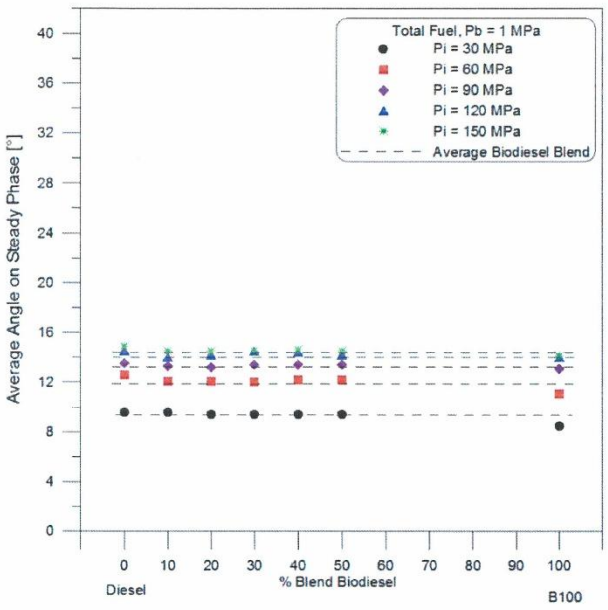

Figure 21. Average angle in steady phase versus percentage biodiesel blend - Pb = 1 MPa.

CONCLUSIONS

The study of the influence of biodiesel and diesel blends on the injection rate and spray injection behavior in non-vaporizing conditions was conducted using an injector with three conical convergent orifices. Measurements of the mass flow rate and visualization of the spray with diesel fuel, biodiesel blends and Biodiesel (B100) were made. The conclusions of this study are summarized as follows:

By increasing the fraction of biodiesel in the blend the discharge coefficient does not change significantly. However, with B100 the discharge coefficient tends to be slightly lower than that of diesel and biodiesel blended fuels.

The spray penetration of diesel fuel and biodiesel blended fuels is similar while with B100, the spray penetration is higher than that of diesel and biodiesel blended fuels. This difference is the result of a smaller spray angle with B100. The fraction of Biodiesel seems to have a slight influence during the transient phase. For low back and injection pressures the maximum spray angle decreases with the percentage of Biodiesel in the fuel.

In this work the fraction of biodiesel in the fuel did not exceed 50% which is in line with the use of biodiesel in many countries (where a biodiesel fraction of 2-20% is mandatory). The results show that increasing the fraction of biodiesel in the blend does not have a significant influence on the discharge coefficient or on the spray behavior.

REFERENCES

1. Demirbas A., "Progress and recent trends in biodiesel fuels," Energy Conversion and Management, 2009,50:14-34.

2. No S.Y., "How vegetable oils and their derivatives affect spray characteristics in CI engines - A review," Atomization and Sprays, 2011, 21(1):87-105.

3. Perdiguero J. and Jiménez J.L., "Sell or not sell biodiesel: Local competition and government measures," Renewable and Sustainable Energy Reviews, 2011, 15:1525-1532.

4. Dernotte J., Hespel C., Foucher F. and Mounaïm-Rousselle C., "Influence of physical fuel properties on the injection rate in a diesel injector," Fuel, 2012,96:153-160.

5. Dernotte J., Hespel C., Foucher F. and Mounaïm-Rousselle C., "Influence of fuel properties on the diesel injection process in non-vaporizing conditions," Atomization and Sprays, 2012, 22(6):461-492.

6. Bang S.H. and Lee C.S., "Fuel injection characteristics and spray behavior of DME blended with methyl ester derived from soybean oil," Fuel, 2010,89:797-800.

7. Seykens X.L.J., Somers L.M.T. and Baert R.S.G., "Modeling of common rail fuel injection system and influence of fluid properties on injection process," In: Proceedings of VAFSEP," Dublin, Ireland; July 6-9, 2004.

8. Som S., Longman D.E., Ramirez A.I. and Aggarwal S.K., "A comparison of injector flow and spray characteristics of biodiesel with petrodiesel," Fuel, 2010, 89:4014-4024.

9. Desantes J.M., Payri R., Garcia A. and Manin J., "Experimental study of biodiesel blends' effects on diesel injection processes," Energy & Fuels, 2009, 23:3227-3235.

10. Payri R., Salvador F.J., Gimeno J. and Morena J., "Study of cavitation phenomena based on a technique for visualizing bubbles in a liquid pressurized chamber," Fuel, 2009, 30:768-777.

11. Park S.H., Suh H.K. and Lee C.S., "Effect of cavitating flow on the flow and fuel atomization characteristics of biodiesel and diesel fuels," Energy & Fuels, 2008, 22:605-613.

12. Gao Y., Deng J., Li C., Deng F., Liao Z., Wu Z. and Li L., "Experimental study of the spray characteristics of biodiesel based on inedible oil," Biotechnology Advances, 2009, 27:616-624.

13. Chen P.C., Wang W.C., Roberts W.L. and Fang T. "Spray and atomization of diesel fuel and its alternatives from a single-hole injector using a common rail fuel injection system," Fuel, 2012; 103:850-861.

14. Soteriou C., Lambert M., Zuelch S. and Passerel D. "The flow characteristics of high efficiency diesel nozzles with enhanced geometry holes," In: THIESEL Conference on Thermo and Fluid dynamics in Diesel Engines, Valencia, Spain, September 13-15, 2006.

15. Naber, J. and Siebers, D., "Effects of Gas Density and Vaporization on Penetration and Dispersion of Diesel Sprays," SAE Technical Paper 960034, 1996, doi: 10.4271/960034.

16. Bosch, W., "The Fuel Rate Indicator: A New Measuring Instrument For Display of the Characteristics of Individual

Injection," SAE Technical Paper 660749, 1966, doi: 10.4271/660749.

17. Payri P., Garcia J.M., Salvador F.J. and Gimeno J., "Using spray momentum flux measurements to understand the influence of diesel nozzle geometry on spray characteristics," Fuel, 2005, 84:551-561

18. Otsu N., "A threshold selection method from gray-level histograms," IEEE Trans. Syst. Man Cyber, 1979, Vol. 1: 62-66.

19. Freitas S.V.D., Paredes M.L.L., Daridon J.L., Lima A.S. and Coutinho J.A.P., "Measurement and prediction of the speed of sound of biodiesel fuels," Fuel 2012, 103:1018-1022.

20. Kegl B., "Numerical analysis of injection characteristics using biodiesel fuel," Fuel, 2006, 85:2377-2387.

21. Tat M.E. and Van Gerpen J.H., "Effect of temperature and pressure on the speed of sound and isentropic bulk modulus of biodiesel and diesel fuel," Jam Oil Chem. Soc, 2003, 80:1127-1130.

22. Payri R., Salvador F.J., Gimeno J. and Venegas O., "Study of cavitation phenomenon using different fuels in a transparent nozzle by hydraulic characterization and visualization," Experimental Thermal and Fluid Science, 2013, 44:235-244.

23. Payri F., Bermudez V., Payri R. and Salvador F.J., "The influence of cavitation on the internal flow and the spray characteristics in diesel injection nozzles," Fuel, 2004; 83:419-431.

CONTACT INFORMATION

Corresponding authors :

P. Tinprabath
padipan.tinprabath@etu.univ-orleans.fr

C. Hespel
camille.hespel@univ-orleans.fr

S. Chanchaona
somchai.cha@kmutt.ac.th

F. Foucher
fabric.foucher@univ-orleans.fr

ACKNOWLEDGMENTS

This work was cofinanced by the European Union and the European Regional Development Fund. The authors would like to thank Bruno MOREAU, Julien LEMAIRE and Jérémie DERNOTTE for their contribution to the experimental setup.

ABBREVIATIONS

AR - Degree of conicity (area reduction)

Ap,s/2 - Projected area of upstream half of the spray

a_s - Fuel sound velocity

Cd - Discharge coefficient

Cv - Velocity coefficient

D_o - Outlet diameter

D_i - Inlet diameter

$\dot{m}$ - Mass flow rate

$\dot{m}_{measured}$ - Mean mass flow rate

$\dot{m}_{th}$ - Theoretical mass flow rate

$\dot{m}_e$ - Estimated mass flow rate

$n_{orifice}$ - Number of orifices on the nozzle

p(t) - Dynamic pressure

Pb - Back-pressure

Pi - Injection pressure

Re - Reynolds number

S - Spray penetration length

S_c - Outlet geometric cross-sectional area

S_{tube} - Cross-sectional area of the measuring tube

V_{mean} - Mean velocity at the outlet section

ΔP - Pressure difference

t - Time

t_{inj} - Effective injection duration

ν - Fuel kinematic viscosity

ρ_a - Air density

ρ_f - Fuel density

APPENDIX

Cavitation analysis.

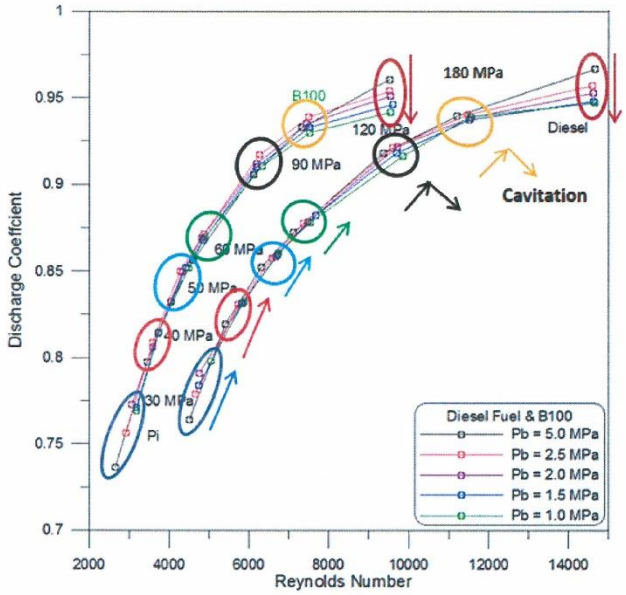

Figure A1. Discharge coefficient versus Reynold number for Diesel fuels and Biodiesel - Pi= 30-180 MPa, P = 1-5 MPa.

ISSN 0148-7191

SAE Customer Service:
Tel: 877-606-7323 (inside USA and Canada)
Tel: 724-776-4970 (outside USA)
Fax: 724-776-0790
Email: CustomerService@sae.org
SAE Web Address: http://www.sae.org
Printed in USA

Appendix III

Article Fuel

Fuel, 144 (2015), pp. 80-89.

Fuel 144 (2015) 80–89

Contents lists available at ScienceDirect

Fuel

journal homepage: www.elsevier.com/locate/fuel

Influence of biodiesel and diesel fuel blends on the injection rate under cold conditions

P. Tinprabath [a,*], C. Hespel [a], S. Chanchaona [b], F. Foucher [a]

[a] Laboratoire PRISME, Université d'Orléans, INSA CVL, Orléans 45072, France
[b] CERL, King Mongkut's University of Technology Thonburi, Bangkok 10140, Thailand

HIGHLIGHTS

- The properties of biodiesel and biodiesel blends were tested in cold conditions.
- A kinematic viscosity correlation of fuel for cold conditions was developed.
- The influence of the percentage of biodiesel blend and temperature decreases on injection rate behavior was investigated.
- The discharge coefficients of biodiesel and biodiesel blends in cold conditions were investigated.

ARTICLE INFO

Article history:
Received 29 September 2014
Received in revised form 1 December 2014
Accepted 3 December 2014
Available online 19 December 2014

Keywords:
Fuel property
Biodiesel blend
Injection rate
Discharge coefficient
Cold conditions

ABSTRACT

During start-up of the engine under cold temperatures, conditions can be different when biodiesel is used due to the low fuel injection pressure and the high cloud point and high pour point. It is consequently of interest to understand the behavior of the injector under cold conditions when operating with biodiesel and the impact on the combustion process. This article presents an experimental study of the influence of diesel fuel and biodiesel blends on injection flow. A Bosch CRI 3.1 piezoelectric injector was used on a typical diesel engine. Five fuel types were tested: diesel fuel, winter diesel fuel, two diesel–biodiesel blends (B20, B50), and pure biodiesel (B100). Injection pressures were set at 30–60 MPa for the study of the injection flow characteristics at room temperature, in non-vaporizing conditions and in cold conditions. The experimental results show that cold temperatures (−5 and −8 °C) have no effect on the injection delay for any of the fuels. The discharge coefficients for all fuels are lower than at room temperature. When the fraction of biodiesel in the blend is increased, the change in the discharge coefficients is insignificant. New correlation coefficients for estimating the kinematic viscosity and the discharge coefficient has been presented for cold conditions.

1. Introduction

Biodiesel is a very interesting fuel because it is renewable, thus increasing energy security, it is environmentally friendly, and it has a higher cetane number and a lower sulfur and aromatic than pure Diesel. The main disadvantages of biodiesel are its higher viscosity, lower energy content, higher cloud point and pour point, higher nitrogen oxide (NOx) emissions, lower power and high cost [1]. However, many countries can produce their own biodiesel and blends with diesel fuel of 2–20% [2,3]. Governments (e.g. the European Union, the U.S.A.) have stipulated that fuel should be blended with biodiesel [3], although consumers are unconvinced about the use of biodiesel fuel blends in automotive engines because of their concerns about combustion efficiency, pollutant emissions and the impact on engine components. Attention has especially focused on pollutant emissions from biodiesel-fuelled vehicles with the implementation in 2014 of the Euro VI regulations.

The new standards involve problems related to cold-start, namely evaluation of post-treatment strategies and EGR at low temperature. The regulations concerning the quality of cold start at −7 °C will become increasingly stringent. At these temperatures the viscosity is higher. The blending of biodiesel with diesel fuel increases the cloud point, the cold filter plugging point (CFPP), or the pour point, which can clog the fuel lines and filters of the vehicle's fuel system [4]. Whatever the type of fuel, diesel–biodiesel

* Corresponding author at: Université d'Orléans, Laboratoire PRISME, 8 rue Léonard de Vinci, 45072 Orléans Cedex 2, France. Tel.: +33 2 38 49 24 57; fax: +33 2 38 41 73 83.
E-mail addresses: padipan.tinprabath@etu.univ-orleans.fr (P. Tinprabath), camille.hespel@univ-orleans.fr (C. Hespel), somchai.cha@kmutt.ac.th (S. Chanchaona), fabrice.foucher@univ-orleans.fr (F. Foucher).

http://dx.doi.org/10.1016/j.fuel.2014.12.010
0016-2361/

Nomenclature

a	fuel sound velocity
AR	degree of conicity (area reduction)
Cd	discharge coefficient
$CFPP$	cold filter plugging point
CP	cloud point
D_i	inlet diameter
D_o	outlet diameter
$\dot{m}$	mass flow rate
$\dot{m}_e$	estimated mass flow rate
$\dot{m}_{measured}$	mean mass flow rate
$\dot{m}_{th}$	theoretical mass flow rate
$n_{orifice}$	number of orifices on the nozzle
Pb	back-pressure
Pi	injection pressure
PP	pour point
$p(t)$	dynamic pressure
ΔP	pressure difference
Re	Reynolds number
S_c	outlet geometric cross-sectional area
SG	specific gravity at 15.5 °C
S_{tube}	cross-sectional area of the measuring tube
V_{mean}	mean velocity at the outlet section
T	fuel temperature
$Troom$	room temperature
v	fuel kinematic viscosity
ρ	fuel density

blends under 5% do not impact cold flow properties [5]. That is why it is important to know the behavior of the diesel injector in these conditions for different fuels.

Several publications [6-12] have highlighted the influence of fuel properties on the performance of the injector under standard temperature conditions. The increased viscosity decreases the flow rate in the nozzle slightly and favors the appearance of larger drops in the spray atomization. However, the decrease in the discharge coefficient is not observed with biodiesel mixtures, only with pure biodiesel [13,14]. On the other hand, the literature shows that it is not easy to find a relation between the fuel mass flow rate and temperature. It depends on the type of injector and type of fuel [15,16]. These two studies show that, in cold conditions, the discharge coefficient (Cd) decreases strongly when the viscosity increases [15]. Kegl [17] studied the impact of temperature on biodiesel for a specific configuration (a single injection assembly of inline fuel injection), and showed that when the temperature decreases, the injection duration, injection timing, mean injection rate and injection pressure increase. No information is available in the literature, however, on the injection rate of diesel–biodiesel blends under cold conditions.

In the present study, the chosen fuels were diesel fuel, biodiesel (rapeseed biodiesel), and diesel fuel blended with 20% and 50% rapeseed biodiesel. We also tested winter diesel which is doubly interesting in that it has the same kinematic viscosity as B20 and the same density as diesel. The fuel properties were measured at the operating temperature and at 8 °C, 0 °C, −5 °C, and −8 °C (very close to the CFPP of Biofuel). We investigated and distinguished the

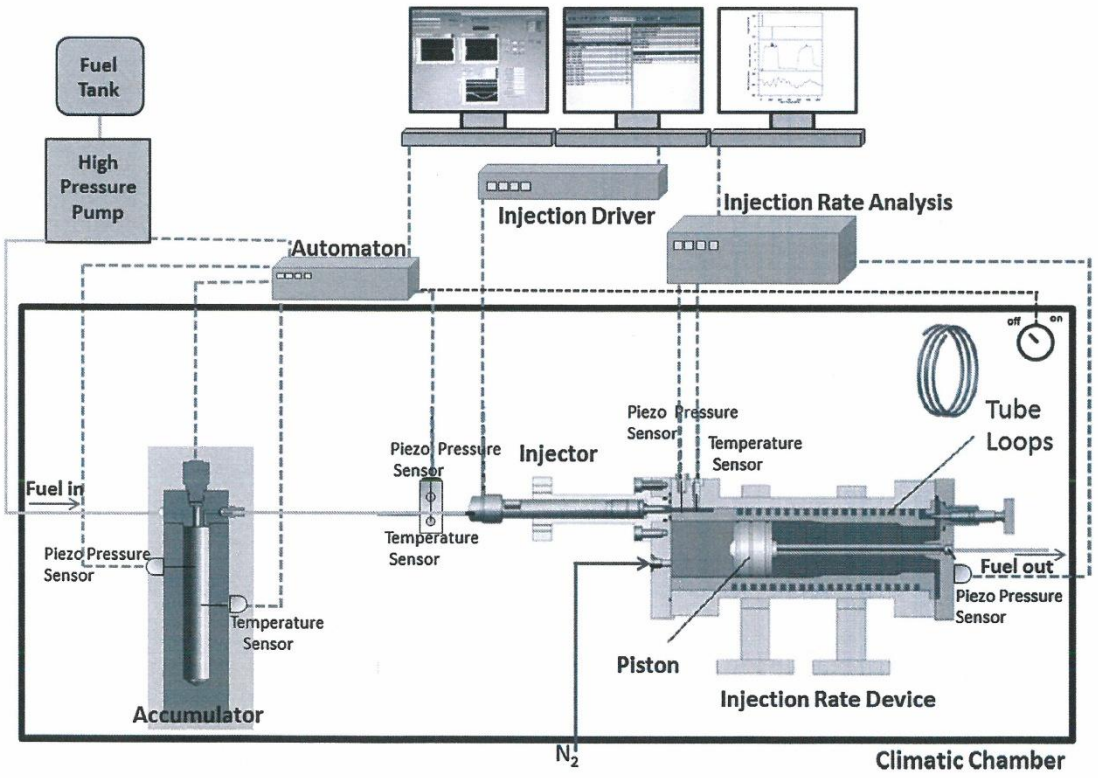

Fig. 1. Injection rate experimental setup (from IAV® technical specification) [10,14].

Table 1
Density and kinematic viscosity of fuels at atmospheric pressure.

T (°C)	Density, ρ (kg/m^3)					Kinematic viscosity, ν (mm^2/s)				
	Diesel	Winter diesel	B20	B50	B100	Diesel	Winter diesel	B20	B50	B100
−8	855.1	853.5	863.3	877.4	900.2	10.38	11.43	11.63	15.42	19.72
−5	852.3	851.4	860.6	874.9	897.7	8.95	9.65	10.07	12.64	16.04
0	848.8	847.4	857.1	871.1	894.1	7.51	8.04	8.24	9.95	13.03
8	843.2	842.4	851.4	865.5	888.3	5.85	6.19	6.40	7.68	9.97
20	834.7	834.1	842.9	856.9	879.6	4.23	4.43	4.61	5.49	7.05

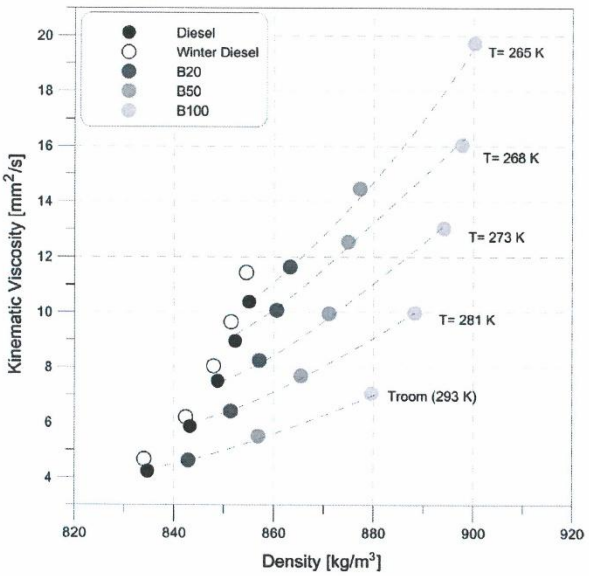

Fig. 2. Fuel matrix – predicted viscosity versus predicted density.

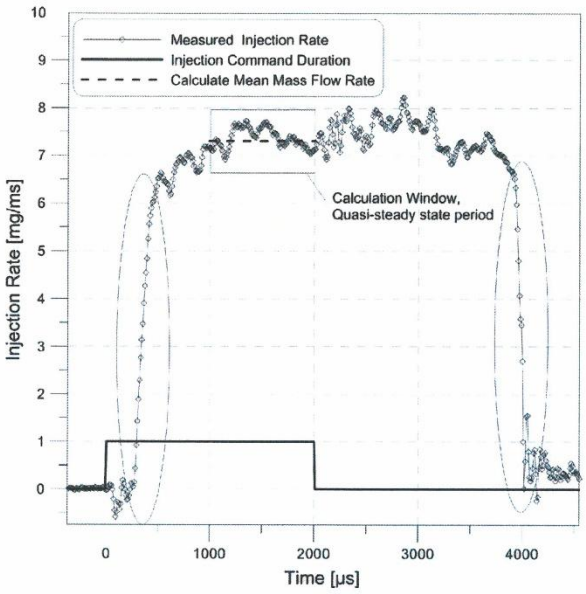

Fig. 4. Mean mass flow rate calculation window during the quasi-steady state period; diesel fuel – Pi = 40 MPa, Pb = 2.5 MPa, room temperature (Troom).

effect of density, viscosity and temperature on the fuel injection rate in cold conditions, and the effect of biodiesel and diesel fuel blends on the injection rate i.e. injection delay, injection duration, discharge coefficient, and fuel mass flow rate.

2. Setup and method

2.1. Experimental setup for injection rate

The fuel injection rate was analyzed according to the Bosch method [18] with an IAV@ Injection Rate system (model

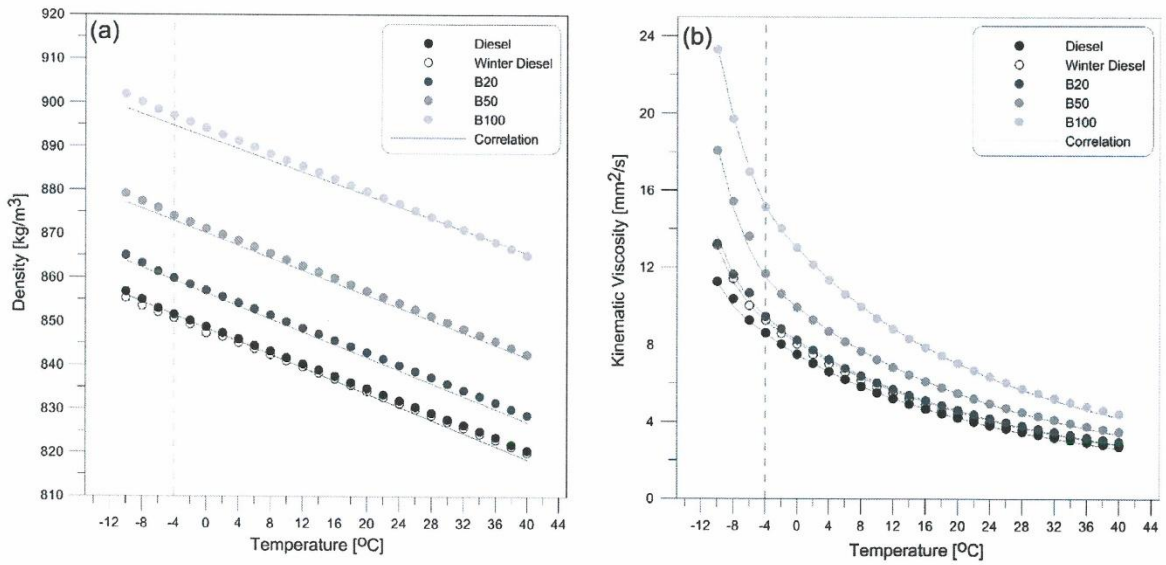

Fig. 3. Experimental data and correlation of (a) density, (b) kinematic viscosity.

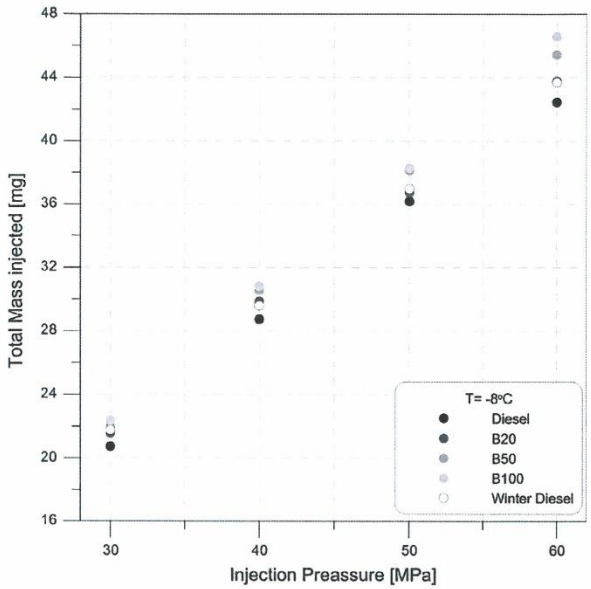

Fig. 5. Total fuel mass injected at $T = -8$ °C.

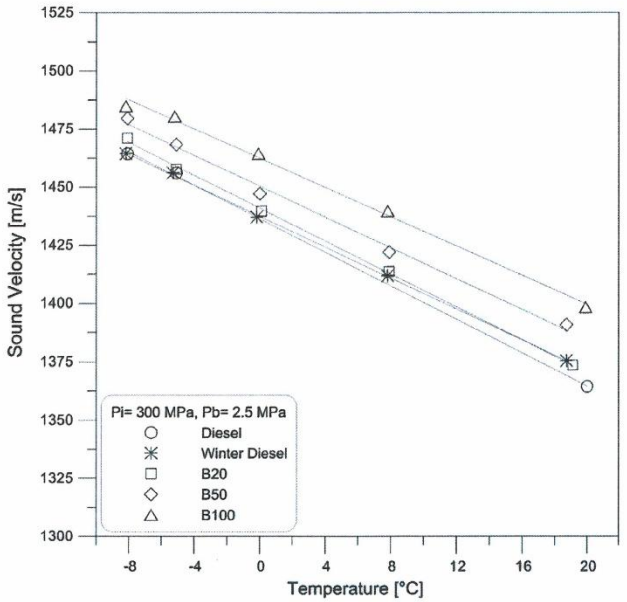

Fig. 7. Sound velocity as a function of temperature for fuels tested at $Pb = 2.5$ MPa.

K-025-50), based on Dernotte et al. [10] and Tinprabath et al. [14]. Since the period 1000–2000 μs does not have any stabilization problem on the injection rate, this period has been used for the main data analysis. The cumulative phenomena is neglected. A high hydraulic pressure pump generates the injection pressure in a small temperature-controlled tank. The accuracy of the pressure regulation is ±10 bar. A 3-hole Bosch CRI 3.1 piezoelectric injector was used for injection into tube loops filled with fuel (Fig. 1). This duct is pressurized by an adjusted nitrogen supply. A piezoelectric sensor and temperature sensor are installed downstream of the injector nozzle in the fuel line and are used to detect the dynamic pressure. The injection rate is computed by Eq. (1), where $\dot{m}$ is the mass flow rate, S_{tube} the cross sectional area of the tube, a the fuel sound velocity and $p(t)$ the dynamic pressure. The injector is a micro-sac type with three nozzles with conical-shaped orifices, and was used in our previous studies [10,11,14]. The outlet diameter (D_o) of the orifice is 100 μm, and the degree of conicity AR is 38% expressed as follow [19]: $AR = 100.(D_i^2 - D_o^2)/D_i^2$ when D_i is the inlet diameter, which limits cavitation phenomena. All the injection equipment was installed in a climatic chamber to control the temperature in the experiment.

$$\dot{m} = \frac{S_{tube}}{a} p(t) \tag{1}$$

2.2. Experimental test fuels

The five fuels chosen in this study were diesel, winter diesel and mixtures of diesel and rapeseed Biodiesel. They are referred to in this study as follows: diesel, winter diesel, B100 (100% biodiesel produced from rapeseed), B20 (diesel 80%, biodiesel 20%) and B50 (diesel 50%, biodiesel 50%). The fuel density and viscosity were analyzed by an Anton Paar® Stabinger Viscosimeter (model SVM 3000/G2). The fuel properties are listed in Table 1 and Fig. 2. We experimented to determine density and viscosity, using the

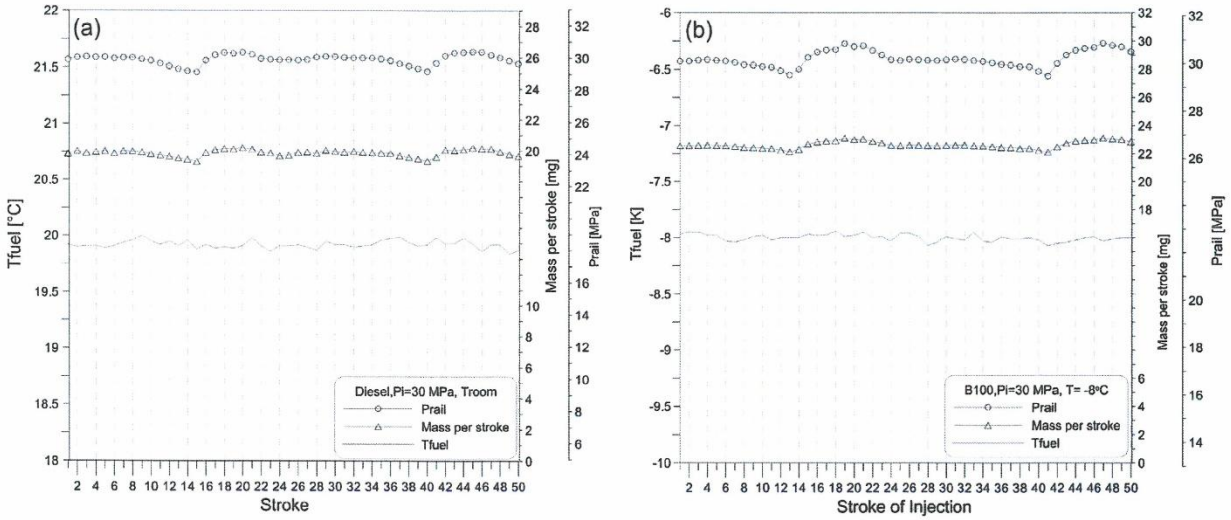

Fig. 6. Tfuel, mass and Prail per stroke of (a) diesel fuel, Troom and (b) B100, $T = -8$ °C.

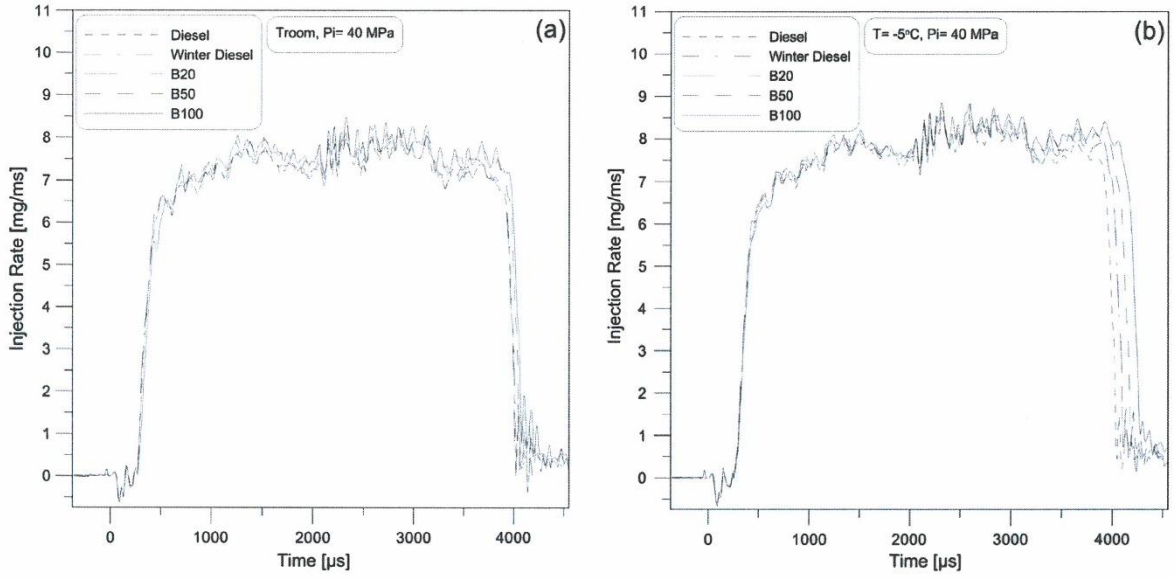

Fig. 8. Mean mass flow rate at injection pressure of (a) T = Troom and (b) T = −5 °C.

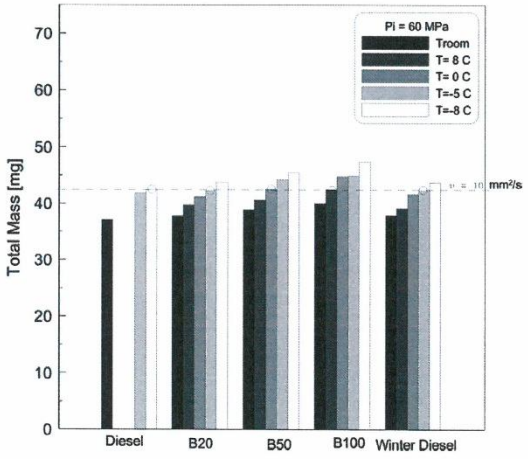

Fig. 9. Total mass injected at Pi = 60 MPa.

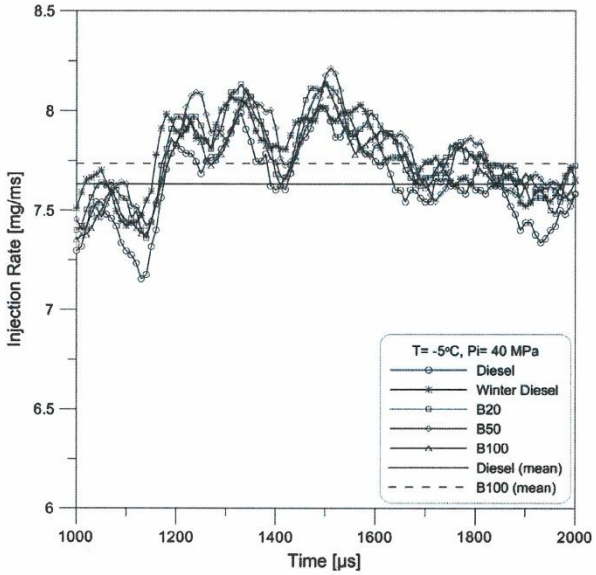

Fig. 10. Injection rate at the interval of 1000–2000 μs.

correlation from Riazi [20]. The density and viscosity can be calculated using Eqs. (2)–(5) where SG is the specific gravity at 15.5 °C and T is fuel temperature [K].

$$\rho(T) = 0.99SG - 10^{-3} \cdot (2.34 - 1.898SG) \cdot (T - 288.7) \quad (2)$$

As a single set of coefficients is not valid to describe the evolution of viscosity for all temperature ranges, we separated the curve into two parts.

For temperatures ranging from −3 °C to 40 °C.

$$\mathrm{Log}_{10}(v(T)) = A\left(\frac{311}{T}\right)^{B} - a \quad (3)$$

$$A = \mathrm{Log}_{10}(v(T = 311)) + a \quad (4)$$

$$B = b \cdot \mathrm{Log}_{10}(v(T = 311)) + c \quad (5)$$

The coefficient values a, b, c were obtained by minimizing the sum of square errors between the correlation and experiment: a = 1.1865, b = −0.4144, c = 2.0082.

For temperatures ranging from −4 °C to −10 °C.

$$\mathrm{Log}_{10}(v(T)) = A\left(\frac{269}{T}\right)^{B} - a \quad (6)$$

$$A = \mathrm{Log}_{10}(v(T = 269)) + a \quad (7)$$

$$B = b \cdot \mathrm{Log}_{10}(v(T = 269)) + c \quad (8)$$

The coefficient values a, b, c were obtained by minimizing the sum of square errors between the correlation and experiment: a = −0.8639, b = −87.6560, c = 124.30. The results from experiment and correlation are shown in Fig. 3. The behavior of different fuels with the same density of 857 kg/m^3 (±0.5%) and the same viscosity of 10 mm^2/s (±4%) were investigated.

2.3. Operating conditions and injection rate analysis

The injection rate experiment was carried out at operating temperatures of 8 °C, 0 °C, −5 °C, and −8 °C. The injection pressure,

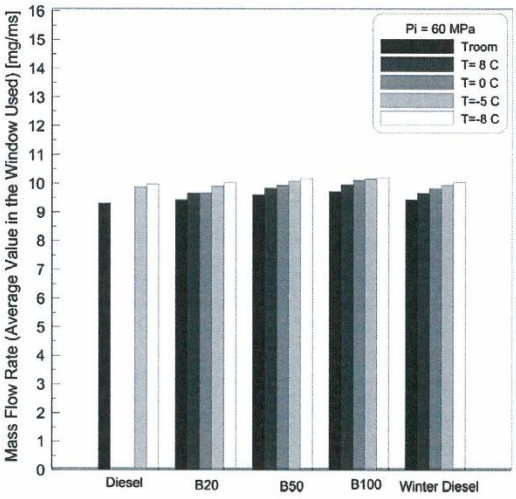

Fig. 11. Mass flow rate (average value in the window used).

Pi, varied from 30 to 60 MPa, it is typical in cold start applications and the back-pressure, *Pb* = 2.5 MPa. The duration of electrical activation of the injector was set at 2000 μs for an effective injection duration of about 4000 μs. Each injection event was reproduced 50 times. The injection frequency was set at 1 Hz to allow the pressure waves in the injection device and in the duct upstream of the injector to be completely dampened [10,14].

For each injection the fuel temperature and the injection pressure were recorded. The temperature was kept constant for all injection strokes, with variations of ±0.3 °C. The behavior of the injector was stable after 18 injections. After 50 injections the standard deviation of injection for the diesel fuel mass was 0.2145 mg. The standard deviation depends on pressure variation.

Each injection rate was divided into three parts: opening, quasi-steady period and closing. The discharge coefficient (*Cd*) calculated for each condition corresponding to the mass flow rate was averaged between 1000 and 2000 μs after the start of activation (SOA) during the quasi-steady state period (Fig. 4).

For each case the total mass injected linearly depends on the square root of the injection pressure. A reduced flow was not observed, demonstrating that there was no cavitation effect in the experiments (the case at −8 °C is illustrated in Fig. 5).

The injection rate was analyzed following the method of Payri et al. [12,19], Dernotte et al. [10] and Tinprabath et al. [14]. Eq. (9) was used to calculate the discharge coefficient *Cd*, by mean mass flow rate, $\dot{m}_{measured}$ from the quasi-steady state period 1000–2000 μs after the start of activation (SOA)(Fig. 6). This period avoids the transient phenomena related to the opening and closing phases of the injector [10,14]. The theoretical mass flow rate (Eq. (10)) is derived from a combination of the continuity equation (Eq. (11)) and Bernoulli's equation (Eq. (12)), assuming that the inlet velocity is negligible:

$$Cd = \frac{\dot{m}_{measured}}{\dot{m}_{th}} \tag{9}$$

$$\dot{m}_{th} = n_{orifice} \cdot S_c \sqrt{2\Delta P \cdot \rho_f} \tag{10}$$

$$\dot{m}_{th} = n_{orifice} \cdot \rho_f \cdot S_c V_{th} \tag{11}$$

$$V_{th} = \sqrt{\frac{2\Delta P}{\rho_f}} \tag{12}$$

where $n_{orifice}$ is the number of orifices on the geometric cross-sectional area of the orifice outlet, ΔP the pressure differential (ΔP = injection pressure *Pi* − back pressure *Pb*), ρ_f the fuel density at the experimental temperature, and V_{th} the theoretical velocity at the fuel outlet section. *Re* the Reynolds number is calculated by Eq. (13), where V_{ef} is the fuel effective velocity at the orifice exit, D_o is the geometric outlet diameter and v is the kinematic viscosity of the fuel at the experimental temperature at atmospheric pressure. V_{mean}, the fuel exit mean velocity (Eq. (14)) can be determined by measuring the mass flow rate and using the continuity equation. Assuming that the real cross-section of the injector outlet is equal to the geometric cross-sectional area (S_c), i.e. that there is no flow contraction generated by cavitation phenomena [9,14], flow losses are attributed to losses of flow velocity. This lower velocity is the effective velocity of the fuel.

$$Re = \frac{V_{ef} \cdot D_O}{v} \tag{13}$$

$$V_{mean} = \frac{\dot{m}_{measured}}{n_{orifice} \cdot S_c \cdot \rho_f} \tag{14}$$

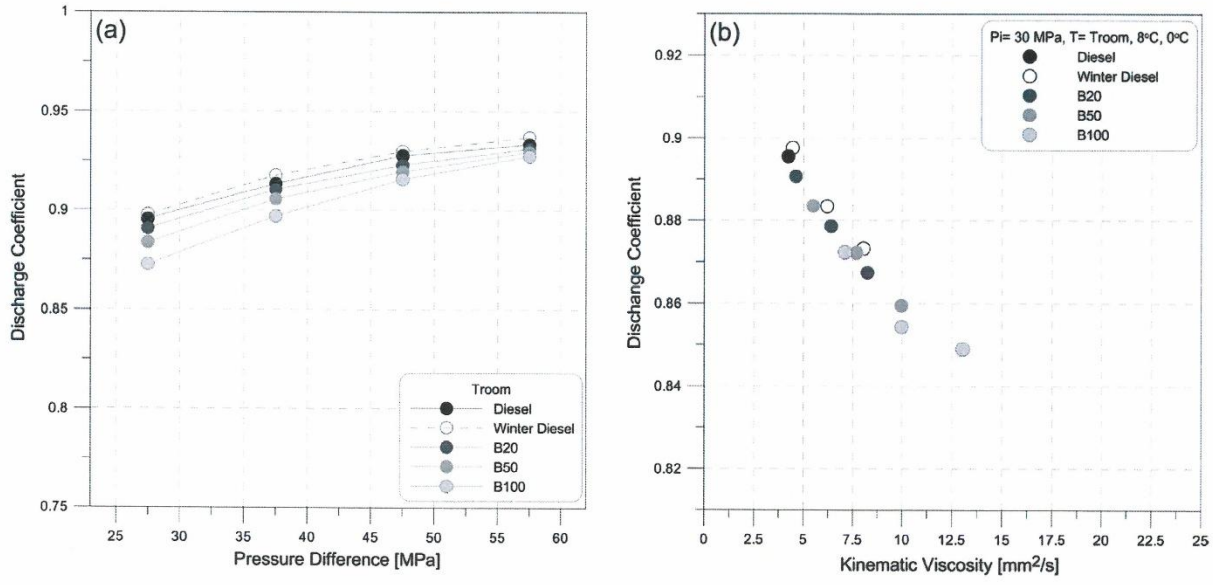

Fig. 12. Impact of fuel blends and temperature on the discharge coefficient – *Pi* = 30–60 MPa at (a) Troom, (b) *T* = Troom, 8 °C, 0 °C.

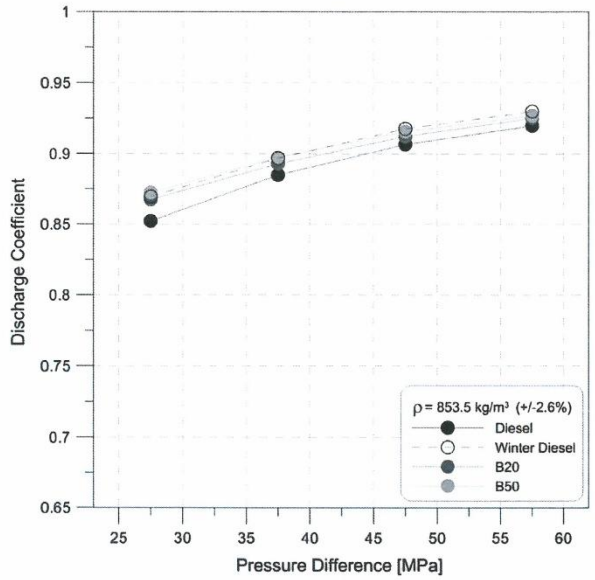

Fig. 13. Impact of the same fuel density (ρ = 857 kg/m^3) on the discharge coefficient – Pi = 30–60 MPa.

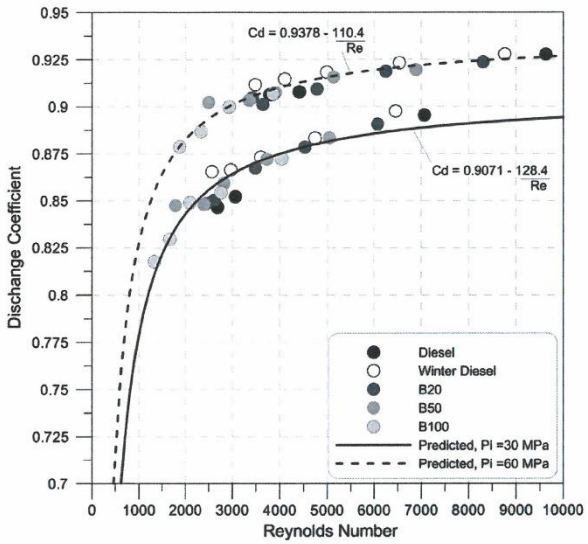

Fig. 15. Discharge coefficient versus Reynolds number for all fuels – Pi = 30, 60 MPa.

2.4. Sound velocity measurement

Sound velocity is an important thermophysical property of fuel, as it directly characterizes the fuel injection and NOx emissions in diesel engines [21]. It is necessary to determine the mass flow rate (see Eq. (1)). The injection rate device can be used to estimate sound velocity [10,22]. The method is based on determination of the time delay between the incident signal induced by the injection event and the first reflection wave [10]. We used the same experiment test bench as Dernotte et al. [10]. They measured the length of the tube loops using two liquids whose sound velocity is known. The two liquids selected were n-Heptane and n-Dodecane and their sound velocity values were taken from the NIST Chemistry WebBook. The distance travelled by the pressure wave is 10.2 m with a maximum error of 0.3%. The acoustic wave is generated by an injection from 30 to 60 MPa in the injection rate system under a back-pressure of 2.5 MPa.

In our case (Fig. 7), we chose a linear fit to show that the sound velocity increases approximately linearly when the temperature decreases. These experimental values at room temperature are close to the measurements made by Dernotte et al. [10] and Tinprabath et al. [14] and the experimental values at cold temperatures are close to the measurements made by Kegl and Hribernik [22].

3. Results and discussion

3.1. Effect of cold temperature and blended fuel properties on injection duration

With the piezoelectric technology and the stronger activation of needle, the change of fuel type or temperature does not modify the injector opening. For Pi = 40 MPa and cold temperature conditions (Fig. 8(b)) the hydraulic delay is the same for approximately 260 μs.

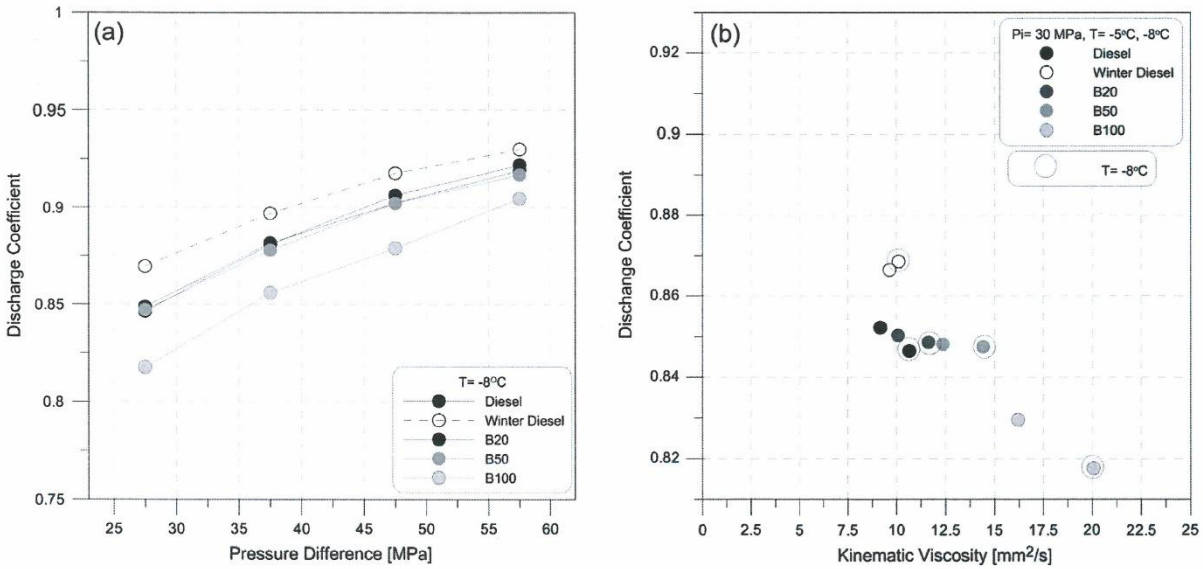

Fig. 14. Impact of fuel kinematic viscosity on the discharge coefficient – Pi = 30 MPa at (a) T = −8 °C and (b) T = −5 °C, −8 °C.

However the modification of fuel and temperature has a significant impact on closing delay, as can be seen in Fig. 8(a) and (b). The closing delay of fuel injection increases with the biodiesel content, with the B100 fuel showing the most delayed closing. The needle displacement due to the pressure drop inside the injector depends on frictional forces and thus on the fuel viscosity. B20 and winter diesel, which have the same viscosity but different densities, show the same closing delay. This behavior is typical for this injector technology. With solenoid activation, the movement of the needle on the opening and the closing of injector is more difficult with a higher viscous fluid [16]. The Bosch piezo technology moves the control orifice near the office, eliminating the plunger typical of solenoid injectors, this produces less moving parts so that friction forces are less important.

The fuel viscosity increases with a decrease in temperature. So the closing delay increases and leads to an increase in injection duration. These results are similar to the findings of Kegl [17].

This increase in injection duration can be explained by the increase in the quantity of fuel injected with the decrease in temperature. This result is illustrated in Fig. 9 where it is shown that the total fuel mass injected increases when the fuel temperature decreases. In cold conditions the fuel density increases, and so basically an increase in the mass flow is expected [16]. But for the same viscosity (in the present case, 10 mm^2/s), a change in the density does not lead to an increase in the total mass of fuel injected. The viscosity causes the duration of injection and hence the quantity of injected fuel.

3.2. Effect of blended fuels and cold conditions on discharge coefficient in quasi steady state period

For the analysis of the discharge coefficient, an injection time between 1000 and 2000 μs was selected, since this corresponds to the steady state period for injection rate (cf. Figs. 4 and 10). The injection rate values for all fuels are similar (Fig. 10). The average flow rate of B100 is slightly higher than that of diesel. In this case, the different in density between diesel and B100 is about 5% and the viscosity of B100 is 2 times higher than that of diesel.

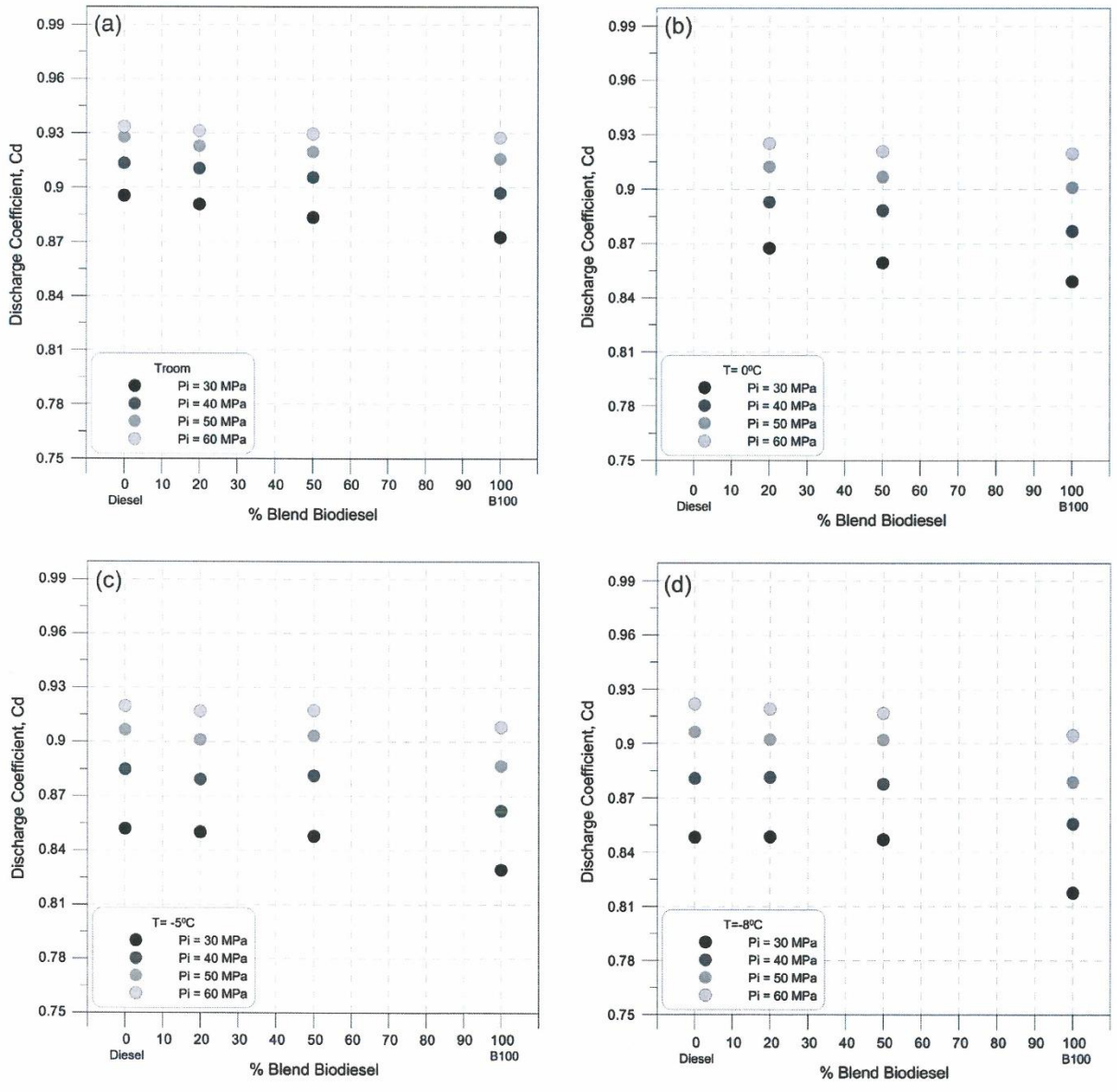

Fig. 16. Discharge coefficient versus percentage of biodiesel blend for all fuels – Pi = 30–60 MPa at (a) Troom, (b) T = 0 °C, (c) T = −5 °C, and (d) T = −8 °C.

Fig. 11 shows that when the temperature is reduced from Troom to −8 °C, the average mass flow rate of all fuels is the same. Substantial changes in viscosity or density do not alter the average mass flow rate during the quasi-steady period. These values are the result of a balance between density and viscosity. In cold conditions and/or with biodiesel, the fuel density increases and so an increase in the mass flow rate can be expected. However, in cold conditions or with biodiesel, the fuel viscosity also increases. This leads to higher frictional forces and contrary to the influence of density, a decrease in the injection rate can be expected. The changes in viscosity compensate almost completely for the changes in density. From the analysis it can be concluded that only a change in viscosity or density can impact on the fuel flow rate.

The data were analyzed according to Eq. (9). The results are given in Fig. 12(a) which shows the discharge coefficient versus the pressure difference for different fuels at room temperature. The discharge coefficient is affected by the biodiesel blend or increase in viscosity at room temperature. These decreases are greater for small injection pressures: 2.6% for $Pi = 30$ MPa and 0.6% for $Pi = 60$ MPa. The results are similar to the findings of Seykens et al. [7], Desantes et al. [9], Park et al. [13] and Tinprabath et al. [14]. This behavior is confirmed down to 0 °C. On Fig. 12(b) the Cd decreases linearly with viscosity at an injection pressure of 30 MPa. For the same density (Fig. 13) the curve arrangement depends on the fuel viscosity except for winter diesel. The discharge coefficient of diesel fuel tends to be the lowest of all the fuels and the maximum difference is 2.4%.

Likewise, Fig. 14(a) shows the discharge coefficient versus the pressure difference for different fuels at a temperature of −8 °C, which is close to the CFPP of biodiesel fuel. The results show that the discharge coefficient of winter diesel fuel is the highest, even if it has the same kinematic viscosity as B20. No significant difference between the discharge coefficients of Diesel or biodiesel blends was observed in the range of test injection pressures used here. However, the discharge coefficient of B100 fuel decreases strongly. At −5 °C and −8 °C the Cd for fuel blends is not determined only by viscosity. In Fig. 14(b), the points are more dispersed; this dispersion can be explained by the fact that fuel additives for winter diesel and diesel improve the discharge coefficient, and that the temperature is very low (−8 °C), close to the CFPP of B100.

Moreover the global behavior shows that the discharge coefficient Cd can be written by this type of equation (Eq. (15)) [16]:

$$Cd = A + \frac{B}{Re} \tag{15}$$

Cases A and B depend on the injection pressure because at a high injection pressure the effect of viscosity is reduced. The coefficient values A and B are obtained by minimizing the sum of square errors between the correlation and experiment: $A = 0.9071$, $B = 128.4$ for Pi = 30 MPa and $A = 0.9378$, $B = 110.4$ for $Pi = 60$ MPa (Fig. 15).

Fig. 16(a)–(d) summarizes the impact of the percentage of biodiesel on the discharge coefficient at room temperature, 0, −5 and −8 °C, respectively. At positive temperatures (Fig. 12), when the amount of biofuel increases, the discharge coefficients decrease. The results are similar to those reported in the literatures [7,9,13,14]. At subzero temperatures (Fig. 14), the mixtures and diesel reach the same discharge coefficient. Only the discharge coefficient of B100 is smaller. At these negative temperatures, the additives in diesel cancel out the influence of viscosity on the discharge coefficient.

4. Conclusions

The study of the influence of biodiesel and diesel blends on the injection rate in cold conditions was conducted using a Bosch CRI 3.1 piezoelectric injector. Measurements of the mass flow rate with diesel fuel, winter diesel fuel, biodiesel blends and Biodiesel (B100) were made.

The study was carried out to reach a new understanding of the injection rate behaviors such as fuel viscosity and density under cold conditions and to focus on low injection pressures, the relationship between the discharge coefficient and the percentage of biodiesel in the blends, and the relationship between the discharge coefficient and the decrease in temperature. New coefficient values for a kinematic viscosity correlation adapted for cold conditions were determined. The results are compared with data available in the literature. The conclusions of this study are summarized as follows:

- For this type of injector, the fuel viscosity changes the injection duration and hence for the same duration of pulse, it also changes the total mass injected.
- Concerning the performance of the injector shown by the value of the discharge coefficient, two behaviors were observed:
  - at positive temperatures or for fuels without additives (B100), the discharge coefficient decreases linearly with increasing viscosity;
  - at negative temperatures for fuels with additives (winter diesel, diesel or blends), the viscosity measured at atmospheric pressure is not the only property which modifies the discharge coefficient. The effect of additives cancels out the impact of viscosity and the diesel and fuel blends then have the same discharge coefficient. For winter diesel with other additives the discharge coefficients are better.

Acknowledgements

This work was cofinanced by the European Union and the European Regional Development Fund. The authors would like to thank Julien LEMAIRE for his contribution to the experimental setup and Ali Zemmit and Yahia Aberdin for their contribution to the measurement campaign.

Appendix A. Supplementary material

Supplementary data associated with this article can be found, in the online version, at http://dx.doi.org/10.1016/j.fuel.2014.12.010.

References

[1] Demirbas A. Progress and recent trends in biodiesel fuels. Energy Convers Manage 2009;50:14–34.
[2] No SY. How vegetable oils and its derivatives affect spray characteristics in CI engines – a review. Atomization Spray 2011;21(1):87–105.
[3] Perdiguero J, Jimenez JL. Sell or not sell biodiesel: local competition and government measures. Renew Sustain Energy Rev 2011;15:1525–32.
[4] Sarin A. Biodiesel production and properties. Cambridge: RSC publishing; 2012.
[5] National Biodiesel Board. Low blends of biodiesel and cold weather operability. [cit. 2014-03-20] <http://www.biodiesel.org>.
[6] Bang SH, Lee CS. Fuel injection characteristics and spray behavior of DME blended with methyl ester derived from soybean oil. Fuel 2010;89:797–800.
[7] Seykens XLJ, Somers LMT, Baert RSG. Modeling of common rail fuel injection system and influence of fluid properties on injection process. In: Proceedings of VAFSEP, Dublin, Ireland; July 6–9, 2004.
[8] Som S, Longman DE, Ramirez AI, Aggarwal SK. A comparison of injection of injector flow and spray characteristics of biodiesel with petrodiesel. Fuel 2010;89:4014–24.
[9] Desantes JM, Payri R, Garcia A, Manin J. Experimental study of biodiesel blends' effects on diesel injection processes. Energy Fuels 2009;23:3227–35.
[10] Dernotte J, Hespel C, Foucher F, Mounaïm-Rousselle C. Influence of physical fuel properties on the injection rate in a diesel injector. Fuel 2012;96:153–60.
[11] Dernotte J, Hespel C, Foucher F, Mounaïm-Rousselle C. Influence of fuel properties on the diesel injection process in non-vaporizing conditions. Atomization Spray 2012;22(6):461–92.

[12] Payri R, Salvador FJ, Gimeno J, Morena J. Study of cavitation phenomena based on a technique for visualizing bubbles in a liquid pressurized chamber. Fuel 2009;30:768–77.
[13] Park SH, Suh HK, Lee CS. Effect of cavitating flow on the flow and fuel atomization characteristics of biodiesel and diesel fuels. Energy Fuels 2008;22:605–13.
[14] Tinprabath P, Hespel C, Chanchona S, Foucher F. Influence of biodiesel and diesel fuel blends on the injection rate and spray injection in non-vaporizing conditions. SAE technical paper, 2013-24-0032; 2013.
[15] Vergnes C, Foucher F, Mounaïm-Rousselle C. Discharge coefficient for a diesel injector during cold starting conditions. Atomization sprays 2009;19(7):621–31.
[16] Payri R, Salvador F J, Gimeno J, Brach G. Effect of fuel properties on diesel spray development in extreme cold conditions. In: Proc. IMechE vol. 222 Part D, J. Automobile Engineering, 2008. p. 1743–53.
[17] Kegl B. Biodiesel usage at low temperature. Fuel 2008;87:1306–17.
[18] Bosch W. The fuel rate indicator: a new measuring instrument for display of the characteristics of individual injection. SAE technical paper, 960749; 1996.
[19] Payri R, Garcia JM, Salvador FJ, Gimeno J. Using spray momentum flux measurements to understand the influence of diesel nozzle geometry on spray characteristics. Fuel 2005;84:551–61.
[20] Riazi MR. Characterization and properties of petroleum fractions. 2nd ed. Danvers: ASTM International; 2007.
[21] Freitas S VD, Paredes Maecio LL, Daridon JL, Lima AS, Coutinho Joao AP. Measurement and prediction of the speed of sound of biodiesel fuels. Fuel 2012;103:1018–22.
[22] Kegl B, Hribernik A. Experimental analysis of injection charcteristics using biodiesel fuel. Energy Fuels 2006;20:2239–48.

References

References

[1] Demirbas A., *Progress and recent trends in biodiesel fuels*, Energy Conversion and Management, 50, (2009), pp. 14-34.

[2] No S.Y., *How vegetable oils and their derivatives affect spray characteristics in CI engines - A review*, Atomization and Sprays, 21, 1(2011), pp. 87-105.

[3] Perdiguero J. and Jiménez J. L., *Sell or not sell biodiesel: Local competition and government measures*, Renewable and Sustainable Energy Reviews, 15, (2011), pp. 1525-1532.

[4] Dardiotis C., Martini G. and Manfredi U., *Revision of low temperature emission standards for petrol vehicles*, JRC Scientific and Policy Report, European Commission, 2012.

[5] Sarin, A., *Biodiesel production and properties*, RSC publishing, 2012.

[6] National Biodiesel Board, *Low blends of biodiesel and cold weather operability [online]*, [cit. 2014-03-20], http://www.biodiesel.org.

[7] Dernotte J., Hespel C., Foucher F. and Mounaïm-Rousselle C., *Influence of physical fuel properties on the injection rate in a diesel injector*, Fuel, 96, (2012), pp. 153-160.

[8] Dernotte J., Hespel C., Foucher F. and Mounaïm-Rousselle C., *Influence of fuel properties on the diesel injection process in non-vaporizing*, Atomization and Spray, 22(6), (2012), pp. 461-492.

[9] Freitas S.V.D., Paredes M.L.L., Daridon J.L., Lima A.S. and Coutinho J.A.P., *Measurement and prediction of the speed of sound of biodiesel fuels*, Fuel, 103, (2012), pp. 1018-1022.

[10] Payri R., Salvador F. J., Gimeno J. and Morena J., *Study of cavitation phenomena based on a technique for visualizing bubbles in a liquid pressurized chamber*, Fuel, 30, (2009), pp. 768-777.

[11] Payri P., Garcia J. M., Salvador F. J. and Gimeno J., *Using spray momentum flux measurements to understand the influence of diesel nozzle geometry on spray characteristics*, Fuel, 84, (2005), pp. 551-561.

[12] Heywood J. B., *Internal combustion engine fundamentals*, McGraw-Hill, New York, 1988.

[13] Nag A., *Biofuels refining and performance*, McGraw Hill, 2008.

[14] Knothe G., *Dependance of biodiesel fuel properties on the structure of fatty acid alkyl esters*, Fuel Processing Technology 86, (2005), pp. 1059-1070.

[15] Weast R. C., *Handbook of chemistry and Physics*, 66th ed., Baca Roton, FL: CRC Press, (1986), pp. D272.

[16] Guntone F. D., Harwood J. L. and Padley F.B., *The lipid handbook*, London: Chapman & Hall, (1994).

[17] Freedman B. and Bagby M. O., *Heat of combustion of fatty esters and triglycer*, Journal of the American Oil Chemists Oil Chemists' Societies 66, (1989), pp. 1601-1605.

[18] Klopfensin E. E., *Effect of molecular weights weghts of fatty acid esters on cetane numbers as diesel fuels*, Journal of the American Oil Chemists' Society 62, (1985), pp. 1029-1031.

[19] Knothe, G., Bagby, M., and Ryan, T., *Cetane numbers of fatty compounds:influence of compound structure and of various potential cetane Improvers*, SAE Technical Paper, 971681, (1997).

[20] Knothe, G., Matheaus A. C., and Ryan T.W., III, *Cetane numbers of branched and straight-chain fatty esters determined in an ignition quality tester*, Fuel, 82, (2003), pp. 971–975.

[21] Allen C. A., Watts K. C., Ackman R. G. and Pegg M. J., *Predicting the viscosity of biodiesel fuels from their fatty acid ester composition*, Fuel, 78, (1999), pp. 1319-1326.

[22] Knothe G. and Steidley K. R., *Kinematic viscosity of biodiesel fuel components, Influence of compound structure and comparison to petrodiesel fuel components*, Fuel, 84 (2005), pp. 1059-1065.

[23] Kent H., *Review of biodiesel composition, properties, and specifications*, Reneable and Sustainable Energy Reviews, 16, (2012), pp. 143-169.

[24] Geller D. P. and Goodrum J. W., *Effects of specific fatty acid methyl esters on diesel fuel lubricity*, Fuel, 83, (2004), pp.2351–2356.

[25] Bhatnagar A. K., Kaul S., Chhibber V. K., and Gupta A. K., *HFRR studies on methyl esters of nonedible vegetable oils*, Energy & Fuels, 20, 3 (2006), pp. 1341–1344.

[26] Schober S. and Mittelbach M., *The impact of antioxidants on biodiesel oxidation stability*, European Journal of Lipid Science and Technology, 106, (2004), pp. 382–389.

[27] Prankl H. and Wörgetter M., *Influence of the iodine number of biodiesel to the engine performance, In: Liquid Fuels and Industrial Products from Renewable Resources*, Proceedings of the 3rd Liquid Fuel Conference, J. S., Cundiff, et al. (Eds.), St Joseph, MI: ASAE, (1996), pp. 191–196.

[28] Lapuerta M., Rodriguez-Fernandez J. and de Mora EF., *Correlation for the estimation of the cetane number of biodiesel fuels and implications on the iodine number*. Energy Policy 37(11), (2009), pp. 4337–4344.

[29] Knothe G. and Steidley K. R., *Lubricity of components of biodiesel and petrodiesel, the origin of biodiesel lubricity*, Energy & Fuels, 19, (2005), pp.1192–1200.

[30] Dunn R. O. and Bagby M. O., *Low-temperature properties of triglyceride-based diesel fuels: Transesterified methyl esters and petroleum middle distillate/ester blends*, Journal of the American Oil Chemists' Society, 72, (1995), pp. 895–904.

[31] Knothe G., Dunn R. O., and Bagby M. O., *Biodiesel: The use of vegetable oils and their derivatives as alternative diesel fuels*, ACS Symposium Series 666, In: Fuels and Chemicals from Biomass, American Chemical Society, Washington, DC, (1997), pp. 172–208.

[32] Knothe G., Dunn R. O., Shockley M. W., and Bagby M. O., *Synthesis and characterization of some long-chain diesters with branched or bulky moieties*, Journal of the American Oil Chemists' Society, 77, (2000), pp. 865–871,.

[33] Dunn R. O., Shockley M. W., and Bagby M. O., *Improving the low-temperature properties of alternative diesel fuels: Vegetable-oil derived methyl esters*, Journal of the American Oil Chemists' Society, 73, (1996), pp. 1719–1728.

[34] Lee I., Johnson L. A., and Hammond E. G., *Reducing the crystallization temperature of biodiesel by winterizing methyl soyate*, Journal of the American Oil Chemists' Society, 73, (1996), pp. 631.

[35] Dunn R. O., Shockley M. W., and Bagby M. O., *Winterized methyl esters from soybean Oil: an alternative diesel fuel with improved low-temperature flow properties*, SAE Technical Paper, 971682, (1997).

[36] Reitz R.D. and Braco F.B., *On the dependence of spray angle and other spray parameters on nozzle design and operating conditions*, SAE Paper, 790494, (1979).

[37] De Filippis P., Giavarini C., Scarsella M. and Sorrentino M., *Transesterification processes for vegetable oils: A simple control method of methyl ester content*, Journal of the American Oil Chemists' Society, 71, (1995), pp. 1399–1404.

[38] Tat M. E. and Van Gerpen J. H., *The kinematic viscosity of biodiesel and its blends with diesel fuel*, Journal of the American Oil Chemists' Society, 76, (1999), pp. 1511–1513.

[39] Allen C. A. W., Watts K. C., Ackman R. G., and Pegg. M. J, *Predicting the viscosity of biodiesel fuels from their fatty acid ester composition*, Fuel, 78, (1999), pp. 1319–1326.

[40] Du L. M. P., *Plant oils as diesel fuel extenders: Stability tests and specifications on different grades of sunflower seed and soyabean oils*, CHEMSA 8, (1982), pp. 150–154.

[41] Knothe G., *Analysis of oxidized biodiesel by 1H-NMR and effect of contact area with air*, European Journal of Lipid Science and Technology, 108, (2006), pp. 493–500.

[42] Allard L. N., Webster G. D., Hole N. J., Ryan III Ott T. W., D., and Fairbridge C. W., *Diesel fuel ignition quality as determined in the ignition quality tester (IQT)*, SAE Technical Paper, 961182, (1996).

[43] Canakci M., Monyem A., and Van Gerpen J., *Accelerated oxidation processes in biodiesel*, Transactions of the American Society of Agricultural Engineers, 42, (1999), pp. 1565–1572.

[44] Knothe G., *Structure indices in FA chemistry. How relevant is the iodine value?*, Journal of the American Oil Chemists' Society, 79, (2002), pp. 847–854.

[45] Prankl H., Wörgetter M., and Rathbauer J., *Technical performance of vegetable oil methyl esters with a high iodine number, In: Biomass*, Proceedings of the 4th Biomass Conference of the Americas, Oakland, California, (1999), pp. 805–810.

[46] Hillion G., Montagne X., and Marchand P., *Methyl esters of plant oils used as additives or organic fuel*. (Les esters méthyliques d'huiles végétales: additif ou biocarburant?), Oleagineux, Corps Gras, Lipides, 6, (1999), pp. 435–438.

[47] Hu J., Du Z., Liu C., and Min E., *Study on the lubrication properties of biodiesel as fuel lubricity enhancers*, Fuel, 84, (2005), pp.1601–1606.

[48] Drown D. C., Harper K. and Frame E., *Screening vegetable oil alcohol esters as fuel lubricity enhancers,* Journal of the American Oil Chemists' Society, 78, (2001), pp. 579–584.

[49] Goodrum J. W. and Geller D. P., *Influence of fatty acid methyl esters from hydroxylated vegetable oils on diesel fuel lubricity*, Bioresource Technology, 96, 7 (2005), pp.851–855.

[50] Desantes J. M., Payri R., Garcia A. and Manin J., *Experimental study of biodiesel blends'effects on diesel injection processes*, Energy & Fuels, 23, (2009), pp. 3227-3235.

[51] Plamondon E. and Seers P., *Development of a simplified dynamic model for a piezoelectric injector using multiple injection strategies with biodiesel/diesel-fuel blends,* Applied Energy, 131, (2014), pp. 411-424.

[52] Vergnes C., Foucher F., and Mounaïm-Rousselle C., *Discharge coefficients for a diesel injector during cold starting conditions,* Atomization and sprays, 19, 7 (2009), pp. 621-631.

[53] Lichtarowicz A. and Pearce I. D., *Cavitation and aeration effects in long orifices*. (L. Mech. Eng. Publ. Ltd., Ed.) Cavitation, Proc. of Fluid Machinery Group of Inst, of Mech. Engineers, (1974), pp. 437.

[54] Payri F., Garcia J.M., Salvador F., and Gi- meno J., *Influenceof nozzle geometryon spray characteristics in non-evaporating and evaporative conditions*, SAE Paper, 2007240023, (2007).

[55] Dernotte J., Hespel C., Foucher F. and Mounaïm-Rousselle C., *Experimental Study of the Influence of Fuel Physical Properties on the Diesel Injection Process in Non-Vaporizing Conditions,* ILASS–Europe 2011, 24th European Conference on Liquid Atomization and Spray Systems, Estoril, Portugal, September 2011.

[56] Miller H. E. and Beardsley E. G., *Spray penetration with a simple fuel injection nozzle*. NACA Annual Report 11, 1926.

[57] Naber J. D. and Siebers D.L., *Effects of gas density and vaporization on penetration and dispersion of diesel sprays*, SAE paper, 960034, (1996).

[58] Musculus M. B. and Kattke K., *Entrainment waves in diesel jets,* SAE Paper, 2009-01-1355.

[59] Siebers, D. L., *Scaling Liquid-Phase Fuel Penetration in Diesel Sprays Based on Mixing-Limited Vaporization*, SAE paper, 1999-01-0528, 1-26.

[60] Hiroyasu H., Arai M., *Structures of fuel sprays in diesel engines*. SAE paper, 900475.

[61] Hiroyasu H., Kadota T. and Tasaka S., *Study of the penetration of diesel. JSME International Journal*, 44(385):3208–3219, (1978).

[62] Levy N., Amara S. and Champoussin J. C., *Simulation of a diesel jet assumed fully atomized at the nozzle exit*. SAE International, 981067, (1998).

[63] Desantes J. M., Payri R., Salvador F. J. and Gil A., *Development and validation of a theoretical model for diesel spray penetration.* Fuel, 85, (2006), pp. 910-917.

[64] Payri R., Salvador F. J., Gimeno J. and Novella R., *Flow regime effects on non-cavitating injection nozzles over spray behavior*, International Journal of Heat and Fluid Flow, 32, (2010), pp. 273¬284.

[65] Sazhin S.S., Feng G. and Heikal M.R., *A model for fuel spray penetration*, Fuel, 80, (2001), pp. 2171-2180.

[66] Arregle J. M., Pastor J. V. and Ruiz S., *The influence of injection parameters on diesel spray characteristics*, SAE paper, 1999-01-0200.

[67] Soteriou C., Lambert M., Zuelch S. and Passerel D., *The flow characteristics of high efficiency diesel nozzles with enhanced geometry holes*, In: THIESEL Conference on Thermo and Fluid dynamics in Diesel Engines, Valencia, Spain, September 13-15, 2006.

[68] Giannadakis E., Gavaises M. and Theodorakakos A., *The influence of variable fuel properties in high-pressure diesel injectors*, SAE paper, 2009-01-0832.

[69] Payri R., Salvador F. J., Gimeno J. and Morena J., *Study of cavitation phenomena based on a technique for visualizing bubbles in a liquid pressurized chamber*, International Journal of Heat and Fluid Flow, 30, (2009), pp. 768-777.

[70] Dernotte J., *Influence des propriétés physic-chimiques des hydrocarbures sur l'injection et la combustion diesel*, Thesis, Université d'Orléans, 2012.

[71] IAV GmbH, *Injection Analyzer simultaneous measurement of injection rate and injection quantity (Version K-025-50)*, 2013.

[72] Bosch W., *The Fuel Rate Indicator: A New Measuring Instrument for Display of the Characteristics of Individual Injection*, SAE Paper, 660749, (1966).

[73] Lefebvre A. H., *Atomization and Sprays*, Hemisphere Publishing Corporation, (1989).

[74] Soteriou C., Andrews R and Smith M., *Direct injection diesel sprays and the effect of cavitation and hydraulic flip on atomization*, SAE Paper 950080, (1995).

[75] Chaves H., Knapp M., Kubitzek A., Obermeier F. and Schneider T., *Experimental study of caviation in the nozzle hole of diesel injectors using transparent nozzles*, SAE Paper, 950290, (1995).

[76] Suh H. K., Park S. H. and Lee C. S., *Experimental investigation of nozzle cavitating flow characteristics for diesel and biodiesel fuels*, International Journal of Automotive Technology, 9, 2 (2008), pp. 217-224.

[77] Otsu N., *A threshold selection method from gray-level histograms*, IEEE Trans. Syst. Man Cyber, 1979, vol. 1: 62-66

[78] Anton Paar GmbH, *Instruction manual SVM 3000 stabinger viscometer*, Austria, 2005.

[79] Riazi M.R., *Characterization and properties of petroleum fractions*, ASTM manual series: MNL50, 2005.

[80] Nadir Yilmaz, *Temperature-dependent viscosity correlations of vegetable oils and biofuel–diesel mixtures.* Biomass & Bioenergy, 35, (2011), pp. 2936-2938.

[81] Wang Z., Ding H., Wyszynki M.L., Tian J. and Xu H., *Experimental study on diesel fuel injection characteristics under cold start conditions with single and split injection strategies.* Fuel Processing Technology, 131, (2015), pp. 213-222.

[82] Tesfa B., Mishra R., Gu F. and Powles N., *Prediction models for density and viscosity of biodiesel and their effects on fuel supply system in CI engines.* Renewable Energy, 35, (2010), pp. 2752-2760.

[83] Verduzco L.F.R., Flores B.E.G., Rodriguez J.E.R. and Jacob A.R.J., *Prediction of the density and viscosity in biodiesel blends at various temperatures.* Fuel, 90, (2011), pp. 1751-1761.

[84] Kegl B., *Numerical analysis of injection characteristics using biodiesel fuel*, Fuel, 85, (2006), pp. 2377-2387.

[85] Tat M.E. and Van Gerpen J.H., *Effect of temperature and pressure on the speed of sound and isentropic bulk modulus of biodiesel and diesel fuel*, Jam Oil Chem. Soc, , 80, (2003), pp. 1127-1130.

[86] Kegl B. and Hribernik A., *Experimental analysis of injection charcteristics using biodiesel fuel*, Energy Fuels, 20, (2006), pp. 2239–2248.

[87] Payri R, Salvador F J, Gimeno J, Brach G., *Effect of fuel properties on diesel spray development in extreme cold conditions*. In; Proc. IMechE Vol.222 Part D, J. Automobile Engineering , (2008), pp. 1743-1753.

[88] Park S.H., Suh H.K. and Lee C.S., *Effect of cavitating flow on the flow and fuel atomization characteristics of biodiesel and diesel fuels,* Energy & Fuels, 22, (2008), pp. 605-613.

[89] Seykens X.L.J., Somers L.M.T. and Baert R.S.G., *Modeling of common rail fuel injection system and influence of fluid properties on injection process*, In: Proceedings of VAFSEP, Dublin, Ireland; July 6-9, 2004.

[90] Payri R., Salvador F.J., Gimeno J. and Venegas O., *Study of cavitation phenomenon using different fuels in a transparent nozzle by hydraulic characterization and visualization*, Experimental Thermal and Fluid Science, 44, (2013), pp. 235-244.

[91] Chen P.C., Wang W.C., Roberts W.L. and Fang T., *Spray and atomization of diesel fuel and its alternatives from a single-hole injector using a common rail fuel injection system*, Fuel,103, (2012), pp. 850-861.

[92] Bang S.H. and Lee C.S., *Fuel injection characteristics and spray behavior of DME blended with methyl ester derived from soybean oil*, Fuel, 89, (2010), pp. 797-800.

[93] Gao Y., Deng J., Li C., Deng F., Liao Z., Wu Z. and Li L., *Experimental study of the spray characteristics of biodiesel based on inedible oil*, Biotechnology Advances, 27, (2009), pp. 616-624.

[94] Kegl B., *Biodiesel usage at low temperature*, Fuel, 87, 2008, pp. 1306–1317.

[95] Tinprabath P., Hespel C., Chanchaona S. and Foucher F., *Influence of biodiesel and diesel fuel blends on the injection rate and spray injection in non-vaporizing conditions,* SAE paper, 2013-24-0032.

[96] White, F., *Fluid Mechanics*, McGraw-Hill, 4rd Ed., Singapore, 1999.

Padipan TINPRABATH

L'Influence des Propriétés Physiques et Chimiques du Biodiesel, Diesel et de leur Mélange sur l'Injection et le Spray

Résumé:

Le biodiesel est un carburant très intéressant car du fait de son caractère renouvelable il augmente la sécurité énergétique et est plus respectueux de l'environnement. De plus il a un indice de cétane plus élevé et une plus faible teneur en soufre et en aromatique que le Diesel pur. Les principaux inconvénients de biodiesel sont sa viscosité élevées, sa faible teneur en énergie, un point trouble et le point d'écoulement plus élevé, une émission d'oxyde d'azote (NOx) plus élevée lors de sa combustion et un coût élevé. Cependant, de nombreux pays peuvent produire leur propre biodiesel et assurer des mélanges d'une teneur entre 2 et 20% de biodiesel avec du carburant diesel. Les nouvelles normes Euro VI impliquent des problèmes liés au démarrage à froid. Pour approfondir notre compréhension de ces mélanges, il est nécessaire de tester un plus large éventail de carburants de 10 à 50% de biodiesel jusqu'à -8°C pour pallier le manque d'information dans la littérature.

La présente thèse porte sur une étude expérimentale sur l'influence des propriétés physiques et chimiques des mélanges de carburants Biodiesel/Diesel sur l'injection : taux et répartition des sprays dans des conditions de non évaporation.

L'originalité de l'approche concerne la définition d'une matrice de carburant (un total de neuf combustibles) dont les propriétés sont modifiées via le pourcentage de biodiesel ou la température. En outre tous les stades de l'injection diesel sont considérés. Des expériences ont été menées en enceinte contrôlée en température. L'analyse se concentre principalement sur la phase quasi-stationnaire de l'événement d'injection et les résultats expérimentaux sont disponibles pour calibrer des modèles physiques et de nouvelles corrélations empiriques sont proposées.

Mots clés: Propriétés des carburants, mélange entre diesel et biodiesel, taux d'introduction, comportement du spray

The Influence of Physical Properties of Biodiesel, Diesel and Their Blended Fuels on Injection and Spray

Abstract:

Biodiesel is a very interesting fuel because it is renewable, thus increasing energy security, it is environmentally friendly, and it has a higher cetane number and a lower sulfur and aromatic content than pure Diesel. The main disadvantages of biodiesel are its higher viscosity, lower energy content, higher cloud point and pour point, higher nitrogen oxide (NOx) emissions, lower power and high cost. However, many countries can produce their own biodiesel and blends with diesel fuel of 2–20%. The new Euro VI standards involve problems related to cold-start. To further our understanding of these mixtures, it is necessary to test a larger range of fuels with a biodiesel fraction of 10 to 50%, and under cold temperatures, no information is available in the literature, however, on the injection rate and spray penetration of Diesel–Biodiesel blends in cold conditions.

The present thesis focuses on an experimental study of the Influence of physical and chemical properties of biodiesel, Diesel and their blended fuels on injection and spray for Diesel engine application.

The originality of the approach concerns the definition of a fuel matrix (a total of 9 fuels) for which properties are varied by varying the percentage of biodiesel and the temperature. Moreover all the stages of Diesel injection are considered. Experiments were conducted in dedicated temperature-controlled vessels. The analysis focuses mainly on the quasi-stationary phase of the injection event and experimental results are scaled to physics-based models and new empirical correlations are proposed.

Keywords : Fuel Properties, Biodiesel Bend, Injection Rate, Spray Behavior

UNIVERSITE D'ORLEANS

Laboratoire PRISME
8 rue Léonard de Vinci
45072 Orléans cedex
FRANCE

PRISME
Laboratoire Pluridisciplinaire de Recherche Ingénierie des Systèmes, Mécanique, Énergétique